Université de Montréal

Polymeric micelles as versatile carriers for drugs and nucleic acids

par

Mahmoud El Sabahy

Faculté de Pharmacie

Thèse présentée à la Faculté des études supérieures
en vue de l'obtention du grade de doctorat
en sciences pharmaceutiques
option technologie pharmaceutique

Août, 2009

© Mahmoud El Sabahy, 2009

Université de Montréal

Faculté des études supérieures

Cette thèse intitulée :

Polymeric micelles as versatile carriers for drugs and nucleic acids

Présentée par :

Mahmoud El Sabahy

A été évaluée par un jury composé des personnes suivantes :

Prof. Patrice Hildgen, président-rapporteur

Prof. Jean-Christophe Leroux, directeur de recherche

Prof. Yue Zhao, membre du jury

Prof. Frédéric Calon, examinateur externe

Résumé

Le cancer est la principale cause de mortalité au Canada. Les taxanes (*e.g.* le paclitaxel et le docétaxel (DCTX)) constituent des remèdes efficaces contre une série de tumeurs solides telles que les cancers du sein, du poumon et de l'ovaire. Par ailleurs, des acides nucléiques (*e.g.* les oligonucléotides antisens (AON) ou les petits ARN interférents (siRNAs)), capables de supprimer sélectivement certains oncogènes impliqués dans la carcinogénèse, sont actuellement étudiés pour traiter une large gamme de cancers. Bien que l'activité des taxanes et des acides nucléiques soit bien établie sur des modèles humains et/ou animaux, plusieurs aspects physico-chimiques et cliniques restent encore à améliorer. Leur solubilité limitée (pour les taxanes), leur dégradation rapide dans le sang (pour les acides nucléiques), leur élimination précoce, leur absence de sélectivité et leur toxicité envers les tissus sains sont les principaux facteurs limitant leur efficacité. C'est pourquoi de nombreux efforts ont porté sur l'élaboration de systèmes de vectorisation ciblés à base de polymères, dans le but de surmonter les problèmes associés aux thérapies actuelles. Dans cette thèse, deux types de micelles polymères ont été développés pour la vectorisation de DCTX et d'acides nucléiques. D'une part, des micelles de poly(oxyde d'éthylène)-*bloc*-poly(oxyde de butylène/styrène) ont été étudiées pour la première fois pour solubiliser le DCTX et le protéger de l'hydrolyse. Ces polymères se sont révélés moins toxiques que le surfactant utilisé commercialement pour solubiliser le DCTX (*i.e.* polysorbate 80) et ont permis une libération prolongée du principe actif. D'autre part, deux systèmes différents de micelles polyioniques (PICM) ont été mis au point pour la vectorisation d'acides nucléiques. De nouveaux conjugués de poly(éthylène

glycol) (PEG)-oligonucléotide ont été proposés pour la protection et la libération contrôlée d'AON. Lorsque ces conjugués ont été formulés avec des dendrimères de poly(amidoamine) (PAMAM), des complexes de taille homogène ont été obtenus. Ces PICM ont permis de prolonger la libération de l'AON et de le protéger efficacement contre la dégradation enzymatique. De plus, des polymères de poly(oxyde d'éthylène)-*bloc*-poly(méthacrylate de propyle-*co*-acide méthacrylique) ont été incorporés afin de conférer des propriétés acido-sensibles aux PICM. Dans ces micelles, formées de ce dernier polymère formulé avec le dendrimère PAMAM, des oligonucléotides (AON et siRNA) ciblant l'oncogène Bcl-2 ont été encapsulés. L'internalisation cellulaire fut assurée par un fragment d'anticorps monoclonal (Fab') situé à l'extrémité de la couronne de PEG. Après l'internalisation cellulaire et la protonation des unités d'acide méthacrylique sous l'effet de l'acidification des endosomes, les micelles se sont affranchies de leur couronne. Elles ont ainsi exposé leur cœur composé d'acide nucléique et de dendrimère PAMAM, qui possède une charge positive et des propriétés endosomolytiques. En effet, ces PICM acido-sensibles ciblées ont permis d'augmenter la biodisponibilité des acides nucléiques vectorisés et se sont avérées plus efficaces pour silencer l'oncoprotéine Bcl-2 que les micelles non ciblées ou que le dendrimère de PAMAM commercial seul. Finalement, les nanovecteurs polymères présentés dans cette thèse se révèlent être des systèmes prometteurs pour la vectorisation des anticancéreux et des acides nucléiques.

Mots-clés : micelles polymères, micelles polyioniques, docétaxel, oligonucléotide antisens, siRNA, dendrimères de poly(amidoamine), vectorisation de médicament, vectorisation d'acides nucléiques, sensibilité au pH, ciblage.

Abstract

Cancer is considered as the leading cause of premature death in Canada. Taxanes (*e.g.* paclitaxel and docetaxel (DCTX)) are effective against a range of solid tumors including breast, lung, and ovarian malignancies. In addition, nucleic acids (*e.g.* antisense oligonucleotides (AON) and short interfering RNA (siRNA)) which are capable of selectively suppressing oncogenes involved in carcinogenesis are currently being investigated for the treatment of a wide variety of cancers. Although the activity of taxanes and nucleic acid drugs is well-established in human and/or animal models, several physicochemical and clinical issues still need to be addressed. Low aqueous solubility (*i.e.* taxanes), rapid degradation in the blood (*i.e.* nucleic acids), fast clearance, non-selectivity and toxicity to normal tissues are limiting factors to their effectiveness. Hence, many efforts have been focused on developing targeted polymeric delivery systems to overcome the problems associated with the current therapies. In this thesis, two types of polymeric micelles have been developed for the delivery of DCTX and nucleic acids. On the one hand, poly(ethylene oxide)-*block*-poly(butylene oxide/styrene oxide) micelles were tested for the first time to solubilize and protect DCTX from hydrolytic degradation. The polymers showed less toxicity than the surfactant used commercially to dissolve DCTX (*i.e.* polysorbate 80) and released the drug in a sustained fashion. On the other hand, two different systems of polyion complex micelles (PICM) were developed for the sustained release and intracellular delivery of nucleic acids. Novel poly(ethylene glycol) (PEG)-oligonucleotide conjugates were assessed to protect AON against degradation and release them in a sustained manner. When these conjugates were mixed with

poly(amidoamine) (PAMAM) dendrimers, monodisperse PICM were formed. These PICM further slowed down AON release and significantly protected it against enzymatic degradation. In addition, the incorporation of poly(ethylene oxide)-*block*-poly(*propyl* methacrylate-*co*-methacrylic acid) was exploited to impart pH-sensitivity to PAMAM-based PICM. This system was composed of the previous copolymer mixed with PAMAM dendrimer. Such PICM were loaded with AON or siRNA targeting the Bcl-2 oncogene. Micelles uptake by the cancer cells was mediated by a monoclonal antibody fragment (*i.e.* Fab') positioned at the extremity of the PEG corona. Upon cellular uptake and protonation of the methacrylic acid units in the acidic endosomal environment, the micelles lost their corona, thereby exposing their positively-charged endosomolytic PAMAM/nucleic acid core. The targeted, pH-sensitive PICM were found to increase the intracellular bioavailability of the entrapped nucleic acids and knock down the Bcl-2 oncoprotein more than either non-targeted micelles or commercial PAMAM dendrimers. The polymeric nanocarriers reported in this thesis appear to be promising vehicles for the delivery of anticancer drugs and nucleic acids.

Keywords: Polymeric micelles, polyion complex micelles, docetaxel, antisense oligonucleotide, siRNA, poly(amidoamine) dendrimers, drug delivery, nucleic acid delivery, pH-sensitivity, targeted delivery.

Table of contents

List of tables

CHAPTER 1 - General overview

CHAPTER 2 - Polymeric micelles as versatile carriers for drugs and nucleic acids delivery

CHAPTER 3 - Solubilization of docetaxel in poly(ethylene oxide)-*block*-poly(butylene/styrene oxide) micelles

CHAPTER 4 - Synthesis and enzymatic stability of PEGylated oligonucleotide duplexes and their self-assemblies with polyamidoamine dendrimers

CHAPTER 5 - Delivery of nucleic acids through the controlled disassembly of multifunctional nanocomplexes

CHAPTER 6 - Discussion

List of figures

CHAPTER 1 - General overview

CHAPTER 2 - Polymeric micelles as versatile carriers for drugs and nucleic acids delivery

CHAPTER 3 - Solubilization of docetaxel in poly(ethylene oxide)-*block*-poly(butylene/styrene oxide) micelles

CHAPTER 6 – Discussion

List of schemes

CHAPTER 4 - Synthesis and enzymatic stability of PEGylated oligonucleotide duplexes and their self-assemblies with polyamidoamine dendrimers

CHAPTER 5 - Delivery of nucleic acids through the controlled disassembly of multifunctional nanocomplexes

List of abbreviations

2′F-ANA	2′-deoxy-2′-fluoro-β-D-arabinonucleic acid
AON	Antisense oligonucleotides
ASGPR	Asialoglycoprotein receptor
ATRP	Atom transfer radical polymerization
AUC	Area under the concentration-time curve
BGE	Background electrolyte
CAC	Critical association concentration
CDN	Candesartan cilexetil
CE-LIF	Laser-induced fluorescence detection coupled to capillary electrophoresis
CMC	Critical micelle concentration
DCTX	Docetaxel
DEAE Sephadex®	Diethylaminoethyl Sephadex®
d_h	Hydrodynamic diameter
DLS	Dynamic light scattering
DOX	Doxorubicin
EPR	Enhanced permeation and retention
Fab'	Fragment antigen binding
FAM	3′-Fluorescein
FOL	Folic acid
FRET	Fluorescence resonance energy transfer
G	Generation

GPC	Gel permeation chromatography
HPLC	High performance liquid chromatography
IP	Inflection points
ITC	Isothermal titration calorimetry
K^2	Scattering vectors
K_v	Partition coefficient
LCST	Lower critical solution temperature
LNA	Locked nucleic acid
MASLS	Multiangle static light scattering
M_n	Number-average molecular weight
MPS	Mononuclear phagocyte system
MTD	Maximum tolerated dose
MTT	3-[4,5-dimethylthiaolyl]-2,5-diphenyl-tetrazolium bromide
M_W	Weight-average molecular weight
N	Nitrogen
N_{agg}	Aggregation number
NHS	*N*-hydroxysuccinimide
ON(s)	Oligonucleotide(s)
P	Phosphate
P	Packing parameter
P(Al(M)A-*co*-MAA)s	Poly(alkyl(meth)acrylate-*co*-methacrylic acid)
PBMA	Poly(butyl methacrylate)

P(MAA-*co*-EA-*co*-BMA)	Poly(methacrylic acid-*co*-ethyl acrylate-*co*-butyl methacrylate)
PAMAM	Poly(amidoamine)
PBLG	Poly(γ-benzyl-L-glutamate)
PBO	Poly(butylene oxide)
PBS	Phosphate buffered saline
PCL	Poly(ε-caprolactone)
PCTX	Paclitaxel
PD	Phosphodiester
PDI	Polydispersity index
PDLA	Poly(D-lactide)
PDLLA	Poly(D,L-lactide)
pDNA	Plasmid DNA
PDPT	Poly(3-[(3-aminopropyl)amino]propylaspartamide)
PEG	Poly(ethylene glycol)
PEG-*b*-P(Asp)	PEG-*b*-poly(aspartic acid)
PEG-*b*-PBO	PEG-*b*-poly(butylene oxide)
PEG-*b*-PPS	PEG-*b*-poly(propylene sulfide)
PEG-*b*-PSO	PEG-*b*-poly(styrene oxide)
PEG-PE	PEG-phosphatidyl ethanolamine
PEI	Polyethylenimine
PEO	Poly(ethylene oxide)
PICM	Polyion complex micelles

PLGA	Poly(D,L-lactide-*co*-glycolide)
PLL	Poly(L-lysine)
PLLA	Poly(L-lactide)
PM	Polymeric micelles
PMPA	Poly[(3-morpholinopropyl) aspartamide]
PNA	Peptide nucleic acid
PNIPAM	Poly(*N*-isopropylacrylamide)
PPO	Poly(propylene oxide)
PS	Phosphorothioate
PSO	Poly(styrene oxide)
PVP	Poly(*N*-vinylpyrrolidone)
R_g	Radius of gyration
R_h	Hydrodynamic radius
RISC	RNA-induced silencing complex
RNAi	RNA interference
S	Specific surface area
scF_V	Single-chain variable
S_{CP}	Solubilizing capacity
SDS	Sodium dodecyl sulfate
siRNA	Short interfering RNA
SNALP	Stable nucleic-acid-lipid particles
SON	Nuclease-sensitive sequence or Sense oligonucleotide
SPARC	Secreted protein acid and rich in cysteine

TBA	*tert*-butanol
*t*BMA	*tert*-butyl methacrylate
TEM	Transmission electron microscopy
T_m	Melting temperature
UPM	Unimolecular polymeric micelles
VEGF	Vascular endothelial growth factor
λ_{em}	Emission wavelength
λ_{ex}	Excitation wavelength
χ_{sc}	Flory-Huggins interaction parameter

Acknowledgments

First and foremost, **Professor Jean-Christophe Leroux, Faculty of Pharmacy, University of Montreal,** deserves recognition for his tremendous contribution to this work, in addition to recognition for the immeasurable impact he has had on my career and professional development. Professor Leroux provided guidance, knowledge, insight and direction whenever it was needed. He introduced me to many of the pioneers in multidisciplinary fields, giving me an opportunity to learn from them as well. He also supported me and my family financially during my Ph.D. studies. He is the one who gave me the chance to come to Canada and continue in my graduate studies. Honestly, most of my knowledge in the modern Pharmaceutical Sciences was acquired from Professor Leroux.

I am also thankful for everyone in my lab. All of them helped me in different ways. It is difficult to mention certain names because all of them contributed to my Ph.D. However, I acknowledge **François Plourde, Marie-Ève Perron, Nicolas Bertrand, Marie-Hélène Dufresne, Nada Wazen** and **Núria Bayó** who were directly involved in my research. I also acknowledge **Jeanne Leblond** for her critical reading of the thesis.

Other individuals deserve special recognition for their impact on this thesis. **Professor Masad Damha, Department of Chemistry, McGill University,** and his students introduced me to a new field (*i.e.* latest advances in the nucleic acid chemistry). Communication and attendance of meetings with this lab were very useful and contributed significantly to my Ph.D. **Glen Deleavey** has synthesized several modified nucleic acids to be combined with our nanomedicines.

Professor Marc Servant, Faculty of Pharmacy, University of Montreal, and his students helped me a lot in evaluating the effect of my formulations on the expression of Bcl-2 (*i.e.* oncoprotein) which is a very important part in my thesis. **Jean-François Clément, Priscilla Doyon** and **Myriam Archambault** are specially acknowledged for helping me with the Bcl-2 assay.

I also would like to acknowledge **Professor Patrice Hildgen, Faculty of Pharmacy, University of Montreal** and all the members of my jury for their contribution to this thesis**.**

I also acknowledge **the Faculté des études supérieures** for financial assistance and the **Egyptian cultural office** for involving me in the exemption program.

I really appreciate the efforts that my **WIFE** did to support me throughout my Ph.D. She provided encouragement, help, care, time and understanding throughout my study.

Last but not least, I would like to thank my **mother, father, grandmother, wife, daughter (Jana), son (Mohamed), brother** and **sister** for providing encouragement and understanding throughout my educational career.

CHAPTER 1 - General overview

Cancer is the uncontrolled division of cells. Cancerous cells are abnormal and can invade and damage nearby tissues or separate from the tumor and spread to other parts of the body[1]. Cancer is considered to be the leading cause of premature death in Canada. In 2003, 2.5% of Canadian men and 2.8% of Canadian women were diagnosed with cancer. According to Canadian cancer statistics, 171,000 new cases of cancer and 75,300 deaths from cancer are anticipated in Canada in 2009.

Many factors, such as, tobacco smoking, prolonged exposure to radiation, free radicals and alcohol can cause cancer[2-5]. In addition, cancer can occur due to viral infections[6]. There are over 100 distinct types of cancer which are classified according to the type of initially-affected cell[7].

Tumorigenesis, a multistep process, reflects the accumulation of genetic damages that drives the progressive transformation of normal cells into malignant cells[8]. These mutations usually produce oncogenes with dominant gain of function and tumor suppressor genes with recessive loss of function. Both activation of oncogenes and loss of tumor suppressor genes allow cancer cells to avoid apoptosis (programmed cell death). The normal function of proteins encoded by tumor suppressor genes is to provide growth restraint[9]. Oncogenes are mutated genes that allow unregulated cell growth by yielding a large number of proteins required for tumor progression[10]. These proteins are usually expressed in normal cells. However, they can be made oncogenic by mutation or overexpression. For example, epidermal growth factor receptors and platelet-derived growth factor receptors are either mutated or overexpressed in tumor cells[10].

Cancer cells usually have distinct properties: evading apoptosis, limitless replicative potential, self-sufficiency of growth factors, insensitivity to anti-growth signals, angiogenesis (recruitment of new blood vessels from pre-existing ones), invasion and metastasis[7]. In addition, some morphological changes are characteristic of tumor cells, such as, variations in cell shape and nuclear size with loss of normal tissue organization[11]. These alterations can be characteristic of a given tumor type and stage.

Cancer is treated by different modalities, such as, surgery[12,13], radiation[13,14], immunotherapy[15,16], hormonal therapy[17,18], angiogenesis inhibition[19-21] and chemotherapy[22-26]. The choice of treatment depends on tumor location and grade. Two or more of these therapies are often combined.

Tumor mass can be completely removed by surgery. However, the tendency of cancer to spread to other sites limits its effectiveness[12,13]. Therefore, dissection of cancer is usually followed by chemotherapy and/or radiotherapy[13].

Radiotherapy employs ionizing radiation to kill cancer cells and shrink tumors. It usually acts by destroying genetic materials to prevent cell growth and division[14]. It is included after surgery, sometimes in combination with chemotherapy, to prevent the spread of cancer[13]. Different types of radiation can be administered, depending on the tumor site and grade. Some can reach deep areas while others can be controlled to treat only small sites[14]. Nevertheless, radiotherapy is toxic to normal tissues, and this restricts its clinical application[27].

Immunotherapy can be specific or non-specific. Non-specific immunotherapy consists of cytokine-based regimens to modulate the immune response[15,16]. Specific

immunotherapies, designed to elicit or enhance the immune response to tumor antigens, involve the administration of cancer cells obtained from the patient (after certain manipulations and are usually combined with immunity activators) to strengthen immunity against specific tumor types[28]. In addition, specific immunotherapies deploy antibodies or immunotoxins against tumor antigens[29]. The main problem with immunotherapies is immunological tolerance. The tumor can violate regulatory mechanisms (*e.g.* loss of tumor antigens) which diminish the activities of these antibodies[30].

Hormonal therapy generally targets tumors that are sensitive to hormones (*e.g.* breast and prostate cancers). In these tumors, certain hormones (*e.g.* estrogen and testosterone) can bind to cancer cell receptors and promote cellular proliferation. Blocking these receptors[17], or inhibiting hormonal production[18] can reduce tumor growth. Drugs that interfere with estrogen binding to breast cancer cell receptors (*e.g.* tamoxifen), or turn off its production from the ovaries (*e.g.* aromatase inhibitors), can serve to treat breast cancer[17,18].

Angiogenesis inhibitors prevent the extensive growth of blood vessels required for tumor growth[19-21]. These inhibitors can prevent vascular endothelial cells from proliferating or migrating in response to a spectrum of pro-angiogenic proteins (*e.g.* vascular endothelial growth factor, VEGF)[19-21]. In addition, they can inhibit the expression of angiogenic proteins (*e.g. via* RNA interference, RNAi)[31-34].

Cancer chemotherapy relies on the use of drugs that prevent the dissemination of neoplasias by interfering with specific molecules involved in tumor growth[22, 23, 26,35]. Although these drugs are effective in killing tumoral cells, they are usually

harmful to normal tissues and cause toxicity[22]. Alternatively, by focusing on the molecular and cellular changes that are specific to cancer (*e.g.* expression of specific extracellular receptors or differences in pH inside the cancer cells), targeted cancer therapies can be more effective and less harmful than current interventions[23]. Taxanes (*e.g.* paclitaxel and docetaxel) are used against a range of solid tumors including breast, lung, and ovarian malignancies[36,37]. In addition, nucleic acids (*e.g.* antisense oligonucleotides (AON) and short interfering RNA (siRNA)) which are capable of selectively suppressing oncogenes (*e.g.* Bcl-2) involved in carcinogenesis have been investigated for the treatment of a wide variety of cancers[38,39]. The mechanisms of action of taxanes, AON and siRNA will be discussed in details in the following sections. Although the effectiveness of both types of compounds is well-established in human and/or animal models, the clinical outcomes still need to be improved. Low aqueous solubility (*i.e.* taxanes), rapid degradation in the blood (*i.e.* nucleic acids), rapid clearance, non-selectivity and toxicity to normal tissues are limiting factors to an optimal activity. Hence, many efforts have been focused on developing targeted polymeric delivery systems to overcome the problems associated with current therapies[40-43].

Targeted polymeric carriers, such as liposomes[44], lipoplexes[45], polyplexes[46] and polymeric micelles[47] (PM), have been tested for the delivery of taxanes, nucleic acids and other drugs. These delivery systems provide a reservoir for either solubilizing water-insoluble agents (*e.g.* antitumor drugs) or accommodating and protecting charged biomacromolecules (*e.g.* proteins and nucleic acids) from enzymatic degradation. These systems are usually coated with a non-ionic

hydrophilic shell to prevent the adsorption of opsonins, thereby limiting the rapid uptake by the mononuclear phagocyte system (MPS) and prolonging the circulation half-life of the encapsulated drug. Prolonged circulation time allows the passive targeting of the nanoparticles into tumors *via* the enhanced permeation and retention (EPR) effect (Chapter 2, Figure 2)[48]. The EPR effect is explained by the vascular leakage and impaired lymphatic drainage at tumor sites, resulting in the peripheral deposition of colloidal particles. In addition, colloids can be decorated with specific ligands that bind to extracellular receptors over-expressed by tumors. In this chapter, some delivery systems that have been examined for the delivery of hydrophobic drugs (*e.g.* taxanes) and nucleic acids will be discussed (Tables 1 and 2).

1. Formulations of taxanes

Taxanes are mitotic inhibitors that include paclitaxel and docetaxel. Their anticancer activity is achieved through binding to tubulins, thus inhibiting cell mitosis at the G2/M phase by stabilizing the microtubules, which triggers apoptosis[49]. Taxanes are effective against a range of solid tumors, such as breast, lung, and ovarian malignancies. However, conventional use of taxanes can be very toxic and only a small proportion of injected drug molecules reaches target cells, whereas the rest damages healthy cells and tissues. In addition, taxanes have poor aqueous solubility. For example, the aqueous solubility of paclitaxel and docetaxel is 1.6 and 2 μg/mL, respectively[50,51]. To improve their solubility, a vehicle composed of polyethoxylated castor oil (Cremophor® EL) and ethanol is used for paclitaxel (commercial formulation Taxol®) while docetaxel is formulated in polysorbate 80

(Tween® 80) and ethanol (commercial formulation Taxotere®). These solvents can cause histamine-mediated hypersensitivity reactions which usually requires premedication[22]. Even with prophylactic antihistaminic agents and corticosteroids, severe reactions can still occur. Furthermore, these surfactants modulate the disposition profiles of paclitaxel and docetaxel after intravenous administration, resulting in non-linear pharmacokinetics[22,52]. To overcome the disadvantages of current formulations and to increase the therapeutic index of taxanes, various colloidal drug carriers, such as emulsions, liposomes, nanoparticles, and PM, are currently being studied (Table 1 and Figure 1).

Table 1. Examples of colloidal taxane formulations currently being tested in clinical trials or approved for cancer treatment.

Formulation	Drug	Carrier	Reference
Taxol®	Paclitaxel	Cremophor® EL	53
Taxotere®	Docetaxel	Tween® 80	38
Xyotax® Polymeric conjugate	Paclitaxel	Poly(L-glutamic acid)	54
Tocosol® Emulsion	Paclitaxel	Tocopherol	55
Abraxane® Nanoparticles	Paclitaxel	Albumin nanoparticles	56

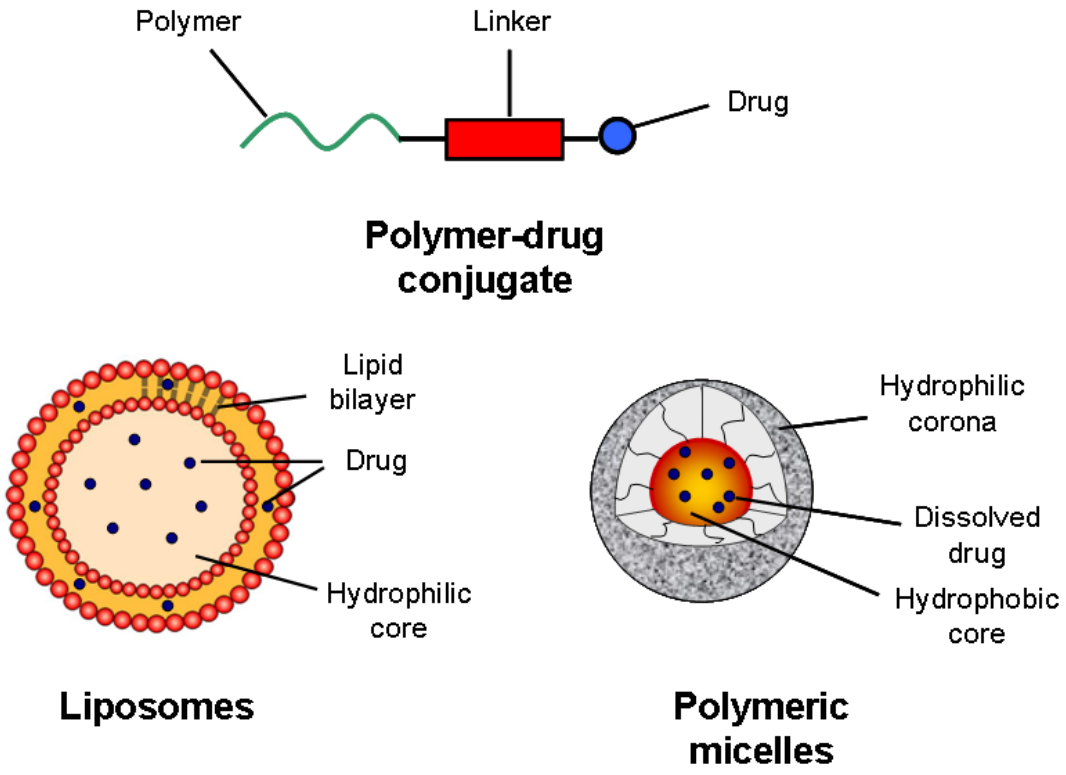

Figure 1. Some delivery systems (liposomes, PM and polymeric-drug conjugates) currently being exploited for the delivery of anticancer drugs.

1.1 Polymeric macromolecular carriers

Chemotherapeutic agents can be conjugated to hydrophilic polymeric backbones to increase their aqueous solubility (Figure 1). This conjugation can modulate the pharmacokinetics and decrease the side-effects of drugs. Moreover, it can be applied for active targeting by attaching a targeting moiety to the polymeric carrier so as to favor its recognition by a specific cell receptor. The idea was first proposed by Ringsdorf in the mid-1970s and then extended to many therapeutic applications[57]. Several polymers have been employed for these purposes, such as

poly(ethylene glycol) (PEG), poly(*N*-(2-hydroxypropyl) methacrylamide) and poly(glutamic acid)[54,58]. Among all these polymeric-drug conjugates, poly(L-glutamic acid)-paclitaxel (Xyotax®) (Table 1) has received special impetus. In this system, paclitaxel is conjugated to poly(L-glutamic acid) *via* ester linkage. The resulting conjugate is highly water-soluble. The active drug is then released by enzymatic cleavage of the poly(glutamic acid) backbone through the action of cellular proteases in tumors, particularly cathepsin B, which is upregulated by malignant tissues[54]. Xyotax® has demonstrated significantly enhanced antitumor efficacy and improved safety compared to paclitaxel in preclinical studies and advanced to phase III clinical trials[59].

1.2 Emulsions

Emulsion is an heterogeneous mixture of two immiscible liquids with emulsifier that stabilizes the dispersed droplets. They can be utilized as carriers for hydrophilic or hydrophobic drugs for different therapeutic applications. For instance, oil-in-water emulsions have served as carriers for lipophilic drugs and many of them are available commercially[60]. These emulsions can alter the biodistribution of the incorporated drugs and enhance their accumulation in target tissues. For example, Constantinides *et al.*[61] have formulated a submicron emulsion of paclitaxel using vitamin E (tocopherol) as the internal phase (Tocosol®-paclitaxel) (Table 1). When the emulsion was injected into melanoma-bearing mice, it was found to be less toxic and had greater antitumor activity than Taxol®. However, Tocosol®-paclitaxel, unexpectedly, failed in a phase III study conducted in breast cancer patients. The response rate was 37% for Tocosol®-paclitaxel *vs.* 45% for Taxol®, and it was linked

to more side effects than Taxol®[62]. Although there is no clear explanation for this failure, the weak interactions between tocopherol and paclitaxel might explain the lower efficacy of the formulation.

1.3 Liposomes

Liposomes are spherical vesicles composed of lipid bilayers with an hydrophilic core (Figure 1). They are usually classified according to the number of lipid bilayers into unilamellar and multilamellar vesicles. Normally, both hydrophilic and lipophilic drugs can be loaded into the core and lipid bilayer of liposomes, respectively[63]. However, the loading of hydrophobic drugs can be limited by the space in the hydrophobic lipid layers. Steric stabilization is usually required to avoid the rapid clearance by the MPS and is usually achieved by grafting hydrophilic polymers (*i.e.* PEG) to the surface of the liposomes. Active targeting can also be carried out by attaching targeting moieties to the surface coating. Liposomes have been employed as delivery vehicles for various chemotherapeutic agents[63]. In particular, doxorubicin-loaded liposomes (Doxil™) have been approved for the treatment of ovarian cancer[44]. These liposomes showed extended circulation time and enhanced accumulation in tumors, compared to the free drug. Liposomes have been tested with several other anticancer drugs, such as paclitaxel and docetaxel[51,64]. For instance, Immordino *et al.*[64] reported that upon intravenous injection of docetaxel formulated in polysorbate 80, the β half-life was 52.3 min. Conversely, the half life rose to 665 min when docetaxel was formulated in PEGylated liposomes. Nevertheless, the low loading capacity of liposomes for taxanes and poor physical stability limited their progress to the clinic[51].

1.4 Polymeric micelles

PM are formed *via* the self-assembly of amphiphilic copolymer chains in aqueous milieu. They present a core/shell architecture wherein the hydrophobic core serves as a microenvironment for the solubilization of poorly water-soluble drugs while the hydrophilic corona acts as a stabilizing interface between the core and the external medium (Figure 1). In water, hydrophobic interactions are generally the main driving force behind the micellization process. PM usually have fairly narrow size distributions with diameters ranging from 10 to 100 nm. Incorporation of the drug inside the micelles often decreases the toxicity of the entrapped drug, allowing for higher doses to be administered and greater efficacy. For example, D. Le Garrec *et al.*[65] demonstrated that paclitaxel incorporated in poly(*N*-vinylpyrrolidone)-*b*-poly(D,L-lactide) (PVP-*b*-PDLLA) did not reach the maximum tolerated dose (MTD) even at 100 mg/kg and showed greater antitumor activity than Cremophor® EL micelles whose MTD was established at 20 mg/kg. Because of the higher MTD, paclitaxel could be injected at higher doses (60 mg/kg) where it induced three- and twofold increases in the plasma and tumor area under the concentration-time curves, respectively, *vs*. Cremophor® EL (20 mg/kg). Indeed, paclitaxel formulated in PEG-*b*-PDLLA micelles is now in phase II clinical trials, either alone or in combination with cisplatin[66,67]. The applications of PM to deliver various therapeutic agents will be discussed in detail in Chapter 2.

1.5 Nanoparticles

Nanoparticles are colloidal particles with a rigid core. They are either made from i) a polymeric or lipidic matrix in which a drug is dissolved or dispersed or ii) from drug nanocrystals stabilized by a polymer[56, 68,69]. They are usually larger than micelles (100-200 nm) and are generally more polydisperse. Amphiphilic copolymers have been exploited as emulsifiers for the preparation of nanoparticles. They form stable films, where the hydrophobic block is oriented toward the core while the hydrophilic block creates a hydrated corona and provides steric stabilization for the nanoparticles. Many copolymers have been employed in the preparation of nanoparticles for the delivery of anticancer drugs. Examples of these polymers include PEG-*b*-PDLLA and PEG-*b*-poly(lactide-*co*-glycolide)[68-71]. Alternatively, albumin nanoparticles (nab-paclitaxel; Abraxane®) have been used for paclitaxel delivery (Table 1)[56,72]. These protein nanoparticles consist of albumin-bound paclitaxel with a mean particle size of 130 nm. They facilitate drug transport into tumors through albumin receptors and caveolae-mediated transport across endothelial cells, which increase the intratumoral accumulation of paclitaxel[56]. Preliminary evidence suggests that this process may be facilitated through binding of albumin to SPARC (secreted protein acid and rich in cysteine), an extracellular matrix glycoprotein that is overexpressed and associated with poor prognosis in a variety of cancers. In a recent *in vivo* study, intratumoral paclitaxel accumulation was found to be 33% higher for nab-paclitaxel compared to Cremophor® EL-paclitaxel when each formulation was administered using equal doses of paclitaxel[37]. These nanoparticles have been recently approved for patients with metastatic breast cancer.

2. Formulations of nucleic acids

The introduction of nucleic acids into eukaryotic cells to investigate gene function and regulate gene expression has drawn considerable attention. Nucleic acids, such as plasmid DNA (pDNA), AON and siRNA have been tested to treat several diseases including cancer[33,34,38,73-76]. For example, AON and siRNA have been implicated in the downregulation of oncogenes involved in the carcinogenesis, such as Bcl-2, an important antiapoptotic protein found in a wide variety of human cancer cells. Bcl-2 protein controls the mitochondrial outer membrane permeabilization. Overexpression of Bcl-2 causes stabilization of the mitochondrial membrane and prevents the release of cytochrome *c* (which plays a role in apoptosis) thus interrupting the intrinsic apoptotic pathway. The latter confers resistance to malignant cells against chemotherapeutic agents that work by inducing apoptosis[39]. Bcl-2 Inhibition would sensitize cancer cells to chemotherapy. Bcl-2 expression can be downregulated by both AON and siRNA (Figure 2)[77]. AON cause protein knockdown by selectively binding to mRNA, blocking mRNA translation or inducing its degradation by activating RNase H endonuclease activity that cleaves RNA in RNA–DNA heteroduplexes. This leads to the selective degradation of target mRNA while leaving AON intact. Alternatively, RNAi cleaves the mRNA and knocks down a target protein *via* a different mechanism. In the RNAi process, long double stranded RNA are cleaved into shorter double stranded RNA segments (siRNA) by the Dicer protein, ribonuclease III type protein. siRNA possesses a well-defined structure consisting of a short (19-22 nucleotides) double stranded RNA with 2-nucleotides 3′ overhangs on each strand. After cellular entry, the siRNA duplex is assembled into

large protein assemblies, called the RNA-induced silencing complexes (RISC), where the sense strand of siRNA is removed by a helicase associated with the RISC. The RISC with the antisense strand specifically cleaves target mRNA which has a complementary sequence to the antisense strand[78]. Both AON and siRNA lead at the end to the target gene downregulation (Figure 2). To date, one AON has been approved for local administration to treat cytomegalovirus (fomivirsen). However, other AON and siRNA are currently in various stages of clinical development (Table 2)[73,79,80].

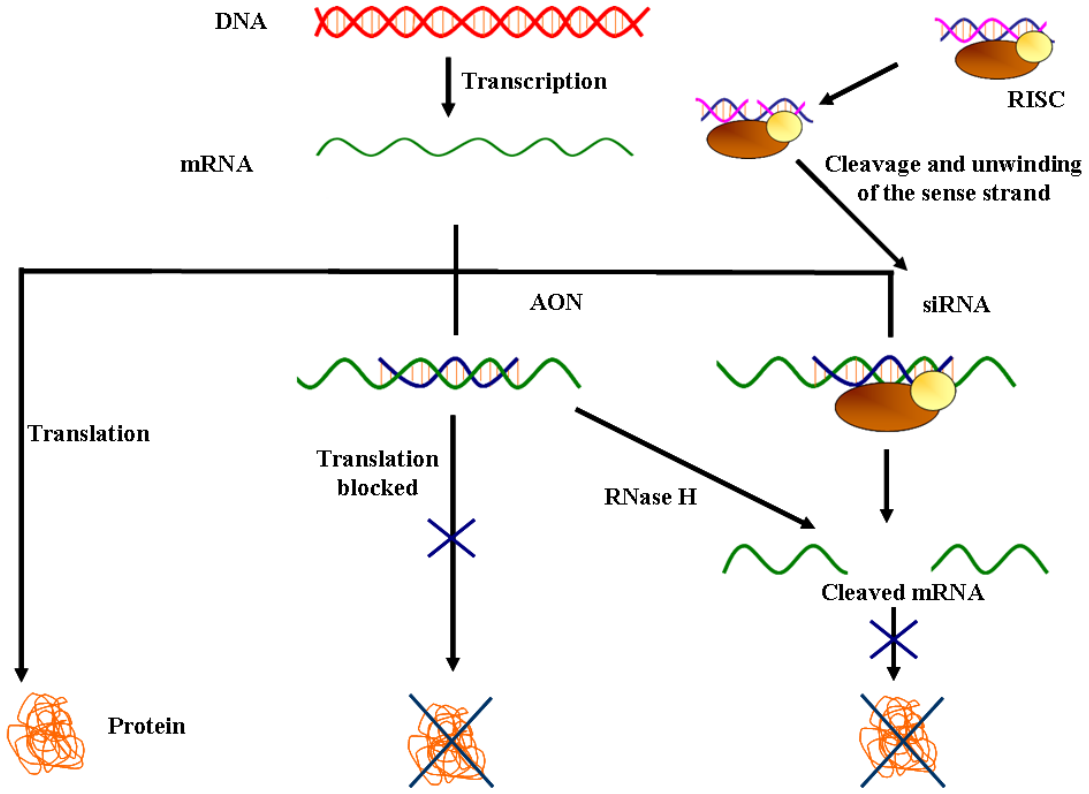

Figure 2. Mechanism of action of AON and siRNA. AON pair with their complementary target RNA and block mRNA translation or induce its degradation. siRNA duplexes are assembled into the RISC where the sense strand is cleaved and unwound, leaving single-stranded RNA associated with the RISC. These complexes hybridize and cleave complementary target mRNA. Both actions result in target protein downregulation.

Table 2. Some AON and siRNA currently in clinical trials for the treatment of cancer[73,79,80].

AON or siRNA	Molecular target	Status	Sponsor
Oblimersen AON (Genasense, G3139)	Bcl-2	Phase II/III	Aventis/Genta
LY900003 AON (Affinitak, ISIS 3521)	Protein kinase C-α	Phase II/III	Lilly/Isis
ISIS 2503 AON	Ha-ras	Phase II	ISIS Pharmaceuticals
Oncomyc-NG AON	c-myc	Phase I/II	AVI BioPharma
CALAA-01 siRNA	RPM2	Phase I	Calando Pharmaceuticals
ALN-VSP siRNA	KSP and VEGF	Phase I	Alnylam Pharmaceuticals

However, the clinical use of nucleic acid-based drugs is still largely hampered by their inability to reach their site of action in sufficient amounts. Parameters, such as circulation time in the blood stream[81,82], deposition at the target site and intracellular transport[83], play a detrimental role in their *in vivo* activity. Unmodified nucleic acids have very limited cellular uptake due to their polyanionic nature and high molecular weight. In addition, naked AON or siRNA usually have a short half-life in serum (usually a few minutes) due to enzymatic degradation, and are rapidly cleared from the body. Numerous efforts have been made to develop efficient vectors for nucleic acid delivery and various methods have been proposed to accomplish their transfer into eukaryotic cells.

2.1 Chemical modifications

Unmodified oligonucleotides (ONs) are seldom tested in animal models as they rapidly degrade in biological fluids and cells[84-87]. The chemical instability issue has been partially solved through specific modifications of the ON backbone.

Among all ON derivatives, phosphorothioate (PS) analogs have been widely studied (Figure 3)[79,84]. In PS modifications, one of the non-bridging oxygen atoms of the phosphodiester linkage is substituted by a sulfur atom. PS modifications confer moderate resistance against nuclease degradation and increase the half-life in human serum compared to the native ON. The major disadvantage of the PS modification is that the sulfur atom promotes non-specific binding to certain proteins, which can cause severe adverse reactions (especially at high doses)[82,88]. Another shortcoming is the reduced affinity towards the mRNA compared to the phosphodiester ON[82,88].

Regarding sugar modifications, 2'-O-methylation is one of the most widely-studied sugar modifications for both AON and siRNA (Figure 3) because it increases their nuclease stability[79,84]. However, many groups have found that large numbers of 2'-O-methyl modifications do not induce the RNase H endonuclease activity and decrease siRNA potency[89,90]. Other modifications of ribose sugar include peptide nucleic acid (PNA) and locked nucleic acid (LNA) (Figure 3)[73,79]. PNA is a synthetic DNA in which the deoxyribose phosphate backbone is replaced by polyamide linkages. LNA is a conformationally restricted nucleotide containing a 2'-*O*, 4'-C-methylene bridge in the β-D-ribofuranosyl configuration. Both PNA and LNA can bind to complementary DNA or RNA with high affinity and specificity. In addition, they have high stability against nuclease degradation. However, both PNA and LNA do not elicit target RNA cleavage by RNase H. Therefore, their applications might be limited as antisense agents and they can be exploited to modulate gene expression[91].

Alternatively, 2′-deoxy-2′-fluoro-β-D-arabinonucleic acid (2′F-ANA) sugar modifications of the ON have been found to maintain high intracellular

concentrations for prolonged periods of time leading to long-term gene silencing (Figure 3)[92]. This was explained by increased serum stability and higher binding affinity to the target mRNA. The 2′F-ANA modifications have been successfully applied to both AON and siRNA[78]. They are well-tolerated throughout both sense and antisense strands of siRNA[92-94]. Although the use of modified nucleic acids has partially overcome the problem of rapid degradation, most chemical modifications are partially ineffective in reducing their renal clearance or improving their intracellular and site-specific delivery.

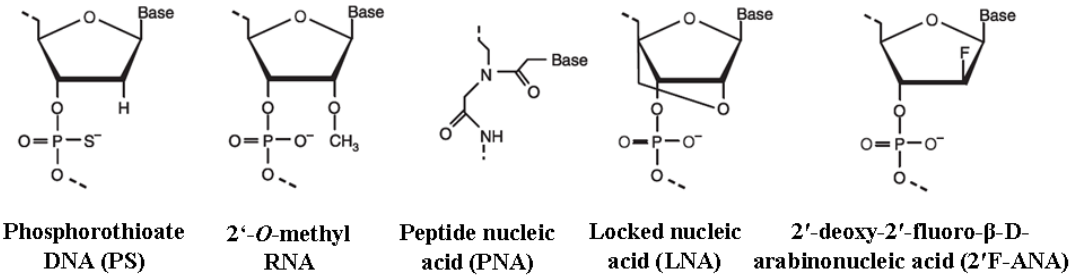

Figure 3. Chemical structure of PS DNA, 2′-*O*-methyl RNA, PNA, LNA and 2′F-ANA

Likewise, conjugates have been employed to enhance transfection efficiency and resistance to nucleases. Covalent conjugation to hydrophilic polymers (*e.g.* PEG) or lipophilic moieties (*e.g.* cholesterol) have been shown to improve the pharmacokinetics and enhance the efficacy of many nucleic acids[95-97]. For instance, conjugation to cholesterol has been reported to slow ON clearance[95,98] and enhance cellular association and transport[96]. However, these conjugates are mainly taken up

by the liver by interacting with lipoprotein particles[97], and their applications to target other tissues are limited.

2.2 Viral vectors

Viruses are composed of an envelope or capsid that contains genetic material (DNA or RNA) in a compact form. They possess sizes ranging from 20 to 100 nm[99]. A variety of these viruses have been converted to vectors to deliver genes to cells (*e.g.* adenoviruses, retroviruses and adeno-associated viruses). Some viruses and their characteristics are presented in Table 3. Although a detailed discussion of viral vectors in nucleic acid delivery is beyond the scope of this introduction, it is worth mentioning that they have been implicated in 70% of gene therapy clinical trials[99]. Indeed, viral vectors offer superior transfection efficiency than their synthetic counterparts, can infect most kinds of cells and are among the first carriers adopted for the delivery of different nucleic acid materials. Nevertheless, their use is limited because of inherent safety concerns. The use of viral vectors for gene therapy can be associated with severe inflammation and immunological problems[100,101]. The toxicity of viral vectors is usually due to random integration of the transported genes[99,102]. In addition, the size of the DNA and the type of the genetic material that can be encapsulated into viral vectors restrict their applicability. Hence, there is a need for alternative synthetic approaches for the delivery of nucleic acids.

Table 3. Characteristics of viral vectors. Adapted from reference[99].

Features	Adenovirus	Adeno-associated virus	Retrovirus
Particle size	70-100	20-25	100
Insert size (kb)	8-10	4.9	8
Chromosomal integration	No	No	Yes
Long-term expression	Weeks to months	>1 year	Long-term
Emergence of replication-competent vector in vivo?	Possible	Possible	Risk

2.3 Non-viral vectors

2.3.1 Non-complexing polymers

Amphiphilic copolymers such as, poloxamers, have been exploited as non-viral gene vectors to deliver different genetic materials[103]. Poloxamers consist of linear triblock copolymers with an A-B-A structure ((ethylene oxide)$_x$-(propylene oxide)$_x$-(ethylene oxide)$_x$). For instance, poloxamer 407 has been used to deliver AON by intravenous injection into *mdx* mice for the treatment of Duchene muscular dystrophy (DMD). DMD is a degenerative muscle disease caused by the low expression of dystrophin protein in skeletal muscles evoked by a mutation in the dystrophin gene. Repeated injections of this formulation enhanced dystrophin induction in skeletal muscles by restoring the dystrophin gene[104].

Polymeric nanocapsules have also been deployed for the delivery of nucleic acids[105]. This method was developed by Lambert *et al.*[106] who prepared poly(isobutylcyanoacrylate) nanocapsules containing an aqueous core. The incorporation of AON into the aqueous core of nanocapsules improved their stability

against enzymatic degradation and increased their serum half-lives as compared to naked AON. Alternatively, the incorporation of AON and siRNA into the aqueous core of non-ionic polymersomes was achieved recently by Discher and coworkers[107]. The exact mechanism of interactions between these non-charged (*i.e.* non-complexing) polymers and nucleic acids is still unclear and needs further investigation. Indeed, the delivery of nucleic acids by complexing them with cationic lipids and polymers has stirred more interest and has produced promising results.

2.3.2 Lipoplexes and polyplexes

A common approach to enhance the stability of nucleic acids and improve their transfection efficiency consists in complexing them with positively-charged lipids and polymers to form lipoplexes and polyplexes, respectively. Both cationic lipids and polymers (*e.g.* polyethylenimine[108,109] (PEI) and poly(amidoamine)[110,111] (PAMAM)) have been studied as non-viral gene carriers because of their ability to protect DNA/RNA from enzymatic degradation and to increase cellular uptake by adsorptive endocytosis. Usually, excess positive charges are required for high transfection efficiency. Although, lipoplexes and polyplexes are considered to be the most promising candidates for non-viral gene delivery systems, they are rapidly inactivated in the presence of serum. This inactivation is probably elicited by interactions with negatively-charged serum proteins which shield the positive charges on the surface of lipoplexes and polyplexes[112]. Moreover, after intravenous injection, the large size and positive character of these complexes result in rapid opsonization, clearance from the circulation and the risk of occlusion of lung capillaries. In many situations, intravenous injection of those complexes led to damage of body tissues

and a high rate of mortality in laboratory animals[113-115]. On the other hand, when these complexes are prepared at stoichiometric (+/-) molar ratios, they tend to aggregate. In addition, these neutralized complexes usually have poor cellular uptake and limited stability.

2.3.3 PEGylated lipoplexes and PICM

The limited stability and rapid elimination of lipoplexes and polyplexes can be partially solved by the use of hydrophilic polymers, such as PEG, to from a shell surrounding the neutralized particles. The PEGylated polyplexes are often referred to as polyion complex micelles (PICM), which form through the complexation of oppositely-charged polyions, followed by the self-association of the neutralized condensates into micelles (Chapter 2, Figure 1). This self-assembly requires at least one of the polymers to have a hydrophilic uncharged segment. The PEGylation of lipoplexes and polyplexes reduces the toxicity and increases their circulation time in the body, allowing passive targeting of tumors *via* the EPR effect. Loading of nucleic acids into these carriers also helps protecting them from enzymatic degradation. For example, when PEG-*b*-poly(L-lysine)/pDNA PICM were intravenously injected to mice, an intact pDNA was observed in the blood circulation even at 3-h post injection whereas the naked pDNA was degraded within 5 min[116]. On the other hand, stable nucleic-acid-lipid particles (SNALP) have been successfully exploited for the delivery of siRNA[117,118]. These SNALP consist of PEGylated lipoplexes that contain a mixture of cationic and fusogenic lipids. Many of these systems have been employed for the delivery of pDNA, AON and siRNA and could enhance their stability [32, 34, 119-121]. Some of them were successfully adopted for the *in vivo* delivery

of nucleic acids to their target sites and were able to partially knockdown the targeted proteins. Despite promising data obtained, there are still hurdles to be overcome before such systems can be considered for a clinical application. Among them, it is imperative to develop a system sufficiently stable to withstand long-term storage and sufficient circulation in the bloodstream while at the same time rapidly releasing the polynucleotide in the appropriate cellular compartment after uptake.

2.3.4 Targeted complexes

The PEGylation of complexes sterically hinders the cellular uptake of the lipoplexes and polyplexes. One way of circumventing this problem consists in attaching targeting ligands at their surface which will bind to specific cellular receptors and promote uptake of the micelles by receptor-mediated endocytosis (Chapter 2, Figure 2). For efficient targeting, the receptors must be over-expressed by target cells (*e.g.* tumor cells) compared to normal tissues[122]. The ligands can be attached either before or after assembly of the carrier. A variety of molecules including monoclonal antibodies[123,124], peptides[125,126], aptamers[23,127] and sugar moieties[128] have been employed to achieve cell targeting. Usually, the ligand should be available on the surface of the carrier for efficient binding to the receptors. In one study, PEGylated PEI/pDNA/transferrin was shown to have a long circulation *in vivo*[113]. However, the transferrin was not attached at the PEG surface but rather conjugated with the PEI in the core. Therefore, selective uptake of these formulations by specific target cells was not demonstrated. In contrast, Oishi *et al.*[46] attached lactose on the surface of PEGylated polyplexes. These formulations allowed the specific uptake of their cargo (pDNA) by hepatocytes through the asialoglycoprotein

receptor-mediated endocytosis. Selecting monoclonal antibodies as targeting moieties has the advantage of selectivity, high affinity, and minimal competition for the receptor, contrary to what is observed with endogenous molecules such as folic acid or transferrin[129-131]. Whole or fragmented antibodies (*e.g.* fragment antigen binding (Fab')) have been used to functionalize micelles. In general, targeted micelles showed higher cellular uptake than non-targeted micelles[124,132]. The whole antibody, however, presents a large size, potentially putting strain on micelle self-assembly. Moreover, it can favor the systemic clearance of the carrier *via* Fc region recognition by the MPS.

2.3.5 pH-sensitive PICM

Despite the afore-mentioned endeavors to prepare targeted, long-circulating and stable nanocarriers, improvement of intracellular delivery remains an important issue to be addressed. Targeted micellar carriers are taken up by cells *via* endocytosis. During this process, the delivery system is first internalized into endosomes and then processed to lysosomes, where degradation occurs. Different groups have investigated the use of pH-sensitive PICM to destabilize endosomes/lysosomes and enhance the intracellular bioavailability of nucleic acids. A detailed discussion of the subject is provided in Chapter 2 (Section 8).

Now, it can be seen how controlled drug delivery systems can offer benefits by improving the biodistribution of anticancer drugs and nucleic acids in terms of protection from hydrolytic or enzymatic degradation, prolonged circulation in the bloodstream and tumor-specific accumulation.

The strategies exploited in this thesis rely on the rational development of delivery vectors based on PM and PICM, which are aimed at increasing the solubility and chemical stability of docetaxel and enhancing the intracellular bioavailability of nucleic acids. Chapter 2 provides a detailed overview of the critical features of both PM and PICM as delivery systems for different anticancer and nucleotide-based drugs.

3. References

1. Chambers, A. F., Groom, A. C., MacDonald, I. C. *Nat Rev Cancer* **2**, 563-572 (2002).
2. Dumitrescu, R. G., Shields, P. G. *Alcohol* **35**, 213-225 (2005).
3. Hussain, S. P., Hofseth, L. J., Harris, C. C. *Nat Rev Cancer* **3**, 276-285 (2003).
4. Hecht, S. S. *Nat Rev Cancer* **3**, 733-744 (2003).
5. Schulman, J. M., Fisher, D. E. *Curr Opin Oncol* **21**, 144-149 (2009).
6. Block, T. M., Mehta, A. S., Fimmel, C. J., Jordan, R. *Oncogene* **22**, 5093-5107 (2003).
7. Hanahan, D., Weinberg, R. A. *Cell* **100**, 57-70 (2000).
8. Bergers, G., Benjamin, L. E. *Nat Rev Cancer* **3**, 401-410 (2003).
9. Meek, D. W. *Nat Rev Cancer* **9**, 714-723 (2009).
10. Darnell, J. E., Jr. *Nat Rev Cancer* **2**, 740-749 (2002).
11. Zink, D., Fischer, A. H., Nickerson, J. A. *Nat Rev Cancer* **4**, 677-687 (2004).
12. Aapro, M., Monfardini, S., Jirillo, A., Basso, U. *Cancer Treat Rev* **35**, 503-508 (2009).
13. Miller, R. C., Iott, M. J., Corsini, M. M. *Int J Radiat Oncol Biol Phys* **75**, 364-368 (2009).
14. Finger, P. T. *Surv Ophthalmol* **54**, 545-568 (2009).
15. Carter, P. *Nat Rev Cancer* **1**, 118-129 (2001).
16. Peggs, K. S., Quezada, S. A., Allison, J. P. *Clin Exp Immunol* **157**, 9-19 (2009).

17. Brauch, H., Jordan, V. C. *Eur J Cancer* **45**, 2274-2283 (2009).

18. Miller, W. R. *Minerva Endocrinol* **31**, 27-46 (2006).

19. Kerbel, R., Folkman, J. *Nat Rev Cancer* **2**, 727-739 (2002).

20. Fischer, C., Mazzone, M., Jonckx, B., Carmeliet, P. *Nat Rev Cancer* **8**, 942-956 (2008).

21. Lu, P. Y., Xie, F. Y., Woodle, M. C. *Trends Mol Med* **11**, 104-113 (2005).

22. ten Tije, A. J., Verweij, J., Loos, W. J., Sparreboom, A. *Clin Pharmacokinet* **42**, 665-685 (2003).

23. Farokhzad, O. C., Cheng, J., Teply, B. A., Sherifi, I., Jon, S., Kantoff, P. W., Richie, J. P., Langer, R. *Proc Natl Acad Sci U S A* **103**, 6315-6320 (2006).

24. Bae, Y., Diezi, T. A., Zhao, A., Kwon, G. S. *J Control Release* **122**, 324-330 (2007).

25. Bromberg, L. *J Control Release* **128**, 99-112 (2008).

26. Kratz, F., Muller, I. A., Ryppa, C., Warnecke, A. *ChemMedChem* **3**, 20-53 (2008).

27. Kirwan, J. M., Symonds, P., Green, J. A., Tierney, J., Collingwood, M., Williams, C. J. *Radiother Oncol* **68**, 217-226 (2003).

28. Kirkwood, J. M., Moschos, S., Wang, W. *Clin Cancer Res* **12**, 2331s-2336s (2006).

29. Pastan, I., Hassan, R., Fitzgerald, D. J., Kreitman, R. J. *Nat Rev Cancer* **6**, 559-565 (2006).

30. Nedospasov, S. A., Kuprash, D. V. *Mol Biol (Mosk)* **41**, 355-368 (2007).

31. Kim, S. H., Jeong, J. H., Lee, S. H., Kim, S. W., Park, T. G. *J Control Release* **116**, 123-129 (2006).

32. Lee, S. H., Kim, S. H., Park, T. G. *Biochem Biophys Res Commun* **357**, 511-516 (2007).

33. Schiffelers, R. M., Ansari, A., Xu, J., Zhou, Q., Tang, Q., Storm, G., Molema, G., Lu, P. Y., Scaria, P. V., Woodle, M. C. *Nucleic Acids Res* **32**, e149 (2004).

34. Kim, S. H., Jeong, J. H., Lee, S. H., Kim, S. W., Park, T. G. *J Control Release* **129**, 107-116 (2008).

35. Wong, H. L., Bendayan, R., Rauth, A. M., Li, Y., Wu, X. Y. *Adv Drug Deliv Rev* **59**, 491-504 (2007).

36. Harries, M., O'Donnell, A., Scurr, M., Reade, S., Cole, C., Judson, I., Greystoke, A., Twelves, C., Kaye, S. *Br J Cancer* **91**, 1651-1655 (2004).

37. Desai, N., Trieu, V., Yao, Z., Louie, L., Ci, S., Yang, A., Tao, C., De, T., Beals, B., Dykes, D., Noker, P., Yao, R., Labao, E., Hawkins, M., Soon-Shiong, P. *Clin Cancer Res* **12**, 1317-1324 (2006).

38. Marshall, J., Chen, H., Yang, D., Figueira, M., Bouker, K. B., Ling, Y., Lippman, M., Frankel, S. R., Hayes, D. F. *Ann Oncol* **15**, 1274-1283 (2004).

39. Chanan-Khan, A. *Blood Rev* **19**, 213-221 (2005).

40. Sutton, D., Nasongkla, N., Blanco, E., Gao, J. *Pharm Res* **24**, 1029-1046 (2007).

41. Torchilin, V. P. *Pharm Res* **24**, 1-16 (2007).

42. Nishiyama, N., Kataoka, K. *Pharmacol Ther* **112**, 630-648 (2006).

43. Torchilin, V. P. *Annu Rev Biomed Eng* **8,** 343-375 (2006).

44. Lukyanov, A. N., Elbayoumi, T. A., Chakilam, A. R., Torchilin, V. P. *J Control Release* **100**, 135-144 (2004).

45. Sakaguchi, N., Kojima, C., Harada, A., Koiwai, K., Shimizu, K., Emi, N., Kono, K. *Int J Pharm* **325**, 186-190 (2006).

46. Oishi, M., Kataoka, K., Nagasaki, Y. *Bioconjug Chem* **17**, 677-688 (2006).

47. Dufresne, M. H., Gauthier, M. A., Leroux, J. C. *Bioconjug Chem* **16**, 1027-1033 (2005).

48. Jones, M., Leroux, J. C. *Eur J Pharm Biopharm* **48**, 101-111 (1999).

49. Nogales, E., Wolf, S. G., Khan, I. A., Luduena, R. F., Downing, K. H. *Nature* **375**, 424-427 (1995).

50. Elsabahy, M., Perron, M. E., Bertrand, N., Yu, G. E., Leroux, J. C. *Biomacromolecules* **8**, 2250-2257 (2007).

51. Yang, T., Cui, F. D., Choi, M. K., Cho, J. W., Chung, S. J., Shim, C. K., Kim, D. D. *Int J Pharm* **338**, 317-326 (2007).

52. McLeod, H. L., Kearns, C. M., Kuhn, J. G., Bruno, R. *Cancer Chemother Pharmacol* **42**, 155-159 (1998).

53. Wiernik, P. H., Schwartz, E. L., Strauman, J. J., Dutcher, J. P., Lipton, R. B., Paietta, E. *Cancer Res* **47**, 2486-2493 (1987).

54. Li, C., Wallace, S. *Adv Drug Deliv Rev* **60**, 886-898 (2008).

55. Constantinides, P. P., Han, J., Davis, S. S. *Pharm Res* **23**, 243-255 (2006).

56. Hawkins, M. J., Soon-Shiong, P., Desai, N. *Adv Drug Deliv Rev* **60**, 876-885 (2008).

57. Ringsdorf, H. *J. Polym. Sci. Symp.* **51**, 135-153 (1975).

58. Posey, J. A., Saif, M. W., Carlisle, R., Goetz, A., Rizzo, J., Stevenson, S., Rudoltz, M. S., Kwiatek, J., Simmons, P., Rowinsky, E. K., Takimoto, C. H., Tolcher, A. W. *Clin Cancer Res* **11**, 7866-7871 (2005).

59. Auzenne, E., Donato, N. J., Li, C., Leroux, E., Price, R. E., Farquhar, D., Klostergaard, J. *Clin Cancer Res* **8**, 573-581 (2002).

60. Rossi, J., Leroux, J. C. in: K. Wasan (Ed.), Role of lipids in modifying oral and parenteral drug delivery, John Wiley & Sons Inc., Hoboken, **2007**, pp. 88-123.

61. Constantinides, P. P., Lambert, K. J., Tustian, A. K., Schneider, B., Lalji, S., Ma, W., Wentzel, B., Kessler, D., Worah, D., Quay, S. C. *Pharm Res* **17**, 175-182 (2000).

62. Bulitta, J. B., Zhao, P., Arnold, R. D., Kessler, D. R., Daifuku, R., Pratt, J., Luciano, G., Hanauske, A. R., Gelderblom, H., Awada, A., Jusko, W. J. *Cancer Chemother Pharmacol* **63**, 1035-1048 (2009).

63. Simard, P., Allen, C., Meyer, O. Leroux, J. C. in: Domb, J., Tabata, Y. Kumar, M. and Farber, S. (Eds.), Nanoparticles for Pharmaceutical Applications, American Scientific Publishers, Valencia, **2007**, pp. 1-62.

64. Immordino, M. L., Brusa, P., Arpicco, S., Stella, B., Dosio, F., Cattel, L. *J Control Release* **91**, 417-429 (2003).

65. Le Garrec, D., Gori, S., Luo, L., Lessard, D., Smith, D. C., Yessine, M. A., Ranger, M., Leroux, J. C. *J Control Release* **99**, 83-101 (2004).

66. Lee, K. S., Chung, H. C., Im, S. A., Park, Y. H., Kim, C. S., Kim, S. B., Rha, S. Y., Lee, M. Y., Ro, J. *Breast Cancer Res Treat* **108**, 241-250 (2008).

67. Kim, D. W., Kim, S. Y., Kim, H. K., Kim, S. W., Shin, S. W., Kim, J. S., Park, K., Lee, M. Y., Heo, D. S. *Ann Oncol* **18**, 2009-2014 (2007).

68. Gaucher, G., Asahina, K., Wang, J., Leroux, J. C. *Biomacromolecules* **10**, 408-416 (2009).

69. Gaucher, G., Poreba, M., Ravenelle, F., Leroux, J. C. *J Pharm Sci* **96**, 1763-1775 (2007).

70. Esmaeili, F., Ghahremani, M. H., Esmaeili, B., Khoshayand, M. R., Atyabi, F., Dinarvand, R. *Int J Pharm* **349**, 249-255 (2008).

71. Owens, D. E., Peppas, N. A. *Int J Pharm* **307**, 93-102 (2006).

72. Roy, V., LaPlant, B. R., Gross, G. G., Bane, C. L., Palmieri, F. M. *Ann Oncol* **20**, 449-453 (2009).

73. Dean, N. M., Bennett, C. F. *Oncogene* **22**, 9087-9096 (2003).

74. Hu-Lieskovan, S., Heidel, J. D., Bartlett, D. W., Davis, M. E., Triche, T. J. *Cancer Res* **65**, 8984-8992 (2005).

75. Horton, H. M., Anderson, D., Hernandez, P., Barnhart, K. M., Norman, J. A., Parker, S. E. *Proc Natl Acad Sci U S A* **96**, 1553-1558 (1999).

76. Meyer, M., Wagner, E. *Hum Gene Ther* **17**, 1062-1076 (2006).

77. Anderson, E. M., Miller, P., Ilsley, D., Marshall, W., Khvorova, A., Stein, C. A., Benimetskaya, L. *Cancer Gene Ther* **13**, 406-414 (2006).

78. Watts, J. K., Deleavey, G. F., Damha, M. J. *Drug Discov Today* **13,** 842-855 (2008).

79. Chan, J. H., Lim, S., Wong, W. S. *Clin Exp Pharmacol Physiol* **33**, 533-540 (2006).

80. Davis, M. E. *Mol Pharm* **6**, 659-668 (2009).

81. De Oliveira, M. C., Boutet, V., Fattal, E., Boquet, D., Grognet, J. M., Couvreur, P., Deverre, J. R. *Life Sci* **67**, 1625-1637 (2000).

82. Kurreck, J. *Eur J Biochem* **270**, 1628-1644 (2003).

83. Li, S. D., Huang, L. *Gene Ther* **13**, 1313-1319 (2006).

84. Dias, N., Stein, C. A. *Mol Cancer Ther* **1**, 347-355 (2002).

85. Hogrefe, R. I. *Antisense Nucleic Acid Drug Dev* **9**, 351-357 (1999).

86. Agrawal, S., Temsamani, J., Tang, J. Y. *Proc Natl Acad Sci U S A* **88**, 7595-7599 (1991).

87. Kausch, I., Bohle, A. *J Urol* **168**, 239-247 (2002).

88. Brown, D. A., Kang, S. H., Gryaznov, S. M., DeDionisio, L., Heidenreich, O., Sullivan, S., Xu, X., Nerenberg, M. I. *J Biol Chem* **269**, 26801-26805 (1994).

89. Chiu, Y. L., Rana, T. M. *RNA* **9**, 1034-1048 (2003).

90. Czauderna, F., Fechtner, M., Dames, S., Aygun, H., Klippel, A., Pronk, G. J., Giese, K., Kaufmann, J. *Nucleic Acids Res* **31**, 2705-2716 (2003).

91. Sazani, P., Kole, R. *J Clin Invest* **112**, 481-486 (2003).

92. Kalota, A., Karabon, L., Swider, C. R., Viazovkina, E., Elzagheid, M., Damha, M. J., Gewirtz, A. M. *Nucleic Acids Res* **34**, 451-461 (2006).

93. Dowler, T., Bergeron, D., Tedeschi, A. L., Paquet, L., Ferrari, N., Damha, M. J. *Nucleic Acids Res* **34**, 1669-1675 (2006).

94. Wilds, C. J., Damha, M. J. *Nucleic Acids Res* **28**, 3625-3635 (2000).

95. Manoharan, M. *Antisense Nucleic Acid Drug Dev* **12**, 103-128 (2002).

96. Krieg, A. M., Tonkinson, J., Matson, S., Zhao, Q., Saxon, M., Zhang, L. M., Bhanja, U., Yakubov, L., Stein, C. A. *Proc Natl Acad Sci U S A* **90**, 1048-1052 (1993).

97. Wolfrum, C., Shi, S., Jayaprakash, K. N., Jayaraman, M., Wang, G., Pandey, R. K., Rajeev, K. G., Nakayama, T., Charrise, K., Ndungo, E. M., Zimmermann, T., Koteliansky, V., Manoharan, M., Stoffel, M. *Nat Biotechnol* **25,** 1149-1157 (2007).

98. Crooke, S. T., Graham, M. J., Zuckerman, J. E., Brooks, D., Conklin, B. S., Cummins, L. L., Greig, M. J., Guinosso, C. J., Kornbrust, D., Manoharan, M., Sasmor, H. M., Schleich, T., Tivel, K. L., Griffey, R. H. *J Pharmacol Exp Ther* **277**, 923-937 (1996).

99. Waehler, R., Russell, S. J., Curiel, D. T. *Nat Rev Genet* **8**, 573-587 (2007).

100. Verma, I. M., Somia, N. *Nature* **389**, 239-242 (1997).

101. Lehrman, S. *Nature* **401**, 517-518 (1999).

102. Young, L. S., Searle, P. F., Onion, D., Mautner, V. *J Pathol* **208**, 299-318 (2006).

103. Roques, C., Fattal, E., Fromes, Y. *J Gene Med* **11**, 240-249 (2009).

104. Lu, Q. L., Rabinowitz, A., Chen, Y. C., Yokota, T., Yin, H., Alter, J., Jadoon, A., Bou-Gharios, G., Partridge, T. *Proc Natl Acad Sci U S A* **102**, 198-203 (2005).

105. Fattal, E., Bochot, A. *Int J Pharm* **364**, 237-248 (2008).

106. Lambert, G., Fattal, E., Pinto-Alphandary, H., Gulik, A., Couvreur, P. *Pharm Res* **17**, 707-714 (2000).

107. Kim, Y., Tewari, M., Pajerowski, J. D., Cai, S., Sen, S., Williams, J., Sirsi, S., Lutz, G., Discher, D. E. *J Control Release* **134**, 132-140 (2009).

108. Akinc, A., Thomas, M., Klibanov, A. M., Langer, R. *J Gene Med* **7**, 657-663 (2005).

109. Sundaram, S., Lee, L. K., Roth, C. M. *Nucleic Acids Res* **35,** 4396-4408 (2007).

110. Yoo, H., Juliano, R. L. *Nucleic Acids Res* **28**, 4225-4231 (2000).

111. Eichman, J. D., Bielinska, A. U., Kukowska-Latallo, J. F., Baker, J. R., Jr. *Pharm Sci Technolo Today* **3**, 232-245 (2000).

112. Sakaguchi, N., Kojima, C., Harada, A., Koiwai, K., Shimizu, K., Emi, N., Kono, K. *Biomaterials* **29**, 1262-1272 (2008).

113. Ogris, M., Brunner, S., Schuller, S., Kircheis, R., Wagner, E. *Gene Ther* **6**, 595-605 (1999).

114. Mahato, R. I., Kawabata, K., Takakura, Y., Hashida, M. *J Drug Target* **3**, 149-157 (1995).

115. Ward, C. M., Read, M. L., Seymour, L. W. *Blood* **97**, 2221-2229 (2001).

116. Harada-Shiba, M., Yamauchi, K., Harada, A., Takamisawa, I., Shimokado, K., Kataoka, K. *Gene Ther* **9**, 407-414 (2002).

117. Zimmermann, T. S., Lee, A. C., Akinc, A., Bramlage, B., Bumcrot, D., Fedoruk, M. N., Harborth, J., Heyes, J. A., Jeffs, L. B., John, M., Judge, A. D., Lam, K., McClintock, K., Nechev, L. V., Palmer, L. R., Racie, T., Rohl,

I., Seiffert, S., Shanmugam, S., Sood, V., Soutschek, J., Toudjarska, I., Wheat, A. J., Yaworski, E., Zedalis, W., Koteliansky, V., Manoharan, M., Vornlocher, H. P., MacLachlan, I. *Nature* **441**, 111-114 (2006).

118. Morrissey, D. V., Lockridge, J. A., Shaw, L., Blanchard, K., Jensen, K., Breen, W., Hartsough, K., Machemer, L., Radka, S., Jadhav, V., Vaish, N., Zinnen, S., Vargeese, C., Bowman, K., Shaffer, C. S., Jeffs, L. B., Judge, A., MacLachlan, I., Polisky, B. *Nat Biotechnol* **23**, 1002-1007 (2005).

119. Jeong, J. H., Kim, S. W., Park, T. G. *J Control Release* **93**, 183-191 (2003).

120. Jeong, J. H., Kim, S. H., Kim, S. W., Park, T. G. *Bioconjug Chem* **16**, 1034-1037 (2005).

121. Jeong, J. H., Kim, S. W., Park, T. G. *Bioconjug Chem.* **14**, 473-479 (2003).

122. Ross, J. F., Chaudhuri, P. K., Ratnam, M. *Cancer* **73**, 2432-2443 (1994).

123. Ulbrich, K., Etrych, T., Chytil, P., Jelinkova, M., Rihova, B. *J. Controlled Release* **87**, 33-47 (2003).

124. Merdan, T., Callahan, J., Petersen, H., Kunath, K., Bakowsky, U., Kopeckova, P., Kissel, T., Kopecek, J. *Bioconjug Chem* **14**, 989-996 (2003).

125. Vinogradov, S., Batrakova, E., Li, S., Kabanov, A. *Bioconjug Chem.* **10**, 851-860 (1999).

126. Nah, J. W., Yu, L., Han, S. O., Ahn, C. H., Kim, S. W. *J Control Release* **78**, 273-284 (2002).

127. Farokhzad, O. C., Jon, S., Khademhosseini, A., Tran, T. N., Lavan, D. A., Langer, R. *Cancer Res* **64**, 7668-7672 (2004).

128. Lim, D. W., Yeom, Y. I., Park, T. G. *Bioconjug Chem* **11**, 688-695 (2000).

129. Singh, M. *Curr Pharm Des* **5**, 443-451 (1999).

130. King, G. L., Feener, E. P. *Adv Drug Deliv Rev* **29**, 197-213 (1998).

131. Qian, Z. M., Li, H., Sun, H., Ho, K. *Pharmacol Rev* **54**, 561-587 (2002).

132. Torchilin, V. P., Lukyanov, A. N., Gao, Z., Papahadjopoulos-Sternberg, B. *Proc Natl Acad Sci U S A* **100**, 6039-6044 (2003).

CHAPTER 2 - Polymeric micelles as versatile carriers for drugs and nucleic acids delivery[1]

Mahmoud Elsabahy[1], Marie-Hélène Dufresne[1] and Jean-Christophe Leroux[1*]

[*]Canada Research Chair in Drug Delivery, [1]Faculty of Pharmacy, University of Montreal, C.P. 6128, Succursale Centre-Ville, Montreal (QC) H3C 3J7, Canada

[1]Materials for Nanomedicine, Pan Stanford Publishing, Hackensack, in press (2009).

Abstract

Polymeric micelles (PM) are a promising nanomedicine platform for drug and nucleic acid delivery. In aqueous solution, PM are formed *via* the self-assembly of amphiphilic copolymers into nanoscopic core/shell architectures presenting a hydrophobic core surrounded by a hydrophilic corona. Polyion complex micelles (PICM) are a subclass of PM and are obtained from electrostatic interactions between oppositely-charged copolymer and drug followed by self-assembly of the charge-neutralized blocks. Both PM and PICM typically have fairly narrow size distributions, with diameters ranging from 10 to 100 nm, and demonstrate a series of attractive properties that warrant them interest as drug delivery carriers. The core of both PM and PICM can serve as a reservoir for drugs, which may be loaded by chemical, physical, or electrostatic means depending on the chemistry of the drug and of the core-forming block. Solubilization, protection and delivery of either hydrophobic or charged macromolecules (*i.e.* antisense-oligonucleotides and short interfering RNA) can then be achieved with the nanocarriers. Furthermore, the composition of the micelles can be tailored to reduce the drug toxicity and enhance the specificity of the drug-loaded micelles. Finally, the properties of the micelles can be adjusted to comply with both intravenous and oral drug delivery requirements. This chapter provides an overview of the critical features of both PM and PICM as delivery systems and discusses the recent advances in their preparation, characterization and pharmaceutical evaluation.

1. Introduction

Polymeric micelles (PM) are formed *via* the self-assembly of amphiphilic copolymer chains in aqueous milieu. They present a core/shell architecture wherein the hydrophobic core serves as a microenvironment for the incorporation of drugs while the hydrophilic corona acts as a stabilizing interface between the core and the external medium. In water, hydrophobic interactions are generally the main driving force behind the micellization process (Figure 1, A and B). However, the self-association of polymeric chains can involve additional forces. For example, electrostatic interactions were shown to induce the complexation and neutralization of oppositely-charged polymers, thereby allowing the formation of polyion complex micelles (PICM) (Figure 1, C-E). In addition, substitution of ligands on a metal drug by charged groups of the copolymer through coordination bonds can trigger micelle formation (Figure 1F). The latter are termed polymer-metal complex micelles. Most of these self-assemblies have fairly narrow size distributions with diameters ranging from 10 to 100 nm.

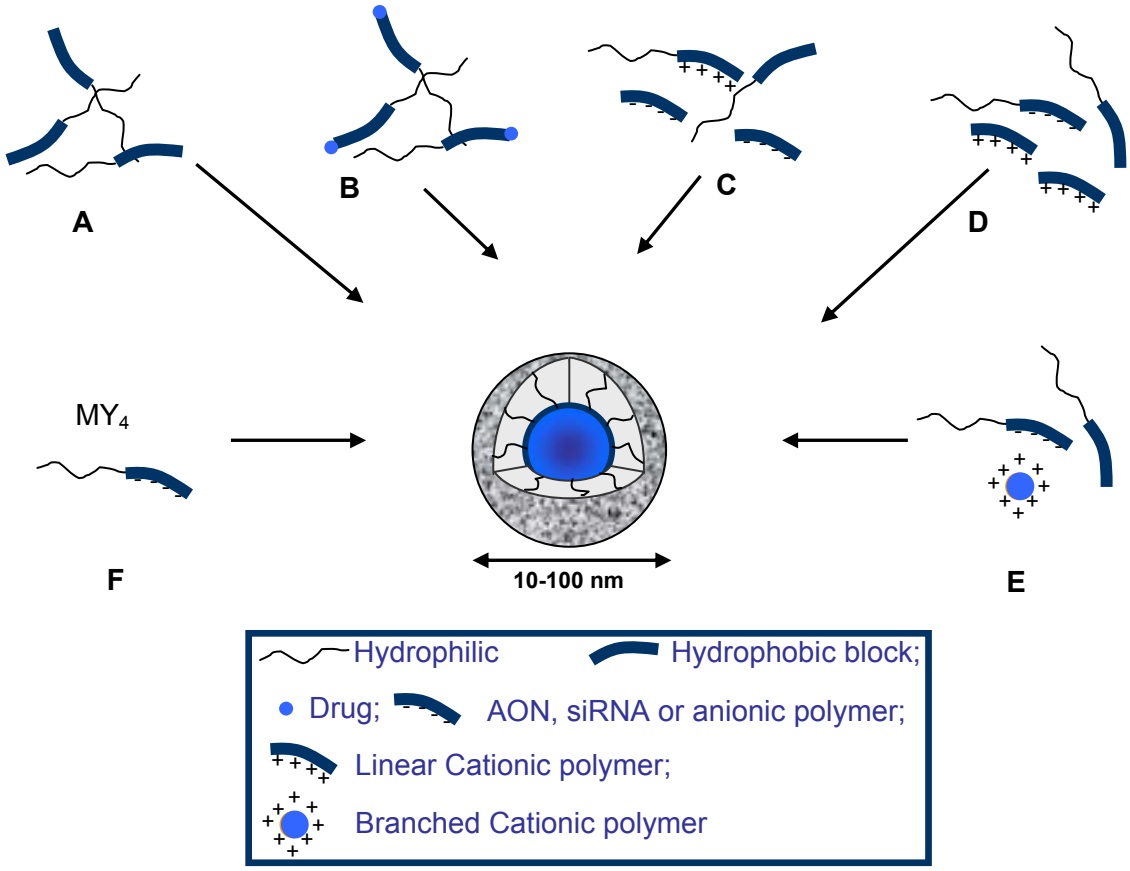

Figure 1. Conventional PM (A); drug-conjugated PM (B); and PICM with the polyionic block consisting of cationic polymer (C) or polynucleic acid (antisense oligonucleotide (AON) or short interfering RNA (siRNA)) (D and E). In D and E, the core forming agent is either linear or branched cationic polymer, respectively. Polymer-metal complex micelles formed *via* the ligand substitution reaction where M and Y are the metal and the ligand, respectively (F).

Many important therapeutic compounds present a low aqueous solubility and poor accumulation at their target site which lower their efficacy and can promote systemic adverse effects. Alternatively, macromolecular drugs such as peptides, DNA and RNA suffer from premature degradation upon administration, low bioavailability and inefficient cellular entry, compromising their therapeutic outcome. The versatile attributes of PM and PICM make these systems an attractive nanomedicine platform for the delivery of various therapeutic agents *via* both

parenteral (*i.e.* intravenous) and oral routes. Indeed, micelles provide a reservoir for either solubilizing water-insoluble drugs or accommodating charged compounds. Sequestration of the drug inside the micellar core may protect it from premature degradation by the surrounding environment. When intravenous applications are sought, the nonionic hydrophilic corona can prevent the adsorption of opsonins, thereby limiting the rapid uptake by the mononuclear phagocyte system (MPS) and prolonging the circulation half-life of the encapsulated drug [1]. Amphiphilic copolymers can be also designed to express low toxicity, biocompatibility and/or biodegradability making them attractive alternatives to low molecular weight surfactants, such as Cremophor® EL, which have been associated with serious side-effects [2]. Finally, PM can be used to target the drug either passively or actively [3]. In passive targeting, the drug-loaded micelles can permeate in pathological sites with leaky vasculature (such as tumors) and accumulate due to impaired lymphatic drainage at these areas (this phenomenon is best known as the enhanced permeation and retention (EPR) effect; Figure 2A) [1]. On the other hand, active targeting is achieved through the attachment of targeting ligands to the micelle surface so as to favor its recognition by a specific cell receptor (Figure 2B) [4]. Alternatively, stimuli-responsive polymers can be used to induce a response to external stimuli such as pH or temperature variations [5-9].

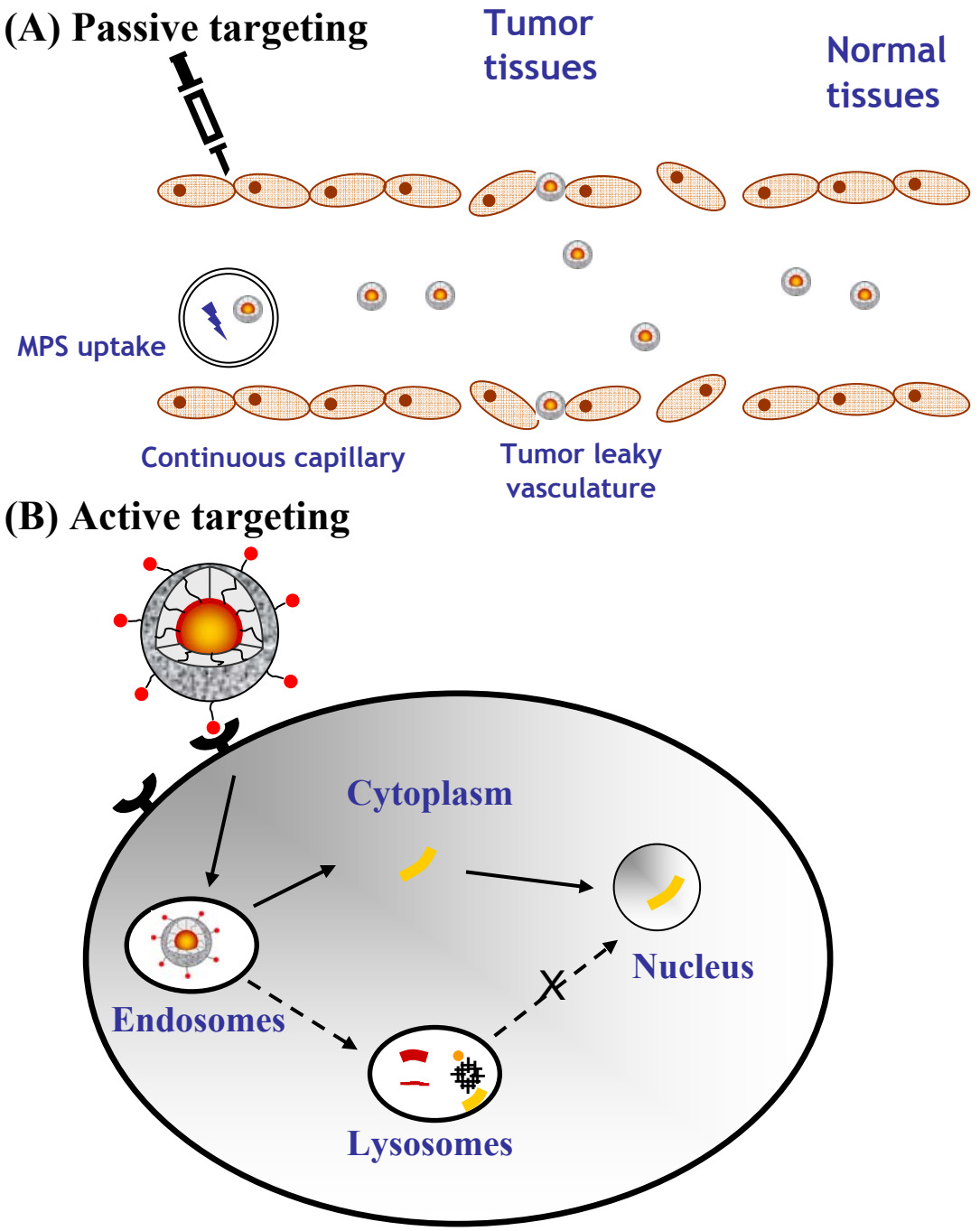

Figure 2. Passive (A) and active (B) targeting. In passive targeting, the non-functionalized micelles extravasate in tissues presenting leaky vasculatures (*e.g.* tumors) and accumulate through the EPR effect. In active targeting, the micelles bind to specific receptors expressed on the surface of the target cells, after which they are internalized. The entrapped drug should be able to escape from the endosomes in order to reach to the cytoplasm and/or nucleus (the solid lines).

As will be highlighted later in this chapter, all these attributes allow the use of micelles as nanocarriers to deliver various drugs including anti-tumor agents and small nucleic acid-based drugs (antisense oligonucleotides (AON) and short interfering RNA (siRNA)). While similar systems have been used to deliver plasmid DNA (pDNA) [10-12], this chapter will focus mainly on the delivery of small nucleic acid fragments for which the molecular weight (*MW*) of both the drug and cationic polymer are of the same size range. This chapter provides a comprehensive analysis of the critical features of PM as drug carriers, including control over size, morphology, stability, drug-loading and release of the incorporated drugs. Furthermore, advanced features, such as site-specific delivery to reduce the toxicity and enhance the specificity of the drug-loaded micelles, are presented.

2. Micellization

The micellization process can simplistically be described as a fine tuned equilibrium between attractive and repulsive forces. In an aqueous milieu, the attractive forces are associated to the core-forming block of the copolymers and can be either purely hydrophobic or involve other mechanisms such as electrostatic interactions or polymer-metal coordination interactions. Regardless of the nature of the attraction, the segregation or coalescence of polymeric chains is entropically driven, with the loss in entropy originating from the ordering of the polymer chains being counter-balanced by the solvent contribution to the entropy. Indeed, it is argued that solvent molecules organize themselves to form a clathrate cage around the hydrophobic segment of the free copolymer chains, prior to micellization, and that

this organized structure decreases the entropy of water [13]. To offset this high free energy, the hydrophobic segments tend to withdraw from the aqueous phase and herd into small clusters or micelles. Segregation of the non-polar moieties decreases their contacts with water molecules, thereby increasing the entropy of the solvent. The formation of PICM, on the other hand, can be best described as the sequential complexation of the polyions followed by the self-association of the neutralized condensates into micelles. The driving force for the cooperative electrostatic interactions between polyions in aqueous solution comes from the entropy gain associated with the release of low molecular weight counter ions [14]. Condensation of the polyions yields neutral and water-insoluble moieties that self-assemble in the same fashion as copolymers featuring a hydrophobic block. Polymer–metal complex micelles is yet another class of PM that has been used for the delivery of platinous anticancer drugs such as cisplatin [cis-dichlorodiamineplatinum (II)] and 1,2-diaminocyclohexane platinum (II) [12]. In this case, micellization occurs *via* substitution of the metal ligand (*i.e.* chloride of platinum (II)) by the carboxylate groups of the copolymer, with the polymer establishing multiple coordination bonds with the drug (Figure 1F).

The repulsive forces controlling the micellization process, on the other hand, are mostly brought about by the shell-forming blocks of the copolymers. The hydrophilic segments generally present large degrees of hydration and large exclusion volumes. They contribute to micelle formation by limiting the interactions between the core and external medium and stabilizing the hydrophobic/hydrophilic interface [15]. Hydrophilic segments are also known to limit or hinder micelle growth

by providing steric repulsions between the hydrated chains. These repulsive forces further hamper secondary aggregation and coagulation by overwhelming the attractive forces operating between micelles. Coronas obtained from nonionic chains are usually preferred over those obtained from charged polymers in order to diminish the non-specific adsorption of opsonins *in vivo* and limit the toxicity of the PM.

It can now be seen how factors such as the nature of the hydrophobic block (being more or less hydrophobic) or hydrophilic segment (neutral *vs.* charged) and their respective length may alter the attraction/repulsion balance and dictate the size, morphology and stability of the resulting micelles. Understanding the underlying dynamics of micellization clearly provides insight for the design of micelles with tailored properties.

3. Composition of the micellar carriers

Several polymers have been characterized for their ability to form PM and PICM and are presented in Table 1. The hydrophilic segment can consist of polysaccharides, such as chitosan [16] and pullulan [17], or synthetic polymers, such as poly(ethylene glycol) (PEG) [18], poly(*N*-vinylpyrrolidone) (PVP) [19, 20], poly(*N*-isopropylacrylamide) (PNIPAM) [21], poly(2-ethyl-2-oxazoline) [22] and poly(acrylic acid) [23]. Of all hydrophilic polymers, PEG (with a molecular weight of 1-20 kD) is undoubtedly the most widely used shell forming component of both PM and PICM. The neutrality, hydrophilicity and flexibility of PEG diminish the possibility of undesirable electrostatic interactions with plasma proteins [24].

Furthermore, the presence of reactive groups at both chain ends can be exploited for further micelle derivatization, such as attachment of ligands for active targeting.

Table 1. Selection of polymers most often used for the preparation of micelles in drug delivery

Shell-component	Ref	Core-component			
		Hydrophobic	Ref	Polyion	Ref
Chitosan	[16]	Poly(D,L-lactide)	[19]	Poly((alkyl)aminoethyl methacrylate)	[39, 64]
Pullulan	[17]	Poly(D,L-lactide-*co*-glycolide)	[109]	Poly(ethyleneimine)	[35]
Poly(2-ethyl-2-oxazoline)	[22]	Poly(ε-caprolactone)	[25, 26]	Poly(amidoamine)	[66]
Poly(acrylic acid)	[23]	Poly(alkyl methacrylate)	[30]	Poly(L-aspartic acid)	[41]
Poly(ethylene glycol)	[18]	Poly(alkyl (meth)acrylate-*co*-methacrylic acid)	[182, 183]	Poly(L-lysine)	[34]
Poly(*N*-(2-hydroxypopyl)methacrylamide)	[26]	Poly(propylene oxide)	[29]	Oligonucleotide[1]	[44]
Poly(*N*-isopropylacrylamide)	[21]	Poly(butylene oxide)	[48]	siRNA[1]	[45]
Poly(*N*-vinyl-2-pyrrolidone)	[19, 20]	Poly(styrene oxide)	[48]		
		Poly(β-benzyl-L-aspartate)	[61]		
		Poly(γ-benzyl-L-glutamate)	[27]		
		Poly(N-hexyl stearate L-aspartamide)	[28]		
		Poly(propylene sulfide)	[200]		
		Phospholipid residues	[31, 32]		
		Attached hydrophobic drugs (*e.g.* covalently linked doxorubicin)	[106]		

[1]The oligonucleotide or siRNA is attached to the non-ionic polymer *via* a covalent link.

It is seen from Table 1 that while a relatively limited selection of hydrophilic segments is available, a host of hydrophobic polymers can be used as core-forming segments. These include biodegradable polymers such as poly(D,L-lactide) (PDLLA) [19], poly(ε-caprolactone) (PCL) [25, 26], poly(γ-benzyl-L-glutamate) (PBLG) [27], and poly(*N*-hexyl stearate L-aspartamide) [28], and non-biodegradable hydrophobic polymers like poly(propylene oxide) (PPO) [29] and poly(vinyl) derivatives [30]. The hydrophobic segment can be inert or can possess reactive groups for post-functionalization. A special group of micelles can finally be obtained from lipid conjugates such as PEG-phosphatidyl ethanolamine (PEG-PE) [31-33].

The core-forming blocks of PICM include polycations such as poly(L-lysine) (PLL) [34], poly(ethylenimine) (PEI) [35-37], derivatives of amine methacrylate [38, 39] and polyanions such as poly(aspartic acid). These are typically covalently attached to the hydrophilic polymer and interact with charged macromolecules such as AON, siRNA, porphyrins, and enzymes [40, 41] to form PICM, as illustrated in Figure 1C. Alternatively, the drug can be conjugated to the hydrophilic polymer and then serve as the core segment. Examples include conjugates of PEG-*b*-AON [42-44] and PEG-*b*-siRNA [45]. In this case, interactions with either linear or branched cationic polymers such PEI, poly(amidoamine) (PAMAM) or poly(amino acids) promotes the formation of PICM (Figure 1, D and E).

Of the spectrum of polymers that can in theory form micelles, the requirements of biocompatibility and/or biodegradability have greatly limited the choice of copolymers used in clinical applications. In the case of non-biodegradable

polymers, careful attention should be taken to maintain their molecular weight below the renal excretion threshold in order to ensure their systemic elimination.

4. Micelle stability

4.1 Significance

The physical stability of a micellar drug delivery system is essential to benefit from its favorable pharmacokinetic parameters [46, 47]. Premature disassembly of the micelles after entry into the bloodstream can, for instance, compromise the circulation times and delivery of the encapsulated drug to its target site. Poor stability can also bring about early drug release (burst release) and toxicity problems. For labile drugs such as nucleic acids, stability of the micelles is further crucial to maintain the therapeutic activity of the drug by protecting it from premature degradation. Clearly, the integrity of micelles is a crucial factor governing their effectiveness and success at delivering incorporated drugs.

The stability of micelles can be described with respect to two different properties, namely thermodynamic stability and kinetic stability. Because PICM are obtained through electrostatic interactions, their stability can be further evaluated by their ability to withstand dissociation in presence of salts and other polyions (such as proteins present *in vivo*) and to protect their cargo against enzymatic degradation. These aspects will be discussed in the following sections.

4.2 Thermodynamic stability

A micelle is thermodynamically stable with respect to its micelle-to-unimer equilibrium. At low concentrations in aqueous medium, amphiphilic molecules exist as discrete chains (unimers). However, as their concentration is increased above a critical concentration, aggregation becomes energetically favorable and the amphiphilic molecules self-assemble into micelles. The concentration at which micelles start to appear is called the critical micelle concentration (CMC). Following that definition, it appears that a lower CMC value is indicative of a greater stability upon dilution. Generally speaking, the more hydrophobic or the longer the water-insoluble block, the greater the entropy gain ensuing from micellization and the lower the CMC. For instance, the CMC of PEG-*b*-poly(styrene oxide) (PEG-*b*-PSO) was shown to be 2-fold lower than that of PEG-*b*-poly(butylene oxide) (PEG-*b*-PBO), in accordance with the greater hydrophobicity conferred by the aromatic ring of the SO unit [48]. Alternatively, increasing the length of the SO or BO block further decreased the CMC values [48]. In contrast, increasing the length of the hydrophilic block results in an increase of the CMC when the length of the hydrophobic block is held constant [15]. A rapid calculation suggests that CMC values around 10 mg/L, which are typically found for amphiphilic polymers [48], should prevent the rapid dissociation of the micelles following intravenous administration to humans. This is assuming that a drug-loaded PM formulation is administered to a 70 kg human at a dose of 10 mg/kg. In this particular case, a polymer concentration of 1.3 g/L would be obtained upon injection (considering that the blood takes up a volume of 5 L), which is about 130 times higher than the CMC.

In principle, any technique detecting discontinuities in the physical properties of a solution (such as molar conductivity, surface tension or osmotic pressure) can be used to evaluate the CMC. If this holds true for low molecular weight surfactants (which usually exhibit CMCs in the g/L range), it can rarely apply to copolymer solutions as they present CMCs at concentrations generally too low for any of these changes to be detected experimentally. A preferred method to determine the CMC of polymers is to use hydrophobic fluorescent probes for which the spectral properties are sensitive to the polarity of the surroundings. Pyrene, a condensed aromatic hydrocarbon, is probably the most widely used fluorescent marker for this application. Below the CMC, pyrene is solubilized in water, a medium of high polarity. When micelles are formed, pyrene partitions preferentially within the hydrophobic domain afforded by the micellar core and experiences a less polar environment. Consequently, numerous changes such as an increase in the fluorescence intensity, a change in the vibrational fine structure of the emission spectrum, and a red shift of the (0,0) band in the excitation spectrum of pyrene can be observed. The apparent CMC is then obtained from plots of either the I_1/I_3 (the ratios of the fluorescence intensity of the first and third peaks in the pyrene emission spectra) or the $I_{335\text{-}339}/I_{333}$ (the exact wavelength depends on the polymer) ratio from the excitation spectra *versus* concentration (Figure 3). An abrupt change in the slope as the concentration increases indicates the onset of micellization. The CMC determined by fluorescence techniques needs to be carefully interpreted for two reasons. First, the concentration of pyrene should be kept extremely low (~ 10^{-7} M) so that a change in slope can be precisely detected as micellization occurs. Second, a

gradual change in the fluorescence spectrum can sometimes be attributed to the presence of hydrophobic impurities or association of the probe with individual polymeric chains or premicellar aggregates [1], thereby underestimating the CMC.

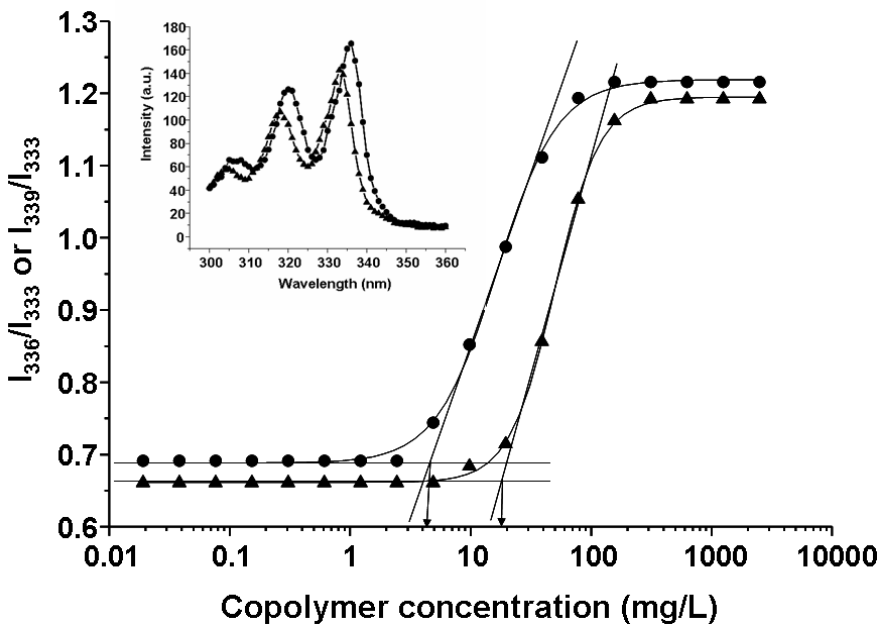

Figure 3. Plot of the intensity ratio I_{336}/I_{333} or I_{339}/I_{333} (from pyrene excitation spectra) as a function of PEG_{45}-*b*-PBO_{15} (▲) and PEG_{45}-*b*-PSO_{15K} (●) concentration. Each value is the mean of three independent measurements. Values of the CMC are indicated by arrows. *Inset*: Excitation spectra of pyrene (2×10^{-7} M aqueous solution) monitored at λ_{em} 390 nm below (▲) and above (●) the PEG_{45}-*b*-PSO_{15} copolymer's CMC.

Other techniques have also been employed to measure the CMC of PM and include light scattering, isothermal titration calorimetry (ITC) and gel permeation chromatography (GPC) [49, 50]. The light scattering technique relies on the fact that the molecular weight of the colloids undergoes a sharp increase as the unimers associate into micellar aggregates. This increase in molecular weight translates into a significant increase of the scattered light. The onset of micellization, however, can

only be detected if the CMC falls within the detection limit of the instrument. The ITC experiment, on the other hand, is carried out by injecting small aliquots of a concentrated micellar solution into water and directly measuring the enthalpy changes occurring after each addition at constant temperature. Each injection below the CMC produces an exothermic peak which is the sum of several contributions: the heat of dilution of the micelles, the enthalpy of demicellization, and the heat of dilution of individual polymer molecules [51]. When the polymer concentration in the cell of the instrument exceeds the CMC, the heat evolved levels off, signaling that the injected micelles remain associated rather than disintegrating into unimers. The CMC is obtained from the plot of the enthalpy change following each injection as a function of polymer concentration where the break point in the slope corresponds to the onset of polymer association. The advantage of using the ITC is that, in addition to the CMC determination, other thermodynamic parameters can be measured such as the enthalpy and entropy of micellization [52]. GPC under aqueous conditions can finally be employed to evaluate CMC and rests on the fact that unimers and micelles exhibit different elution volumes. The method is particularly appealing in that it can simultaneously permit the determination of the micellar *MW* and aggregation number (N_{agg}). However, for this technique to be valid, it is important that the integrity of the PM be maintained during their elution through the size exclusion column. Adsorption of the polymer on the column may also present a problem, especially at concentrations close to the CMC where micelles consist of large loose aggregates.

The same methods used to determine the CMC of amphiphilic PM can in theory serve to evaluate the CMC of PICM. For instance, reports can be found where

fluorescence (pyrene) [53] and light scattering techniques [34] are being used. The CMC values for PICM are comparable to those of PM which indicates that, despite a partly different self-association mechanism, the PICM are also susceptible to dissociation upon dilution.

4.3 Kinetic stability

Another crucial factor characterizing PM is their kinetic stability. The kinetic stability of micelles refers to the actual rate of micelle dissociation below the CMC. Thus, even below the CMC, PM may still be kinetically stable, provided that the dissociation into unimers proceeds slowly. Systems for which dissociation takes place over hours or even days have been reported, as opposed to low molecular weight surfactants that dissociate within milliseconds below their CMC [54, 55]. Several properties of the copolymer can be modified to improve the kinetic stability. These include the hydrophobic/hydrophilic balance, the physical state of the micelle core, the size of the hydrophobic block, and the incorporation of hydrophobic compounds (Figure 4) [56]. For instance, Creutz *et al.* [57] showed that the rate of disassembly could be slowed down by increasing the hydrophobic/hydrophilic balance of the core-forming block. Increases in the hydrophobicity of the copolymers led to reduced rates of unimer exchanges, which is indicative of increased stability. Alternatively, increased kinetic stability can be met by using hydrophobic segments that will yield micelles with crystalline or highly viscous cores below their glass transition temperature. In this light, monodisperse stereocomplex PMs were prepared through the self-assembly of equimolar mixtures of PEG-*b*-poly(L-lactide) (PLLA) and PEG-*b*-poly(D-lactide) (PDLA) in water [58]. When present in an equimolar

ratio, PDLA and PLLA form a crystalline triclinic unit cell in which the chains exhibit a 3_1 helical conformation and display a melting point 50°C above that reported for the enantiomeric component. The micelles presenting such stereocomplexes exhibited enhanced kinetic stability and were less prone to secondary aggregation than either PEG-*b*-PLLA or PEG-*b*-PDLA micelles. The gain in stability ensues from limited and hindered mobility of the hydrophobic chains [18]. The viscosity of the micellar core, which serves as an indicator of kinetic stability, can be evaluated using fluorescent probes, such as 1,2-(1,1'-dipyrenyl)propane, for which the intensity ratio of excimer to monomer can be related to the fluidity of the environment [48, 59] and by ^{1}H nuclear magnetic resonance [60]. Finally, Kataoka and colleagues [61, 62] reported instances where micellar stability increased following incorporation of a hydrophobic drug (doxorubicin (DOX)) in the core of PM. It was proposed that the occurrence of π-π stacking between the hydrophobic drug and the side groups of the core-forming segments as well as increased hydrophobic interactions both contributed to this gain in kinetic stability.

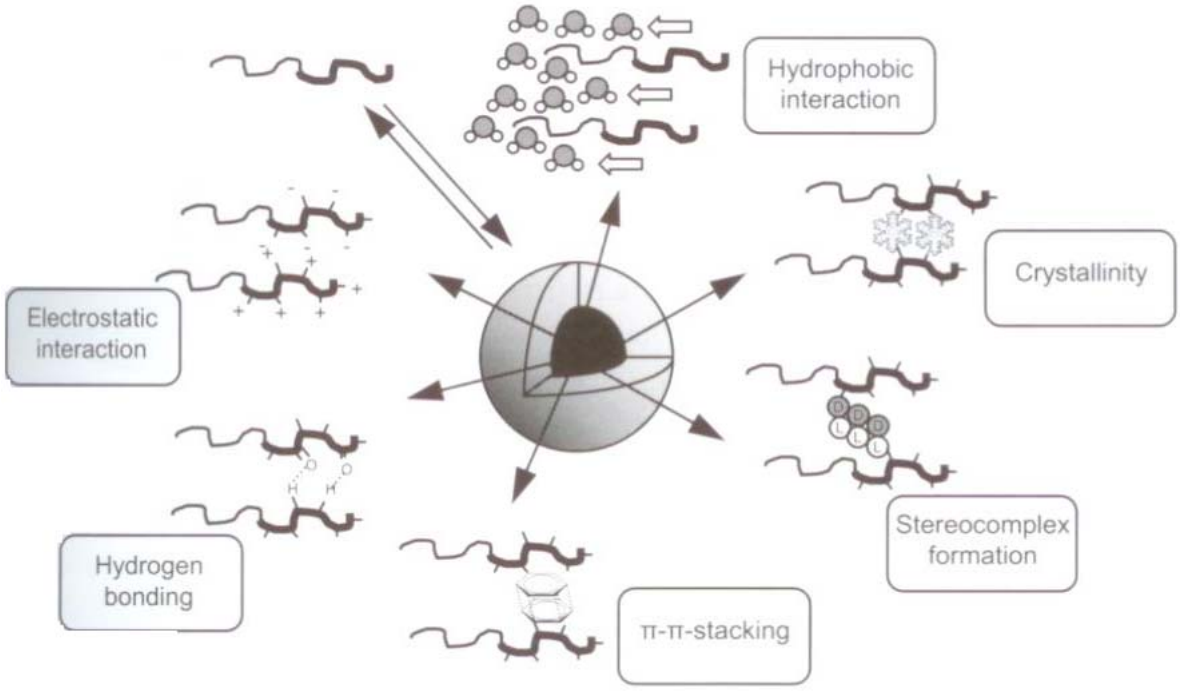

Figure 4. Interactions in the micellar core that enhance the kinetic stability of PM. Reproduced from Carstens, M. *et al.* [56] Copyright 2008, with permission from Springer Science.

4.4 Stability of PICM towards dissociation

The stability of PICM towards dissociation can be assessed by displacement assays in which the micelles are incubated with macromolecular polyions of identical charge to the loaded drug. Polyanions (such as heparin, which is typically found in the blood, or synthetic polymers such as poly(methacrylic acid)) have been used to displace negatively-charged drugs (*e.g.* nucleic acids). In such situations, both the drug and the added polyanion can interact with the cationic polymer so that a competition for the cationic sites is set. At high enough concentrations, the polyanion will eventually occupy all cationic sites, thereby expelling the complexed compounds

out of the micellar system. The release of the nucleic acids is typically monitored by gel electrophoresis or fluorescence techniques (in which case ethidium bromide is often used). Similar to amphiphilic micelles, the balance between the charged and the hydrophilic (nonionic) segments affects the stability of the micelles. Generally speaking, the longer the charged components (either the genetic material or the cationic moiety) are, the greater the cooperativity of the electrostatic interactions and the less favorable the exchange reactions [63]. In contrast, at constant ionic block length, the longer the hydrophilic nonionic segment, the less stable the micelles. This was demonstrated by Dufresne *et al.* [64] who prepared PICM of an AON and copolymers of the type PEG-*b*-poly(aminoethyl methacrylate) of increasing PEG length. Other factors can influence the electrostatic binding with the cationic polymers. These include the nitrogen-to-phosphate (N/P) ratio, hydrophobicity, pH and the ionic strength of the medium [53, 65, 66].

4.5 Protection of the drugs towards enzymatic degradation

Incorporation of peptides, nucleic acids or other macromolecules in the core of PICM prevents the action of the enzyme by limiting the access of the enzyme to the drug either through the steric hindrance afforded by the corona segments or the protection ensuing from complexation with the cationic segments [34]. Usually, a correlation between PICM stability against dissociation and the ability of the micelles to protect their cargo against enzymatic degradation can be established. It comes out that factors such as the balance between the ionic and nonionic hydrophilic segments, the N/P ratio or degree of ionization also affect protection of the drugs towards enzymatic degradation. For instance, Elsabahy *et al.* [66] have recently studied the

effect of different molecular weight PAMAM on the stability of PICM formed through the interaction with a PEGylated oligonucleotide duplex. It was found that the stability of the entrapped oligonucleotide increased with an increase in the PAMAM molecular weight. This was attributed to the enhanced cooperative interaction afforded by the greater surface amine density of the highly branched PAMAM. It is also worth mentioning that an increase in the N/P ratio of the PAMAM/oligonucleotide duplex within the PICM resulted in enhanced stability against degradation by nucleases (Figure 5).

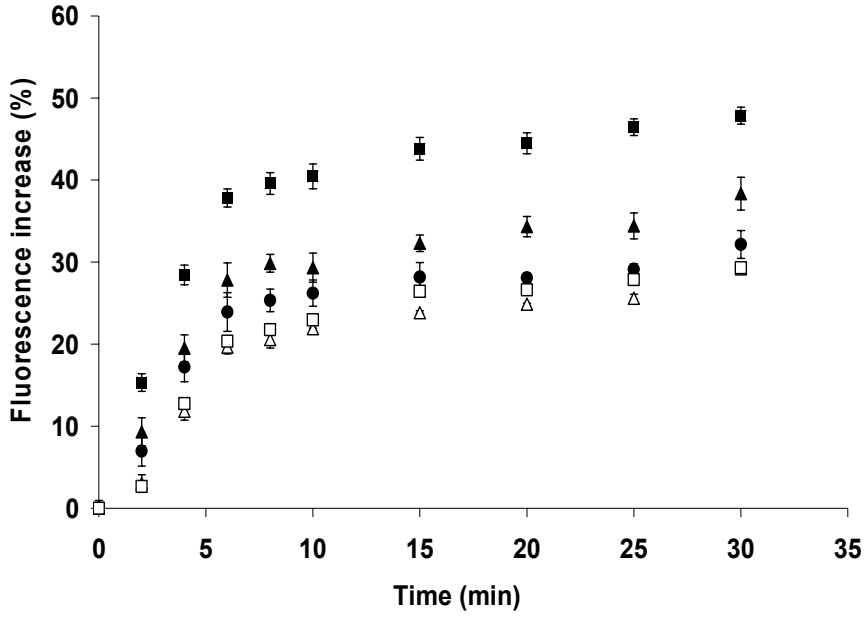

Figure 5. Dequenching of fluorescein-labeled sense oligonucleotide (SON) fluorescence following the incubation of PEG_{10K}-SON/AON-PAMAM generation 3 (*Mw* = 6,909) PICM at N/P ratios of 1:1 (■), 2:1 (▲), 3:1 (●), 4:1 (Δ) and 5:1 (□) with DNase 1 (60 U/μg oligonucleotide, 37°C, pH 7.4). Mean ± SD (n=3). The λ_{ex} and λ_{em} were measured at 490 and 520 nm, respectively. The SON release was indirectly assessed by measuring the dequenching of the SON fluorescence. The fluorescence intensity corresponding to 100% release was determined at the end of the experiment by adding an excess of heparin to destabilize the micelles followed by the addition of DNase 1 and letting the reaction run for another 24 h.

4.6 Towards greater micelle stability

Despite these efforts in adjusting the properties of the block copolymers to yield carriers presenting increasing stability, PM remain equilibrium systems that are intrinsically susceptible to dilution. Strategies which rely on the chemical bonding or cross-linking of the different micelle components have thus been explored to proscribe dissociation (Figure 6). There generally are three approaches to the preparation of core cross-linked micelles: polymerization or cross-linking (i) of entrapped low molecular weight monomers, (ii) of reactive groups present at the core chain end or (iii) of reactive groups introduced on the side chain. Kim *et al.* [67] revealed that the stability of a micelles could be improved by incorporating and polymerizing low molecular weight monomers (namely ethylene glycol dimethacrylate) in the core. Interestingly, the drug loading in core-polymerized micelles was at the same level as that of the non-crosslinked micelles. Iijima *et al.* [68] have prepared copolymers of PEG-*b*-PDLLA presenting a methacryloyl polymerizable group at the lactide chain end. They showed that the polymerization of the methacryloyl groups in the core of pre-formed micelles conferred increased stability to the system towards the presence of sodium dodecyl sulfate or following dissolution in organic solvents. Kakizawa *et al.* [69], have synthesized PEG-*b*-PLL copolymers presenting side-chain thiol groups to complex AON. Oxidation of the thiol groups of pre-formed PICM yielded complexes with cross-linked cores. This method of micelles stabilization has been applied successfully and permitted the dissociation of the complexes into cells due to the cleavage of the disulfide bonds in the intracellular reducing medium.

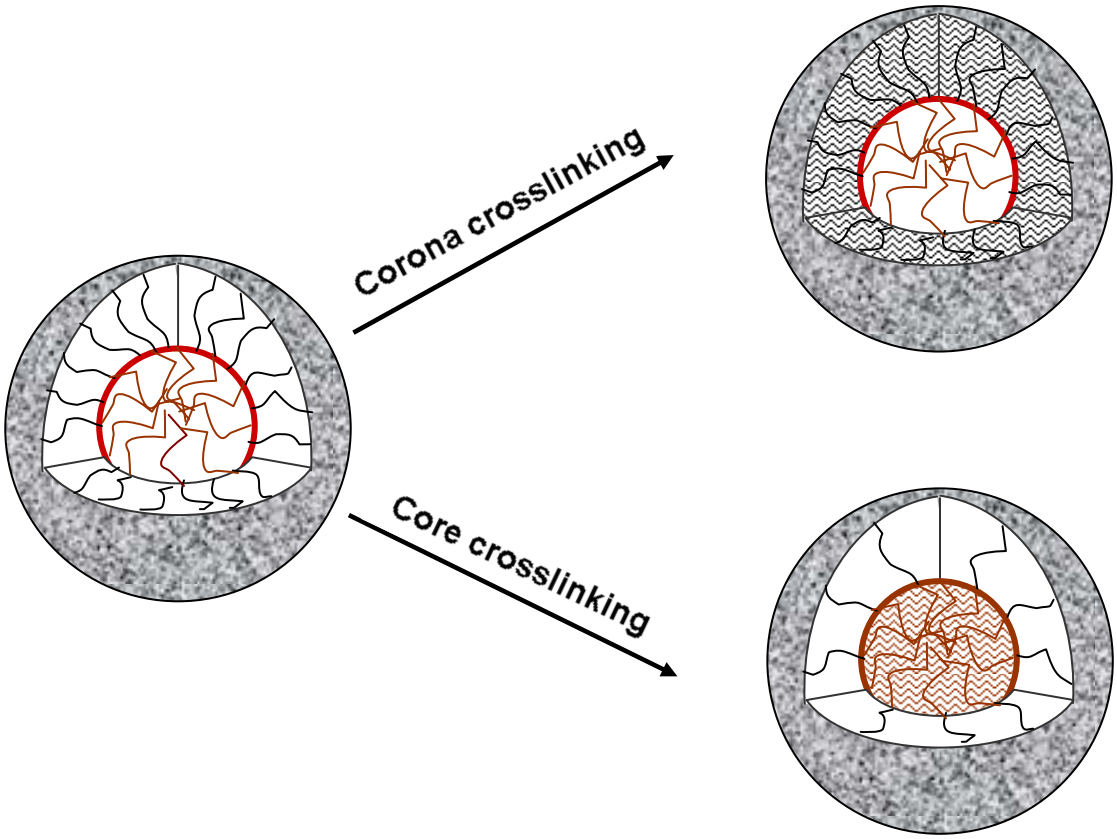

Figure 6. Crosslinking of the micellar corona or core as means to interplay with the micellar stability and drug release.

An alternative scheme to the chemical stabilization of the cores is to fix the shell blocks of the micelles. Particularly, the group of Wooley has gained expertise in preparing shell cross-linked PM [70]. A common strategy is to react carboxylic acid groups present along the shell segment with diamines to form amide bonds. However, if not optimized properly, shell cross-linking presents inherent limitations in that cross-linking restrains the mobility of the hydrophilic segments, which in turn reduces the entropy factor and impairs the stabilizing capabilities of the shell. Furthermore, shell cross-linking must be carried out at high dilution in order to avoid extensive intermicellar cross-linking. Armes and colleagues [71, 72] have

successfully addressed these issues by using ABC triblock copolymers rather than conventional AB diblocks. ABC triblock copolymers yield onion-like micelles for which the inner corona (B) can be selectively cross-linked. For instance, a bifunctional alkyl iodide was used to quaternize (and cross-link) the tertiary amine units of the center segment of PEG-*b*-poly(2-(*N,N*-dimethylamino)ethyl methacrylate) (DMAEMA)-*b*-poly(2-(*N,N*-diethylamino)ethyl methacrylate) triblocks [71]. The PEG outer corona provided the steric repulsion that ensured minimal interpenetration of the micelles just as minimal intermicellar cross-linking.

One concern associated with such chemical stabilization of micelles is that it may impair the end elimination of the system, especially in the case of non-biodegradable materials. Cross-linked or polymerized micelles are often large entities that can no longer be eliminated by glomerular filtration. Likewise, cross-linking may impair the biodegradability of some polymers. To overcome these potential problems, hydrolysable cross-links have recently been used [73].

Small assemblies that topologically mimic the micelle architecture but that present covalently bound amphiphilic chains have been synthesized as an alternative approach to provide intrinsic stability. These nanocarriers are referred to as unimolecular polymeric micelles (UPM) and consist of single macromolecules such that their formation and dissociation are intrinsically independent on polymer concentration (no apparent CMC). UPM can be obtained from both dendrimers [74] and star-block copolymers [26, 75], with the latter form involving fewer synthetic steps and being simpler to prepare.

5. Micelle dimensions and morphology

5.1 Theoretical prediction of the micelle morphology

The interaction forces between amphiphiles within aggregates and the strength of forces between aggregates, determine the equilibrium structure of the assemblies, and are affected by the relative block length, temperature, and solution conditions (*i.e.* ionic strength and pH of the solution). As micelles are entities formed by the non-covalent aggregation of individual amphiphilic polymers, they can self-assemble into different morphologies including spherical, small rod, worm-like and vesicular geometries [76-79]. Spherical micelles can grow one- or two-dimensionally into cylindrical or bilayer structures, respectively. This growth is controlled primarily by the nature of the corona segments since both one and two-dimensional growth require bringing the polymer heads in close proximity to each other in order to reduce the curvature of the micelle surface, and hence the available area per polymer molecule at the micelle surface [80]. Generally, the interior of the spherical micelle presents a radius of approximately the length of the fully extended hydrophobic chains. Based on the geometry of various monomers and the space occupied by the hydrophilic and hydrophobic groups of the amphiphilic polymer, it is possible to predict the morphology of a micelle. One of the most common methods used to this end is to calculate the packing parameter (P) according to Equation 1:

$$P = \frac{v}{l_c a_\circ} \tag{1}$$

where v corresponds to the volume of the hydrophobic group in the micellar core, l_c is the length of the hydrophobic group and $a_\circ$ is the cross-sectional area occupied by

the hydrophilic group at the micelle-solution interface [80, 81]. The *P* values of spherical, cylindrical and lamellar micelles are usually 0-⅓, ⅓-½ and ½-1, respectively. These values can be explained by the fact that core volumes increase on going from spherical to cylindrical and lamellar micelles. Concomitantly, the surface area per monomer, averaged over the entire surface, decreases as the micelle size increases. Thus, it can be predicted that if the molecular shape of an amphiphile is in the form of a cone, wedge or cylinder, then spherical, rod-like, or vesicular morphologies will respectively be obtained (Table 2). This average molecular shape can be more simply expressed as the hydrophilic-to-total mass or volume ratio (*f*). Here, it can be seen that as the monomer shape goes from cone to wedge to cylinder, the $f_{\text{hydrophilic}}$ decreases and the $f_{\text{hydrophobic}}$ increases. A survey of the literature indicates that spherical micelles are observed when $f_{\text{hydrophilic}} > 0.5$ while cylindrical and vesicular morphologies are observed when $f_{\text{hydrophilic}}$ is 0.4-0.5 and 0.25-0.45, respectively (Table 2) [48, 76, 79, 82-88]. If the *f* ratio can be useful in predicting the morphology of various polymeric assemblies, it remains an empirical rule and deviations have been found upon changing the molecular weight and chemistry of the copolymer.

5.2 Analysis of the micelle morphology

A common method to examine the morphology of the formed micelles is to compute the ratio of the radius of gyration over the hydrodynamic radius (R_g/R_h). This ratio takes a value of 0.78 for a polymer chain in a hard sphere conformation while it reaches 1.30 or higher for polymers in a random coil and 1 or less for

vesicles (Table 2) [89, 90]. In the case of PM, values close to 0.78 are typically obtained, indicating that PM often form spherical aggregates in solution. Deviations from this predicted value can be encountered and are explained by a higher R_g measured when the polymeric chains of the micelles expand in water to adopt other conformations (*i.e.* cylinders and vesicles) [48, 91].

Table 2. Different parameters that can be used to predict the micelle morphology

$v/l_c a^o$	Monomer shape	R_g/R_h	$f_{hydrophilic}$	Expected Morphology
0-⅓	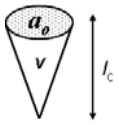	0.78	> 0.5	Spherical 
⅓-½		≥1.3	0.4-0.5	Cylindrical 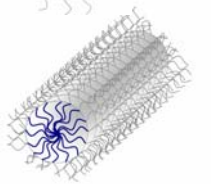
½-1		~1	0.25-0.45	Lamellar 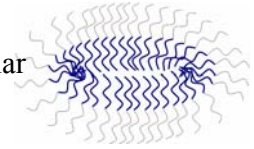

Other methodologies only allow establishing whether micelles are spherical or not. For instance, the sphericity of PM can be confirmed by performing dynamic light scattering measurements at multiple angles. For spherical particles, the intensity of the scattered light is equal in all directions such that plots of the diameter as a function of the scattering vectors (K^2) are linear [92]. Angular dependency is then indicative of non-spherical morphologies [48]. Alternatively, deviation from

spherical morphology can be confirmed by comparing experimental N_{agg} to theoretical values predicted for a sphere using equation 2.

$$N_{max} = \frac{4\pi r^3 \rho N_A}{3m} \quad (2)$$

In Equation 2, r stands for the maximum possible radius for an anhydrous core of a spherical micelle (*i.e.* the extended chain length of the hydrophobic segment), ρ is the density of the hydrophobic segment, N_A is Avogadro's number and m is the molecular weight of the hydrophobic part. Since no void can exist in the center of the micelles, and as the hydrophobic chains in the liquid state are not usually fully extended, one dimension is always limited by the maximum possible extension of the hydrophobic chain. Therefore, the equation allows the calculation of the maximum possible aggregation number (N_{max}) for spherical micelles. If N_{agg} exceeds the maximum theoretical number, an expanded morphology has to be assumed and deviation from sphericity is inferred. The main limitation of this approach is that a lower value of N_{agg} compared to N_{max} cannot confirm a spherical morphology. In addition, predictions lose in precision for micelles of large diameter.

Finally, the morphology of PM can be directly visualized by microscopic methods such as transmission electron microscopy (TEM) and atomic force microscopy. Protocols where the micelles are imaged in their hydrated state are to be preferred for better agreement with reality.

5.3 Transformation between different morphologies

In addition to adjusting polymer composition, various morphologies are attainable by changing the solution conditions (*i.e.* water content, ionic strength and pH). This is illustrated by the work of Eisenberg and coworkers [86, 93] who have shown how the solution properties can control the architecture of aggregates from spherical micelles to other closely related structures such as rods, vesicles, tubules, and lamellae in a reversible fashion (depending on the polymer concentration and block length). For example, TEM images for a solution of 1% (*w/w*) poly(styrene)$_{310}$-*b*-poly(acrylic acid)$_{52}$ in dioxane (Figure 7) revealed that the water content in the solution determined the shape and size of the formed aggregates. The spheres in solution at 9.1% (*w/w*) water, for example, morphed into short rods when the water content was increased to 11.5% (*w/w*) and into long rods and vesicles when the water content was further increased. An increase in water content makes the solvent of poorer quality for the hydrophobic block. In response to this, the system tends to minimize the total interfacial area by increasing the micellar size (*i.e.* by increasing the N_{agg}) while reducing the total number of aggregates. However, this increase in micellar radius is accompanied by a thermodynamically unfavorable increase in core-chain stretching and in corona chain repulsion. When the thermodynamic penalty associated with these factors exceeds the gain met with reducing the interfacial area, the spherical micelles undergo a morphological transition into smaller-diameter rods so as to reduce the core-chain stretching, the intercorona repulsion and, ultimately, the total free energy of the system. With further increases in the water content, a similar tendency to reduce to the total free energy of the system drives the

transformation of rods into vesicles. For the same copolymer, different morphologies can be attained by varying the polymer concentration at a given water content. Another interesting concept for engineering uniform rod PM while controlling the rod length has recently been introduced through the use of molecular recognition. Spherical 22-mer-oligonucleotide-*b*-PPO_{115} micelles were hybridized with long single stranded-DNA template molecules that encode the complementary sequence of the micelle corona multiple times. Upon this molecular recognition event, the shape of the micelles changed from spheres to uniform rods as confirmed by scanning force microscopy and fluorescence correlation spectroscopy [94].

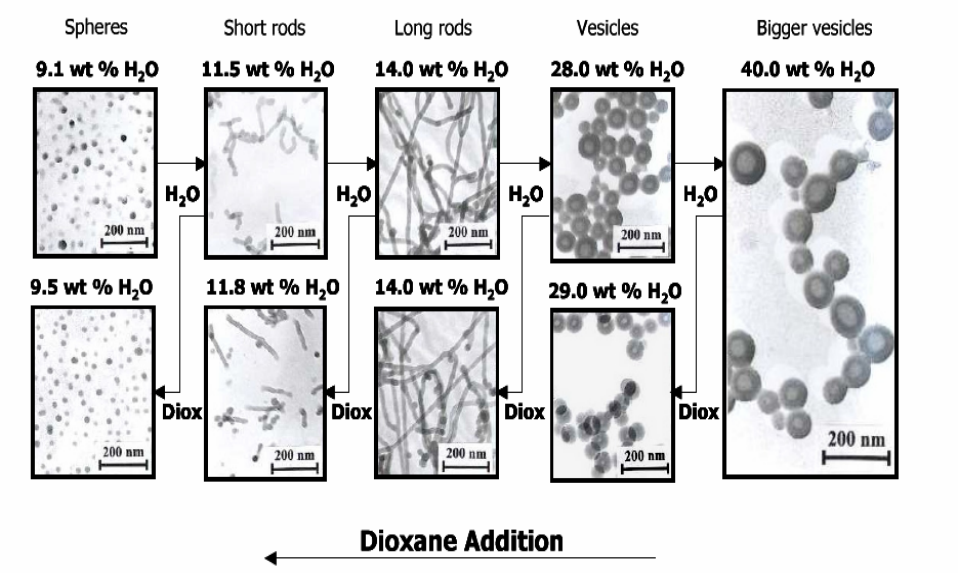

Figure 7. The control of micelles morphology by changing the solvent conditions. Representative TEM pictures showing the reversibility of various morphological transitions for a solution of 1% (*w*/*w*) poly(styrene)$_{310}$-*b*-poly(acrylic acid)$_{52}$. Reprinted from Shen, H. *et al.* [93] Copyright 1999, with permission from American Chemical Society.

5.4 Morphologies attainable with PICM

Similar to PM, PICM with different morphologies can be obtained. Most of the PICM reported to date were of spherical morphology although other morphologies are attainable depending on the polymer composition and the genetic material structure [38, 43, 66]. For instance, complexes of pDNA and PDMAEMA$_{20}$-*b*-poly[2-methacryloyloxyethyl phosphorylcholine]$_{30}$ copolymer formed rod-like aggregates as confirmed by TEM [95].

5.5 Significance in drug delivery

Aggregates of different morphologies have received significant attention since they have the potential to display different characteristics. For example, assemblies of cylindrical shape are usually associated with greater solubilization capacity, given their higher N_{agg} and core volume, than spherical ones [48, 88, 96, 97]. The pharmacokinetics of micelles of different morphologies is also expected to vary. Discher and coworkers [83-85] have prepared PM of PEG-*b*-PCL and PEG-*b*-polyethylethylene known as filomicelles ($f_{hydrophilic}$ = 0.42-0.44) and compared them with spheres of similar chemistry. In rodents, filomicelles provided drastically different pharmacokinetic properties and persisted in the circulation about ten times longer than their spherical counterparts. It was found that the long filomicelles were not taken up by the macrophages. On the contrary, shorter micelles are taken up by cells, thus resulting in more rapid clearance. The clearance of the filomicelles occurred upon the persistent decrease in length which was more significant for the

biodegradable PCL than the non-degradable polyethylethylene due to the hydrolysis of PCL over time.

6. Drug incorporation

6.1 Drug loading procedures

Several procedures have been considered for the incorporation of hydrophobic drugs into micelles (Figure 8), the most direct of which consists in the dissolution of the drug into a solution of pre-formed micelles. Unfortunately, this simple equilibration process can only be used with the most hydrophilic copolymers and often results in low levels of loading given that diffusion of the drug in the PM core is slow. Instead, physical entrapment of the drug performed in tandem with the micellization procedure is preferred and is often achieved using the dialysis or oil-in-water emulsion methods. The dialysis method involves the solubilization of both the polymer and drug in a common water-miscible organic solvent (such as ethanol or *N*-*N*-dimethylformamide). As the good solvent is replaced with water, the surface free energy associated with both the drug and hydrophobic segment of the copolymer increases, thereby driving their segregation into the core of drug loaded-micelles. Extensive dialysis (over several days) ensures complete removal of the organic solvents. The oil-in-water emulsion method, on the other hand, consists in the emulsification of a water-insoluble organic drug solution into an aqueous polymer solution. The copolymer partitions at the solvent/water interface of the organic droplets and drug incorporation proceeds as the solvent evaporates. Solution casting

is yet another drug encapsulation method whereby a drug/polymer solid dispersion is obtained after dissolving both the polymer and drug in an organic solvent and evaporating the solvent. Drug-loaded micelles are obtained as the film is rehydrated with hot water. The success of this procedure was shown to depend on the nature of the organic solvent employed to form the polymer/drug matrix. In an attempt to incorporate paclitaxel in PEG-*b*-PDLLA, Zhang *et al.* [60] found that of an extensive list of solvents, only acetonitrile gave a clear solution following reconstitution in water. Furthermore, the use of this method remains limited to drugs and copolymers that are thermally stable. Another efficient procedure for the production of drug-loaded PM consists in dissolving both the drug and copolymer in a *tert*-butanol (TBA)/water mixture and freeze-drying the solvents to produce a drug/copolymer cake [98]. The presence of TBA in the solvent mixture induces the formation of a pre-micellar structure with a swollen core where the drug can easily diffuse and partition. Dynamic light scattering studies revealed that the greater the TBA fraction, the larger and the more swollen the micelles [98]. Rehydration of the freeze-dried cake produces an aqueous solution of drug-loaded micelles. Of marked interest is the fact that the drug/polymer TBA/water solution can easily be sterilized by filtration and freeze-dried under aseptic conditions. Using this method, paclitaxel and docetaxel were incorporated into the PM with efficiencies reaching almost 100% [98].

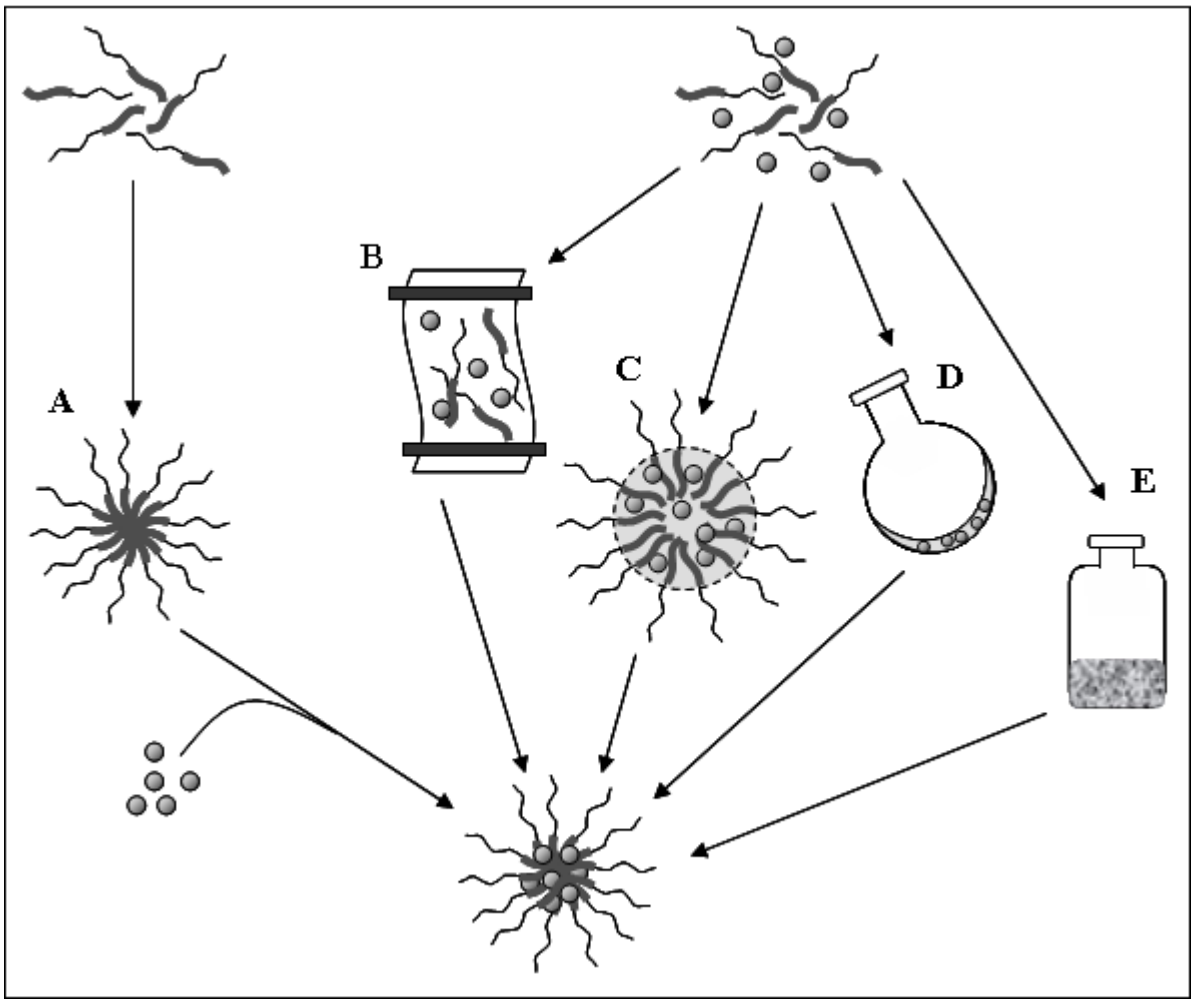

Figure 8. Most often used drug-loading procedures; simple equilibrium (A), dialysis (B), oil-in-water emulsion (C), solution casting (D) and freeze-drying (E). Reproduced from Dufresne *et al.* [46].

The incorporation of charged drugs or polyanions into the core of PICM, in contrast, results from the straightforward mixing of an aqueous drug solution and an aqueous polymer solution (Figure 1, C-E). Electrostatic interactions between the copolymer and the oppositely-charged drug provoke condensation, neutralization and self-association of the condensates into PICM. Drug entrapment proceeds

simultaneously with micelle formation [14]. Usually, most of the nucleic acid is incorporated in the PICM at an N/P ratio approaching 1.

6.2 Achieving high drug loading

Optimization of the loading efficiency is crucial in order to reduce the amount of vehicle to be administered. Not only is this vital to limit the toxicity or adverse effects that could be associated with the carrier, but also to minimize the overall cost of the formulation. Achieving high drug loading is also desirable considering that the micelle core, *i.e.* the space available for drug incorporation, only makes up a small volume of the micelle solution. This is particularly true for UPM where the free loading space is limited by the length and number of the core-forming blocks. Several properties of both the copolymer and drug are known to affect the drug loading and are discussed below.

If different loading procedures can lead to varying entrapment efficiencies, the extent of incorporation of drugs is still mostly influenced by the nature of the polymer/drug combination. In a study where the degree of solubilization of different aromatic and aliphatic hydrocarbons in PM was evaluated, Nagarajan *et al.* [99] showed that the affinity between the core and solubilizate dictated the magnitude of incorporation. The Flory-Huggins interaction parameter χ_{sc} was used as an adequate variable to correlate and evaluate solubilization in block copolymer micelles [99]. The value of χ_{sc} can be computed as follows:

$$\chi_{sc} = \frac{(\delta_s - \delta_c)^2 V_s}{RT} \tag{3}$$

where δ_s and δ_c are the Scatchard-Hildebrand solubility parameters of the solubilizate and core-forming polymer block respectively, and V_s is the molar volume of the solubilizate. The lower the interaction parameter χ_{sc}, the greater the compatibility between the solubilizate and the micelle core. The relevance of the Flory-Huggins interaction parameter is that it shows that no universal delivery system is likely to be ever designed; each drug presents unique properties that will be best complimented by selective copolymer systems [15, 100]. Some caution, however, should be exercised in using χ_{sc} for a quantitative description of the extent of solubilization because only positive χ_{sc} values can be obtained from this simplified equation and, in addition, concentration dependence cannot be studied.

Another predictor of the drug affinity for the PM is the partition coefficient (K_v) of the solubilizate between the core and the surrounding environment. The higher the K_v value, the higher the affinity of the drug toward the micellar phase. K_v values can be obtained by plotting the ratio of drug solubility in the presence of PM (S_{tot}) over that in pure water (S_w) against micellar concentration according to Equation 4 [101]:

$$\frac{S_{\mathrm{tot}}}{S_{\mathrm{w}}} = 1 + K_{\mathrm{v}} \cdot C_{\mathrm{mic}} \cdot V_{\mathrm{m}} \tag{4}$$

where C_{mic} is the micellar concentration (defined as the polymer concentration minus the CMC divided by N_{agg}). V_m is the micellar partial molar volume and is given by:

$$V_{\mathrm{m}} = \frac{M_{\mathrm{wmic}} \cdot Q_{\mathrm{h}}}{d_{\mathrm{h}}} \tag{5}$$

where M_{wmic} is the micellar molecular weight, Q_h is the hydrophobic block weight fraction and d_h is the density of the core. The K_v of docetaxel between water and

copolymer micelles of PEG-*b*-PBO, PEG-*b*-PSO and PVP-*b*-PDLLA were calculated according to Equations 4 and 5 [48, 98]. The K_v values ranged from 2 x 10^4 to 36 x 10^4 with the highest affinity found towards the PSO micelles. The difference in the K_v values between those micelles might be explained by the higher hydrophobicity of the PSO core as well as better compatibility between their aromatic structure and docetaxel. K_v values are calculated under the assumption that the drug partitions between two phases, namely the PM (as a whole) and water. Under such a premise, K_v should remain constant as a function of the drug concentration. However, deviations from this behavior have been observed, with K_v decreasing as the drug concentration increases. In such cases, solubilization of the drug occurs at the micellar interface, which becomes saturated at higher drug concentration. Thus, solubilization takes place in an adsorption-like manner and the data can be best fitted to the Langmuir adsorption isotherm [102].

The above discussion reveals that the maximum drug loading might be achieved when high affinity exists between the core-forming block and the drug to be loaded. The loading capacity of micelles can also be influenced by other important variables such as the occurrence of interactions between the drug and hydrophilic block of the copolymer [19]. For instance, higher entrapment efficiencies could be attained when using PVP rather than PEG as the hydrophilic segment. This might be due to the binding of the drug (*i.e.* indomethacin) to PVP probably *via* intermolecular hydrogen bonding between the drug hydroxyl and PVP carbonyl groups [19, 103]. Drugs with high affinity for both the core and shell blocks are likely to be solubilized in the core of micelles but also at the core/shell interface, and even within the shell

[15]. Alternatively, the efficiency of drug incorporation can be affected by the length of both the core-forming and corona-forming blocks [104]. The longer the hydrophobic block, the larger the hydrophobic core or cargo space available, and the higher the ability to entrap hydrophobic drugs. In contrast, a significant increase in the hydrophilic block length can result in an increase of the CMC, which reflects a smaller fraction of amphiphilic copolymers present in micellar form and a drop in the hydrophobic volume available for solubilization. Furthermore, copolymers presenting increased hydrophilic block lengths will experience increased surface densities and produce small particles with reduced cargo space. Another factor affecting drug loading is the state of the core. While crystallinity enhances micelle stability, it may well reduce drug loading. Crystalline cores are highly ordered and their physical cross-linking reduces the free cargo space and hinders diffusion of drugs into the core [105]. The drug loading can be increased by covalently linking drug molecule to the hydrophobic segment [62, 106]. For example, the chemical fixation of DOX on PEG-*b*-poly(aspartic acid) (PEG-*b*-P(Asp)) was shown to cause an increase in the level of physically loaded drug due to enhanced affinity resulting from π-π interactions [62]. Finally, entrapment efficiencies can depend on the initial amount of drug to be solubilized. Trying to solubilize larger amounts of drug than what can be accommodated by the micelle core can induce precipitation of the drug and reduce the loading yield [107, 108].

7. Drug release

7.1 Release from PM

In the previous sections, it was emphasized how PM need to retain their integrity following the large *in vivo* dilution to achieve applications such as passive targeting and sustained release. Moreover, maximization of the drug loading revealed to be crucial given the small cargo volume available. An issue now to be addressed is the identification of the parameters affecting the drug release and, ultimately, the effectiveness of the system.

One such parameter is micelle stability. Indeed, it is easily seen how dissociation of micelles into single chains will free the entrapped molecules. Likewise, erosion or biodegradation of the carrier could provoke the escape of drug molecules. For instance, biodegradable poly(D,L-lactide-*co*-glycolide) (PLGA)-AON conjugates were shown to release the AON in a sustained manner by controlled degradation of the hydrophobic PLGA chains [109].

In cases where the system is stable, slowly biodegradable or non-biodegradable and above the CMC, however, drug release will instead depend on the rate of diffusion from the micelle. The rate of diffusion was shown to be influenced by various factors, most of which concurrently affect micelle stability and drug loading. Of those factors, one can state the core-forming block length, the micelle morphology, the physical state of the core, the presence of cross-links (within either the core or the corona segments), and the compatibility of the copolymer/drug pair. For instance, an increase in the length of the core forming block is known to favor the

self-association of amphiphilic copolymers into micelles and to provide a larger cargo space where more drug can be accommodated. The consequence on drug release is such that drugs located in the core have to diffuse through a longer path (larger core radius) and present a slower release rate [110]. Similarly, various micelle morphologies (spherical, cylindrical, bilayer, etc.) are associated with different diameters and surface (and interface) areas per micelle, thus affecting the release rate. The physical state of the micelle core, whether solid-like or liquid-like, was also shown to influence micelle stability and, in parallel, the release of the entrapped drug. For example, Teng *et al.* [111] revealed that the diffusion constant of a fluorescent probe from a poly(styrene) core was smaller than from a poly(*tert*-butyl acrylate) core. This tendency could be qualitatively correlated with the respective glass transition temperatures of the core components (*i.e.* 100 *vs.* 40-43°C) and indicated that the diffusion of a drug through a glassy core was slower than through a more mobile core. In turn, cross-linking of the corona-forming blocks affects the permeability of the corona and the period within which drugs diffuse [112]. The polymer/drug compatibility can concurrently influence drug release and drug incorporation. Just as the Flory-Huggins interaction parameter was used to predict the extent of drug incorporation, it can be used to infer the characteristics of drug release of a system. Generally speaking, the stronger the interaction between the drug and the core-forming block, the slower its release from the micelle.

In addition to factors affecting the properties of the micelles, the localization of the drug within the micellar assembly is expected to influence the release, with

molecules located at the core/corona interface or within the corona diffusing faster than those located in the core [111].

Other properties influencing the release kinetics include properties inherent to the drug molecule such as its molecular volume and its physical state in the micelle core. On the one hand, a relationship between the molecular volume of the drug and diffusion constant can be obtained by studying differences in the release rates of different probes from a particular micellar system [111]. Such data suggest that the larger the molecular volume, the smaller the diffusion constant and the release rate. On the other hand, the physical state of a drug in the micelle core can alter the drug release profile. Jeong *et al.* [110] showed that an increase in the amount of clonazepam loaded into PEG-*b*-PBLG micelles (12.1 to 32.8% (*w/w*)) resulted in a slower drug release. Differential scanning calorimetry thermograms revealed that crystallization of the drug occurred at the higher loading.

Release kinetics are often biphasic and exhibit an initial burst associated to the fast release of drug molecules located in the shell or at the core-shell interface [111], followed by a slow release phase corresponding to the diffusion of the drug from the core. If drug release profiles determined *in vitro* are useful to compare drug formulations within each other and gain some insight on the properties of the formulation, they rarely correlate with the *in vivo* behavior, the release being accelerated *in vivo*. For instance, while the *in vitro* release of hydroxycamptothecin loaded in PEG-*b*-PCL micelles occurred over several days, the drug was cleared from plasma within few hours following i.v. administration of the micelles (Figure 9A) [113]. Results by Savic *et al.* [114] showing the loss of integrity of PM of similar

structure 1 h after intramuscular or subcutaneous injection suggest that the poor pharmacokinetics of the drug might be due to premature micelle disassembly. Likewise, paclitaxel loaded into PEG-*b*-PDLLA was found to have lower plasma levels than the copolymer and a different biodistribution profile following injection, indicating micelle disassembly [115]. It was recently demonstrated that the destabilization of the PM and the release of the loaded drug *in vivo* is possibly due to interactions with plasma proteins (Figure 9B) [116]. However, additional factors, such as the destabilization of the micelles by other molecules in blood, the translocation of hydrophobic drugs to the lipid components in the blood and the degradation of the copolymers, can also contribute to the disassembly of the micelles and the fast release of the drug.

(A)

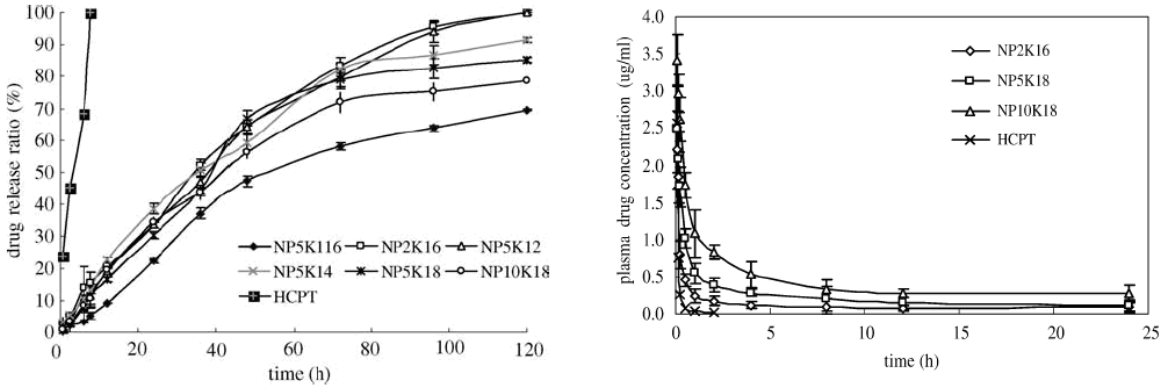

(B)

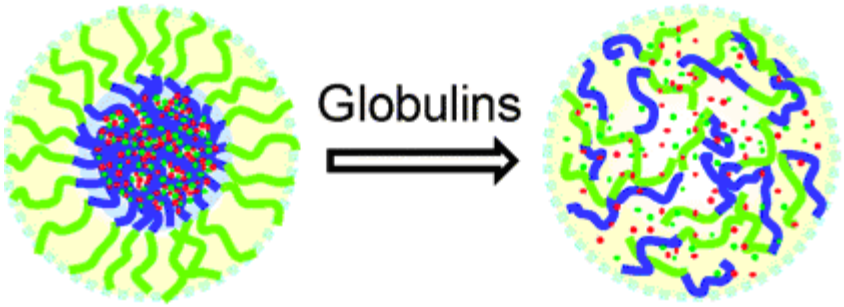

Figure 9. (A) *In vitro* release (left panel) and plasma concentration-time curve (right panel) after i.v. administration of hydroxycamptothecin loaded in PEG-*b*-PCL micelles to rats. **(B)** Destabilization of the PM possibly occurs due to the adsorption of plasma proteins. Reprinted from Shi, B. *et al.* [113] and Chen, H. *et al.* [116] Copyright 2005 and 2008, with permission from Springer Science and American Chemical Society, respectively.

7.2 Release from other micellar systems

In the case of PICM, which result from electrostatic interactions between oppositely charged ions, drug release is not diffusion-based but rather occurs through

dissociation of the assemblies. The dissociation mostly follows from exchange events with charged ions (*i.e.* salts, heparin) which are typically found *in vivo*. Similarly, the dissociation of the polymer-metal complex micelles occurs through the substitution of the metal from the coordinating groups of the copolymer by ions in the medium, thus resulting in the micellar dissociation and subsequent release of the drug.

7.3 Triggered drug-release

Although the above mentioned mechanisms of drug release from the micellar carriers are the most common, other can be involved. Some micellar systems have been adapted to trigger the release of their contents following a change in pH, temperature or in the redox state of the surrounding medium. Ultrasounds have also been utilized to trigger drug release from micellar systems *in vitro* and *in vivo*. However, this chapter will not address this rather specialized subject and the readers are referred to the references [117, 118] for more information.

7.3.1 pH-sensitivity

Changes in pH are one of the most exploited stimuli to trigger drug release. Indeed, pH variations occur at different pathological/physiological sites permitting applications where micelles release their contents upon experiencing a change in the environmental pH. Firstly, the microenvironment in tumors is generally more acidic than in normal tissues. This acidic pH might be explained by the characteristics of cancer cells which have glycolytic rates higher than in normal tissues [119]. However, the pH differences at tumor sites are usually small so that adequately

sensitive systems should be used. Changes in pH are also encountered upon cellular internalization of the drug-loaded carriers *via* clathrin-mediated endocytosis, a process which is accompanied by an increase of acidity inside the endosome. Finally, drugs administered by the oral route experience a pH gradient as they transit from the stomach to the jejunum.

Several strategies have been exploited to achieve pH-sensitivity, most of which rely on changes in the polymer properties following the protonation/deprotonation of acidic and basic groups present along the polymer chain or on the hydrolytic cleavage of hydrophobic functionalities or cross-links. For instance, the pH-sensitivity can be imparted by using a corona composed of a PNIPAM copolymer bearing carboxylic acid functionalities. At neutral pH, the carboxylic acid groups make the PNIPAM segment soluble. As the pH is lowered, a sharp decrease in the solubility of the corona occurs. As a result, mixing of the PNIPAM chains and core region takes place, increasing the polarity of the core and promoting the release of the entrapped drug [120]. Another approach consists in conferring amphiphilicity to a copolymer by conjugating hydrophobic moieties to one of the polymer block (the core block) *via* pH-sensitive links. As the pH decreases, the links hydrolyze to expose back polar groups on the core forming block, thus destabilizing the micelles and releasing any encapsulated drug. This was for example achieved by Gillies *et al*. [121, 122] who developed block copolymers of PEG and either PLL or polyester dendrons and attached hydrophobic groups to the dendrimer periphery by highly acid-sensitive cyclic acetals (Figure 10). These polymers self-assembled into micelles that were stable in neutral aqueous solution but disintegrated into unimers at mildly acidic pH

following loss of the hydrophobic groups upon acetal hydrolysis [122]. The same group extended this strategy by directly conjugating a hydrophobic anticancer agent (DOX) to copolymers, thereby producing pH-sensitive micelles able to release the drug at acidic pH values similar to that found in tumor tissues [121]. However, a disadvantage of this method is the requirement of functional groups on the drug molecule that can be covalently modified, and since not all drugs are capable of being conjugated to a polymer in such a way, the scope of this method is limited.

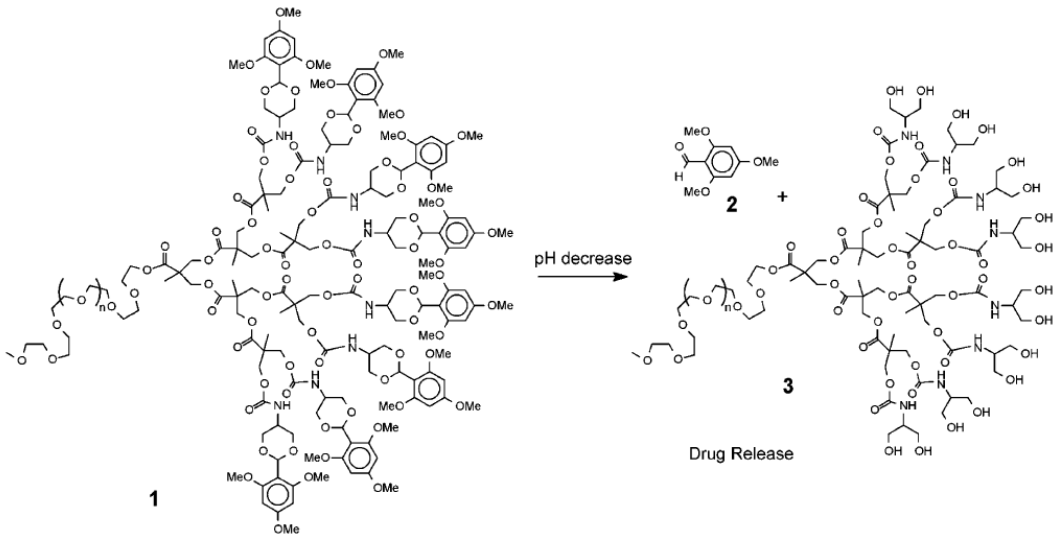

Figure 10. Hydrolysis of acetals on the dendrimer periphery of the micelle-forming copolymer 1 leads to a solubility change which disrupts micelle formation and triggers the drug release. Reprinted from Gillies, E. *et al.* [121] Copyright 2005, with permission from American Chemical Society.

7.3.2 Temperature-sensitivity

Some disease states are associated with local hyperthermia. Alternatively, local increases in body temperature can be induced by exterior means, making

temperature-directed drug release another viable triggered release strategy. To that aim, polymers presenting a lower critical solution temperature (LCST) transition can be incorporated in the composition of micelles. The most widely used polymer for that purpose is PNIPAM. The LCST of PNIPAM can be adjusted within a desired range by copolymerizing it with hydrophilic or hydrophobic monomers which strengthen or weaken the interactions between polymer chains and water, resulting in an increase or decrease in water solubility, respectively [8, 123, 124]. Below the LCST, the nonpolar core is segregated from the hydrated PNIPAM corona. At higher temperature (above the LCST), collapse of the corona is accompanied by increased mixing of the NIPAM corona units and hydrophobic core units, similar to lowering of the pH. This mixing increases the core polarity and releases the micelle-incorporated drug [7, 8, 120, 125].

7.3.3 Redox-sensitivity

The presence of oxygen-reactive species released by activated macrophages in the inflamed tissues and certain tumors has been investigated as yet another stimulus to trigger the release of drugs from the polymeric carriers [126]. Block copolymers of PEG-*b*-poly(propylene sulfide) (PEG-*b*-PPS) that respond to oxidative conditions show promise for that purpose. The hydrophobic PPS is readily converted to hydrophilic poly(sulfoxide) or poly(sulfone) by mild oxidizing agents. Micelles obtained from this polymer could therefore accommodate hydrophobic drugs that would be released during the solubilization or swelling of the polysulfide upon oxidation, as was demonstrated for polymeric vesicles [127, 128]. Another

mechanism could be to take advantage of the reductive conditions met in the cytosol. For example, the cleavage of a disulfide bond linking an AON or siRNA to a PEG segment in the cytosol will cause release of the drug [45, 129].

8. Cellular barriers-Endosomal escape

Micellar carriers can be taken up by cells *via* endocytosis. During this process, the micelles are internalized into vesicles (*i.e.* the endosomes) which end later in lysosomes. Sequestration of the micelles in the endosomal compartments can preclude the drugs from reaching their cytoplasmic or nuclear targets and, in some cases (mostly hydrophilic drugs), is a bottleneck to their efficacy. In such cases, the transient destabilization of (and escape from) the endosomal/lysosomal compartments becomes crucial. This destabilization can, for instance, be achieved using amine-containing polymers exhibiting pK_a values between physiological and lysosomal pH in the preparation of PICM. As the endosomes are acidified, these cationic polymers undergo large changes in their ionization state and become protonated. This protonation of unbound amine groups causes an influx of chloride ions and induces osmotic swelling and subsequent disruption of the endosome [130]. This effect is referred to as the "proton sponge effect" [131]. Both PEI and PAMAM, which have pK_as of 5.5 and 6.9 (for primary amino groups), respectively, have been used for this purpose [132]. Although some controversy exists about the contribution of the proton sponge effect to endosomal release, PEI and PAMAM have undeniably been shown throughout the literature to facilitate efficient delivery of pDNA, AON, and siRNA [133]. The buffering capacity of these cationic polymers depends on the

number of unbound amino groups and may be hampered by complexation with the genetic material [11, 134]. It is possible to overcome this issue by increasing the polymer proportion in the PICM composition (*i.e*. by increasing the N/P ratio). However, this may come at the price of cell toxicity. Hence, A-B-C triblock copolymers forming 3-layered micelles with segments of different pK_as have been proposed (Figure 11A) [11]. Specifically, the micelles consist of PEG as the outer layer, poly[(3-morpholinopropyl) aspartamide] (PMPA) as a low-pK_a middle layer and PLL as a high pK_a inner layer. PLL (pK_a of 9.4) is highly ionized at pH 7.4 and preferentially interacts with the negatively-charged genetic material. On the contrary, the low-pK_a PMPA is only partially ionized at pH 7.4 (~ 10%), providing an opportunity to buffer and prevent acidification of the endosomes. These micelles showed superior transfection efficiency than either PEG-*b*-PLL or a mixture of PEG-*b*-PLL and PEG-*b*-PMPA due to the high buffering capacity of the PMPA segment remaining free in the intermediate layer. Similarly, a PEG-*b*-polycation possessing a diamine structure with 2 distinct pK_as (*i.e.* primary and secondary amino groups in the poly(3-[(3-aminopropyl)amino]propylaspartamide) (PDPT) side chain), was found to be remarkably effective for siRNA delivery (Figure 11B) [135]. It is expected that this unique structure of PEG-*b*-PDPT allows that only the primary amino groups be involved in the PICM formation, thereby maintaining the buffering capacity of the secondary amino groups. Yessine *et al.* [53] took a different approach to promote endosomal destabilization and integrated a synthetic membrane-active polyanion, namely poly(methacrylic acid-*co*-ethyl acrylate-*co*-butyl methacrylate) (P(MAA-*co*-EA-*co*-BMA)) in the composition of PICM. The incorporated polymer

was shown to effectively destabilize the endosomal membrane and promote the release the AON in the cytoplasm.

(A)

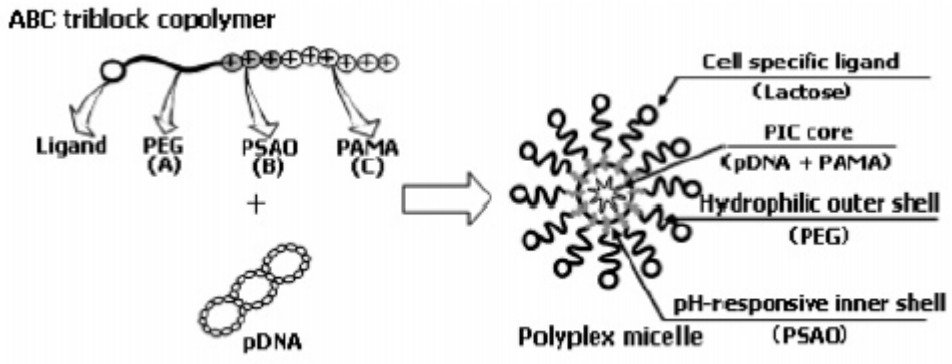

(B)

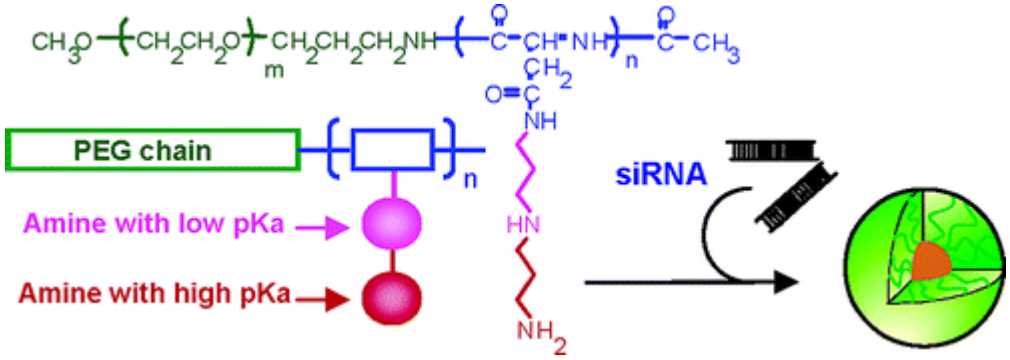

Figure 11. Three-layered micelles (A) and micelles with diamine structure (B) as strategies to enhance endosomal escape and transfection efficiency. Reprinted from Oishi, M. *et al.* and Itaka, K. *et al.* [10, 135] Copyright 2006 and 2004, respectively, with permission from American Chemical Society.

While the endosomal compartments hamper the efficacy of many hydrophilic drugs, it is not a real barrier for most hydrophobic drugs as the later can partition in membranes. In a recent study, Chen, H. *et al.* [136] found that during micelle-membrane interactions, the core-loaded molecules were transferred to the plasma

membrane, from which they could be taken up, independent of the copolymer micelles.

9. *In vitro* and *in vivo* applications

It is one thing to design micelles with targeted properties and behavior yet another to evidence their *in vitro* and *in vivo* applicability. To our benefit, there are numerous instances where the formulation of drugs as PM reduced their cytotoxity, increased the maximum tolerated dose (MTD) or permitted passive accumulation at target sites while accounting for improved therapeutic effects compared to control formulations [137-140]. Some PM and PICM systems are summarized in Tables 3 and 4, respectively, and their performance discussed below.

Table 3. Examples of PM loaded with various antitumor drugs

Polymer composition	Targeting moiety	Micelle-incorporated drug	Size (nm)	Ref
PEG-*b*-PLLA-DOX	-	DOX	90	[201]
Poloxamers 181 (PEG_2-PPO_{30}-PEG_2) and 407 (PEG_{99}-PPO_{65}-PEG_{99})	-	DOX	21-27	[141, 144]
PEG-*b*-P(Asp)-DOX	-	DOX	40	[142]
Poloxamer 181 (PEG_2-PPO_{30}-PEG_2)	-	DOX	-	[202]
PEG-*b*-PLGA-DOX and FOL-PEG-*b*-PLGA	Folic acid	DOX	95-115	[176]
cRGD-PEG-*b*-PCL	cRGD	DOX	20-27	[173]
PEG-*b*-P(Asp)-DOX	-	DOX	65	[203]
PNIPAM-*b*-PBMA	-	DOX	340	[8]
PEG-*b*-PDLLA	-	Paclitaxel	20-25	[143]
Galactose-PEG-*b*-PBLG	Galactose	Paclitaxel	105	[179]
PEG-PE	mAb 2C5 mAb 2G4	Paclitaxel	20	[168]
PEG-*b*-PBO or PEG-*b*-PSO	-	Docetaxel	16-21	[48]
P(NIPAM-*co*-MAA-*co*-ODA)	-	AlClPc	13-35	[6, 125]
P(NIPAM-*co*-VP-*co*-MAA-*co*-ODA)	-	AlClPc	20-34	[5]
PEG-*b*-P(Asp)	-	Cisplatin	20	[146, 204, 205]
PEG-PE	-	Dequalinium	-	[104]
Poloxamer 235 (PEG_{27}-PPO_{40}-PEG_{27})	-	Digoxin	-	[206]
PEG-*b*-poly(*N*-hexyl-L-aspartamide)-stearic acid	-	Amphotericin B	-	[150]
PVP-*b*-PDLLA	-	Paclitaxel Docetaxel Indomethacin	40-100	[19, 98, 149]
Pullulan-Cholesterol	-	Insulin	20-30	[17]

Table 4. Examples of PM loaded with heparin, pDNA, AON or siRNA

Composition	Targeting moiety	Drug (target gene)	Size (nm)	Ref
PEG-*b*-P(DMAEMA)	-	Heparin	31	[38]
PEG-SON/AON and PAMAM G5 and G3	-	AON	70-100	[66]
PEG-*b*-P(AEMA) and P(MAA-*co*-EA-*co*-BMA)	-	AON	30	[53]
AON-PLGA	-	AON (*c-myc*)	80	[109]
PEG-AON and PEI	-	AON (*c-raf*)	70	[42, 43]
PEG-AON and KALA	-	AON (*c-myb*)	70	[44]
FOL-PEG-AON and lipofectamine	Folic acid	AON (GFP)	70-90	[4]
PEG-*b*-PLL	-	AON (*c*-Ha-*ras* or VEGF)	40-50	[34, 69]
PEG-siRNA and PEI	-	siRNA (VEGF)	-	[45]
PEG-siRNA and KALA	-	siRNA (VEGF)	<200	[129]
PEG-*b*-DPT	-	siRNA (luciferase)	-	[135]
Transferrin-PEG-cyclodextrin-containing polycations	Transferrin	siRNA (*EWS-FLI1*)	50	[171]
cRGD-PEG-PEI	cRGD	siRNA (VEGF)	100	[36]
Lactose-PEG-siRNA and PLL	Lactose	siRNA (luciferase)	117	[180]
Fab'-PEG-PEI	Fab'	pDNA (luciferase)	150	[159]

9.1 Non-targeted micelles

The preferential accumulation of micelles in pathological sites presenting leaky vasculature (*i.e.* inflammation and tumors) can increase the efficacy of micelle-encapsulated drugs. This passive targeting, however, is only achievable if the drug-loaded micelles circulate for a long time in the blood to allow for their slow

deposition in the compromised vasculature of the pathological sites. This approach is currently under development by many research groups, with different PM formulations in different phases of clinical trial (Table 3) [141-144]. One clear example of passive targeting was reported by Hamaguchi, T. *et al.* [145] who showed that the incorporation of paclitaxel in PEG-*b*-P(Asp) PM resulted in about 90- and 25-fold increase in plasma and tumor area under the concentration-time curves (AUC), respectively, compared to the free drug. This remarkable increase in the AUC, in spite of using equivalent doses, can be ascribed to the greater stability conferred by the micelles which permits long circulation and minimizes the drug leakage (4-6 times longer elimination half-life *vs.* the free drug) and allow the passage and accumulation of the drug in the tumor. Alternatively, passive targeting has been demonstrated after loading platinous drugs into micelles of PEG-*b*-poly(glutamic acid) *via* polymer-metal complex interactions. Treatment of solid tumor-bearing mice with the micelle formulations reduced the nephrotoxicity, slowed down the clearance and allowed longer circulation time compared to the free cisplatin [146, 147]. Consequently higher and more sustained levels of drug in the tumor tissue were accomplished.

Still, passive targeting remains a strategy that is difficult to demonstrate *in vivo*. Rather, micellar systems usually permit to decrease the toxicity of the entrapped drug, allowing for higher doses to be administered and for greater efficacy. Examples of formulations that have been used to deliver potent antitumor drugs such as paclitaxel and DOX and for which greater efficacy has been achieved will be given below. Paclitaxel was successfully incorporated into the core of either PEG-*b*-

PDLLA or PVP-*b*-PDLLA micelles [143, 148, 149]. D. Le Garrec *et al.* [149] have shown that paclitaxel incorporated in PVP-*b*-PDLLA did not reach the MTD even at 100 mg/kg and showed greater antitumor activity than Cremophor® EL micelles whose MTD was established at 20 mg/kg after single injection. Because of the higher MTD, paclitaxel could be injected at higher doses (*i.e.* 60 mg/kg) where it induced three- and twofold increase in the plasma and tumor AUCs, respectively, *vs*. Cremophor® EL at 20 mg/kg. Other formulations such as SP1049C, where DOX is physically loaded in mixture of poloxamers 181 and 407, or PEG-*b*-P(Asp), where DOX is conjugated to the P(Asp) residues, were used to formulate DOX. Both formulations could prolong the half-life and increase the MTD of the drug compared to the free DOX. Taken together, these data underscore the therapeutic potential of PM to improve cancer therapy.

In addition to modifying the pharmacokinetics and biodistribution and decreasing the systemic toxicity of drugs, PM have been found to stabilize their incorporated drug, as in the case of amphotericin B. Amphotericin B is a membrane-disruptive drug used to treat systemic fungal diseases in its monomeric form. Its direct administration, however, is associated with self-aggregation, leading to loss of selectivity and systemic toxicity. M. Adams *et al.* [150] have shown that when amphotericin B was incorporated into the core of PEG-*b*-poly(*N*-hexyl-L-aspartamide-stearic acid) micelles, it was stabilized in its monomeric form, preventing the non-selective hemolysis of mammalian red blood cells *in vitro*. Moreover, the drug-loaded PM retained potent *in vivo* antifungal activity as compared to the standard clinical Fungizone® formulation.

The utilization of passive targeting to deliver different drugs was extended to different AON and siRNA (Table 4). For instance, PEG-AON/PEI PICM showed a superior antiproliferative activity against ovarian cancer cells where the intravenously injected micelles showed significantly higher accumulation level in the tumor region compared to the naked AON [43].

Clinical data demonstrates the distinct pharmacokinetic advantages of micelle-delivered drugs over free drugs. In addition, some of these examples suggest the feasibility of passive targeting, *i.e.* favoring the local accumulation of PM through the EPR effect. Hence, paclitaxel formulated in PEG-*b*-PDLLA micelles is now in phase II clinical trial either alone or in combination with cisplatin and showing promising results [151, 152].

9.2 Targeted micelles

Finest selectivity in the biodistribution of micelles and improved efficiency could theoretically be achieved by using systems which respond to external stimuli (such as pH and temperature variations) or by attaching specific ligands to the exposed hydrophilic ends of the carriers. These rather intricate targeting mechanisms are referred to as active targeting.

9.2.1 pH-responsive micelles

As mentioned in section 7.3.1, drug release from PM can be triggered by pH changes. If the change in pH is associated to a pathological process (*e.g.* solid tumors presenting acidosis), active targeting can be achieved [153, 154]. Hence, micellar devices have been designed to trigger and/or enhance drug release in response to pH.

An extended application of the pH-sensitive micelles has recently been introduced for the formulation of multiple anticancer agents in the context of combinatorial therapy. Advantages of the combinational therapy include better patient compliance and higher efficacy. Indeed, by simultaneously administering multiple drugs, the number of injections reduces, improving the quality of life of the patient. Furthermore, the combination of two or more drugs can amplify the activity of the drugs through a synergistic mechanism, thereby reducing the therapeutic dose and toxicity of the drugs. This synergistic action is usually brought about by rendering the tumor cells more sensitive to the drug. In this approach, pH-sensitive micelles become interesting seeing that the drugs can be conjugated to a polymer at a precise ratio. For instance, Bae, Y. *et al.* [155] conjugated DOX and wortmannin to PEG-poly(aspartate hydrazide) through an acid-sensitive hydrazone bond. The polymer–drug conjugates then assembled into micelles in which the drug mixing ratio between DOX and wortmannin was precisely controlled. It was shown that these mixed PM could reduce the DOX dose required for cytotoxicity through a synergistic drug action. Although the formulations have not yet been tested *in vivo*, it is expected that they would present several advantages over the conventional PM in the future.

9.2.2 Temperature-sensitive micelles

The efficiency of the micellar carriers can also be improved by combining the EPR effect with temperature-sensitivity. Thermo-responsive PMs were shown to release the loaded drug when the temperature increases beyond the LCST, thereby increasing their therapeutic efficacy. For instance, PM of (PNIPAM-*co*-*N*,*N*-

dimethylacrylamide)-*b*-poly(benzyl methacrylate) [7] and PNIPAM-*b*-poly(butyl methacrylate) (PNIPAM-*b*-PBMA) [8] loaded with DOX not only showed a thermo-responsive drug release behavior but also showed increased cytotoxicity towards bovine aortic endothelial cells *in vitro* above their LCST compared to the free drug. The higher cytotoxicity of the micellar formulation compared to the free drug at an identical dose suggests different routes of drug uptake by the cells. However, no *in vivo* data are available yet on the feasibility of hyperthermia targeting with PM.

9.2.3 Functionalized micelles

Up till this point, PM systems with highly hydrated, nonionic hydrophilic shells have mostly been discussed. The shell-components, primarily selected to hinder non-specific interactions and increase blood circulation times, may prevent internalization of the carriers by target cells [156]. Hence, systems presenting ligands at their water-exposed surface have been designed to enhance their selective binding to specific receptors on the cells, promote the uptake of the drug loaded micelles by receptor-mediated endocytosis and enhance efficacy. For efficient targeting, the receptors must be over-expressed by target cells (*e.g.* tumor cells) compared to normal tissues [157]. A variety of molecules including antibodies [158, 159], peptides [35, 160], aptamers [161, 162], vitamins and sugar moieties [163] have been used to achieve cell targeting (Table 3 and 4). The use of antibodies as the targeting moiety presents the advantage of selectivity, high affinity, and minimal competition for the receptor, contrary to what is observed with endogenous molecules such as folic acid (FOL) or transferrin [164-166]. Antibodies, however, might induce immunogenicity, can be difficult to produce/handle and present a large size,

potentially putting strain on micelle self-assembly. The use of small molecules such as sugars and vitamins can then become advantageous. As reported in many studies, it is important that the functional groups be readily available on the surface for efficient attachment to the receptors. The ligands can be attached either before or after the assembly of the particulate carrier.

9.2.3.1 Monoclonal antibodies and antigen binding fragments.

Targeting can be achieved by the whole antibody or its fragments such as the fragment antigen binding (Fab') and $F(ab')_2$ or scF_V (single-chain variable) [167] (Figure 12). The advantage of using an antigen binding fragment (*e.g.* Fab') instead of the whole monoclonal antibody is that, in view of its lower molecular weight, a lower level of steric hindrance during complex formation can be accomplished. In addition, it can induce less immunogenicity when *in vivo* applications are sought. Micelles functionalized with either monoclonal antibody or Fab' have both shown higher cellular uptake compared to non-targeted micelles. For instance, targeting of ovarian carcinoma cells using Fab'-PEG-PEI/pDNA PICM was demonstrated by Merdan, T. *et al.* [159] who observed more than 6-fold greater binding of the targeted micelles to the OVCAR-3 cells and measured 80-fold higher luciferase reporter gene expression compared to the unmodified system. Increased cellular uptake was also reported by Torchilin and coworkers [168] for whole antibody-PM targeting lung cancer cells. The increased cellular uptake was associated with a four-fold higher tumor accumulation of the drug (paclitaxel) *in vivo* after 2 h and with higher anti-tumor efficacy.

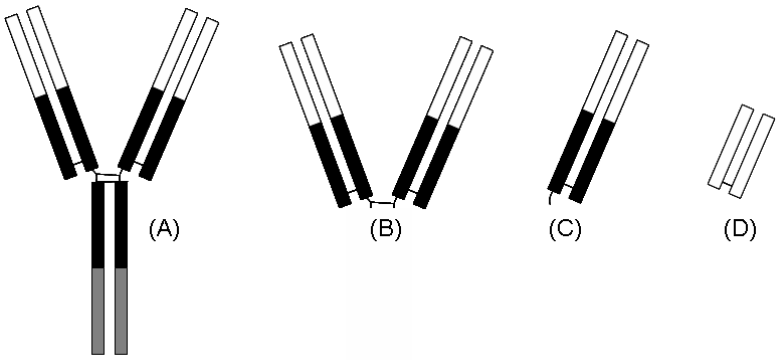

Figure 12. Targeting can be achieved with the whole antibody (A) or its fragments such as $F(ab')_2$ (B), (Fab') (C) or scF_V (D).

9.2.3.2 Aptamers.

Nucleic acid ligands (aptamers) have been used recently for the targeting of drug encapsulated PMs. Such molecules can fold by intramolecular interactions into unique three-dimensional conformations capable of binding to target antigens with high affinity and specificity. They are usually selected by screening a random library of nucleic acids to specific molecular targets [169, 170]. An RNA aptamer targeting the prostate specific membrane antigen, a well-known prostate cancer tumor marker that is overexpressed on prostate acinar epithelial cells, was used to decorate PEG-*b*-PLA or PEG-*b*-PLGA micelles [161, 162]. The targeted PM showed a marked increase in the cellular uptake over the non-targeted PM. When the targeted PEG-*b*-PLGA PMs were loaded with docetaxel, this increased uptake translated into increased cytotoxicity *in vitro* and in increased anti-tumor efficacy *in vivo*. However, the instability of DNA or RNA molecules in the blood may limit the use of these ligands in the clinic.

9.2.3.3 Non-immune peptides and proteins.

Proteins like transferrin, an iron transporter, can be used to target rapidly dividing cells that are in need of nutrients such as tumor cells. In this light, Hu-Lieskovan *et al*. [171] developed a multicomponent delivery system for metastatic tumor treatment. The system included a cyclodextrin-containing polycation that self-assembled with a siRNA inhibiting *EWS-FLI1* (a gene that is found in 85% of patients with Ewing's tumor). The surface of the complexes was then decorated with PEG and targeted with transferrin. Systemic administration of the targeted carriers downregulated oncoproteins and suppressed the spread of metastatic tumors. Removal of the targeting ligand eliminated the antitumor effects. While promising results were obtained with transferrin, this protein is a big molecule (80 kDa) that can put strain on micelles so that smaller peptides might be advantageous.

Small, tightly binding peptides and proteins have been utilized for cancer-targeted drug delivery. One example is the cRGD peptide, which targets the $\alpha_v\beta_3$ integrin. This integrin is a cellular transmembrane protein that has a marked role in tumor growth and metastasis [37, 172]. The cRGD peptide was conjugated to maleimide-terminated PEG-*b*-PCL PM encapsulating DOX. A three-fold increase in cellular uptake was observed by flow cytometry when the surface density was adjusted to 5% cRGD. A more pronounced 30-fold increase was even observed with 76% cRGD attachment [173]. Similar studies with a PEGylated branched PEI modified with an RGD peptide at the distal end of the PEG further demonstrated the possibility of *in vivo* targeting with this peptide [36]. Indeed, increased siRNA uptake in the tumor and decreased uptake in the lung and liver were observed following

intravenous administration of the modified complexes. This resulted in inhibition of both tumor angiogenesis and growth.

9.2.3.4 Vitamins.

The expression levels of FOL receptors in tumors have been reported to be 100-300 times higher than those observed in normal tissues [157]. FOL has high affinity for the FOL receptor (especially for FOL receptors alpha) and retains its receptor binding affinity when it is covalently derivatized *via* its gamma-carboxyl group [157, 174, 175]. In view of this, Yoo and Park have functionalized PEG-*b*-PLGA chains with FOL by covalently conjugating the ligand *via* its γ-carboxyl group [176]. The polymer was physically mixed with PEG-*b*-PLGA-DOX and free-DOX to produce targeted micelles. The micelles decreased the tumor growth rate compared to control non-targeted micelles and enhanced the antitumor efficacy when administered at the same dose level. However, selective derivatization through the γ-carboxyl group is difficult to be achieved, thereby decreasing the yield/potency of such systems.

9.2.3.5 Sugars.

One of the most common cancers affecting human is the hepatocarcinoma. The development of liver-targeted drug carriers is therefore highly desirable. Advances in this area rely on the fact that hepatocytes express carbohydrate receptors *i.e.*, asialoglycoprotein receptors (ASGPR), that recognize different sugar moieties such as lactose, galactose or mannose, allowing for liver-specific delivery [177, 178]. Cho and coworkers [179] have prepared paclitaxel-loaded galactose-PEG-*b*-PBLG

micelles, and showed a greater *in vitro* uptake and cytotoxicity of the micelles in an ASGPR-expressing cancer cell line compared to an analogous non-ASGPR expressing cell line. Alternatively, lactose was attached to the surface of PICM for siRNA delivery. The formulation exhibited gene silencing of firefly luciferase expression in HuH-7 cells expressing ASGPR that was comparable to cationic liposomes (oligofectamine) [180].

9.3 PM for oral drug delivery

Drugs administered by the oral route experience a pH gradient as they transit from the stomach to the jejunum. This pH gradient can be exploited to trigger drug release by using PM that exhibit a pH-dependant ionization/dissociation profile. These micelles are typically optimized to present minimal release of the encapsulated drug in the stomach, where the pH is acidic. As the micelles progress through the intestine (pH > 5), however, they become partially or completely ionized, thereby triggering the release of the entrapped drug in the small bowel (where absorption is maximal). Both multimolecular or unimolecular pH-responsive micelles have been reported [75, 181] and differ in their drug release mechanism. In the case of unimolecular systems, drug release is based on a decreased affinity of the ionized core for the encapsulated drug while release from multimolecular micelles further proceeds through micelle dissociation. Leroux and coworkers has shown that copolymers of PEG and poly(alkyl(meth)acrylate-*co*-methacrylic acid) (P(Al(M)A-*co*-MAA)s) display pH-dependent micellization/release behavior in aqueous media [19, 75, 181-183]. The pH-sensitivity of the polymers is conferred by the pendant carboxylic acid groups of the MAA moieties, whereas the self-association into well-

defined core-shell structure is facilitated by the inclusion of the hydrophobic non-ionizable AI(M)A units. pH-dependent release profiles have been recorded for a number of hydrophobic drugs (*i.e.* indomethacin, fenofibrate, progesterone, and candesartan cilexetil (CDN)) using these micelles [19, 75, 181-183]. In rats, the PM were found to improve the oral bioavailability of fenofibrate and CDN. The oral bioavailability of fenofibrate from these self-assemblies was measured to be 156% and 15% greater than a fenofibrate coarse suspension and Lipidil Micro®, respectively [184]. In the case of CDN, the pH-sensitive PM yielded greater AUC compared to the non pH-sensitive PM, the commercial formulation and a CDN powder suspension [183]. These results suggest that pH-sensitive self-assemblies have potential for improving the oral bioavailability of poorly water-soluble drugs. The use of PM for oral administration has been also extended to different cancer therapeutic agents [185, 186].

9.4 Reverse PM

In non-aqueous media, amphiphilic polymers self-assemble into nanostructures, termed reverse PM, presenting a polar core and a hydrophobic shell (Figure 13). These micelles have been used to dissolve hydrophilic compounds (*i.e.* peptides) in non-aqueous solvents (*i.e.* oils). As for PM, the loading capacity of the reverse PM depends on the core size, the hydrophobic/hydrophilic balance and the affinity between the drug and the core segments. Reverse PM have been obtained from unimolecular dentritic [187-189] or hyperbranched structures [190-192] and from the self-assembly of amphiphilic polymers [193, 194]. For instance, it was shown that star-shaped alkylated poly(glycerol methacrylate)s could form multimolecular

micelles in different organic solvents and oils [195-197]. The assemblies were able to encapsulate hydrophilic dyes, peptides and proteins. As for conventional micelles, premature release of the encapsulated drug can follow from the rapid diffusion of the encapsulated molecules and/or the disassembly of the micelles upon dilution. Cross-linking of either the shell [198] or the core [199] comes here again as a promising strategy to improve the stability of the micelles. For instance, core cross-linking of alkylated poly(glycerol methacrylate)s reverse PM with divinyl sulphone allowed for enhanced retention of the encapsulated dye without compromising the loading capacity (Figure 13) [199].

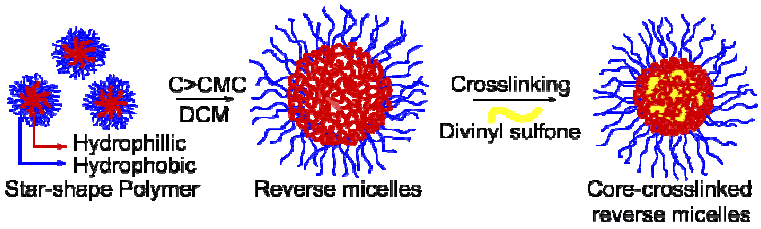

Figure 13. Assembly of reverse PM in organic solvent (CH_2Cl_2 (DCM)) and crosslinking of the micelle core.

10. Conclusion

Micelles are a promising nanomedicine platform for drug delivery. These core-shell self-assemblies can be tailored to increase the solubility of poorly water-soluble drugs just as protect labile hydrophilic drugs from premature degradation. Because of their nanometer size and hydrated outer layer, micelles can prolong the circulation time of an encapsulated drug and passively accumulate at tumor sites, thereby reducing its systemic toxicity and enhancing its efficacy. Micelles that actively target tissues can also be prepared by utilizing stimuli-responsive components or by

attaching recognition groups at their surface. It must be emphasized that the polymeric carriers need to be stable and retain the encapsulated drug long enough for any of these applications to be achievable. To this end, both the thermodynamic stability and kinetic stability of the micelles can be improved by varying the nature of the hydrophobic block, increasing the hydrophobic/hydrophilic balance, increasing the hydrophobic block length or by accommodating hydrophobic molecules in the core. Alternatively, micelle stabilization can be achieved by cross-linking either the core or the corona of pre-formed micelles, by preparing crystalline micelles or by designing intrinsically stable UPM. The parameters affecting micelle stability, however, need to be carefully optimized as many also affect and influence the extent of drug solubilization, release kinetics and the pharmaceutical outcome.

While many progresses have been achieved to modulate the stability and stimuli-responsiveness of PM *in vitro*, many of the strategies put forth remain to be tested *in vivo* to demonstrate real control over the pharmacological properties of the encapsulated drugs. In view of the conflicting structural requirements for micelle stability and drug release, future work should focus on the development and clinical application of multifunctional yet easy to formulate micelles capable of delivering drugs at target sites in a controlled/triggered fashion. In the end, PM rise as very attractive drug delivery systems in that their physicochemical properties and *in vivo* fate are interrelated, creating opportunities for their performance to be fine-tuned.

11. Acknowledgements

Financial support from the Natural Sciences and Engineering Research Council of Canada and Canada Research Chair Program is acknowledged.

12. References

[1] Jones, M. C. & Leroux, J. C. *Eur. J. Pharm. Biopharm.* **48,** 101-111 (1999).

[2] Ardavanis, A., Tryfonopoulos, D., Yiotis, I., Gerasimidis, G., Baziotis, N. & Rigatos, G. *Anticancer Drugs* **15,** 581-585 (2004).

[3] Torchilin, V. P. *Cell. Mol. Life Sci.* **61,** 2549-2559 (2004).

[4] Kim, S. H., Jeong, J. H., Mok, H., Lee, S. H., Kim, S. W. & Park, T. G. *Biotechnol. Prog.* **23,** 232-237 (2007).

[5] Le Garrec, D., Taillefer, J., van Lier, J. E., Lenaerts, V. & Leroux, J. C. *J. Drug Target.* **10,** 429-437 (2002).

[6] Taillefer, J., Brasseur, N., van Lier, J. E., Lenaerts, V., Le Garrec, D. & Leroux, J. C. *J. Pharm. Pharmacol.* **53,** 155-166 (2001).

[7] Nakayama, M. & Okano, T. *Biomacromolecules* **6,** 2320-2327 (2005).

[8] Chung, J. E., Yokoyama, M., Yamato, M., Aoyagi, T., Sakurai, Y. & Okano, T. *J. Control. Release* **62,** 115-127 (1999).

[9] Rijcken, C. J., Soga, O., Hennink, W. E. & van Nostrum, C. F. *J. Control. Release* **120**, 131-148 (2007).

[10] Oishi, M., Kataoka, K. & Nagasaki, Y. *Bioconjugate Chem.* **17,** 677-688 (2006).

[11] Fukushima, S., Miyata, K., Nishiyama, N., Kanayama, N., Yamasaki, Y. & Kataoka, K. *J. Am. Chem. Soc.* **127,** 2810-2811 (2005).

[12] Nishiyama, N, & Kataoka, K. *Pharmacol. Ther.* **112,** 630-648 (2006).

[13] Atkins, P. W. Macromolecules and colloids, Physical Chemistry, Oxford University Press, New York, pp. 679-714 (1997).

[14] Kakizawa, Y. & Kataoka, K. *Adv. Drug Deliv. Rev.* **54,** 203-222 (2002).

[15] Allen, C., Maysinger, D. & Eisenberg, A. *Colloid Surf. B-Biointerfaces* **16,** 3-27 (1999).

[16] Miwa, A., Ishibe, A., Nakano, M., Yamahira, T., Itai, S., Jinno, S. & Kawahara, H. *Pharm. Res.* **15,** 1844-1850 (1998).

[17] Akiyoshi, K., Kobayashi, S., Shichibe, S., Mix, D., Baudys, M., Kim, S. W. & Sunamoto, J. *J. Control. Release* **54,** 313-320 (1998).

[18] Lavasanifar, A., Samuel, J. & Kwon, G. S. *Adv. Drug Deliv. Rev.* **54,** 169-190 (2002).

[19] Benahmed, A., Ranger, M. & Leroux, J. C. *Pharm. Res.* **18,** 323-328 (2001).

[20] Luo, L., Ranger, M., Lessard, D. G., Garrec, D. L., Gori, S., Leroux, J. C., Rimmer, S. & Smith, D. *Macromolecules* **37,** 4008 – 4013 (2004).

[21] Kim, I. S., Jeong, Y. I., Cho, C. S. & Kim, S. H. *Int. J. Pharm.* **211,** 1-8 (2000).

[22] Kim, C., Lee, S. C., Kwon, I. C., Chung, H. & Jeong, S. Y. *Macromolecules* **35,** 193-200 (2002).

[23] Inoue, T., Chen, G., Nakamae, K. & Hoffman, A. S. *J. Control. Release* **51,** 221-229 (1998).

[24] Torchilin, V. P. & Trubetskoy, V. S. *Adv. Drug Deliv. Rev.* **16,** 141-155 (1995).

[25] Savic, R., Luo, L., Eisenberg, A. & Maysinger, D. *Science* **300,** 615-618 (2003).

[26] Lele, B. S. & Leroux, J. C. *Polymer* **43,** 5595-5606 (2002).

[27] Oh, I., Lee, K., Kwon, H. Y., Lee, Y. B., Shin, S. C., Cho, C. S. & Kim, C. K. *Int. J. Pharm.* **181,** 107-115 (1999).

[28] Lavasanifar, A., Samuel, J. & Kwon, G. S. *J. Control. Release* **77,** 155-160 (2001).

[29] Kabanov, A., Lemieux, P., Vinogradov, S. & Alakhov, V. *Adv. Drug Deliv. Rev.* **54,** 223-233 (2002).

[30] Ranger, M., Jones, M. C., Yessine, M. A. & Leroux, J. C. *J. Polym. Sci. Polym. Chem.* **39,** 3861–3874 (2001).

[31] Torchilin, V. P. *Pharm. Res.* **24,** 1-16 (2007).

[32] Lukyanov, A. N. & Torchilin, V. P. *Adv. Drug Deliv. Rev.* **56,** 1273-1289 (2004).

[33] Torchilin, V. P., Levchenko, T. S., Whiteman, K. R., Yaroslavov, A. A., Tsatsakis, A. M., Rizos, A. K., Michailova, E. V. & Shtilman, M. I. *Biomaterials* **22,** 3035-3044 (2001).

[34] Harada, A., Togawa, H. & Kataoka, K. *Eur. J. Pharm. Sci.* **13,** 35-42 (2001).

[35] Vinogradov, S., Batrakova, E., Li, S. & Kabanov, A. *Bioconjugate Chem.* **10,** 851-860 (1999).

[36] Schiffelers, R. M., Ansari, A., Xu, J., Zhou, Q., Tang, Q., Storm, G., Molema, G., Lu, P. Y., Scaria, P. V. & Woodle, M. C. *Nucleic Acids Res.* **32,** e149 (2004).

[37] Woodle, M. C., Scaria, P., Ganesh, S., Subramanian, K., Titmas, R., Cheng, C., Yang, J., Pan, Y., Weng, K., Gu, C. & Torkelson, S. *J. Control. Release* **74,** 309-311 (2001).

[38] Dufresne, M. H. & Leroux, J. C. *Pharm. Res.* **21,** 160-169 (2004).

[39] Rungsardthong, U., Deshpande, M., Bailey, L., Vamvakaki, M., Armes, S. P., Garnett, M. C. & Stolnik, S. *J. Control. Release* **73,** 359-380 (2001).

[40] Harada, A. & Kataoka, K. *Macromolecules* **31,** 288-294 (1998).

[41] Zhang, G. D., Nishiyama, N., Harada, A., Jiang, D. L., Aida, T. & Kataoka, K. *Macromolecules* **36,** 1304-1309 (2003).

[42] Jeong, J. H., Kim, S. W. & Park, T. G. *J. Control. Release* **93,** 183-191 (2003).

[43] Jeong, J. H., Kim, S. H., Kim, S. W. & Park, T. G. *Bioconjugate Chem.* **16,** 1034-1037 (2005).

[44] Jeong, J. H., Kim, S. W. & Park, T. G. *Bioconjugate Chem.* **14,** 473-479 (2003).

[45] Kim, S. H., Jeong, J. H., Lee, S. H., Kim, S. W. & Park, T.G. *J. Control. Release* **116,** 123-129 (2006).

[46] Dufresne, M.H., Fournier, E., Jones, M.-C., Ranger, M. & Leroux, J.C. *Challenge in drug delivery for the new millennium*. R. Gurny (Ed.). Saint-Priest, Bulletin technique Gattefossé **96,** 87-102 (2003).

[47] Gaucher, G., Dufresne, M. H., Sant, V. P., Kang, N., Maysinger, D. & Leroux, J. C. *J. Control. Release* **109,** 169-188 (2005).

[48] Elsabahy, M., Perron, M., Bertrand, N., Yu, G. & Leroux, J. C. *Biomacromolecules* **8,** 2250-2257 (2007).

[49] Yan, H., Kawamitsu, H., Kushi, Y., Kuwajima, T., Ishii, K. & Toshima, N. *J. Colloid Interface Sci.* **315,** 94-98 (2007).

[50] Li, X., Wettig, S. D. & Verrall, R. E. *J. Colloid Interface Sci.* **282,** 466-477 (2005).

[51] Laukkanen, A., Valtola, L., Winnik, F. M. & Tenhu, H. *Polymer* **46,** 7055–7065 (2005).

[52] Wettig, S. D., Nowak, P. & Verrall, R. E. *Langmuir* **18,** 5354-5359 (2002).

[53] Yessine, M. A., Dufresne, M. H., Meier, C., Petereit, H. U. & Leroux, J. C. *Bioconjugate Chem.* **18,** 1010-1014 (2007).

[54] Kwon, G. S. & Kataoka, K. *Adv. Drug Deliv. Rev.* **16,** 295-309 (1995).

[55] Nakagawa, T. *Colloid Polym. Sci.* **252**, 56-64 (1974).

[56] Carstens, M. G., Rijcken, C. J. F., Nostrum, C. F. & Hennink, W. E. in: Torchilin, V. (Ed.), *Multifunctional Pharmaceutical Nanocarriers*, Springer, New York, pp. 263-308 (2008).

[57] Creutz, S., van Stam, J., De Schryver, F. C. & Jérôme, R. *Macromolecules* **31,** 681-689 (1998).

[58] Kang, N., Perron, M. E., Prud'homme, R. E., Zhang, Y., Gaucher, G. & Leroux, J. C. *Nano Lett.* **5,** 315-319 (2005).

[59] Lavasanifar, A., Samuel, J. & Kwon, G. S. *Colloid Surf. B-Biointerfaces* **22,** 115-126 (2001).

[60] Zhange, X., Jackson, J. K. & Burt, H. M. *Int. J. Pharm.* **132,** 195-206 (1996).

[61] Kataoka, K., Matsumoto, T., Yokoyama, M., Okano, T., Sakurai, Y., Fukushima, S., Okamoto, K. & Kwon, G. S. *J. Control. Release* **64,** 143-153 (2000).

[62] Yokoyama, M., Fukushima, S., Uehara, R., Okamoto, K., Kataoka, K., Sakurai, Y. & Okano, T. *J. Control. Release* **50,** 79-92 (1998).

[63] Sundaram, S., Lee, L. K. & Roth, C. M. *Nucleic Acids Res.* **35,** 4396-4408 (2007).

[64] Dufresne, M.H., Elsabahy, M. & Leroux J.C. *Pharm. Res.* **25,** 2083-2093 (2008).

[65] Gary, D. J., Puri, N. & Won, Y. Y. *J. Control. Release* **121,** 64-73 (2007).

[66] Elsabahy, M., Zhang, M., Gan, S., Waldron, K. C. & Leroux, J. C. *Soft Matter* **4,** 294-302 (2008).

[67] Kim, J. H., Emoto, K., Iijima, M., Nagasaki, Y., Aoyagi, T., Okano, T., Sakurai, Y. & Kataoka, K. *Adv. Polym. Technol.* **10,** 647-654 (1999).

[68] Iijima, M., Nagasaki, Y., Okada, T., Kato, M. & Kataoka, K. *Macromolecules* **32,** 1140-1146 (1999).

[69] Kakizawa, Y., Harada, A. & Kataoka, K. *Biomacromolecules* **2,** 491-497 (2001).

[70] O'Reilly, R. K., Hawker, C. J. & Wooley, K. L. *Chem. Soc. Rev.* **35**, 1068-1083 (2006).

[71] Liu, S., Weaver, J. V. M., Tang, Y. T., Billingham, N. C. & Armes, S. P. *Macromolecules* **35,** 6121-6131 (2002).

[72] Bütün, V., Wang, X. S., de Paz Banez, M. V., Robinson, K. L., Billingham, N. C., Armes, S. P. & Tuzar, Z. *Macromolecules* **33,** 1-3 (2000).

[73] Chan, Y., Wong, T., Byrne, F., Kavallaris, M. & Bulmus, V. *Biomacromolecules* **9,** 1826-1836 (2008).

[74] Hawker, C. J., Wooley, K. L. & Fréchet, J. M. *J. Chem. Soc. Perkin Trans. I* **1**, 1287-1297 (1993).

[75] Jones, M. C., Ranger, M. & Leroux, J. C. *Bioconjugate Chem.* **14,** 774-781 (2003).

[76] Fairclough, J. P. A., Norman, A. I., Shaw, B., Nace, V. M. & Heenan, R. K. *Polym. Int.* **55,** 793-797 (2006).

[77] Liu, L., Gao, X., Cong, Y., Li, B. & Han, Y, *Macromol. Rapid Commun.* **27,** 260-265 (2006).

[78] Castelletto, V. & Hamley, I. W. *Adv. Polym. Technol.* **17,** 137-144 (2006).

[79] Norman, A. I., Ho, D. L., Lee, J. H. & Karim, A. *J. Phys. Chem. B* **110,** 62-67 (2006).

[80] Israelachvili, J. N. Intermolecular and surface forces: with applications to colloidal and biological systems, Academic Press, London; Toronto, pp. 296 (1985).

[81] Tanford, C. The hydrophobic effect: formation of micelles and biological membranes, Wiley, New York, pp.233 (1980).

[82] Yang, Z., Crothers, M., Attwood, D., Collett, J. H., Ricardo, N. M. P. S., Martini, L. G. A. & Booth, C. *Colloid Interface Sci.* **263,** 312-317 (2003).

[83] Geng, Y., Dalhaimer, P., Cai, S., Tsai, R., Tewari, M., Minko, T. & Discher, D. E. *Nat. Nanotechnol.* **2,** 249-255 (2007).

[84] Kim, Y., Dalhaimer, P., Christian, D. A. & Discher, D. E. *Nanotechnology* **16,** S484–S491 (2005).

[85] Dalhaimer, P., Engler, A. J., Parthasarathy, R. & Discher, D. E. *Biomacromolecules* **5,** 1714-1719 (2004).

[86] Choucair, A. & Eisenberg, A. *Eur. Phys. J. E* **10,** 37-44 (2003).

[87] Discher, D. E. & Eisenberg, A. *Science* **297,** 967-973 (2002).

[88] Cai, S., Vijayan, K., Cheng, D., Lima, E. M. & Discher, D. E. *Pharm. Res.* **24,** 2099-2109 (2007).

[89] Stauch, O., Schubert, R., Savin, G. & Burchard, W. *Biomacromolecules* **3,** 565-578 (2002).

[90] Schuch, H., Klingler, J., Rossmanith, P., Frechen, T., Gerst, M., Feldthusen, J., & Muller, A. H. *Macromolecules* **33,** 1734-1740 (2000).

[91] Müller, A. & Burchard, W. *Colloid Polym. Sci.* **273,** 866-875 (1995).

[92] Yasugi, K., Nagasaki, Y., Kato, M. & Kataoka, K. *J. Control. Release* **62,** 89-100 (1999).

[93] Shen, H. & Eisenberg, A. *J. Phys. Chem. B.* **103,** 9473-9487 (1999).

[94] Ding, K., Alemdaroglu, F. E., Borsch, M., Berger, R. & Herrmann, A. *Angew. Chem. Int. Ed. Engl.* **46,** 1172-1175 (2007).

[95] Chim, Y. T., Lam, J. K., Ma, Y., Armes, S. P., Lewis, A. L., Roberts, C. J., Stolnik, S., Tendler, S. J. & Davies, M. C. *Langmuir* **21,** 3591-3598 (2005).

[96] Crothers, M., Zhou, Z., Ricardo, N. M., Yang, Z., Taboada, P., Chaibundit, C., Attwood, D. & Booth, C. *Int. J. Pharm.* **293,** 91-100 (2005).

[97] Chaibundit, C., Ricardo, N. M. P. S., Crothers, M. & Booth, C. *Langmuir* **18,** 4277-4283 (2002).

[98] Fournier, E., Dufresne, M. H., Smith, D. C., Ranger, M. & Leroux, J. C. *Pharm. Res.* **21,** 962-968 (2004).

[99] Nagarajan, R., Barry, M. & Ruckenstein, E. *Langmuir* **2,** 210-215 (1986).

[100] Liu, J., Xiao, Y. & Allen, C. *J. Pharm. Sci.* **93,** 132-143 (2004).

[101] Krishna, A. K. & Flanagan, D. R. *J. Pharm. Sci.* **78,** 574-576 (1989).

[102] Choucair, A. & Eisenberg, A. *J. Am. Chem. Soc.* **125**, 11993-12000 (2003).

[103] Taylor, L. S. & Zografi, G. *Pharm. Res.* **14,** 1691-1698 (1997).

[104] Torchilin, V.P. *J. Control. Release* **73,** 137-172 (2001).

[105] Müller, R. H., Radtke, M. & Wissing, S. A. *Adv. Drug Deliv. Rev.* **54,** S131-S155 (2002).

[106] Nakanishi, T., Fukushima, S., Okamoto, K., Suzuki, M., Matsumura, Y., Yokoyama, M., Okano, T., Sakurai, Y. & Kataoka, K. *J. Control. Release* **74,** 295-302 (2001).

[107] Yokoyama, M., Satoh, A., Sakurai, Y., Okano, T., Matsumura, Y., Kakizoe, T. & Kataoka, K. *J. Control. Release* **55,** 219-229 (1998).

[108] Kwon, G., Naitob, M., Yokoyamac, M., Okanoc, T., Sakuraic, Y. & Kataoka, K. *J. Control. Release* **48,** 195-201 (1997).

[109] Jeong, J. H. & Park, T. G. *Bioconjugate Chem.* **12,** 917-923 (2001).

[110] Jeong, Y. I., Cheon, J. B., Kim, S. H., Nah, J. W., Lee, Y. M., Sung, Y. K., Akaike, T. & Cho, C. S. *J. Control. Release* **51,** 169-178 (1998).

[111] Teng, Y., Morrison, M. E., Munk, P. & Webber, S. E. *Macromolecules* **31,** 3578-3587 (1998).

[112] Rösler, A., Vandermeulen, G. W. M. & Klok, H. A. *Adv. Drug Deliv. Rev*. **53,** 95-108 (2001).

[113] Shi, B., Fang, C., You, M. X., Zhang, Y., Fu, S. & Pei, Y. *Colloid Polym. Sci.* **283**, 954–967 (2005).

[114] Savic, R., Azzam, T., Eisenberg, A. & Maysinger, D. *Langmuir* **22,** 3570-3578 (2006).

[115] Burt, H. M., Zhang, X., Toleikis, P., Embree, L. & Hunter, W. L. *Colloid Surf. B-Biointerfaces* **16,** 161–171 (1999).

[116] Chen, H., Kim, S., He, W., Wang, H., Low, P. S. Park, K., Cheng, J. X. *Langmuir* **24,** 5213-5217 (2008).

[117] Gao, Z., Fain, H. D. & Rapoport, N. *Mol. Pharm.* **1,** 317-330 (2004).

[118] Gao, Z., Fain, H. D. & Rapoport, N. *J. Control. Release* **102,** 203-222 (2005).

[119] Tannock, I. F. & Rotin, D. *Cancer Res.* **49,** 4373-4384 (1989).

[120] Schild, H. G. & Tirrell, D. A. *Langmuir* **7,** 1319-1324 (1991).

[121] Gillies, E. R. & Frechet, J. M. *Bioconjugate Chem.* **16,** 361-368 (2005).

[122] Gillies, E. R., Jonsson, T. B. & Frechet, J. M. *J. Am. Chem. Soc.* **126,** 11936-11943 (2004).

[123] Chung, J. E., Yokoyama, M., Aoyagi, T., Sakurai, Y. & Okano T. *J. Control. Release* **53,** 119-130 (1998).

[124] Chen, G. & Hoffman, A. S. *Nature* **373,** 49-52 (1995).

[125] Taillefer, J., Jones, M. C., Brasseur, N., van Lier, J. E. & Leroux, J. C. *J. Pharm. Sci.* **89,** 52-62 (2000).

[126] Coussens, L. M. & Werb, Z. *Nature* **420,** 860-867 (2002).

[127] Rehor, A., Schmoekel, H., Tirelli, N. & Hubbell, J. A. *Biomaterials* **29**, 1958-1966 (2008).

[128] Rehor, A., Hubbell, J. A. & Tirelli, N. *Langmuir* **21,** 411-417 (2005).

[129] Lee, S. H., Kim, S. H. & Park, T. G. *Biochem. Biophys. Res. Commun.* **357,** 511-516 (2007).

[130] Sonawane, N. D., Szoka, F. C. & Verkman, A. S. *J. Biol. Chem.* **278,** 44826-44831 (2003).

[131] Akinc, A., Thomas, M., Klibanov, A. M. & Langer, R. *J. Gene. Med.* **7,** 657-663 (2005).

[132] De Smedt, S. C., Demeester, J. & Hennink, W. E. *Pharm. Res.* **17,** 113-126 (2000).

[133] Cho, Y. W., Kim, J. D. & Park, K. *J. Pharm. Pharmacol.* **55,** 721-734 (2003).

[134] Kabanov, A. V., Bronich, T. K., Kabanov, V. A., Yu, K. & Eisenberg, A. *Macromolecules* **29,** 6797-6802 (1996).

[135] Itaka, K., Kanayama, N., Nishiyama, N., Jang, W. D., Yamasaki, Y., Nakamura, K., Kawaguchi, H. & Kataoka, K. *J. Am. Chem. Soc.* **126,** 13612-13613 (2004).

[136] Chen, H., Kim, S., Li, L., Wang, S., Park, K. & Cheng, J. X. *Proc. Natl. Acad. Sci. U.S.A.* **105**, 6596-6601 (2008).

[137] Li, S. D. & Huang, L. *Gene Ther.* **13,** 1313-1319 (2006).

[138] Sutton, D., Nasongkla, N., Blanco, E. & Gao, J. *Pharm. Res.* **24,** 1029-1046 (2007).

[139] Torchilin, V. P. *Annu. Rev. Biomed. Eng.* **8,** 343-375 (2006).

[140] Savic, R., Eisenberg, A. & Maysinger, D. *J. Drug Target.* **14,** 343-355 (2006).

[141] Danson, S., Ferry, D., Alakhov, V., Margison, J., Kerr, D., Jowle, D., Brampton, M., Halbert, G. & Ranson, M. *Br. J. Cancer* **90,** 2085-2091 (2004).

[142] Matsumura, Y., Hamaguchi, T., Ura, T., Muro, K., Yamada, Y., Shimada, Y., Shirao, K., Okusaka, T., Ueno, H., Ikeda, M. & Watanabe, N. *Br. J. Cancer* **91,** 1775-1781 (2004).

[143] Kim, T. Y., Kim, D. W., Chung, J. Y., Shin, S. G., Kim, S. C., Heo, D. S., Kim, N. K. & Bang, Y. J. *Clin. Cancer Res.* **10,** 3708-3716 (2004).

[144] Alakhov, V., Klinski, E., Li, S., Pietrzynski, G., Venne, A., Batrakova, E., Bronitch, T. & Kabanov, A. *Colloid Surf. B-Biointerfaces* **16,** 113-134 (1999).

[145] Hamaguchi, T., Matsumura, Y., Suzuki, M., Shimizu, K., Goda, R., Nakamura, I., Nakatomi, I., Yokoyama, M., Kataoka, K. & Kakizoe, T. *Br. J. Cancer* **92**, 1240-1246 (2005).

[146] Mizumura, Y., Matsumura, Y., Hamaguchi, T., Nishiyama, N., Kataoka, K., Kawaguchi, T., Hrushesky, W. J. M., Moriyasu, F. & Kakizoe, T. *Jpn. J. Cancer Res.* **92,** 328-336 (2001).

[147] Uchino, H., Matsumura, Y., Negishi, T., Koizumi, F., Hayashi, T., Honda, T., Nishiyama, N., Kataoka, K., Naito, S. & Kakizoe, T. *Br. J. Cancer* **93,** 678-687 (2005).

[148] Kim, S. C., Kim, D. W., Shim, Y. H., Bang, J. S., Oh, H. S., Kim, S. W. & Seo, M. H. *J. Control. Release* **72,** 191-202 (2001).

[149] Le Garrec, D., Gori, S., Luo, L., Lessard, D., Smith, D. C., Yessine, M. A., Ranger, M. & Leroux, J. C. *J. Control. Release* **99,** 83-101 (2004).

[150] Adams, M. L., Andes, D. R. & Kwon, G. S. *Biomacromolecules* **4,** 750-757 (2003).

[151] Lee, K. S., Chung, H. C., Im, S. A., Park, Y. H., Kim, C. S., Kim, S. B., Rha, S. Y., Lee, M. Y. & Ro, J. *Breast Cancer Res. Treat.* **108,** 241-250 (2008).

[152] Kim, D. W., Kim, S. Y., Kim, H. K., Kim, S. W., Shin, S. W., Kim, J. S., Park, K., Lee, M. Y., Heo, D. S. *Ann. Oncol.* **18**, 2009-2014 (2007).

[153] Engin, K., Leeper, L. D., Cater, J. R., Thistlethwaite, A. J., Tupchong, L. & McFarlane, J. D. *Int. J. Hyperthermia* **11,** 211-216 (1995).

[154] Helmlinger, G., Yuan, F., Dellian, M. & Jain, R. K. *Nat. Med.* **3,** 177-182 (1997).

[155] Bae, Y., Diezi, T. A., Zhao, A. & Kwon, G. S. *J. Control. Release* **122**, 324-330 (2007).

[156] De Jaeghere, F., Allémann, E., Feijen, J., Kissel, T., Doelker, E. & Gurny, R. *J. Drug Target.* **8,** 143-153 (2000).

[157] Ross, J. F., Chaudhuri, P. K. & Ratnam, M. *Cancer* **73,** 2432-2443 (1994).

[158] Ulbrich, K., Etrych, T., Chytil, P., Jelinkova, M. & Rihova, B. *J. Control. Release* **87,** 33-47 (2003).

[159] Merdan, T., Callahan, J., Petersen, H., Kunath, K., Bakowsky, U., Kopeckova, P., Kissel, T. & Kopecek, J. *Bioconjugate Chem.* **14,** 989-996 (2003).

[160] Nah, J. W., Yu, L., Han, S. O., Ahn, S. H. & Kim, S. W. *J. Control. Release* **78,** 273-284 (2002).

[161] Farokhzad, O. C., Jon, S., Khademhosseini, A., Tran, T. N., Lavan, D. A. & Langer, R. *Cancer Res.* **64**, 7668-7672 (2004).

[162] Farokhzad, O. C., Cheng, J., Teply, B. A., Sherifi, I., Jon, S., Kantoff, P. W., Richie, J. P. & Langer, R. *Proc. Natl. Acad. Sci. U.S.A.* **103,** 6315-6320 (2006).

[163] Lim, D. W., Yeom, Y. I. & Park, T. G. *Bioconjugate Chem.* **11,** 688-695 (2000).

[164] Singh, M. *Curr. Pharm. Design* **5**, 443-451 (1999).

[165] King, G. L. & Feener, E. P. *Adv. Drug Deliv. Rev.* **29**, 197-213 (1998).

[166] Qian, Z. M., Li, H., Sun, H. & Ho, K. *Pharmacol. Rev.* **54**, 561-587 (2002).

[167] Allen, T. M. *Nat. Rev. Cancer* **2**, 750-763 (2002).

[168] Torchilin, V. P., Lukyanov, A. N., Gao, Z. & Papahadjopoulos-Sternberg, B. *Proc. Natl. Acad. Sci. U.S.A.* **100,** 6039-6044 (2003).

[169] Ellington, A. D. & Szostak, J. W. *Nature* **346**, 818-822 (1990).

[170] Lupold, S. E., Hicke, B. J., Lin, Y. & Coffey, D. S. *Cancer Res.* **62**, 4029-4033 (2002).

[171] Hu-Lieskovan, S., Heidel, J. D., Bartlett, D. W., Davis, M. E. & Triche, T. G. *Cancer Res.* **65,** 8984-8992 (2005).

[172] Mizejewski, G. J. *Proc. Soc. Exp. Biol. Med.* **222,** 124-138 (1999).

[173] Nasongkla, N., Shuai, X., Ai, H., Weinberg, B. D., Pink, J., Boothman, D. A. & Gao, J. *Angew. Chem. Int. Ed. Engl.* **43,** 6323-6327 (2004).

[174] Guo, W. & Lee, R. L. *AAPS Pharm. Sci.* **1,** E19 (1999).

[175] Kamen, B. A. & Smith, A. K. *Adv. Drug Deliv. Rev.* **56**, 1085-1097 (2004).

[176] Yoo, H. S. & Park, T. G. *J. Control. Release* **96,** 273-283 (2004).

[177] Jule, E., Nagasaki, Y. & Kataoka, K. *Bioconjugate Chem.* **14,** 177-186 (2003).

[178] Sugahara, K., Togashi, H., Takahashi, K., Onodera, Y., Sanjo, M., Misawa, K., Suzuki, A., Adachi, T., Ito, J., Okumoto, K., Hattori, E., Takeda, T., Watanabe, H., Saito, K., Saito, T., Sugai, Y. & Kawata, S. *Hepatology* **38,** 1401-1409 (2003).

[179] Jeong, Y. I., Seo, S. J., Park, I. K., Lee, H. C., Kang, I. C., Akaike, T. & Cho, C. S. *Int. J. Pharm.* **296,** 151-161 (2005).

[180] Oishi, M., Nagasaki, Y., Itaka, K., Nishiyama, N. & Kataoka, K. *J. Am. Chem. Soc.* **127,** 1624-1625 (2005).

[181] Sant, V. P., Smith, D. & Leroux, J. C. *J. Control. Release* **97,** 301-312 (2004).

[182] Satturwar, P., Eddine, M. N., Ravenelle, F. & Leroux, J. C. *Eur. J. Pharm. Biopharm.* **65**, 379-387 (2007).

[183] Satturwar, P., Gaucher. G, Jones. M. C., Furtos. A. & Leroux. J. C. In: Lavasanifar A and Arshady R (Ed.). *Polymeric Micelles and Related Nanodelivery Systems*, Kentus Books, London, in press (2008).

[184] Sant, V. P., Smith, D. & Leroux, J. C. *J. Control. Release* **104,** 289-300 (2005).

[185] Bromberg, L. *J. Control. Release* **128**, 99-112 (2008).

[186] Benny, O., Fainaru, O., Adini, A., Cassiola, F., Bazinet, L., Adini, I., Pravda, E., Nahmias, Y., Koirala, S., Corfas, G., D'Amato, R. J. & Folkman, J. *Nat. Biotechnol* **26,** 799-807 (2008).

[187] Cooper, A. I., Londono, J. D., Wignall, G., McClain, J. B., Samulski, E. T., Lin, J. S., Dobrynin, A., Rubinstein, M., Burke, A. L. C., Frechet, M. J. & DeSimone, J. M. *Nature* **389,** 368-371 (1997).

[188] Sayed-Sweet, Y., Hedstrand, D. M., Spinder, R. & Tomalia, D. A. *J. Mater. Chem.* **7**, 1199-1205 (1997).

[189] Vutukuri, D. R., Basu, S. & Thayumanavan, S. *J. Am. Chem. Soc.* **126**, 15636-15637 (2004).

[190] Sunder, A., Kramer, M., Hanselmann, R., Mulhaupt, R. & Frey, H. *Angew. Chem. Int. Ed. Engl.* **38**, 3552-3555 (1999).

[191] Chen, Y., Shen, Z., Frey, H., Perez-Prieto, J. & Stiriba, S. E. *Chem. Commun.* **6,** 755-757 (2005).

[192] Antonietti, L., Aymonier, C., Schlotterbeck, U., Garamus, V. M., Maksimova, T., Richtering, W. & Mecking, S. *Macromolecules* **38**, 5914-5920 (2005).

[193] Teng, J. & Zubarev, E. R. *J. Am. Chem. Soc.* **125**, 11840-11841 (2003).

[194] Xu, J. & Zubarev, E. R. *Angew. Chem. Int. Ed. Engl.* **43,** 5491-5496 (2004).

[195] Jones, M. C., Gao, H. & Leroux, J. C. *J. Control. Release* **132**, 208-215 (2008).

[196] Jones, M. C., Tewari, P., Blei, C., Hales, K., Pochan, D. J. & Leroux, J. C. *J. Am. Chem. Soc.* **128**, 14599-14605 (2006).

[197] Gao, H., Jones, M. C., Tewari, P., Ranger, M. & Leroux, J. C. *J. Polym. Sci. Polym. Chem.* **45,** 2425–2435 (2007).

[198] Babin, J., Lepage, M. & Zhao, Y. *Macromolecules* **41,** 1246-1253 (2008).

[199] Gao, H., Jones, M. C., Chen, J., Prud'homme, R. E. & Leroux, J. C. *Chem. Mat.* **20,** 3063–3067 (2008).

[200] Segura, T. & Hubbell, J. A. *Bioconjugate Chem.* **18,** 736-745 (2007).

[201] Yoo, H. S., Lee, E. A. & Park, T. G. *J. Control. Release* **82,** 17-27 (2002).

[202] Venne, A., Li, S., Mandeville, R., Kabanov, A. & Alakhov, V. *Cancer Res.* **56,** 3626-3629 (1996).

[203] Bae, Y., Nishiyama, N., Fukushima, S., Koyama, H., Yasuhiro, M. & Kataoka, K. *Bioconjugate Chem.* **16,** 122-130 (2005).

[204] Nishiyama, N., Kato, Y., Sugiyama, Y. & Kataoka, K. *Pharm. Res.* **18,** 1035-1041 (2001).

[205] Nishiyama, N., Yokoyama, M., Aoyagi, T., Okano, T., Sakurai, Y. & Kataoka, K. *Langmuir* **15,** 377 -383 (1999).

[206] Batrakova, E. V., Miller, D. W., Li, S., Alakhov, V. Y., Kabanov, A. V. & Elmquist, W. F. *J. Pharmacol. Exp. Ther.* **296,** 551-557 (2001).

Objectives and hypotheses of the thesis

In this thesis, two types of polymeric micelles (PM) have been developed for the delivery of anticancer drugs (*i.e.* docetaxel) and nucleic acids (*i.e.* antisense oligonucleotides (AON) and short interfering RNA (siRNA)). The hypothesis of the research program to which this thesis belongs is that polymeric nanocarriers can overcome many disadvantages associated with the conventional formulations, such as toxicity and non-selectivity. More particularly, we assumed that entrapment of docetaxel into PM would increase its water-solubility and afford protection against hydrolytic degradation. In addition, encapsulation of nucleic acids (either AON or siRNA) in polyion complex micelles (PICM) may protect them against enzymatic degradation and increase their intracellular bioavailability.

In **Chapter 3,** poly(ethylene oxide)-*block*-poly(butylene oxide/styrene oxide) micelles were investigated to solubilize and protect docetaxel from hydrolytic degradation. The objectives of this part were to formulate and characterize docetaxel-loaded PM in terms of size, maximum loading capacity and stability against degradation. In addition, we compared the toxicity of the polymers *vs.* the surfactant used commercially to dissolve docetaxel (*i.e.* polysorbate 80).

In **Chapter 4,** poly(ethylene glycol) (PEG)-oligonucleotide conjugates were assessed to protect AON against degradation and to release them in a sustained manner. When these conjugates were mixed with poly(amidoamine) (PAMAM) dendrimers, monodisperse PICM were formed. A fluorimetric assay was undertaken to monitor AON and siRNA degradation. With this assay, it was found that these PICM slowed down AON release and significantly protected it against enzymatic

degradation. In **Chapter 5,** PEG-*block*-poly(*propyl* methacrylate-*co*-methacrylic acid) was exploited to impart pH sensitivity to PAMAM-based PICMs. This system was composed of the previous copolymer mixed with PAMAM dendrimer. Such PICM were loaded with AON or siRNA targeting the Bcl-2 oncogene. Micelle uptake by the cancer cells was mediated by a monoclonal antibody fragment (*i.e.* Fab') positioned at the extremity of the PEG corona. We assumed that upon cellular uptake and protonation of the methacrylic acid units in the acidic endosomal environment, the micelles would lose their corona and expose their positively-charged endosomolytic PAMAM/nucleic acid core. The objective of this part was to test whether these pH-sensitive micelles were able to increase the intracellular bioavailability of AON and siRNA. **Chapter 6** summarizes and discusses the results. Finally, we propose the future work required to enhance the stability and potency of the formulations.

CHAPTER 3 - Solubilization of docetaxel in poly(ethylene oxide)-*block*-poly(butylene/styrene oxide) micelles[2]

Mahmoud Elsabahy[1], Marie-Ève Perron[1], Nicolas Bertrand[1], Ga-er Yu[2] and Jean-Christophe Leroux[1*]

[*]Canada Research Chair in Drug Delivery, [1]Faculty of Pharmacy, University of Montreal, C.P. 6128, Succ. Centre-Ville, Montreal (QC) H3C 3J7, Canada

[2]Advanced Polymer Materials Inc., 5020 Fairway, Suite 224, Montreal (QC) H8T 1B8, Canada

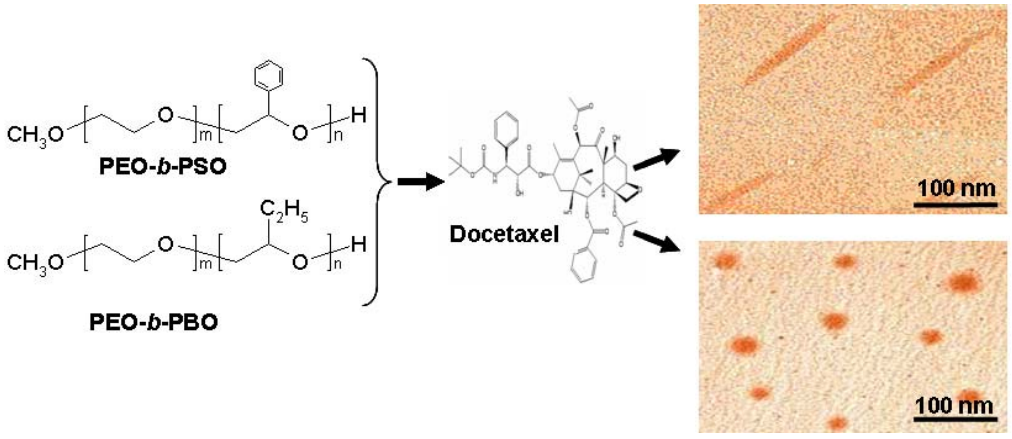

[2]*Biomacromolecules* **8**, 2250-2257 (2007); reproduced with permission from the American Chemical Society.

Abstract

Poly(ethylene oxide)-*block*-poly(styrene oxide) (PEO-*b*-PSO) and PEO-*b*-poly(butylene oxide) (PEO-*b*-PBO) of different chain lengths were synthesized and characterized for their self-assembling properties in water by dynamic/static light scattering, spectrofluorimetry and transmission electron microscopy. The resulting polymeric micelles were evaluated for their ability to solubilize and protect the anticancer drug docetaxel (DCTX) from degradation. The drug release kinetics as well as the cytotoxicity of the loaded micelles were assessed *in vitro*. All polymers formed micelles with a highly viscous core at low critical association concentrations (<10 mg/L). Micelle morphology depended on the nature of the hydrophobic block, with PBO- and PSO-based micelles yielding monodisperse spherical and cylindrical nanosized aggregates, respectively. The maximum solubilization capacity for DCTX ranged from 0.7 to 4.2% and was the highest for PSO micelles exhibiting the longest hydrophobic segment. Despite their high affinity for DCTX, PEO-*b*-PSO micelles were not able to efficiently protect DCTX against hydrolysis under accelerated stability testing conditions. Only PEO-*b*-PBO bearing 24 BO units afforded significant protection against degradation. *In vitro*, DCTX was released slower from the latter micelles but all formulations possessed a similar cytotoxic effect against PC-3 prostate cancer cells. These data suggest that PEO-*b*-P(SO/BO) micelles could be used as alternatives to conventional surfactants for the solubilization of taxanes.

1. Introduction

Docetaxel (DCTX) is an anticancer drug which displays a broad spectrum of antitumor activity. It is currently approved for the treatment of advanced breast cancer, which remains a major cause of morbidity and mortality in women worldwide [1, 2]. Furthermore, it has been used with success in patients with various tumors, including advanced non-small cell lung cancer and ovarian cancer. Due to its poor aqueous solubility, DCTX is currently formulated in polysorbate 80 (Taxotere®). This formulation is devoid of water because DCTX degrades over time in protic solvents [2]. The polysorbate 80 formulation is known to cause severe allergic reactions and peripheral neuropathy [3, 4]. Early clinical studies of Taxotere® revealed that the incidence of hypersensitivity reactions ranged from 5 to 40% [4]. Moreover, after dilution with the hydroalcoholic vehicle provided, the Taxotere® formulation is physically unstable and must be administered to the patient within 8 h.

To overcome the disadvantages of the current formulation and to increase the therapeutic index of DCTX, various colloidal drug carriers, such as emulsions [5], liposomes [6] and nanoparticles [7], are currently being investigated. Likewise, block copolymer micelles have recently attracted considerable attention for the delivery of taxanes [8-12]. In aqueous media, amphiphilic block copolymers can spontaneously self-assemble into nanoscopic core-shell type structures having different morphologies (spheres, small rods, worm-like geometries, etc) [13-16], wherein the hydrophobic blocks form the micelle core and the hydrophilic segments make up the corona. The hydrophobic core serves as a reservoir for poorly water-soluble drugs

while the hydrophilic shell interacts with the biological milieu and can alter the pharmacokinetics and biodistribution of the incorporated drug [17].

Among the different amphiphilic block copolymers that have been evaluated for drug delivery applications, diblock copolymers of poly(ethylene oxide) (PEO) and poly(butylene oxide) (PBO) or poly(styrene oxide) (PSO) are of particular interest. These polymers can self-assemble at low concentrations into micelles of various shapes, depending on relative block lengths, concentration and temperature [18-21]. Their hydrophobic segments exhibit low glass transition temperatures (ca. 40°C), allowing for the incorporation of drugs at temperatures that are compatible with thermolabile agents [22, 23]. Although PSO- and PBO-based copolymer micelles have been characterized in several studies [18-21], their role as solubilizers has been reported only for the antifungal drug griseofulvin, which is of low clinical significance as it is currently administered orally in a micronized form [22, 24].

The aim of this project was to characterize the self-assembling properties of short PEO-*b*-PBOs and PEO-*b*-PSOs and assess their ability to dissolve and chemically protect DCTX. The molecular weight of the PEO segment was fixed at 2000 while the nature and length of the hydrophobic block were varied. The micelles were analyzed by light scattering, transmission electron microscopy (TEM) and fluorescence spectroscopy. The effect of micellar solubilization on the aqueous stability of DCTX was examined by high performance liquid chromatography (HPLC). In addition, drug release and cytotoxicity were also evaluated *in vitro*.

2. Materials

Methoxy-PEO and BO were purchased from Fluka *via* Sigma-Aldrich (Oakville, ON, Canada). Pyrene, SO, polysorbate 80 and 3-[4,5-dimethylthiaolyl]-2,5-diphenyl-tetrazolium bromide (MTT) were procured from Sigma-Aldrich. DCTX was kindly provided by the Shanghai Fudan Taxusal New Technology Co. (Shanghai, China). ^{14}C-labelled docetaxel (60 mCi/mmol) was obtained from American Radiolabeled Chemicals Inc. (St. Louis, MO). 1,3-bis-(1-pyrenyl)propane, RPMI medium, penicillin G and streptomycin were obtained from Invitrogen Canada Co. (Burlington, ON, Canada). 200-mesh copper grids, poly(L-lysine) and uranyl acetate for TEM sample preparation came from Canemco & Marivac Inc. (Montreal, QC, Canada). Franz diffusion cells and membrane filters were purchased from Cole Parmer (Vernon Hills, IL) and Avestin (Ottawa, ON, Canada), respectively. PC-3 prostate cancer cells were purchased from American Type Culture Collection (Manassas, VA). Fetal bovine serum was purchased from Hyclone (Logan, UT). Ultima Gold™ was obtained from Perkin Elmer (Woodbridge, ON, Canada). Deionized water was generated by a Millipore Milli-Q system (Bedford, MA).

3. Methods

3.1 Characterization of unloaded polymeric micelles

3.1.1 Synthesis and characterization of polymers

EO_{45}-SO_{26}, EO_{45}-SO_{15}, EO_{45}-BO_{24} and EO_{45}-BO_{15} (subscripts denote number-average block lengths in repeat units) diblock copolymers were prepared by

sequential oxyanionic polymerization, as described elsewhere [25]. Methoxy-PEO with a number-average molecular weight (M_n) of 2000 was partly converted to its potassium salt to initiate BO and SO polymerization. The monomers were dried over CaH_2, and were vacuum-transferred to ampoules containing activated PEO. The polymerization temperature was set at 80°C. Weight-average molecular weight (M_w) and M_n were determined at 28°C using a Waters gel permeation chromatography (GPC) system equipped with a 1515 isocratic pump and 2410 refractive index detector (Waters, Milford, MA). Choloroform was the eluent and monodisperse PEO was employed as standard. ^{1}H-NMR spectra were recorded on a Bruker ARX400 spectrometer (Bruker, Milton, ON, Canada) in deuterated choloroform. The number of SO and BO units in each polymer was determined by ^{1}H-NMR from Equations 1 and 2, respectively:

$$2(I_{4.2-5.0\,ppm}) + n(4 + \frac{3}{45}) = I_{3.2-3.9\,ppm} \quad (1)$$

$$3(I_{0.8-1.0\,ppm}) + n(4 + \frac{3}{45}) = I_{3.2-3.9\,ppm} \quad (2)$$

In both cases, n refers to the number of EO units while factor 3/45 takes into account the contribution of the methoxy end group of the PEO chain (M_n = 2000). In Equation 1, $I_{4.2\text{-}5.0\,ppm}$ corresponds to the intensity of the methylene proton of the PSO backbone ($OCH_2CH(C_6H_5)$), and was set to 1. In turn, $I_{3.2\text{-}3.9\,ppm}$ corresponds to the intensity of the methylene groups of the PEO chain and methylene protons of the PSO backbone ($OCH_2CH(C_6H_5)$). Solving the equation for n allows the determination of a SO/EO ratio (where SO = 1) that can be balanced for PEO 2000 (45 EO units). Equation 2 is used in a similar fashion. In this case, $I_{0.8\text{-}1.0\,ppm}$

corresponds to the intensity of the methyl protons of the PBO pendant group ($OCH_2CH(CH_2CH_3)$), and was set to 3. On the other hand, $I_{3.2\text{-}3.9\ ppm}$ corresponds to the methylene groups of the PEO and PBO backbones.

3.1.2 Determination of the critical association concentration (CAC)

The apparent CAC of the polymers was estimated by a steady-state pyrene fluorescence method [26], based on shifts of the third excitation band of pyrene from 333 to 336 and 339 nm due to its incorporation in the hydrophobic core of PEO-*b*-PBO and PEO-*b*-PSO micelles, respectively. Serial dilutions of stock solutions of different copolymers were prepared to contain 2 x 10^{-7} M of pyrene and stirred overnight in the dark. Their excitation spectra were recorded at room temperature in an Aminco Bowman Series 2 luminescence spectrometer (Spectronic Instruments Inc., Rochester, NY) at λ_{em} = 390 nm (bandpass = 2 nm). The CAC was determined from the intersection of 2 straight lines (the horizontal line with an almost constant value of the ratio $I_{336\ or\ 339}/I_{333}$, and the vertical line with a steady increase in the ratio value) on the graph of the fluorescence intensity ratio $I_{336\ or\ 339}/I_{333}$ *vs.* log polymer concentration. Experiments were performed in triplicate.

3.1.3 Measurement of core viscosity

1,3-bis-(1-pyrenyl)propane, a hydrophobic probe similar to pyrene, diffuses from an aqueous phase to the hydrophobic core of micelles. Given that the extent of excimer formation depends on the viscosity of the surrounding environment, the ratio

of the excimer to monomer intensity (I_e/I_m) at 376 and 480 nm can be exploited to measure effective micelle core viscosity. 1,3-bis-(1-pyrenyl)propane was dissolved in 5 mL of chloroform to give a final concentration of 2×10^{-7} M. The solvent was then evaporated and replaced by 5 mL of aqueous polymer solutions at concentrations above the CAC (0.5 mg/mL). Sodium dodecyl sulfate (SDS) at 5 mg/mL served as a control, low molecular weight surfactant. The solutions were stirred for 24 h in the dark. The emission spectrum of 1,3-bis-(1-pyrenyl)propane was obtained at room temperature with an Aminco Bowman Series 2 luminescence spectrometer. The excitation wavelength and the emission bandwidth were set at 333 and 4 nm, respectively. All measurements were done in triplicate.

3.1.4 Dynamic light scattering (DLS) measurements

The mean hydrodynamic diameters (d_h) and the polydispersity indices (PDI) of polymeric micelles were measured by DLS with a Malvern Autosizer 4800 instrument (Malvern Instrument, Worcestershire, UK). All samples were filtered (Acrodisc® 13-mm syringe filter with 0.45-µm nylon membrane, Pall Co., Mississauga, ON, Canada) prior to analysis. The different polymers were dissolved in water to a final concentration of 2 mg/mL. Measurements were taken at a fixed scattering angle of 90°. DLS measurements were also performed at different angles (50-140º) to examine micelle sphericity. For spherical particles, diameter is independent of detection angle due to the undetectable rotational motion [27]. The CONTIN program was used to extract size distributions from the autocorrelation functions. Measurements were performed in triplicate at room temperature.

3.1.5 Multiangle static light scattering (MASLS) measurements

Polymer solutions were prepared in Millipore water at room temperature and stirred overnight. All samples were passed through a 0.45-μm nylon filter prior to analysis. Then, samples were subjected to MASLS measurements in a Malvern Autosizer 4800 at 6 angles ranging from 50 to 120°, for 5 polymer concentrations above the CAC (0.25 to 2 mg/mL). The M_ws of the micelles were extracted from Equation 3, which describes the intensity of light scattered from a dilute solution of macromolecules:

$$\frac{Kc}{R_0} = \frac{1}{M_W P(\theta)} + 2A_2 c + 3A_3 c^2 \quad (3)$$

In this equation, c stands for the polymer concentration, R_0 is the Rayleigh ratio of the solution, and A_2 and A_3 are the second and third virial coefficients. K is, in turn, defined by:

$$K = \frac{4\pi^2 n_0^2 \left(\frac{dn}{dc}\right)^2}{\lambda^4 N} \quad (4)$$

where n_0 is the refractive index of the solvent, λ is the laser wavelength *in vacuo*, and N is Avogadro's number. Specific refractive index increments (dn/dc) were determined using a differential Rudolph J157 automatic refractometer (Rudolph Research Analytical, Flanders, NJ), at a wavelength of 589.3 nm. The dn/dc values for EO_{45}-SO_{26}, EO_{45}-SO_{15}, EO_{45}-BO_{24}, and EO_{45}-BO_{15} solutions were 0.160, 0.154, 0.112, and 0.120 cm^3/g, respectively. Aggregation number (N_{agg}) was calculated by dividing micelle M_w by that of the corresponding polymer. Radii of gyration (r_g) were also extracted from MASLS analysis.

3.2 TEM

Copper grids (200 mesh) were coated with a drop of aqueous poly(L-lysine) solution (0.1% *w/v*) 5 min prior to sample deposition to ensure good adhesion between the samples and the grids. Excess solution was wicked off, the grids were allowed to dry, and a drop of different micelle solutions (2 mg/mL) was placed on the grid for 2 min. After the removal of excess solution, a droplet of uranyl acetate (3% *w/v* in water) was added to provide negative staining. After 5 min, the grids were gently washed with water, and excess fluid was removed with filter paper. The samples were then analyzed under a Philips CM100 transmission electron microscope (FEI Company, Tokyo, Japan) operating at 60 kV. Micrographs were taken at a magnification of 50,000.

3.3 Characterization of DCTX-loaded polymeric micelles

3.3.1 Preparation and characterization of DCTX-loaded micelles

Both DCTX and the polymer were dissolved in ethanol. The solvent was then evaporated under vacuum at room temperature, and replaced by Millipore water, and the solutions were stirred overnight prior to analysis. The solutions of drug-loaded micelles were centrifuged (18,000 *g*, 30 min), the supernatant was collected and passed through a 0.2-μm nylon filter. Drug concentration was assayed in the supernatant using a Waters HPLC system equipped with a 1525 binary pump, a 2487 dual wavelength absorbance detector and Breeze chromatography software (Waters, Milford, MA). *N*-heptylbenzamide served as internal standard. The mobile phase

consisted of acetonitrile, methanol and water (48:11:41 *v/v*). The column was Waters Nova-Pack C18 60 Å 4 µm (3.9 × 300 mm). Flow rate, detection wavelength, temperature and injection volume were set at 1 mL/min, 232 nm, 4ºC and 55 µL, respectively. Size analyses were performed by DLS on freshly-prepared micelles and freeze-dried formulations after reconstitution in water.

3.3.2 Determination of the partition coefficient (Kv)

DCTX-loaded micelles were prepared with the drug present in large excess (2 mg) and increasing polymer concentrations (from 2 to 10 mg/mL). The solutions were stirred overnight and then centrifuged (18,000 *g*, 30 min). Drug concentration was assayed in the supernatant with the HPLC method detailed above. K_v values were obtained by plotting the ratio of DCTX solubility in the presence of polymeric micelles (S_{tot}) over that in pure water (S_w = 2 µg/mL) against micellar concentration according to Equation 5 [28]:

$$S_{tot} / S_w = 1 + K_v \,.\, C_{mic} \,.V_m \qquad (5)$$

where C_{mic} is the micellar concentration (defined as the polymer concentration minus the CAC divided by N_{agg}). V_m is given by:

$$V_m = (M_{wmic} . Q_h)/d_h \qquad (6)$$

where V_m is the micellar partial molar volume, M_{wmic} is the micellar molecular weight (as determined by MASLS), and Q_h is the hydrophobic block weight fraction. The density of the core, d_h, was assumed to be that of a homopolymer of the hydrophobic segment of similar molecular weight.

3.4 Chemical stability of DCTX-loaded micelles

DCTX-loaded micelles were subjected to accelerated stability testing by heating the polymer solutions at 50°C for 24 h. The polymer concentrations (5 mg/mL) were kept above the CAC, and the drug concentration was set at 2 μg/mL in all solutions. At scheduled time intervals, samples were withdrawn and assayed by HPLC for intact DCTX, as described above. An aqueous solution of free DCTX was used as control.

3.5 Calculation of solubility parameters by the group contribution method

Total (δ_t) and partial (δ_d, δ_p and δ_h) solubility parameters of the drug, PEO, PBO and PSO blocks were calculated by the following 4 equations according to the group contribution method:

$$\delta_d = \frac{\sum F_{di}}{V} \quad (7)$$

$$\delta_p = \frac{\sqrt{\sum F_{pi}^2}}{V} \quad (8)$$

$$\delta_h = \sqrt{\frac{\sum E_{hi}}{V}} \quad (9)$$

$$\delta_t = \sqrt{\delta_d^2 + \delta_p^2 + \delta_h^2} \quad (10)$$

where F_{di}, F_{pi} and E_{hi} describe the functional group contributions from van der Waals dispersion forces, dipole-dipole interactions and hydrogen bonding, respectively [29]. The total molar volumes (V) of DCTX, PEO, PBO and PSO polymer repeat units were obtained by the Fedors method [30].

3.6 In vitro release kinetics

DCTX-loaded polymeric micelles (0.7% (*w/w*) for EO_{45}-BO_{24}, 0.7 and 3.5% (*w/w*) for EO_{45}-SO_{26}), spiked with ^{14}C-labelled DCTX (2 μCi/mg DCTX) were prepared in phosphate buffered saline (PBS, pH 7.4) as previously described. The release of DCTX from the different formulations was studied by following the time course of drug transfer from the donor to the acceptor compartment using jacketed Franz diffusion cells. Both compartments were separated from each other by two superimposed 50-nm polycarbonate membranes. The release medium was maintained under continuous agitation (700 rpm) and at a constant temperature of 37±0.2°C using a circulating water bath. To ensure sink conditions, DCTX-loaded polymeric micelles were dispersed to a final drug concentration of 0.5 μg/mL in the donor compartment. At various time points, a 200-μL aliquot was withdrawn from the acceptor compartment and replaced by 200 μL of fresh PBS. Ultima Gold™ scintillation cocktail (5 mL) was added to the sample and DCTX was quantified by radioactivity counting (Liquid Scintillation Analyzer, Tri-Carb 2100TR, Packard, Meridan, CT).

3.7 In vitro cytotoxicity assay

PC-3 prostate cancer cells were maintained in RPMI 1640 supplemented with fetal bovine serum (10%) and penicillinG/ streptomycin (100 units/mL). For the cytotoxicity assays, DCTX-loaded polymeric micelles (0.7% (*w/w*) for EO_{45}-BO_{24}, 0.7 and 3.5% (*w/w*) for EO_{45}-SO_{26}) were passed through 0.45-μm nylon filters, then the drug content was assayed by HPLC. DCTX-loaded micelles and control DCTX solution mimicking Taxotere® (polysorbate 80/ethanol/DCTX 72.8:24.3:2.9 *wt%*) were serially diluted in cell culture medium prior to their addition. Control unloaded-micelles were tested at polymer/polysorbate 80 concentrations ranging from $7x10^{-7}$ to 4.2 mg/mL. Cells were seeded in 96-well plates at a density of $5x10^3$ cells/well and cultured for 24 h at 37°C in a humidified atmosphere containing 5% CO_2. The medium was then refreshed (100 μL) prior to the addition of 20-μL aliquots of either the micelle solutions or medium alone. After a 72-h incubation period, cells were rinsed with PBS, fed with 100 μL of fresh medium, and exposed to 10 μL/well of a MTT solution (5 mg/mL in PBS). After a 3.5 h-incubation, 100 μL of a SDS solution (10% in HCl 0.01 N) was added to each well to dissolve the blue formazan product generated by the oxidation of MTT by living cells. The absorbance was read 16 h later at 570 nm using Tecan Safire plate reader (Durham, NC).

4. Results and discussion

4.1 Characterization of the polymers and unloaded micelles

The molecular characteristics of PEO-*b*-PBO and PEO-*b*-PSO copolymers are reported in Table 1. Given that these polymers are not biodegradable, relatively low molecular weights were targeted (<6000) to avoid exceeding the renal filtration threshold for the elimination of unimers [31, 32]. GPC revealed that PEO-*b*-PBOs had narrow distribution peaks while the curves of PEO-*b*-PSOs showed a small shoulder on the low volume side of the main narrow peak, which was attributed to the initiation of homo PSO by moisture (data not included). The PEO-*b*-PSOs were further purified by precipitation of the copolymers from a product solution of dichloromethane into hexane to give the final products with a single peak in GPC. ^{1}H-NMR spectra were recorded and confirmed the compositions of the block copolymers [33].

Table 1. Molecular characteristics of PEO-*b*-PBO and PEO-*b*-PSO

Copolymer [a]	M_n [a]	M_n [b]	M_w [b]	M_w/M_n [b]
EO_{45}-BO_{15}	3080	2700	2900	1.05
EO_{45}-BO_{24}	3730	3400	3600	1.05
EO_{45}-SO_{15}	3800	3000	3350	1.11
EO_{45}-SO_{26}	5120	3460	4150	1.20

[a] The subscripts denote the number of repeat units as measured by ^{1}H-NMR.
[b] Measured by GPC.

All polymers exhibited low CAC, ranging from 1 to 10 mg/L (Table 2). The CAC was found to decrease with increasing hydrophobic chain length and

substituting BO for SO. Indeed, the CAC of EO_{45}-BO_{15} was twice that of the EO_{45}-SO_{15} copolymer, reflecting the stronger hydrophobic interactions conferred by the aromatic ring. In a recent review, Booth et al. [34] ranked the relative hydrophobicities of various oxyalkylene units and attributed values of 1, 6 and 12 to propylene oxide, BO and SO, respectively. All polymeric micelles possessed highly viscous cores, as evidenced by the low I_e/I_m ratios (0.05 to 0.12) compared to that of SDS (0.69), which is liquid-like (Figure 1 and Table 2). PSO-based micelles presented higher core viscosity than their PBO counterparts. The latter showed I_e/I_m values similar to those of PEO-*b*-poly(L-aspartamide) derivatives [35].

Table 2. Size, CAC and core viscosity of unloaded micelles. Mean of 3 independent experiments

Copolymer	d_h (nm)	PDI	CAC (mg/L) ± SD	I_e/I_m ± SD
EO_{45}-BO_{15}	16	0.04	9.5 ± 0.5	0.15 ± 0.01
EO_{45}-BO_{24}	21	0.07	4.0 ± 0.2	0.12 ± 0.02
EO_{45}-SO_{15}	19	0.06	4.5 ± 0.2	0.05 ± 0.01
EO_{45}-SO_{26}	21	0.17	1.5 ± 0.1	0.04 ± 0.01

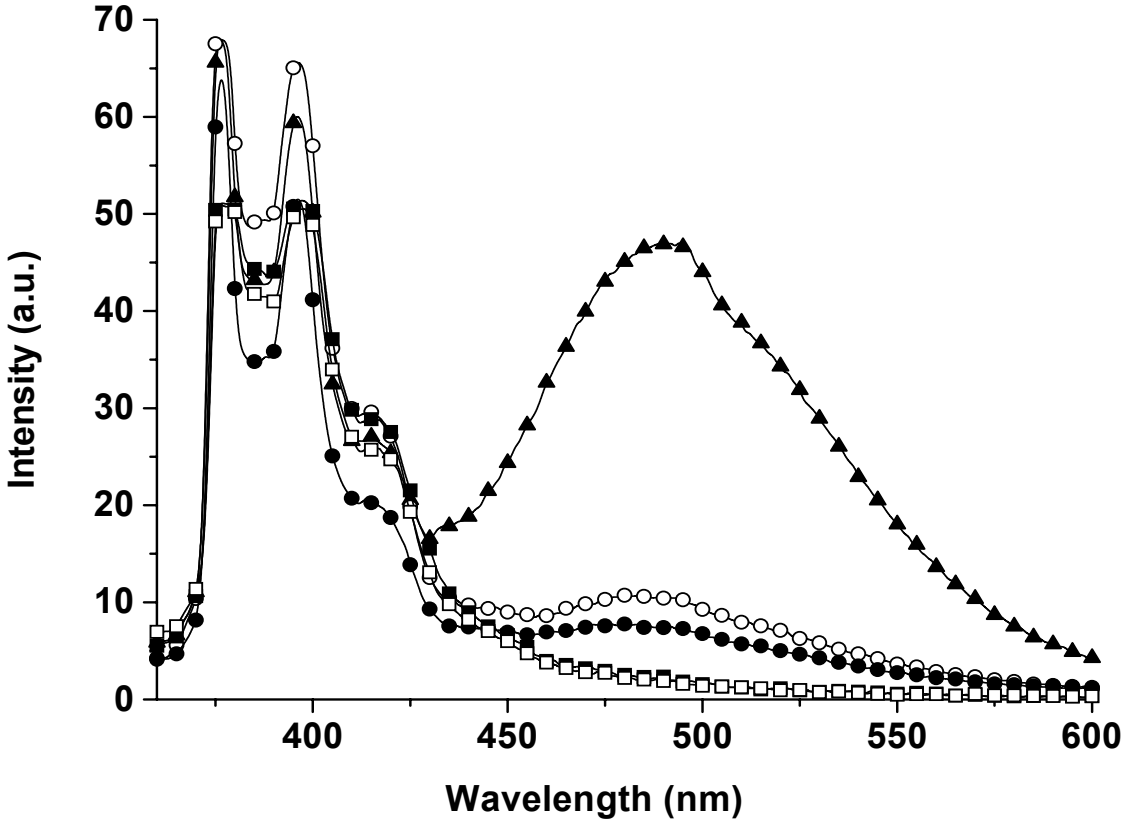

Figure 1. Fluorescence emission spectra of 1,3-bis-(1-pyrenyl)propane in EO_{45}-BO_{15} (○), EO_{45}-BO_{24} (●), EO_{45}-SO_{15} (□), EO_{45}-SO_{26} (■), and SDS (▲) micellar aqueous solutions.

The size of micelles is controlled by various factors, among which the length and nature of the core-forming segment and corona-forming chain are predominant. As reported in Table 2, mean d_h of the micelles ranged from 16 to 21 nm. N_{agg}s were above 300 for all copolymers except EO_{45}-BO_{15} which was about one-third of this value (Table 3). This polymer also formed the smallest micelles, as determined by DLS (16 nm). In all cases, size distribution was unimodal and of low polydispersity. Micelle diameter was augmented when chain length of the oxyalkylene block was increased. The latter observation is in agreement with earlier data obtained for similar

systems [19-21]. DLS measurements were also performed at different angles (50-140°) to assess whether the micelles were spherical. Figure 2 shows mean diameter as a function of the scattering vector (K^2). No angular dependence was found for EO_{45}-BO_{24} and EO_{45}-BO_{15} copolymers, the mean diameters being almost identical at every angle. This suggests that the BO polymers probably self-assembled into spheres. In contrast, angular dependence was evidenced in the case of both EO_{45}-SO_{15} and EO_{45}-SO_{26} copolymers, indicating that the self-assemblies were not spherical in shape.

Table 3. MASLS analysis of unloaded micelles

Copolymer	M_{wmic}	N_{agg}	r_g/r_h[a]
EO_{45}-BO_{15}	263,500	90	0.9
EO_{45}-BO_{24}	1,193,700	330	0.9
EO_{45}-SO_{15}	1,030,700	307	1.3
EO_{45}-SO_{26}	1,235,000	310	3.6

[a] r_h is the hydrodynamic radius.

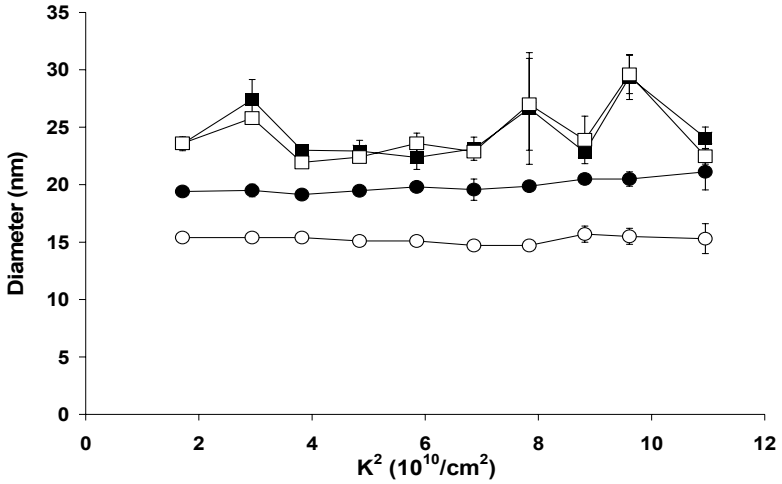

Figure 2. Change of diameter with the magnitude of K^2 for EO_{45}-BO_{15} (○), EO_{45}-BO_{24} (●), EO_{45}-SO_{15} (□), and EO_{45}-SO_{26} (■) micelles (detection angles 50-140°). Each value is the mean of 3 experiments ± SD. The mean diameter was found to be independent on the polymer concentration above the CAC.

The morphology of the unloaded micelles was then examined by computing the r_g/r_h ratio for the different polymers (Table 3). For PEO-*b*-PBO micelles, the r_g/r_h values were close to that of a hard sphere (0.78), in agreement with the formation of nearly spherical micelles. On the other hand, the ratios found for PEO-*b*-PSO copolymers were more than 1, consistent with significantly elongated micelles [36]. TEM imaging was undertaken in order to directly visualize the shape of the aggregates. As anticipated, PEO-*b*-PBO formed nearly spherical micelles in water (Figure 3 A-i and B-i), whereas the PEO-*b*-PSOs self-assembled into small rods (Figure 3 C-i and D-i). Under TEM, the diameters of all micelles were close to those obtained by DLS, while the mean length of the EO_{45}-SO_{15} and EO_{45}-SO_{26} rods were approximately 80 ± 15 and 90 ± 10 nm (n=20), respectively. PSO-based micelles have been proposed to adopt both spherical and cylindrical arrangements, depending on the length of the respective PSO and PEO blocks. Indeed, Crothers et al. [37]

found that the r_g/r_h of EO_{45}-*b*-SO_{10} micelles (same PEO length but shorter PSO block) was consistent with spherical micelle formation, thus confirming the determining role of polymer hydrophilic/ hydrophobic balance on micelle morphology [38]. In another study, Yang et al. [21] compared the N_{agg} of EO_{17}-BO_8 and EO_{17}-SO_8. These polymers have lower molecular weight than those studied in the present work, but their EO/BO and EO/SO ratios are comparable. They found that substituting BO for SO brought about a rise of N_{agg} which was superior to the theoretical increase expected for spherical micelles. They hypothesized that the difference in N_{agg} between these 2 polymers could be explained by elongation of the micelles to accommodate the high N_{agg}. While the formation of rod micelles with PEO-*b*-PSO has been predicted theoretically [21, 22], this is the first time that the cylindrical morphology of PSO-based micelles is observed. Although the difference in shape between the 2 types of micelles can be related to differences in the hydrophobicity (being twice for the SO) [34] and conformations of BO and SO, it is worth mentioning that the possible residual homopolymer of SO dissolved in the micelle core may also have contributed to the formation of cylindrical PEO-*b*-PSO micelles [39].

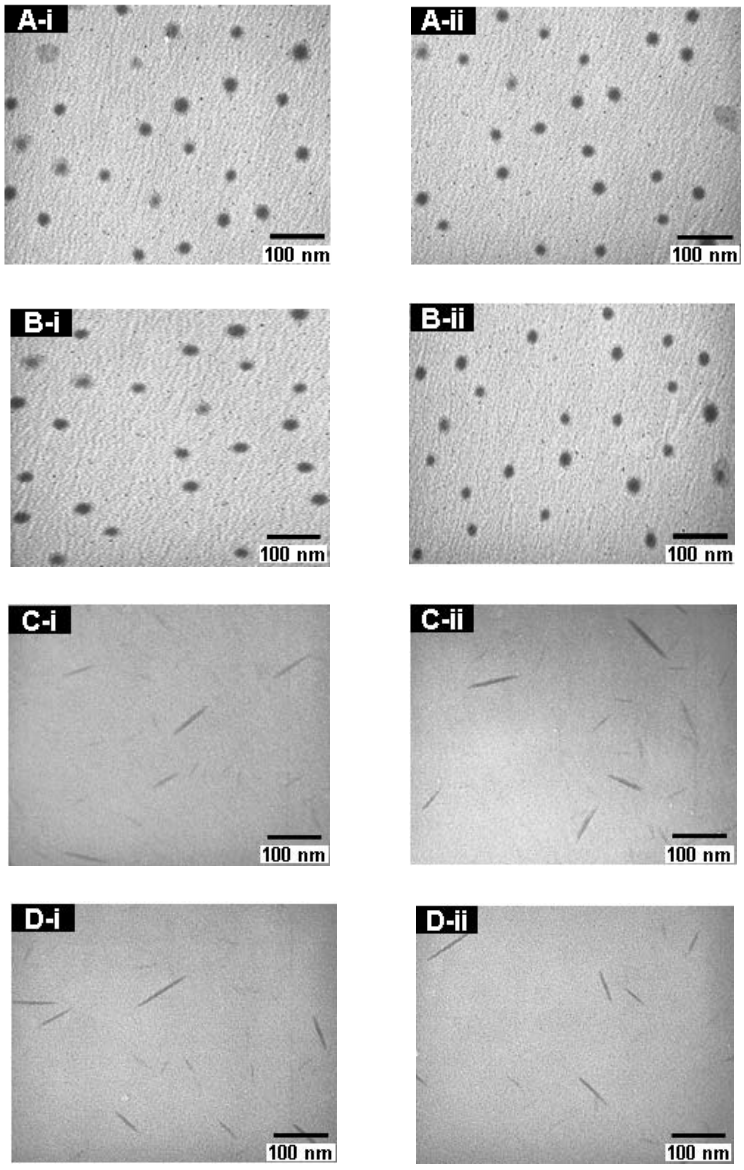

Figure 3. TEM imaging of unloaded (i) and DCTX-loaded (ii) EO_{45}-BO_{15} (A), EO_{45}-BO_{24} (B), EO_{45}-SO_{15} (C) and EO_{45}-SO_{26} (D) micelles.

4.2 Characterization of DCTX-loaded micelles

The drug-loaded micelles were prepared according to a procedure which was initially proposed for PEO-*b*-poly(D,L lactide) (PEO-*b*-PDLLA) [40]. Attempts at dissolving DCTX into preformed micelles resulted in low drug loading, probably

because of slow diffusion of the drug into the viscous micelle core (data not shown). Accordingly, it was decided to first co-dissolve both the drug and polymer in a pharmaceutically-acceptable organic solvent (*i.e.* ethanol) to form a homogeneous polymeric matrix, evaporate the organic solvent, and then add the water phase. The size of DCTX-loaded micelles was measured by DLS (Table 4), and no difference was observed compared to unloaded micelles. Moreover, the loaded micelles preserved their initial shape (Figure 3 A-ii-D-ii). The micelles could be readily freeze-dried, and recovered their initial size distribution upon reconstitution in aqueous media (data not shown). In solution, no crystallization was apparent for at least 14 days. The solubilizing capacity (S_{CP}) of each system was evaluated (Table 4). PSO-based micelles incorporated more DCTX (~3-4%) than PBO micelles (<1%), most likely because of the better compatibility between DCTX and PSO (see below) and to the micelle morphology. Micelles of cylindrical shape are usually associated with greater S_{CP}, given their higher N_{agg} and core volume [22, 24]. Indeed, Crothers et al. [22] demonstrated that griseofulvin was also incorporated to a greater extent into PSO *vs.* PBO micelles having comparable characteristics. For both polymers, S_{CP} rose when the length of the hydrophobic block was increased. More than 4% (*w/w*) drug loading could be achieved with EO_{45}-SO_{26}. With such loading, hydrosolubility of exceeding 2 mg/mL was reached, which was more than 1000-fold the aqueous solubility of free DCTX.

Table 4. Characteristics of DCTX-loaded micelles

Copolymer	S_{CP} ± SD (mg/g)[a]	Q_h	ρ (g/cm^3)[b]	K_v x 10^{-4}	d_h (nm)	PDI
EO_{45}-BO_{15}	4.2 ± 0.8	0.35	0.973	3.9	17	0.07
EO_{45}-BO_{24}	7.4 ± 1.1	0.46	0.973	5.3	22	0.08
EO_{45}-SO_{15}	34.8 ± 1.7	0.47	1.150	35.3	19	0.07
EO_{45}-SO_{26}	41.7 ± 1.2	0.60	1.150	36.7	21	0.19

[a]Solubilizing capacity expressed as mg of DCTX per g of copolymer.
[b]The densities of the hydrophobic block were taken from the literature [21, 24].

The K_v of DCTX between water and the copolymer micelles was calculated using Equations 5 and 6 (Table 4). The K_v values ranged from 4 x 10^4 to 53 x 10^4. The high affinity of DCTX for another hydrophobic block, *i.e.* PDLLA, has been reported earlier by our group [41]. The K_v value of DCTX in poly(*N*-vinyl-2-pyrrolidone)-*block*-PDLLA micelles was found to be 2.46 × 10^4. It is similar to the K_v of the drug in PEO-*b*-PBO micelles, but substantially lower than the K_v for PEO-*b*-PSO.

Solubility parameters are useful to estimate compatibility, interactions and miscibility between drugs and various carrier systems [41]. Difference in loading capacity and the affinity of PEO-*b*-PSO and PEO-*b*-PBO for the drug were correlated with the solubility parameters and the enthalpy of mixing of both the drug and the polymers. As expected, the difference between the total solubility parameters of DCTX and each polymer block was found to be the least important for PSO (Table 5). The enthalpy of mixing (ΔH_M) was then calculated using Equation 11 [42]:

$$\Delta H_M = \phi_1\phi_2\left[(\delta_{d1}-\delta_{d2})^2+(\delta_{p1}-\delta_{p2})^2+(\delta_{h1}-\delta_{h2})^2\right] \qquad (11)$$

where ϕ_1 and ϕ_2 are volume fractions of the drug and the polymers. The ΔH_M values for PSO and PBO were 79.7 and 87.3 MPa, respectively, corroborating the experimental data. Considering the differences in both solubility parameters and ΔH_M, PSO is more suitable than PBO for solubilizing DCTX.

Table 5. Total (δ_t) and partial (δ_d, δ_p and δ_h) solubility parameters of DCTX and individual polymer blocks ($MPa^{1/2}$)

Molecule	δ_d	δ_p	δ_h	δ_t
DCTX	20.6	3.1	14.6	25.5
PEO	17.8	11.1	9.1	22.9
PBO	16.6	5.8	6.6	18.8
PSO	20.8	4.6	5.8	22.1

4.3 In vitro evaluation of micelle formulations

The effect of micellar solubilization on the chemical stability of DCTX in water was investigated over a period of 24 h at 50ºC (Figure 4). For comparison between the different systems, all micelles were loaded at the same drug level (0.04% *w/w*). Despite their higher affinity for the drug, both PSO-based micelles were inefficient at protecting DCTX from degradation under accelerated stability testing conditions. Likewise, EO_{45}-BO_{15} did not afford any protection compared to the control drug solution. Surprisingly, only EO_{45}-BO_{24} was able to preserve most DCTX chemical integrity (92%) after 24 h. This protective effect cannot be accounted for by differences between the drug affinity or core microviscosity of BO_{24} block, since both parameters were inferior to those of PSO block and almost similar to the BO_{15}

segment (Tables 2, 4 and 5). One possible explanation for the observed effect is the difference in specific surface area between micelles. The specific surface area (S) was estimated for spherical and cylindrical micelles using Equations 12 and 13, respectively:

$$S = 4 \pi r^2/M_w \quad (12)$$

$$S = 2 \pi r L /M_w \quad (13)$$

where L is the length of the cylindrical micelles which was extracted from TEM analysis, r is the micelle radius (Table 4) and M_w is the molecular weight of micelles as ascertained by MASLS. BO_{24} micelles yielded the lowest specific surface area (760 m^2/g), whereas the calculated values for BO_{15}, SO_{15} and SO_{26} micelles were 2050, 2800 and 2900 m^2/g, respectively. Thus, the greater protection conferred by EO_{45}-BO_{24} micelles could be partially ascribed to decreased interactions of DCTX with the aqueous medium at the water-micelle interface due to the lower specific surface area.

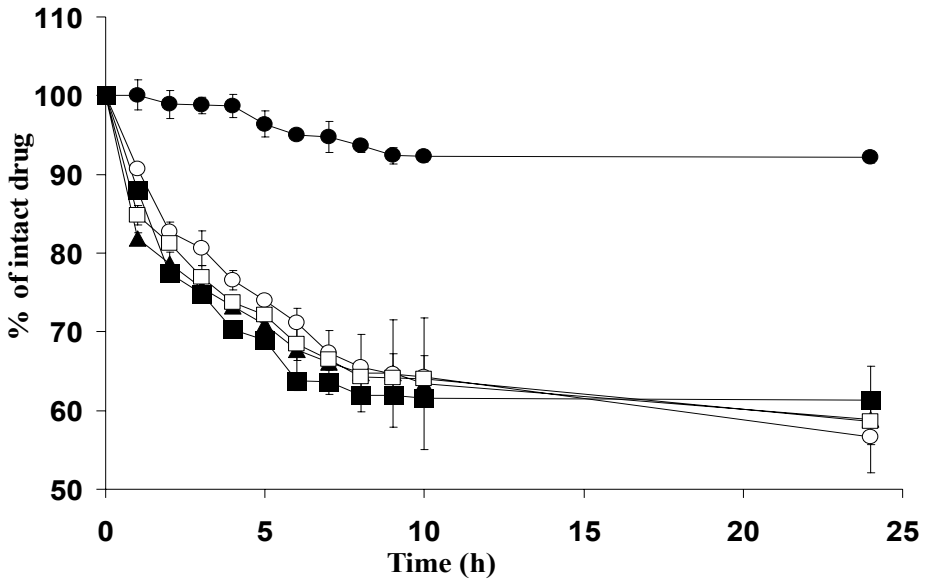

Figure 4. Effect of micellar solubilization on DCTX stability in EO_{45}-BO_{15} (○), EO_{45}-BO_{24} (●), EO_{45}-SO_{15} (□), and EO_{45}-SO_{26} (■) micelles. The stability of free DCTX in water (▲) is also shown. The experiments were carried out at fixed temperature (50ºC) for 24 h. DCTX loading and concentration were set at 0.04 (% *w/w*) and 2 µg/mL, respectively. Mean ± SD (n=3).

The release of DCTX from EO_{45}-BO_{24} and EO_{45}-SO_{26} micelles was studied *in vitro* (Figure 5). The free drug diffused completely in about 24 h, indicating that the two superimposed 50-nm membranes influenced the release rate. However, this particular setting was necessary to prevent the transfer of micelles in the acceptor compartment (<5% after 5 days as estimated by DLS). All micelle formulations displayed similar profiles characterized by a fast initial release (~50% within 12 h) followed by a decelerated rate over 5 days. In order to eliminate the background effect, mathematical kinetic modeling was performed. In the model, the drug release measured in the acceptor compartment was divided into two different transfer rates, namely one from micelles to the donor compartment and one from donor to acceptor compartment. Each transfer relation was defined by a simple first order linear

differential equation defined by microconstant, K_m for the rate of DCTX release from micelles and K_d for the transfer of DCTX to the acceptor compartment (see supporting information). To assess the effect of the two superimposed 50-nm membranes on the release, K_d was determined by fitting the equation on the free DCTX release curve and used subsequently to obtain the specific K_m of each formulation. Comparison of the release rates of the formulations with 0.7% DCTX showed that release was faster for EO_{45}-SO_{26} than for EO_{45}-BO_{24} micelles (K_{mSO26} = 1.31 d^{-1} *vs.* K_{mBO24} = 0.57 d^{-1}, and 83% of the drug had diffused out in 72 h *vs.* 73%, respectively). However, normalization of the constants by specific surface area (K_{mSO26}/S = 4.51 10^{-4} $g.m^{-2}.d^{-1}$ *vs.* K_{mBO24}/S = 7.56 10^{-4} $g.m^{-2}.d^{-1}$) tends to ascribe this difference to the surface dissimilarities between formulations, as previously discussed. Comparison of the release profiles of EO_{45}-SO_{26} formulations with different drug loadings (0.7 and 3.5% DCTX) revealed that surface area was not the only factor affecting drug release. Indeed, similar release profiles were obtained despite the fact that there was a 5-fold difference in micelle concentrations between the 2 formulations. The drug loading may influence DCTX distribution in the micelles or its initial partition between micelles and donor compartment and therefore affect the drug release profile.

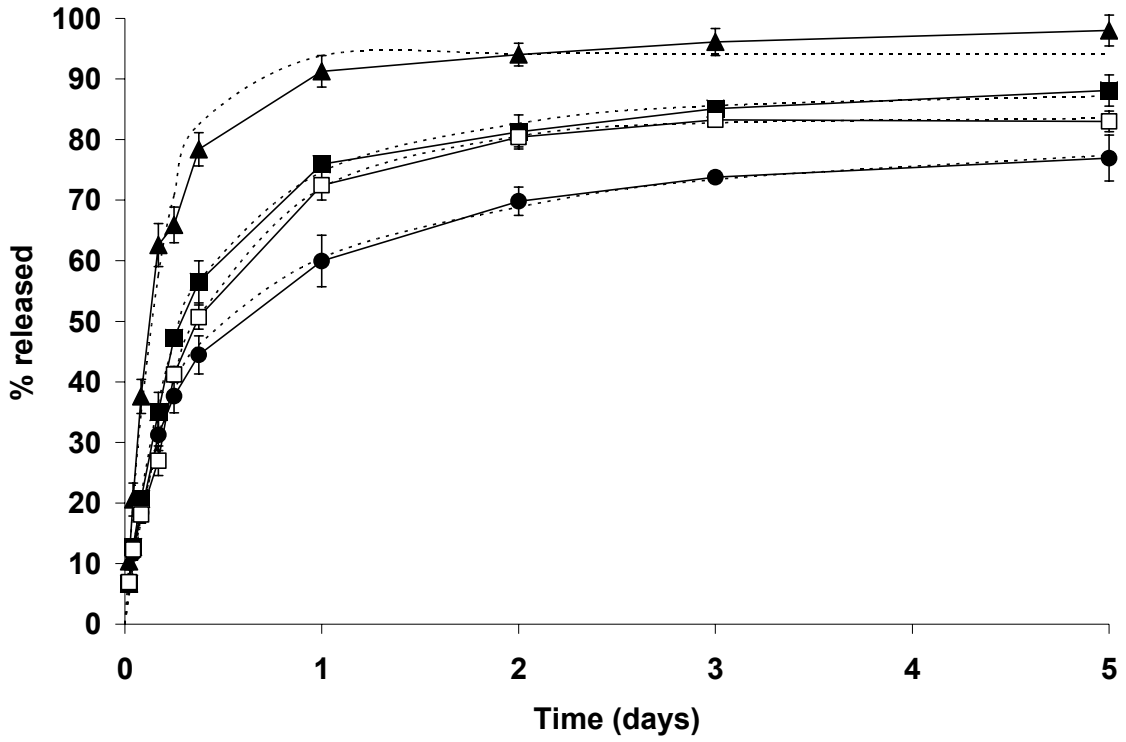

Figure 5. *In vitro* release kinetics of DCTX from EO_{45}-BO_{24} (0.7% DCTX) (●) and EO_{45}-SO_{26} (0.7% DCTX) (□), and EO_{45}-SO_{26} (3.5% DCTX) (■) micelles. DCTX diffusion in the absence of micelles is represented by (▲). The experiments were carried out at 37ºC in PBS (pH 7.4). Mean ± SD (n=3). The dotted lines represent the simulated release kinetics.

The antimitotic activity of DCTX-loaded micelles was then evaluated on human prostate cancer cells PC-3. The cytotoxicity assays revealed that EO_{45}-BO_{24} and EO_{45}-SO_{26} micelles formulations were as efficient as the control commercial formulation to inhibit the growth of these cells (Figure 6). No difference was found between the tested systems with IC_{50} values ranging from 2.2 to 2.5 nM (±0.3 nM). Indeed, the *in vitro* release data can be used to rationalize these results. After 72 h of incubation, most of the DCTX has been released from the polymeric micelles and is thus available to exert its cytotoxic activity. Indeed, Le Garrec *et al.* [8] obtained

similar findings with biodegradable poly(*N*-vinylpyrrolidone)-*b*-poly(D,L-lactide) micelles loaded with DCTX. These micelles exhibited IC_{50} values comparable to those of Taxotere®, indicating the complete release of drug from the hydrophobic core. Neither the unloaded-micelles nor polysorbate 80 caused a significant decrease in cell viability up to a polymer/polysorbate 80 concentration of 0.01 mg/mL (corresponding to a DCTX concentration of $5.4x10^{-9}$ M for the micelles loaded with 0.7% drug) (data not shown). At high concentration (0.7 mg/mL), EO_{45}-SO_{26} was fairly less toxic (86% viability) than polysorbate 80 (51% viability) and EO_{45}-BO_{24} (24% viability). Altogether these data suggest that, at high drug concentrations, PEO-*b*-PSO may potentially improve the therapeutic index of DCTX by decreasing the formulation's non specific toxicity.

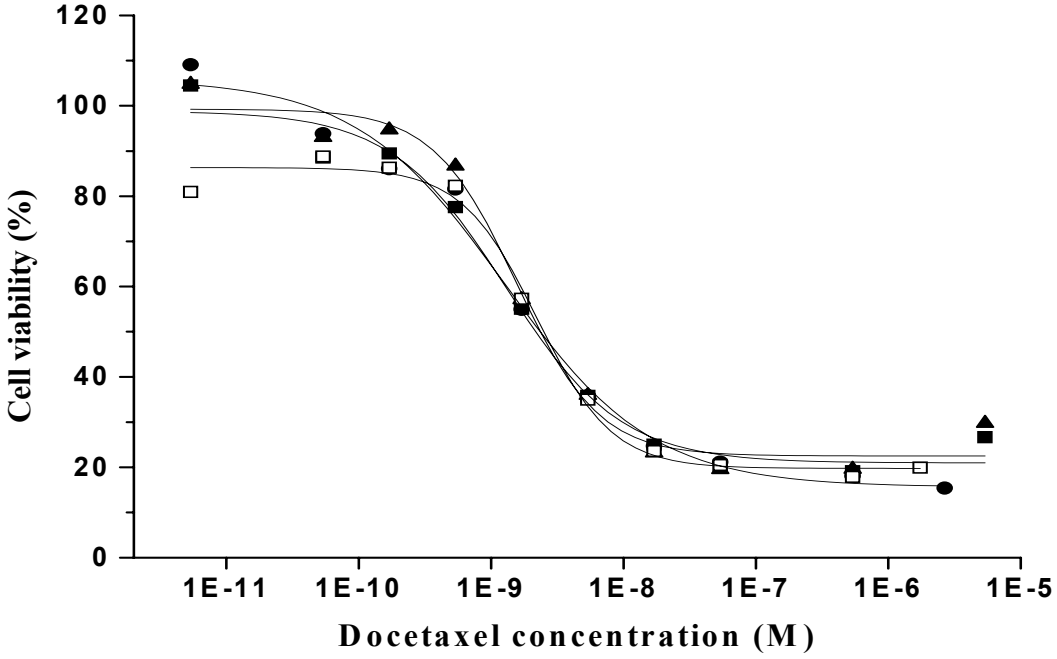

Figure 6. Cell viability of PC-3 cells exposed to EO_{45}-BO_{24} (0.7% DCTX) (●) and EO_{45}-SO_{26} (□) (0.7% DCTX), and (3.5% DCTX) EO_{45}-SO_{26} (■) DCTX-loaded micelles. A polysorbate 80/ethanol formulation of DCTX was used as control (▲). The data represent the mean of 3 experiments. For the purpose of clarity, the error bars of the standard deviation are omitted (CV < 12%).

5. Conclusion

In water, PEO-*b*-PBO and PEO-*b*-PSO block copolymers self-assembled at low concentrations to form spherical and cylindrical micelles, respectively. These micelles possessed diameters ranging from 16 to 21 nm, which make them suitable for sterilization by filtration and administration by intravenous injection. PSO-based copolymers were associated with higher solubilizing capacities for DCTX (~4% *w/w*) than PBO due to the aromatic structure of the core-forming polymer and the cylindrical morphology of the resulting micelles, However, the PBO copolymer

offered a greater protective effect against the hydrolytic degradation of DCTX. Nevertheless, the long term stability for all these systems is guaranteed by the fact that the micelles investigated in this work could be lyophilized and thus stored in dried form. Such polymers could provide useful alternatives to low molecular weight surfactants for the solubilization of taxane derivatives.

6. Acknowledgements

This work was supported financially by the Canada Research Chair Program. Geneviève Gaucher and Marie-Hélène Dufresne are acknowledged for their critical reading of the manuscript.

7. References

[1] Walker, R. A., Jones, J. L., Chappell, S., Walsh, T. & Shaw, J. A. *Cancer Metastasis Rev*. **16,** 5-27 (1997).

[2] Rao, B. M., Chakraborty, A., Srinivasu, M. K., Devi, M. L., Kumar, P. R., Chandrasekhar, K. B., Srinivasan, A. K., Prasad & A. S. Ramanatham, J. *J. Pharm. Biomed. Anal.* **16,** 676-681 (2006).

[3] Ardavanis, A., Tryfonopoulos, D., Yiotis, I., Gerasimidis, G., Baziotis, N. & Rigatos, G. *Anti-Cancer Drugs* **15**, 581-585 (2004).

[4] Tije, A. J., Verweij, J., Loos, W. J. & Sparreboom, A. *Clin. Pharmacokinet.* **42,** 665-685 (2003).

[5] Einhaus, C. M., Retzinger, A. C., Perrotta, A.O., Dentler, M. D., Jakate, A. S., Desai, P. B. & Retzingen, G. S. *Clin. Cancer Res.* **10,** 7001-7010 (2004).

[6] Immordino, M. L., Brusa, P., Arpicco, S., Stella, B., Dosio, F. & Cattel, L. *J. Control. Release* **91,** 417-429 (2003).

[7] Farokhzad, O. C., Cheng, J., Teply, B. A., Sherifi, I., Jon, S., Kantoff, P. W., Richie, J. P. & Langer, R. *Proc. Natl. Acad. Sci. U. S. A.* **103,** 6315-6320 (2006).

[8] Le Garrec, D., Gori, S., Karkan, D., Luo, L., Lessard, D. G., Smith, D., Ranger, M., Yessine, M. A. & Leroux, J. C. *J. Drug Deliv. Sci. Technol.* **15,** 115-120 (2005).

[9] Kataoka, K., Harada, A. & Nagasaki, Y. *Adv. Drug Deliv. Rev.* **47,** 113-131 (2001).

[10] Kim, S. C., Kim, D. W., Shim Y. H., Bang J. S., Oh, H. S., Kim, S. W. & Seo, M. H. *J. Control. Release* **72,** 191-202 (2001).

[11] Jeong, Y. I., Kang, M. K., Sun, H. S., Kang, S. S., Kim, H. W., Moon, K. S., Lee, K. J., Kim, S. H. & Jung, S. *Int. J. Pharm*. **273,** 95-107 (2004).

[12] Kang, N., Perron, M., Prud'homme, R. E., Zhang, Y., Gaucher, G. & Leroux, J. C. *Nano Lett.* **5,** 315-319 (2005).

[13] Fairclough, J. P. A., Norman, A. I., Shaw B., Nace, V. M. & Heenan, R. K. *Polym. Int.* **55,** 793-797 (2006).

[14] Liu, L., Gao, X., Cong, Y., Li, B. & Han, Y. *Macromol. Rapid Commun.* **27,** 260-265 (2006).

[15] Castelletto, V. & Hamley, I. W. *Adv. Polym. Technol.* **17,** 137-144 (2006).

[16] Norman, A. I., Ho, D. L., Lee, J. H. & Karim, A. *J. Phys. Chem. B* **110,** 62-67 (2006).

[17] Hamaguchi, T., Matsumura, Y., Suzuki, M., Shimizu, K., Goda, R., Nakamura, I., Nakatomi, I., Yokoyama, M., Kataoka, K. & Kakizoe, T. *Br. J. Cancer* **92,** 1240-1246 (2005).

[18] Hamley, I. W., Pedersen, J. S., Booth, C. & Nace, V. M. *Langmuir* **17,** 6386-6388 (2001).

[19] Kelarakis, A., Mai, S. M., Havredaki, V., Nace, V. M. & Booth, C. *Phys. Chem. Chem. Phys*. **3,** 4037-4043 (2001).

[20] Kelarakis, A., Havredaki, V., Booth, C. & Nace, V. M. *Macromolecules* **35,** 5591-5594 (2002).

[21] Yang, Z., Crothers, M., Attwood, D., Collett, J. H., Ricardo, N. M. P. S., Martini, L. G. A. & Booth, C. *J. Colloid Interface Sci.* **263,** 312-317 (2003).

[22] Crothers, M., Zhou, Z., Ricardo, N. M. P. S., Yang, Z., Taboada, Z., Chaibundit, C., Attwood*, D.* & Booth, C. *Int. J. Pharm*. **293,** 91-100 (2005).

[23] Zhou, Z., Lodge, T. P. & Bates, F. S. *J. Phys. Chem. B* **110,** 3979-3989 (2006).

[24] Chaibundit, C., Ricardo, N. M. P. S., Crothers, M. & Booth, C. *Langmuir* **18,** 4277-4283 (2002).

[25] Mai, S.-M., Ludhera, S., Heatley, F., Attwood, D. & Booth, C. *J. Chem. Soc., Faraday Trans.* **94,** 567-572 (1998).

[26] Wilhelm, M., Zhao, C. L., Wang, Y., Xu, R., Winnik, M. A., Mura, J. L., Riess, G. & Croucher, M. D. *Macromolecules* **24,** 1033-1044 (1991).

[27] Yasugi, K., Nagasaki, Y., Kato, M. & Kataoka, K. *J. Control. Release* **62,** 89-100 (1999).

[28] Krishna, A. K. & Flanagan, D. R. *J. Pharm. Sci.* **78,** 574-576 (1989).

[29] Krevelen, D. V. Cohesive properties and solubility. *Properties of polymers: their correlation with chemical structure; their numerical estimation and prediction from addition group contributions*. In: Krevelen, D. V. (Ed.), New York: Elsevier Scientific Publishing Co., 189 (1990).

[30] Fedors, R. F. *Polym. Eng. Sci.* **14,** 147-154 (1974).

[31] Yamamoto, Y., Nagasaki, Y., Kato, Y., Sugiyama, Y. & Kataoka, K. *J. Control. Release* **77,** 27-38 (2001).

[32] Seymour, L. W., Duncan, R., Strohalm, J. & Kopecek, J. *J. Biomed. Mater. Res.* **21,** 1341-1358 (1987).

[33] Rekatas, C. J., Mai, S.-M., Crothers, M., Quinn, M., Collett, J. H., Attwood, D., Heatley, F., Martini, L. & Booth, C. *Phys. Chem. Chem. Phys.* **3,** 4769-4773 (2001).

[34] Booth, C. & Attwood, D. *Macromol. Rapid Commun.* **21,** 501-527 (2000).

[35] Lavasanifar, A., Samuel, J. & Kwon, G. S. *Colloid Surf. B-Biointerfaces* **22,** 115-126 (2001).

[36] Müller, A. & Burchard, W. *Colloid Polym. Sci.* **273,** 866-875 (1995).

[37] Crothers, M., Attwood, D., Collett, J. H., Yang, Z., Booth, C., Taboada, P., Mosquera, V., Ricardo, N. M. P. S. & Martini, L. G. A. *Langmuir* **18,** 8685-8691 (2002).

[38] Rangel-Yagui, C. O., Pessoa-Jr, A. & Tavares, L. C. *J. Pharm. Pharm. Sci.* **8,** 147-165 (2005).

[39] Nagarajan, R. *Colloid Surf. B-Biointerfaces* **16,** 55-72 (1999).

[40] Zhange, X., Jackson, J. K. & Burt, H. M. *Int. J. Pharm*. **132,** 195-206 (1996).

[41] Fournier, E., Dufresne, M. H., Smith, D. C., Ranger, M. & Leroux, J. C. *Pharm. Res.* **21,** 962-968 (2004).

[42] Liu, J., Xiao, Y. & Allen, C. *J. Pharm. Sci.* **93,** 132-143 (2004).

Supporting information

The kinetic modeling was applied by using the following equation S1:

$$\frac{M_t}{M_\infty} = \left[P_o\left(1-\exp(-K_d t)\right)\right] + \left[P_m\left(1-\exp(-K_m t)\right)\left(1-\exp(-K_d t)\right)\right] \quad \text{(S1)}$$

where P_o and P_m are constants related to the amount of drug initially present in the donor compartment (free DCTX) and in the micelles, and K_d and K_m are rate constants for diffusion out of donor compartment and micelles, respectively (Figure S1). The K_d used for all simulations was determined by fitting the equation on DCTX release profile with $K_m = 0$.

Figure S1. Kinetic model for DCTX release from micelles in jacketed Franz diffusion cells.

Reference:

[1] Jacquez, J. A. *Compartmental analysis in biology and medicine.* Amsterdam, Elsevier Publishing Company. pp.237 (1972).

CHAPTER 4 - Synthesis and enzymatic stability of PEGylated oligonucleotide duplexes and their self-assemblies with polyamidoamine dendrimers[3]

Mahmoud Elsabahy[1], Mingzhen Zhang[1], Shao-Ming Gan[2], Karen C. Waldron[2] and Jean-Christophe Leroux[1*]

[*]Canada Research Chair in Drug Delivery, [1]Faculty of Pharmacy, [2]Department of Chemistry University of Montreal, C.P. 6128, Succursale Centre-Ville, Montreal (QC) H3C 3J7, Canada

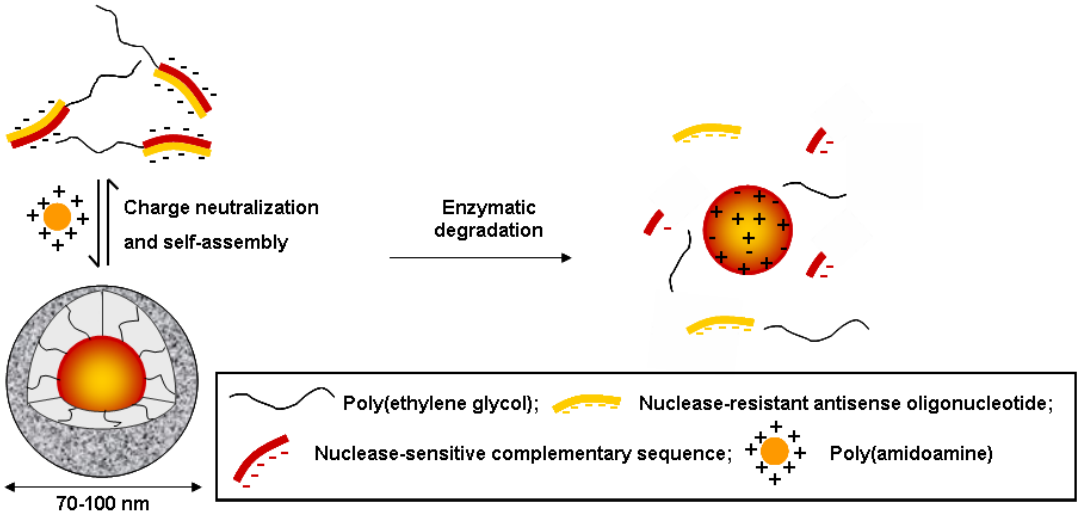

[3]*Soft Matter* **4**, 294-302 (2008); reproduced with permission from the Royal Society of Chemistry.

Abstract

The objectives of the current study were to design and characterize poly(ethylene glycol) (PEG)-based carriers for antisense oligonucleotides (AON) delivery that would gradually release the AON upon the enzymatic degradation of a complementary nuclease-sensitive sequence (SON). A phosphodiester SON was conjugated to one extremity or to the central part of PEG (molecular weight 10 or 20K). The PEG-SON was hybridized to a nuclease-resistant phosphorothioate AON analog. Compared to the non-PEGylated duplex, the PEG-SON/AON derivative had a modest impact on the degradation kinetics of SON as monitored by a fluorescence dequenching assay performed in the presence of DNase 1. The reaction rate depended on the grafting position of SON and on the PEG's molecular weight. To further control the release rate, PEG-SON/AON conjugates were complexed to poly(amidoamine) (PAMAM) dendrimers of different generations (G). Interaction with PAMAMs of G3 and G5 yielded monodisperse polyion complex micelles (PICM) with average mean sizes ranging from 70 to 100 nm. The PICM were found to decrease the catalytic reaction rate by 20 to 100 fold; the slowest release kinetics being achieved with PEG_{10K}-SON/AON/G5 PAMAM. The PEGylated conjugates reported in this manuscript as well as their self-assemblies with PAMAMs, could prove potentially useful to confer prolonged circulating properties to nucleic acid drugs and release them in a sustained manner.

1. Introduction

Selective inhibition of gene expression by DNA/RNA oligonucleotides (ONs) has been shown to be promising in the treatment of numerous diseases, including cancer and viral infections [1-6]. However, the clinical use of nucleic acid based drugs is still largely hampered by their inability to reach their site of action in sufficient amount. Parameters such as the chemical stability [7-10], circulation time in the bloodstream [11, 12], deposition at the target site and intracellular transport [13] play a determinant role in the *in vivo* activity of ONs. Unmodified phosphodiester (PD) ONs are seldom tested in animal models as they rapidly degrade in biological fluids and in cells [7-10]. The chemical instability issue has been partially solved through specific modifications of the ON backbone. Chemically-modified ONs can exhibit enhanced nuclease resistance, prolonged biological half-lives [1, 9] and greater affinity for the target sequence [14]. Among all ON derivatives, phosphorothioate (PS) analogs have been the most widely studied [12]. PS modification confers resistance against nuclease degradation and increases the half-life in human serum compared to the native ON [9, 12].

Likewise, conjugates have also been employed to improve cellular uptake and resistance to nucleases. Indeed, various lipophilic molecules have been attached to ONs. Of these compounds, cholesterol is perhaps the best characterized. It has been reported to slow down ON clearance [15, 16] and enhance cellular association and transport [17]. Concurrently, conjugation with poly(ethylene glycol) (PEG), a hydrophilic and flexible polymer, can extend the circulation time of macromolecular drugs such as ONs and enhance their stability by creating a zone of steric hindrance

around the drug [18]. The polymer chain can also serve as a linker for conjugating targeting ligands [19]. Another means to improve the delivery of ONs consists in complexing them with oppositely charged molecules such as cationic lipids [19] and polymers [20, 21]. Of particular interest are poly(amidoamine) (PAMAM) dendrimers which have been shown to increase the efficacy of nucleic acid drugs [20-25]. The limited toxicity, high transfection efficiency, and the stability of the ON/PAMAM complexes confer significant advantages over other non viral gene delivery vectors [25-27].

In the current study, both the PEGylation and PAMAM/ON complexation approaches were investigated as means to release an antisense ON (AON) in a controlled fashion. A nuclease- sensitive PD-ON sequence (SON) was attached to different functionalized PEGs *via* an amide linkage, and hybridized to its complementary PS-antisense sequence as depicted in Scheme 1A. Enzymatic hydrolysis of the PEGylated PD-SON is expected to gradually release the active nuclease-resistant PS-AON. In order to further increase the delivery time, the PEG-SON/AON duplex was further complexed to PAMAM to generate polyion complex micelles (PICM). PICM possess a core-shell type structure whereby the neutralized SON/AON/PAMAM core is stabilized by a PEG corona [28, 29]. In this case, the enzymatic degradation of the SON would release the AON and/or AON/PAMAM complex which would then be available for transfection (Scheme 1B). Different PEG-SONs were synthesized and characterized for their hybridization properties and ability to release the AON in its intact form upon SON degradation by nucleases. The PEG-SON/AON duplexes were subsequently complexed to PAMAMs of different

generations, and the resulting PICM were analyzed for their size, size distribution and morphology. Finally, the impact of micellization on the degradation of SON was examined.

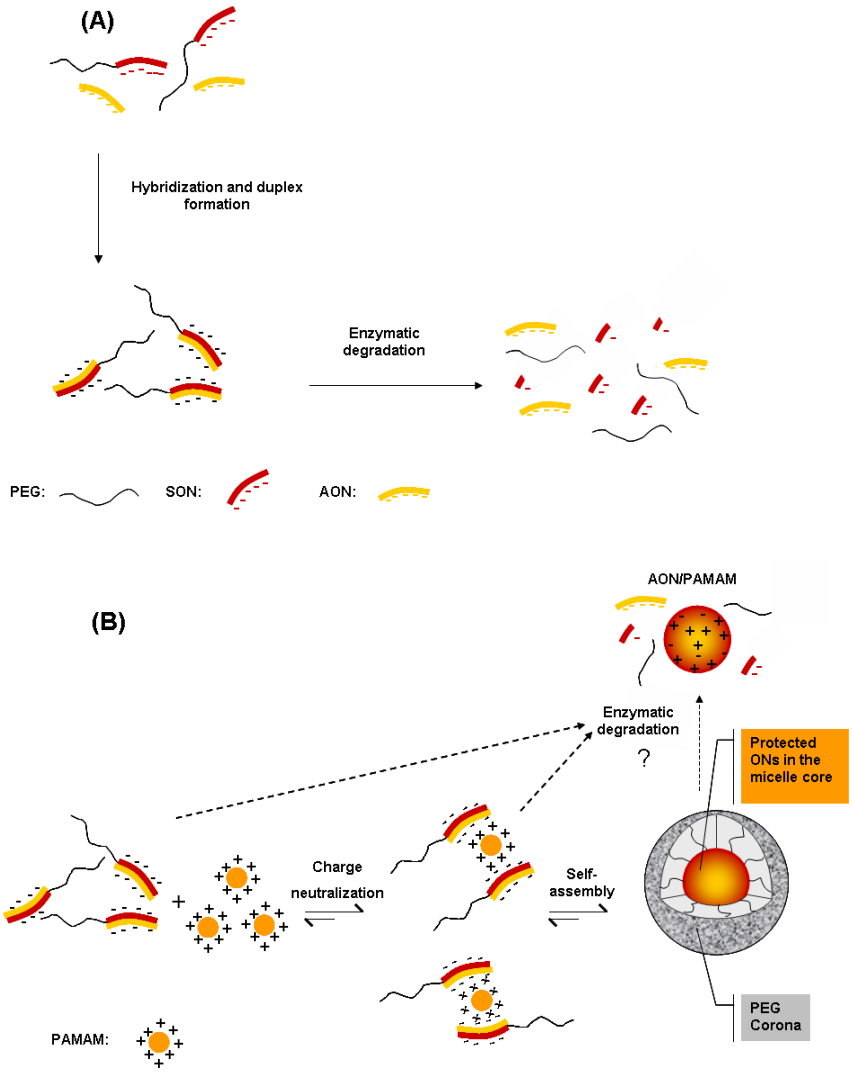

Scheme 1. Approaches investigated to deliver nuclease-resistant AON: (**A**) PEG-conjugation and (**B**) Self-assembly of PEG conjugate with PAMAMs to form PICM. The enzymatic degradation of the nuclease-sensitive SON releases the AON either free or complexed to the PAMAM.

2. Materials

3′-Fluorescein (FAM)-5′-aminoalkyl-PD-SON (5'-TGAAACTCACCAGCGAGAAC) was obtained from Alpha DNA (Montreal, QC, Canada). Both 5′-Cy3-labeled and non-labeled PS-AON (5'-GTTCTCGCTGGTGAGTTTCA) were supplied by Midland Certified Reagent Company Inc. (Midland, TX). Linear methoxy PEG succinimidyl α-methyl butanoate (M_w = 10,500; PDI = 1.01 and M_w = 21,000; PDI = 1.00) (PEG_{10K} and PEG_{20K}) and branched dimethyl PEG succinimidyl butanoate (M_w = 21,000; PDI = 1.02) ($PEG_{20K\text{-}br}$) were purchased from NEKTAR (Huntsville, AL). The *N*-hydroxysuccinimide (NHS) functional group was attached either to the terminal or the middle positions of the linear and branched PEGs, respectively. Regenerated cellulose ultrafiltration membranes (Ultracel, molecular weight cut-off 10,000 and 30,000) were from Millipore (Bedford, MA). Diethylaminoethyl Sephadex® (DEAE Sephadex®) and PAMAM generations 0 (G0), 1 (G1), 3 (G3) and 5 (G5) corresponding to M_w of 517, 1,430, 6,909 and 28,826 g/mol, respectively, and heparin sodium salt from porcine intestinal mucosa (M_w of ~6000) were obtained from Sigma-Aldrich (Oakville, ON, Canada). UltraPure™ Agarose and deoxyribonuclease 1 (DNase 1, 10,000-25,000 units/mg) were obtained from Invitrogen Canada Co. (Burlington, ON, Canada). Fused silica capillary was purchased from Polymicro Technologies (Phoenix, AZ). All chemicals used were of analytical grade. Deionized water was generated by a Millipore Milli-Q system (Bedford, MA).

3. Methods

3.1 Preparation of the PEGylated duplexes

3.1.1 PEGylation of the SON

PEG-SON conjugates were prepared through the formation of an amide bond between the NHS-functionalized PEG and 3′-FAM-5′-aminoalkyl-SON. The reactive group was positioned at one extremity (PEG_{10K} and PEG_{20K}) or in the middle ($PEG_{20K\text{-}br}$) of the PEG chain. The SON (100 µg, 15.1 nmol) was dissolved in 150 µL of phosphate buffered saline (PBS) (pH 8.0, 10 mM NaH_2PO_4/Na_2HPO_4, 100 mM NaCl). Then, 0.47, 0.95 and 0.93 mg of PEG_{10K}, PEG_{20K} and $PEG_{20K\text{-}br}$ (45 nmol) was added to the SON solution (PEG/SON 3:1 mol/mol). The reaction was carried out at 30°C for 24 h under continuous agitation. The PEG-SON conjugate was purified by passage through a DEAE Sephadex® column. The unreacted PEG was eluted using Tris buffer (pH 8.0, 10 mM) containing no NaCl. Then, Tris buffer containing 1 M NaCl was used to elute the PEG-SON. The solutions were concentrated under vacuum and the free SON was removed by ultrafiltration using a cellulose membrane of molecular weight cut-off 10,000.

3.1.2 Hybridization of the PEG-SON with the AON

Equimolar ratios of PEG-SON or SON alone and AON were mixed together and added to the annealing buffer (0.1 M Tris pH 8, $5x10^{-4}$ M EDTA pH 8, 1 M NaCl) in a 5:1 volume ratio. The mixture was heated at 80°C for 3 min, cooled down

to 4°C and left overnight at this temperature. The PEG-SON/AON was purified by ultrafiltration (cellulose membrane of molecular weight cut-off 30,000) to remove the free AON. The purified solutions were stored at 4°C until use.

3.2 Characterization of PEG-ON duplex

3.2.1 Determination of the quenching efficiency

The hybridization and release of the AON was monitored by spectrofluorimetry as described elsewhere [30]. Quenching of the fluorescence of FAM-labeled SON by the Cy3-labeled-AON was exploited to follow hybridization. The quenching efficiency was determined by measuring the fluorescence emission of FAM-labeled SON or PEG-SON in hybridization buffer (150 μL, 0.02 μM) at excitation (λ_{ex}) and emission (λ_{em}) wavelengths of 490 and 520 nm, respectively, using a Tecan Safire plate reader (Durham, NC), in the presence of increasing concentrations of quencher Cy3-AON (up to 0.2 μM). The decrease in fluorescence was monitored until it reached a stable plateau, and the quenching efficiencies were determined as follows [30]:

$$Q_E = 100 - \left[\frac{F_{SON/AON}}{F_{SON}} \times 100 \right] \qquad \text{Eq. 1}$$

where Q_E is the quenching efficiency, $F_{SON/AON}$ and F_{SON} are the respective fluorescence emission intensities of the FAM-labeled SON/AON and SON, when they are both excited at 490 nm.

3.2.2 Determination of melting temperature (T_m)

The T_m of both SON/AON and PEG-SON/AON were measured by monitoring the fluorescence intensity as a function of temperature. The formulations were heated from 20 to 95°C and fluorescence emission at 520 nm was recorded using an Aminco Bowman Series 2 luminescence spectrometer (Spectronic Instruments Inc., Rochester, NY). The T_m was taken as the midpoint of the sigmoidal plot representing the increase in fluorescence intensity as a function of temperature [31, 32].

3.2.3 Agarose gel electrophoresis

Agarose gels (2%) were prepared in Tris-acetate-EDTA buffer (0.04 M Tris, 0.001 M EDTA-$Na_2.2H_2O$, 0.02 M glacial acetic acid, pH 8.5). The samples were mixed with the loading buffer (10 mM Tris-HCl, pH 7.6, 60 mM EDTA and 60% glycerol) at 6:1 volume ratio. Gel electrophoresis was carried out using a Horizon® 11.14 horizontal apparatus (Montreal Biotech Inc., Montreal, QC, Canada) at 122 V for 30 min. Qualitative fluorescence imaging of the separated ONs was performed with a Typhoon™ 9410 Workstation with variable mode imager (Amersham Biosciences, Pittsburgh, PA). The $\lambda_{ex}/\lambda_{em}$ were set at 488/526 and 532/670 nm for FAM and Cy3, respectively.

3.2.4 Capillary electrophoresis

Laser-induced fluorescence detection coupled to capillary electrophoresis (CE-LIF) was performed with a 3-mW argon ion laser having an λ_{ex} of 488 nm and with emission monitored at 520 nm. The analysis was performed on a Beckman P/ACE^{TM} MDQ Capillary Electrophoresis System (Beckman Coulter, Fullerton, CA) with a 61.4 cm long (50.6 cm to detector) fused silica capillary (50 μm ID, 360 μm OD). The capillary was flushed consecutively with 0.1 M NaOH, Milli-Q water and background electrolyte (BGE) for a minimum replacement of ten capillary volumes before each injection. The injection (approx. 10 nL) of samples was performed hydrodynamically at 3.4 kPa for 10 s. An electrolyte plug (3.4 kPa for 5 s) was always injected afterward. The separation voltage was set at 25 kV. The capillary temperature was maintained at 25°C while the samples were kept at 4°C until analysis. A sodium tetraborate buffer (55 mM and pH 8.22) was used as BGE. Detection was achieved on-column at 8.5 cm from the outlet after removing a 5-mm length of the polyimide coating with a resistive heating element. The NHS-PEG was detected by absorbance with a conventional CE-UV/Vis instrument (model HP^{3D}CE, Agilent Technologies, Palo Alto, CA) equipped with a diode-array detector, under the same separation conditions.

3.3 Preparation and characterization of the PICM

3.3.1 Preparation of the PICM

Purified PEG-SON/AON duplexes were mixed with aqueous solutions of PAMAM of different generations at increasing nitrogen-to-phosphate (N/P) ratios in Tris buffer (pH 7.4) to form PICM. To compare the different formulations, the N/P ratio was adjusted to 2:1 because the micelles formed at this ratio exhibited the lowest polydispersity indices (PDI). The micelle solutions were filtered on 0.2 μm-nylon membranes prior to analysis.

3.3.2 Characterization of the PICM

The mean hydrodynamic diameter, PDI, and scattering intensity of PICM were measured in Tris buffer (pH 7.4) at a temperature of 25°C by dynamic light scattering (DLS) using a Malvern Zetasizer Nanoseries ZS (Malvern, Worcestershire, UK) equipped with a backscattered light detector operating at 173º. The CONTIN program was used to extract size distributions from the autocorrelation functions. The effect of NaCl (0.1-1 M) on the stability of the PICM was studied by measuring the scattering intensity of the micelles after each addition of salt. To compare the stability between the different formulations, the inflection points (IP) of the scattering intensity plots were calculated by fitting a sigmoidal curve on the experimental data. The zeta potential was determined in Tris buffer (pH 7.4) at a temperature of 25°C by laser Doppler anemometry with Malvern Zetasizer Nanoseries ZS. The micelles' morphology was examined by atomic force microscopy (AFM).[39] A drop of micelle

solution (2 mg/mL) was deposited on a clean mica grid and nitrogen-dried at room temperature just before measurement. AFM images were recorded on a Nanoscope IIIa Dimension^{TM} 3100 instrument (Digital Instruments, SantaBarbara, CA). The imaging was performed in tapping mode with a silicon tip (tapping mode etched Si probes-RTESP7) operating at a 250–300 kHz resonance frequency, and a 42 N/m constant force.

3.4 Enzymatic degradation

SON/AON, PEG-SON/AON or PICM were incubated with DNase 1 (60 U/μg ON) in the presence of $MgCl_2$ (5 mM) at 37°C. AON release was indirectly measured by monitoring the dequenching of FAM-labeled SON. The λ_{ex} and λ_{em} were set at 490 and 520 nm, respectively. The fluorescence intensity corresponding to 100% release was determined at the end of the experiment by adding excess of the DNase 1 and letting the reaction run for another 24 h. For PICM, the previous step was preceded by adding an excess of heparin before the addition of DNase 1 to destabilize the micelles. The degraded samples were loaded onto a 2%-agarose gel and the ONs were visualized directly on the gel.

The enzymatic degradation reactions were analyzed with the Michaelis-Menten equation [33]:

$$V = \frac{V_{\max}[S]}{(K_m + [S])} \qquad \text{Eq. 2}$$

where [S] is the concentration of SON, V is velocity, V_{max} is maximal velocity, and K_m is the Michaelis constant.

4. Results and discussion

4.1 Preparation and characterization of PEG-SON

The first step in designing the AON formulation involved the conjugation of the nuclease- labile SON to one extremity (PEG_{10K} and PEG_{20K}) or in the middle of the PEG chain ($PEG_{20K\text{-}br}$) (Scheme 1A). The functionalized NHS-PEG was reacted with 5′-aminoalkyl-SON as illustrated in Scheme 2. The PEG-SONs were successfully purified by anion exchange chromatography and ultrafiltration to remove the unconjugated PEG and SON, respectively. The conjugates' purity was first established by CE-LIF, whereby analytes were separated according to their size and charge [34]. Figure 1 presents the electropherograms of FAM-labeled SON (a), PEG_{20K}-SON (b), $PEG_{20K\text{-}br}$-SON (c) and PEG_{10K}-SON (d). These electropherograms confirmed that no free SON remained in the formulations after purification. As expected, PEGylation of the SON reduced its electrophoretic mobility, and thus elution time, due to an increase in the size of the anionic analyte. The fastest migration rate was achieved with the conjugates having the highest molecular weights (*i.e.* PEG_{20K}-SON and $PEG_{20K\text{-}br}$-SON). CE-UV/Vis also established that there was no free functionalized PEG in the solution (data not shown). These results were confirmed by agarose gel electrophoresis (Figure 2A). In this case, the attachment of the different PEGs retarded the migration of the SON. PEG_{20K}-SON and $PEG_{20K\text{-}br}$-SON were associated with the slowest migration rate.

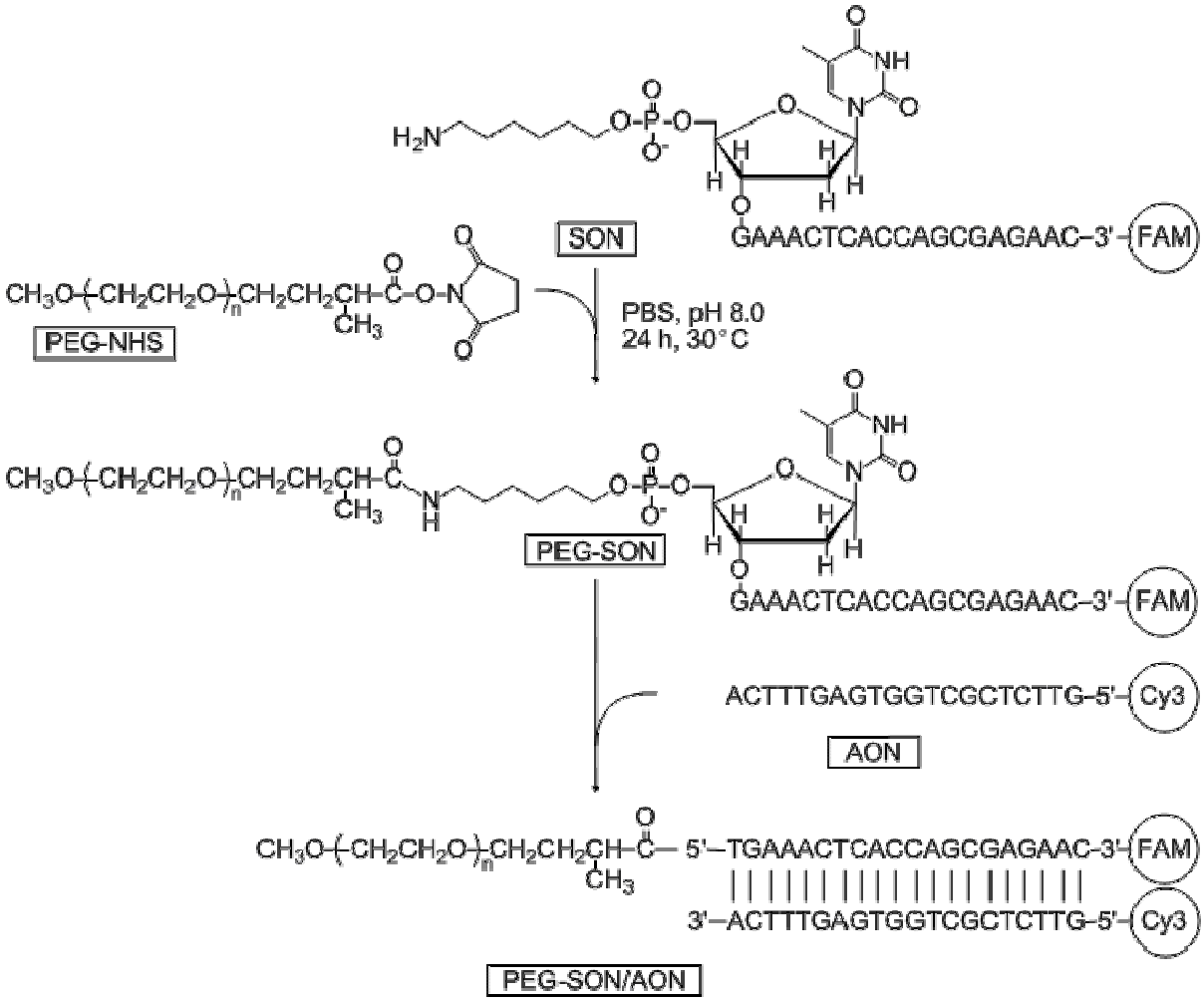

Scheme 2. Synthesis of PEG–SON conjugates and hybridization with AON. In this example, the SON is a PD ON whereas the AON is a PS analog.

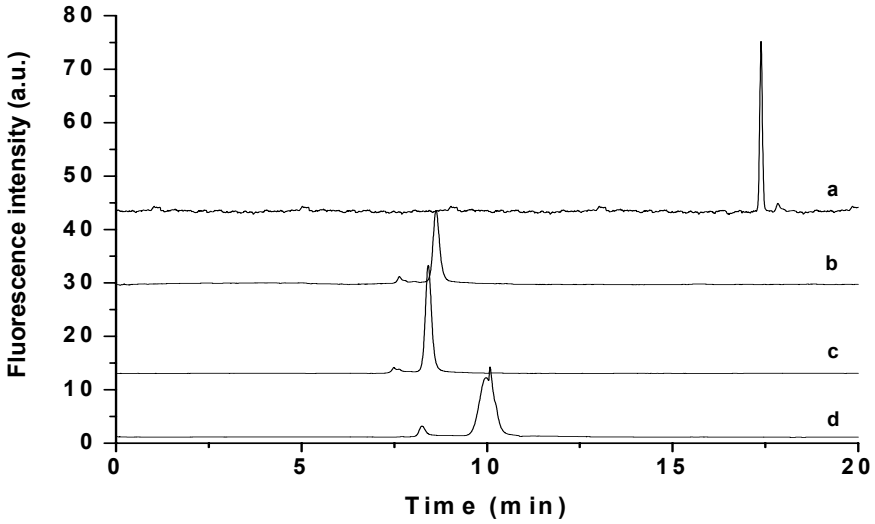

Figure 1. Capillary electropherograms showing the migration of SON (a), PEG_{20K}-SON (b), $PEG_{20K\text{-}br}$-SON (c) and PEG_{10K}-SON (d). The separation was carried out in borate buffer (55 mM, pH 8.22). The voltage was set at 25 kV and the capillary temperature was maintained at 25°C.

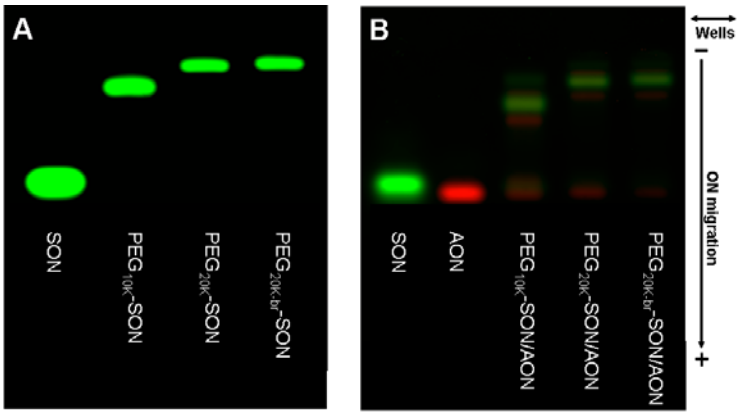

Figure 2. Migration profiles of (**A**) PEG_{10K}-SON, PEG_{20K}-SON and $PEG_{20K\text{-}br}$-SON, and (**B**) PEG_{10K}-SON/AON, PEG_{20K}-SON/AON and $PEG_{20K\text{-}br}$-SON/AON on 2%-agarose gel. Control SON and AON are shown in the first lane. The green and red spots correspond to the fluorescence emission of FAM (λ_{ex} = 488 nm) and Cy3 (λ_{ex} = 532 nm), respectively.

4.2 Preparation and characterization of PEG-SON/AON

The duplexes were prepared by hybridizing the Cy3-labeled AON to the FAM-labeled PEG-SON (Scheme 2) and isolated by ultrafiltration. The purity of the PEG-duplex was established by gel electrophoresis (Figure 2B). It revealed the quasi absence of free AON. Duplex formation was associated with a distinguishable decrease in fluorescence intensity of SON, which reflected the quenching of the FAM-SON fluorescence by Cy3-AON. Upon hybridization, FAM comes into intimate contact with Cy3 (Scheme 2), thereby favoring the contact mode of quenching (static quenching) [30]. The traces of the free AON seen in Figure 2B are due to the high sensitivity of the image analysis used to visualize the quenched bands. Duplex formation was associated with a 93 ± 2% quenching of FAM fluorescence (Figure 3). This property was exploited to measure the T_m of the different conjugates. Heating of the duplexes draws the two strands away from each other resulting in an increase in the fluorescence emission intensity of the FAM-SON. All PEG-SON/AON displayed a T_m of 64°C, similar to that of SON/AON, suggesting that the terminal or central attachment of SON to PEG did not affect its hybridizing capacity, at least under well controlled *in vitro* hybridization conditions. These findings corroborate those of Jeong *et al.* who demonstrated that the attachment of PEG_{2K} to the AON did not sterically hindered duplex formation with the complementary SON sequence [31, 35].

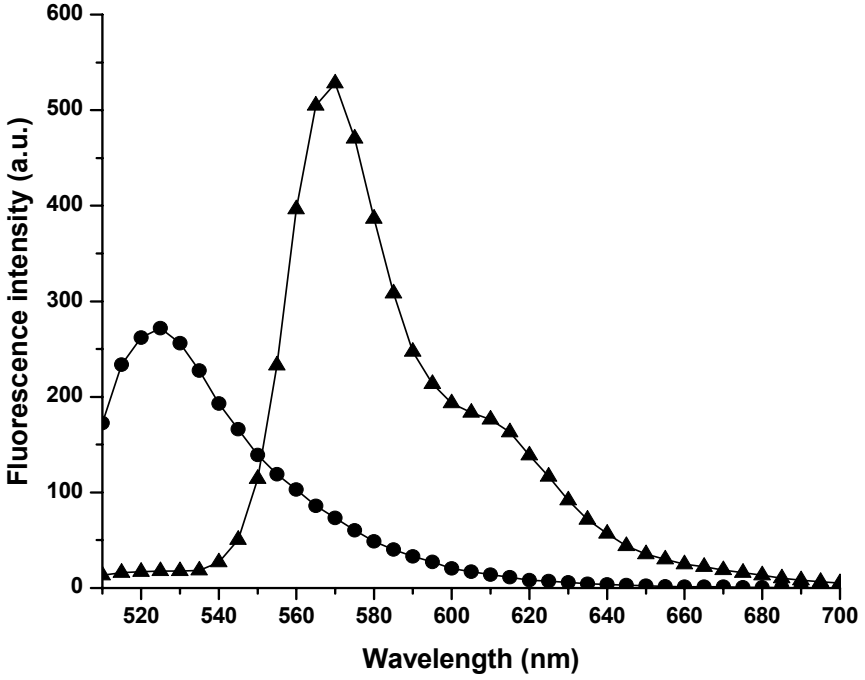

Figure 3. Emission spectrum of FAM-labeled SON prior to (●) and after hybridization with Cy3-labeled AON (▲) (λ_{ex} = 490 nm).

4.3 Preparation and characterization of the PICM

The electrostatic complexation of PEG-SON/AON to G3 and G5 PAMAMs, triggered the self-assembly of the duplexes into monodisperse PICM (Scheme 1, Table 1), where the PEG chains sterically stabilize the neutralized SON/AON/PAMAM core [31, 35, 36]. Comparatively, the addition of G0 and G1 PAMAMs did not induce micelle formation (data not shown). The absence of micellization with the low M_w PAMAMs can be explained by insufficient cooperativity in the electrostatic interactions (4 and 8 surface amine groups for G0 and G1 *vs.* 32 and 128 for G3 and G5, respectively). The multimeric binding through cooperative effects facilitates multiple simultaneous interactions with other molecules

resulting in an increase of binding affinity [37, 38]. Chen *et al.* [37] proposed a binding model for plasmid DNA-dendrimer complexes where the cooperative effect of high M_w PAMAMs (G7) allowed DNA wrapping. Conversely, "earlier generation" dendrimers (G2) were not able to form efficient complexes with the DNA.

Table 1. Characteristics of the ternary PICM prepared at an N/P 2:1 ratio; mean ± SD (n=3).

Formulation	PAMAM[a]	Diameter (nm)	PDI ± SD	Zeta potential ± SD (mV)	IP (M)[b]
PEG_{10K}-PICM	G3	68	0.06±0.02	-1.8±0.3	0.31±0.01
PEG_{20K}-PICM	G3	88	0.09±0.02	-3.2±1.5	0.23±0.01
$PEG_{20K\text{-}br}$-PICM	G3	89	0.14±0.04	3.0±1.6	0.20±0.01
PEG_{10K}-PICM	G5	88	0.08±0.05	-1.7±0.3	0.48±0.01
PEG_{20K}-PICM	G5	93	0.07±0.04	0.5±0.6	0.37±0.01
$PEG_{20K\text{-}br}$-PICM	G5	97	0.11±0.04	0.6±2.9	0.37±0.01

[a]G3 = 6,909 g/mol, G5 = 28,826 g/mol.
[b]Inflection point of sigmoidal plot representing scattering intensity *versus* NaCl concentration (Fig. 5).

In the presence of G3 or G5 PAMAM, and at an optimal N/P ratio of 2:1, PICM with mean hydrodynamic diameters ranging from 68 to 97 nm, a narrow size distribution (PDI<0.15) and nearly neutral surface charge (-1.7 – 3.0 mV) were obtained. Size increased slightly with both PEG (10 *vs*. 20 K) and PAMAM (G3 *vs.* G5) molecular weights. No significant differences were observed between PEG_{20K}- and $PEG_{20K\text{-}br}$-PICM in terms of size or PDI. Figure 4 shows the AFM images of PICM formed between PEG_{20K}-SON/AON and G5 PAMAM on a mica surface. The particles were relatively spherical; however, the average diameter was 139 ± 11 nm, which is about 1.5 times that measured by DLS (Table 1). The difference found here could be due to flattening of the PICM on the mica surface during the drying process [41]. This hypothesis is supported by the fact that the mica-deposited micelles had a

thickness of only 55 ± 5 nm. Dufresne *et al*. [39] have studied the morphology of the PEG-*b*-P(2-(*N*-amino)ethyl methacrylate)-heparin PICM by AFM. These micelles were smaller (25 nm) and relatively spherical. There was also a good correlation between the sizes measured by AFM and DLS. Similarly, Jeong *et al*. [35] have measured the size of the PEG_{2K}-AON/polyethylenimine (branched, M_w = 25,000) PICM by both DLS and AFM. The two methods yielded comparable diameters, while the AFM analysis also demonstrated that the PICM were spherical. In the current study, the observed flattening of the micelles upon drying might be explained by a less dense micelle core due to a less efficient compaction of the oppositely charged polyions.

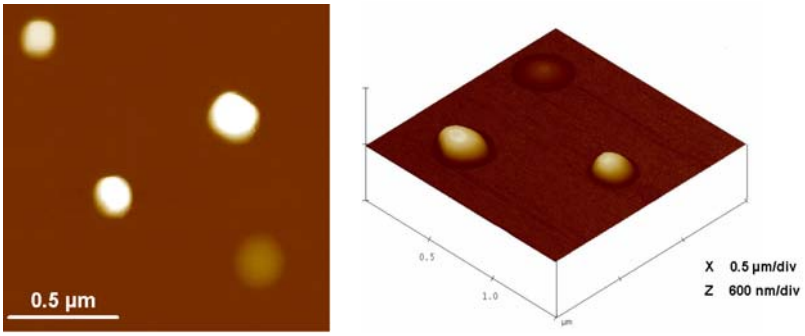

Figure 4. AFM image of PEG_{20K}-SON/AON/G5 PAMAM based PICM.

It is known that the stability of PICM is dependent on the ionic strength of the surrounding medium [39]. Chen *et al*. [37] found that the binding constant between PAMAM and polynucleotides at lower ionic strength is higher which is in agreement with electrostatic contributions to the binding. Salts can compete with the ON-PAMAM interactions, thereby destabilizing the PICM [37, 38]. The influence of NaCl concentration on the stability of micelles was therefore studied by measuring

the scattered light intensity (Figure 5). Apart from the PICM prepared with PEG_{20K} or $PEG_{20K\text{-}br}$ and G3 PAMAM, most micelle formulations were stable up to an NaCl concentration of about 0.2 M (>80% of initial scattering intensity retained), which is above the physiologic isotonic conditions (0.15 M). The inflection point (IP) of the scattering intensity *versus* salt concentration curves was calculated to compare the stability among the different micellar systems (Table 1). The PICM prepared with G5 PAMAM were more resistant towards dissociation than those containing G3 PAMAM (closed *vs.* empty symbols, Figure 5) This reflects the enhanced cooperative interaction afforded by the greater surface amine content of G5 PAMAM. Among the different PEG-SON/AON conjugates, the greater stability against destabilization was afforded by the PICM prepared with the PEG_{10K} derivative (higher IP values, Table 1). These findings can be rationalized in terms of micelle thermodynamics. Owing to its shorter PEG chain, the PEG_{10K}-SON/AON/PAMAM complexes self-assemble at lower concentrations than the PEG_{20K} counterparts (unpublished observations).

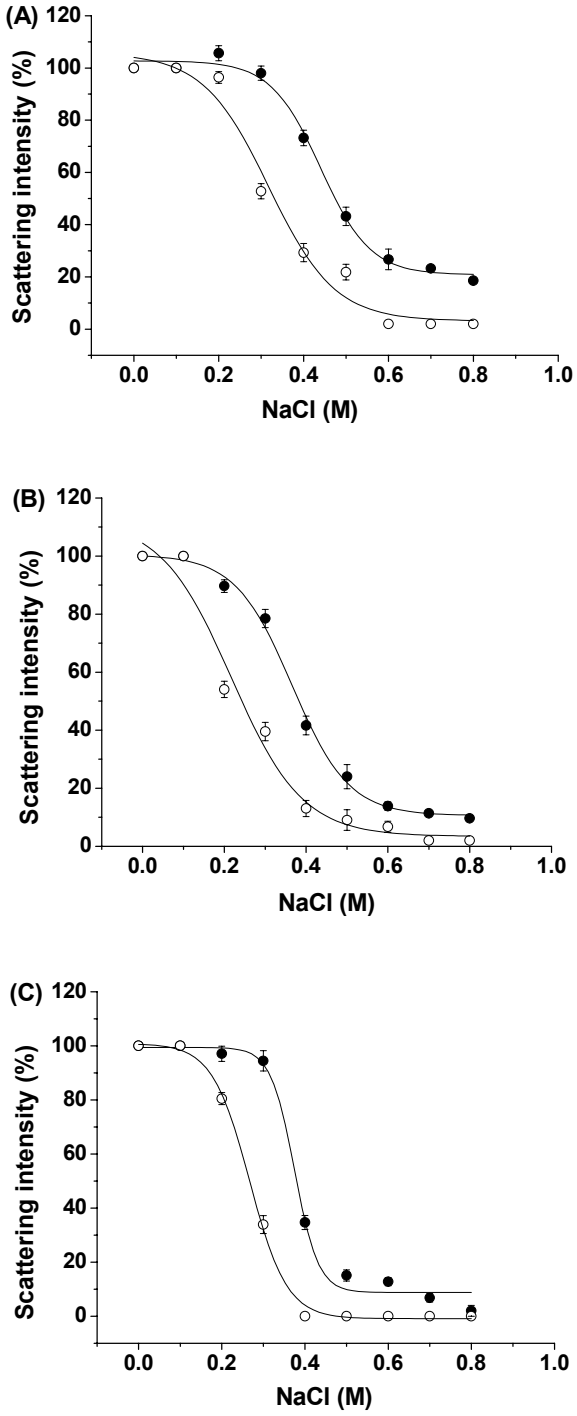

Figure 5. Effect of ionic strength on scattering intensity of PEG_{10K}- (**A**), PEG_{20K}- (**B**) and $PEG_{20K\text{-}br}$-SON/AON/PAMAM (**C**) based PICM prepared with G3 (○) or G5 (●) PAMAM. Mean ± SD (n=3).

4.4 Enzymatic degradation

The main objective of this project was to design a delivery system that releases a nuclease-stable PS-AON upon the enzymatic degradation of the complementary PD-SON sequence. Accordingly, the AON release from PEG-SON/AON systems alone as well as complexed to G3/G5 PAMAMs (PICM) was investigated in the presence of the endonuclease DNase 1 (Figures 6-8, Table 2). The degradation of SON was first monitored by measuring the dequenching of FAM fluorescence which occurs upon the dissociation of the duplex. As shown in Figure 6, the SON in unconjugated SON/AON was rapidly degraded by DNase 1 (>90% of dequenched fluorescence after 5 min incubation). The PEG-SON/AON conjugates appeared more resistant, although 100% of dequenching was achieved after 20 min. The protective effect of PEGylation could be ranked as follows $PEG_{20K\text{-}br}$>PEG_{20K}>PEG_{10K}. The kinetic parameters were calculated by fitting the data to the Michaelis-Menten equations (Table 2). PEGylation of the SON brought about a 50% decrease in V_{max}. Surprisingly, the K_m value remained virtually unchanged, implying that PEGylation did not influence the endonuclease affinity for SON (or at least for the SON nucleotides located away from the PEG chains). However, PEGylation slowed down the enzyme catalytic activity. PEG conjugation has been previously shown to confer resistance against the attack of nucleases. For example, Lee *et al.* [40] reported that siRNA was completely degraded after the RNase treatment for 15 min, whereas the siRNA-PEG_{5K} conjugate maintained more than 40% of intact siRNA.

Table 2. Michaelis-Menten kinetic parameters for SON degradation by DNase 1[a]

Formulation	V_{max} (nM min^{-1})	K_m (nM)	Relative V_{max}
SON/AON	8.15	16.4	1
PEG_{10K}-SON/AON	5.49	16.4	0.670
PEG_{20K}-SON/AON	4.72	16.4	0.580
$PEG_{20K\text{-}br}$-SON/AON	4.01	16.4	0.490
PEG_{10K}-SON/AON/G3	0.39	16.3	0.048
PEG_{20K}-SON/AON/G3	0.43	16.3	0.053
$PEG_{20K\text{-}br}$-SON/AON/G3	0.47	16.4	0.057
PEG_{10K}-SON/AON/G5	0.11	16.2	0.014
PEG_{20K}-SON/AON/G5	0.19	17.3	0.022
$PEG_{20K\text{-}br}$-SON/AON/G5	0.20	16.2	0.025

[a]The enzyme concentration used in all experiments was set at 0.049 nM. G3 and G5 refer to the PAMAM used.

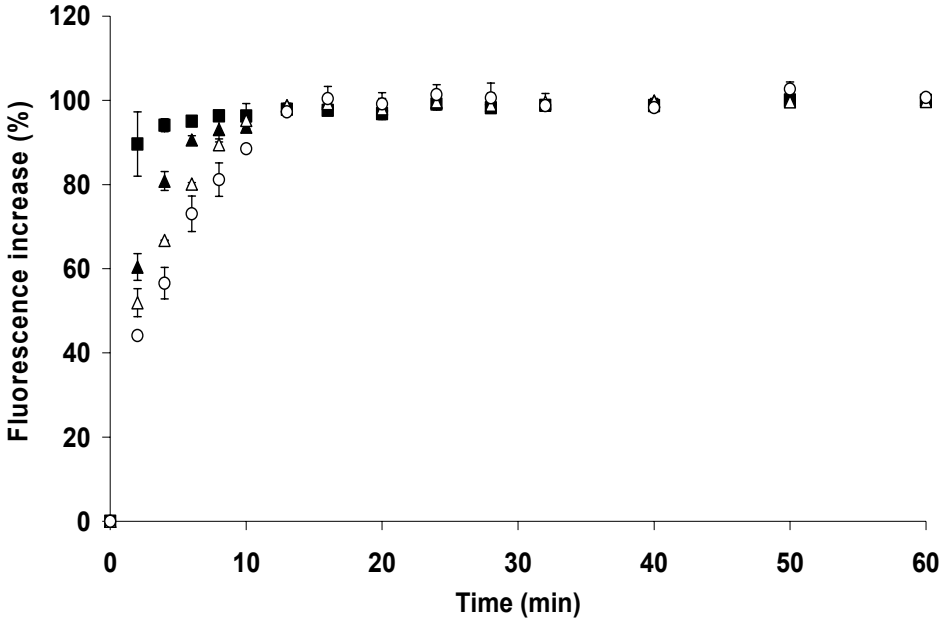

Figure 6. Dequenching of FAM-labeled SON fluorescence following the incubation with DNase 1 (60 U/µg ON, 37°C, pH 7.4) with SON/AON (■), PEG_{10K}- (▲), PEG_{20K}- (Δ) and $PEG_{20K\text{-}br}$-SON/AON (○). Mean ± SD (n=3).

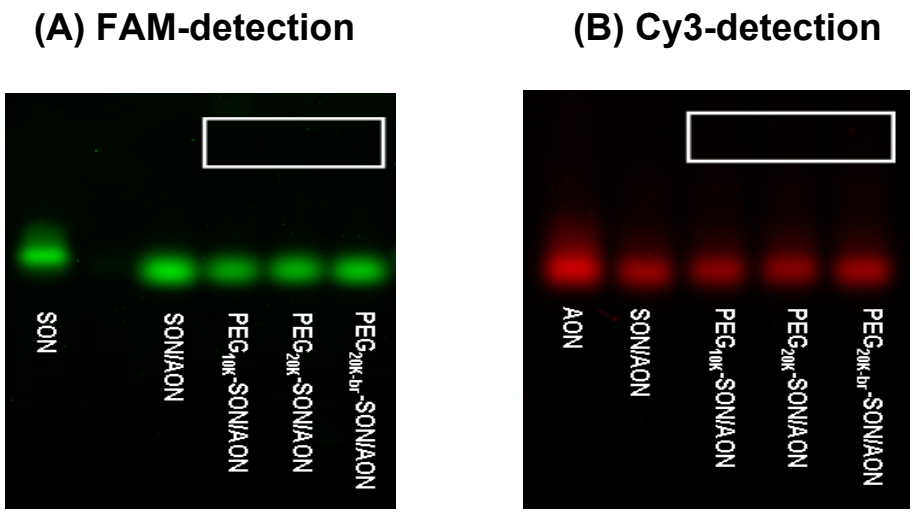

Figure 7. Migration profiles of PEG_{10K}-, PEG_{20K}- and $PEG_{20K\text{-}br}$-SON/AON on 2%-agarose gel after degradation by DNase 1 (60 U/µg ON, 1 h, 37°C, pH 7.4) and of intact SON and AON. The gel was scanned for FAM-labeled SON (λ_{ex} = 488 nm) (**A**) and Cy3-labeled AON (λ_{ex} = 532 nm) (**B**) detection. The empty white box corresponds to the original bands of the non-degraded PEG-SON/AON duplexes.

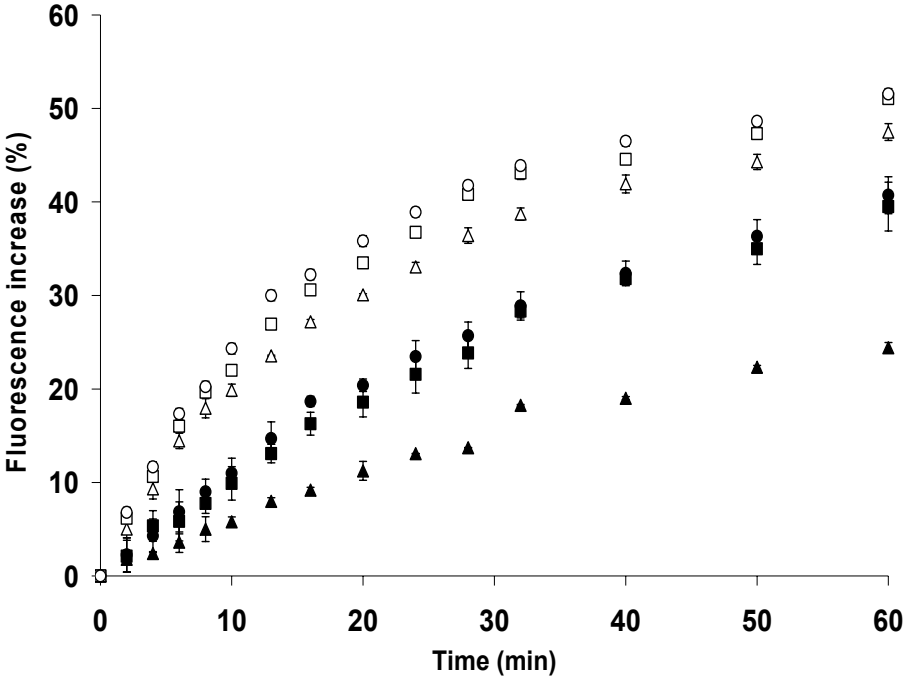

Figure 8. Dequenching of FAM-labeled SON fluorescence following the incubation with DNase 1 (60 U/µg ON, 37°C, pH 7.4) of PEG_{10K}- (triangles), PEG_{20K}- (squares), $PEG_{20K\text{-}br}$- (circles) SON/AON/PAMAM based PICM prepared with G3 (open symbols) or G5 (closed symbols) PAMAM. Mean ± SD (n=3).

To confirm that the dequenching of the FAM fluorescence was associated with the degradation of SON and the release of intact AON, the digests were analyzed by agarose gel electrophoresis (Figure 7). The exposure of SON/AON to DNase 1 resulted in the degradation of the SON as shown by the difference in FAM-SON migration compared to the control SON (panel A). Conversely, the AON from the DNase 1-exposed SON/AON migrated to the same level as the control AON (panel B), suggesting the release of the intact antisense strand. With respect to the PEG-SON/AON conjugates, the disappearance of the signal at the bottom of the gel (box area, panels A-B) confirmed the cleavage of the DNA strands from PEG. As for SON/AON, this was accompanied by the release of degraded SON (panel A) and intact AON (panel B).

As illustrated in Figure 8, the release rate of the AON could be further slowed down by complexing PEG-SON/AON conjugates to G3/G5 PAMAMs. Indeed, a reduction in V_{max} of up to ~20-100 fold was achieved with the PICM. As with the uncomplexed PEG-SON/AON conjugates, K_m values remained unchanged. Given that the DNA is sequestered in the core of the PICM (Scheme 1B), it is unlikely that the endonuclease was able to access the entrapped SON with the same affinity as the uncomplexed strand. As PICM are in dynamic equilibrium with free unimers [39], the enzymatic attack most probably occurred on the unimers (the dotted arrows in Scheme 1B). The degradation of unimers (PEG-SON/AON and/or non-micellized PEG-SON/AON/PAMAM) then shifted the equilibrium towards the unimer side, progressively depleting the micelle population. Generally, G3 PAMAM yielded PICM with faster release rates than G5 PAMAM (Table 2). The greater protection

against enzymatic attack was afforded by the PICM prepared with the PEG_{10K} derivative which might be owing to the fact that these micelles self-assemble at lower concentration making the unimers less available for reacting with DNase 1. These findings are in accordance with the NaCl-stability assays which revealed the greater stability of PEG_{10K}- and/or G5 PAMAM micelles.

5. Conclusion

Conjugates comprised of PEG and a nuclease-sensitive PD-SON were prepared and hybridized with a nuclease-resistant PS-AON. PEGylation did not change the *in vitro* hybridization capacity of the SON for its complementary sequence. The PEGylated derivatives released the AON upon degradation of SON. The cleavage rate was slowed down by about 50-65% *versus* the SON/AON duplex. Complexation of the PEG-SON/AON with G3/G5 PAMAMs yielded the formation of monodisperse PICM with average diameters in the 70-100 nm range, depending on the PAMAM generation and PEG molecular weights. Compared to the SON/AON duplex, the PICM slowed down SON degradation V_{max} by about 20-100 fold. The reaction rates were influenced by both the PEG and PICM molecular weights. The PEGylated conjugates reported in this manuscript as well as their complexes with PAMAMs could prove potentially useful to confer prolonged circulating properties to nucleic acid drugs and release them in a sustained manner.

6. Acknowledgement

This work was supported financially by the Canada Research Chair Program.

7. References

[1] Dean, N. M & Bennett, C. F. *Oncogene* **22,** 9087-9096 (2003).

[2] Lebedeva, I. & Stein, C. A. *Annu. Rev. Pharmacol. Toxicol.* **41**, 403-419 (2001).

[3] Mani, S., Rudin, C. M., Kunkel, K., Holmlund, J. T., Geary, R. S., Kindler, H., L., Dorr, F. A. & Ratain, M. G. *Clin. Cancer Res.* **8**, 1042-1048 (2002).

[4] Nemunaitis, J., Holmlund, J. T., Kraynak, M., Richards, D., Bruce, J., Ognoskie, N., Kwoh, T. J., Geary, R., Dorr, A., Von Hoff, D. & Eckhardt, S. G. *J. Clin. Oncol.* **17**, 3586-3595 (1999).

[5] Wang, H., Hang, J., Shi, Z., Li, M., Yu, D., Kandimalla, E. R., Agrawal, S. & Zhang, R. *Int. J. Oncol.* **21**, 73-80 (2002).

[6] Zellweger, T., Miyake, H., Cooper, S., Chi, K., Conklin, B. S., Monia, B. P. & Gleave, M. E. *J. Pharmacol. Exp. Ther.* **298**, 934-940 (2001).

[7] Dias, N. & Stein, C. A. *Mol. Cancer Ther.* **1**, 347-355 (2002).

[8] Hogrefe, R. E. *Antisense Nucleic Acid Drug Dev.* **9**, 351-357(1999).

[9] Agrawal, S., Temsamani, J. & Tang, J. Y. *Proc. Natl. Acad. Sci. U. S. A.* **88**, 7595-7599 (1991).

[10] Kausch, I. & Bohle, A. *J. Urol.* **168**, 239-247 (2002).

[11] De Oliveira, M. C., Boutet, V., Fattal, E., Boquet, D., Grognet, J. M., Couvreur, P. & Deverre, J. R. *Life Sci.* **67**, 1625-1637 (2000).

[12] Kurreck, J. *Eur. J. Biochem.* **270**, 1628-1644 (2003).

[13] Li, S. D. & Huang, L. *Gene Ther.* **13**, 1313-1319 (2006).

[14] Kalota, A., Karabon, L., Swider, S. R., Viazovkina, E., Elzagheid, M., Damha, M. J. & Gewirtz, A. M. *Nucleic Acids Res.* **34**, 451-461 (2006).

[15] Manoharan, M. *Antisense Nucleic Acid Drug Dev.* **12**, 103-128 (2002).

[16] Crooke, S. T., Graham, M. J., Zuckerman, J. E., Brooks, D., Conklin, B. S., Cummins, L. L., Greig, M. J., Guinosso, C. J., Kornbrust, D., Manoharan, M., Sasmor, H. M., Schleich, T., Tivel, K. L. & Griffey, R. H. *J. Pharmacol. Exp. Ther.* **277**, 923-937 (1996).

[17] Krieg, A. M., Tonkinson, J., Matson, S., Zhao, Q., Saxon, M., Zhang, L. M., Bhanja, U., Yakubov, L. & Stein, C. A. *Proc. Natl. Acad. Sci. U. S. A.* **90**, 1048-1052 (1993).

[18] Tsutsumi, Y., Onda, M., Nagata, S., Lee, B., Kreitman, R. G. & Pastan, I. *Proc. Natl. Acad. Sci. U. S. A.* **97**, 8548-8553 (2000).

[19] Kim, S. H., Jeong, J. H., Mok, H., Lee, S. H., Kim, S. W. & Park, T. G. *Biotechnol. Prog.* **23**, 232-237 (2007).

[20] Kang, H., DeLong, R., Fisher, M. H. & Juliano, R. L. *Pharm. Res.* **22**, 2099-2106 (2005).

[21] Yoo, H. & Juliano, R. L. *Nucleic Acids Res.* **28**, 4225-4231 (2000).

[22] Yoo, H., Sazani, P. & Juliano, R. L. *Pharm. Res.* **16**, 1799-1804 (1999).

[23] Delong, R., Stephenson, R., Loftus, T., Fisher, M., Alahari, S., Nolting, A. & Juliano, R. L. *J. Pharm. Sci.* **86**, 762-764 (1997).

[24] Hussain, M., Shchepinov, M., Sohail, M., Benter, I. F., Hollins, A. J., Southern, E. M. & Akhtar, S. *J. Control. Release* **99**, 139-155 (2004).

[25] Kukowska-Latallo, J. F., Bielinska, A. U., Johnson, J., Spindler, R., Tomalia, D. A. & Baker, J. R. *Proc. Natl. Acad. Sci. U. S. A.* **93**, 4897-4902 (1996).

[26] Eichman, J. D., Bielinska, A. U., Kukowska-Latallo, J. F. & Baker, J. R. *Pharm. Sci. Technol. Today* **3**, 232-245 (2000).

[27] Roberts, J. C., Bhalgat, M. K. & Zera, R. T. *J. Biomed. Mater. Res.* **30**, 53-65 (1996).

[28] Harada, A., Togawa, H. & Kataoka, K. *Eur. J. Pharm. Sci.* **13**, 35-42 (2001).

[29] Harada-Shiba, M., Yamauchi, K., Harada, A., Takamisawa, I., Shimokado, K. & Kataoka, K. *Gene Ther.* **9**, 407-414 (2002).

[30] Marras, S. A., Kramer, F. R. & Tyagi, S. *Nucleic Acids Res.* **30**, e122 (2002).

[31] Jeong, J. H., Kim, S. W. & Park, T. G. *J. Control. Release* **93**, 183-191 (2003).

[32] Karen, T. J., Lewis, J. & Akhtar, S. *J. Control. Release* **37**, 173-183 (1995).

[33] Fersht, A. *Enzyme structure and mechanism*, 2nd ed., W.H. Freeman, New York, pp. 99-109 (1985).

[34] Harris, D. C. *Quantitative chemical analysis*, 6th ed., Freeman, New York, pp. 640-657 (2003).

[35] Jeong, J. H., Kim, S. H., Kim, S. W. & Park, T. G. *Bioconjugate Chem.* **16**, 1034-1037 (2005).

[36] Ogris, M., Brunner, S., Schuller, S., Kircheis, R. & Wagner, E. *Gene Ther.* **6**, 595-605 (1999).

[37] Chen, W., Turro, N. J. & Tomalia, D. A. *Langmuir* **16**, 15-19 (2000).

[38] Dufes, C., Uchegbu, I. F. & Schatzlein, A. G. *Adv. Drug Deliv. Rev.* **57**, 2177-2202 (2005).

[39] Dufresne, M. H. & Leroux, J. C. *Pharm. Res.* **21**, 160-169 (2004).

[40] Lee, S. H., Kim, S. H. & Park, T. G. *Biochem. Biophys. Res. Commun.* **357**, 511-516 (2007).

[41] Oh, J. K., Tang, C., Gao, H., Tsarevsky, N. V. & Matyjaszewski, K. *J. Am. Chem. Soc.* **128**, 5578-5584 (2006).

CHAPTER 5 - Delivery of nucleic acids through the controlled disassembly of multifunctional nanocomplexes[4]

Mahmoud Elsabahy[1], Nada Wazen[1], Núria Bayó-Puxan[1], Glen Deleavey[2], Marc Servant[1], Masad J. Damha[2] and Jean-Christophe Leroux[1,3,4]

[1]Faculty of Pharmacy, University of Montreal, C.P. 6128, Succursale Centre-Ville, Montreal (QC) Canada H3C 3J7, [2]Department of Chemistry, McGill University, Montreal (QC) Canada H3A 2K6, [3]Canada Research Chair in Drug Delivery, [4]Drug Formulation and Delivery, Institute of Pharmaceutical Sciences, ETH Zürich, Wolfgang-Pauli-Str. 10, 8093 Zürich, Switzerland

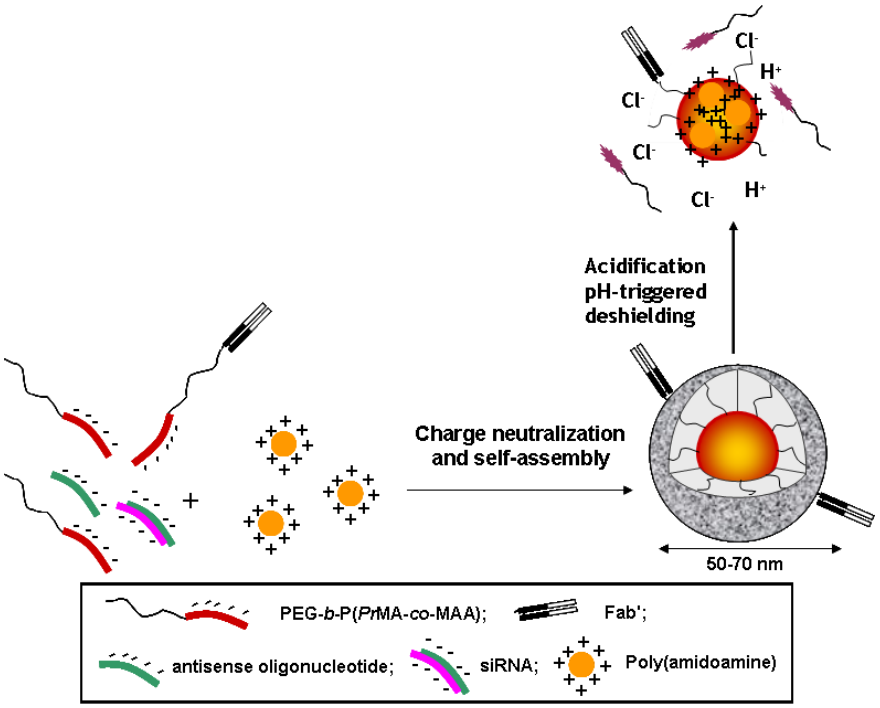

[4] *Adv. Funct. Mater.* in press (2009).

Abstract

In this study, novel pH-responsive polyion complex micelles (PICMs) were developed for the efficient delivery of nucleic acid drugs such as antisense oligonucleotide (AON) and short interfering RNA (siRNA). The PICMs consisted of a poly(amidoamine) (PAMAM) dendrimer-nucleic acid core and a detachable poly(ethylene glycol)-*block*-poly(*propyl* methacrylate-*co*-methacrylic acid) (PEG-*b*-P(*Pr*MA-*co*-MAA)) shell. The micelles displayed a mean hydrodynamic diameters ranging from 50 to 70 nm, a narrow size distribution and a nearly neutral surface charge. They could be lyophilized without any additive and stored in dried form. Upon redispersion in water, no change in complexation efficiency or colloidal properties was observed. Entry of the micelles into cancers cells was mediated by a monoclonal antibody fragment positioned at the extremity of the PEG segment *via* a disulfide linkage. Upon cellular uptake and protonation of the MAA units in the acidic endosomal environment, the micelles lost their corona, thereby exposing their positively-charged endosomolytic PAMAM/nucleic acid core. When these pH-responsive targeted-PICMs were loaded with AON or siRNAs that targeted the oncoprotein Bcl-2, they exhibited a greater transfection activity than non-targeted PICMs or commercial PAMAM dendrimers. Moreover, their non specific cytotoxicity was lower than that of PAMAM. The pH-responsive PICMs reported here appear as promising carriers for the delivery of nucleic acids.

1. Introduction

The use of nucleic acids such as antisense oligonucleotides (AON) and short interfering RNA (siRNA), which are capable of selectively suppressing genes involved in pathological processes is an elegant strategy to tackle diseases such as cancer and viral infections.[1-5] Unfortunately, the efficacy of oligonucleotide-based drugs is still largely hampered by their inability to reach their site of action in sufficient amounts. Parameters such as systemic circulation time, deposition at the target site and intracellular transport play a pivotal role in their *in vivo* activity.[6-8] Unmodified nucleic acids have limited cellular uptake due to their polyanionic nature. In addition, they are rapidly cleared from the body because of their degradation by nucleases in the blood and rapid renal excretion. The chemical instability and fast elimination issues can be partly overcome through specific modifications of the oligonucleotide backbone[9] but achieving high intracellular concentrations solely through chemistry is hardly achievable. Of particular importance is the fate of the nucleic acid after cellular internalization. The intracellular bioavailability of oligonucleotides is poor due to their sequestration in endosomal/lysosomal compartments. Membrane-destabilizing agents are therefore used to permit the escape of biomolecules from endosomes before they reach the lysosomes, where they are otherwise extensively degraded.[10, 11]

An approach to enhance the stability of nucleic acids but also to improve their deposition at the target site consists of loading them into polymeric nanocarriers such as polyion complex micelles (PICMs).[12, 13] PICMs decorated with a targeting ligand are conceptually one of the best vehicles for the delivery of nucleic acids.[14, 15]

PICMs result from cooperative electrostatic interactions between the AON or siRNA and one or several charged polymers presenting a water-soluble nonionic segment. Upon complexation, the charge-compensated nucleic acid/polymeric chains self-assemble into a micellar core while the hydrophilic segments form a protecting corona. Entrapment of nucleic acids in such carriers has been shown to protect them from enzymatic degradation while allowing a greater proportion of intact drug to reach the target cell.[16-18]

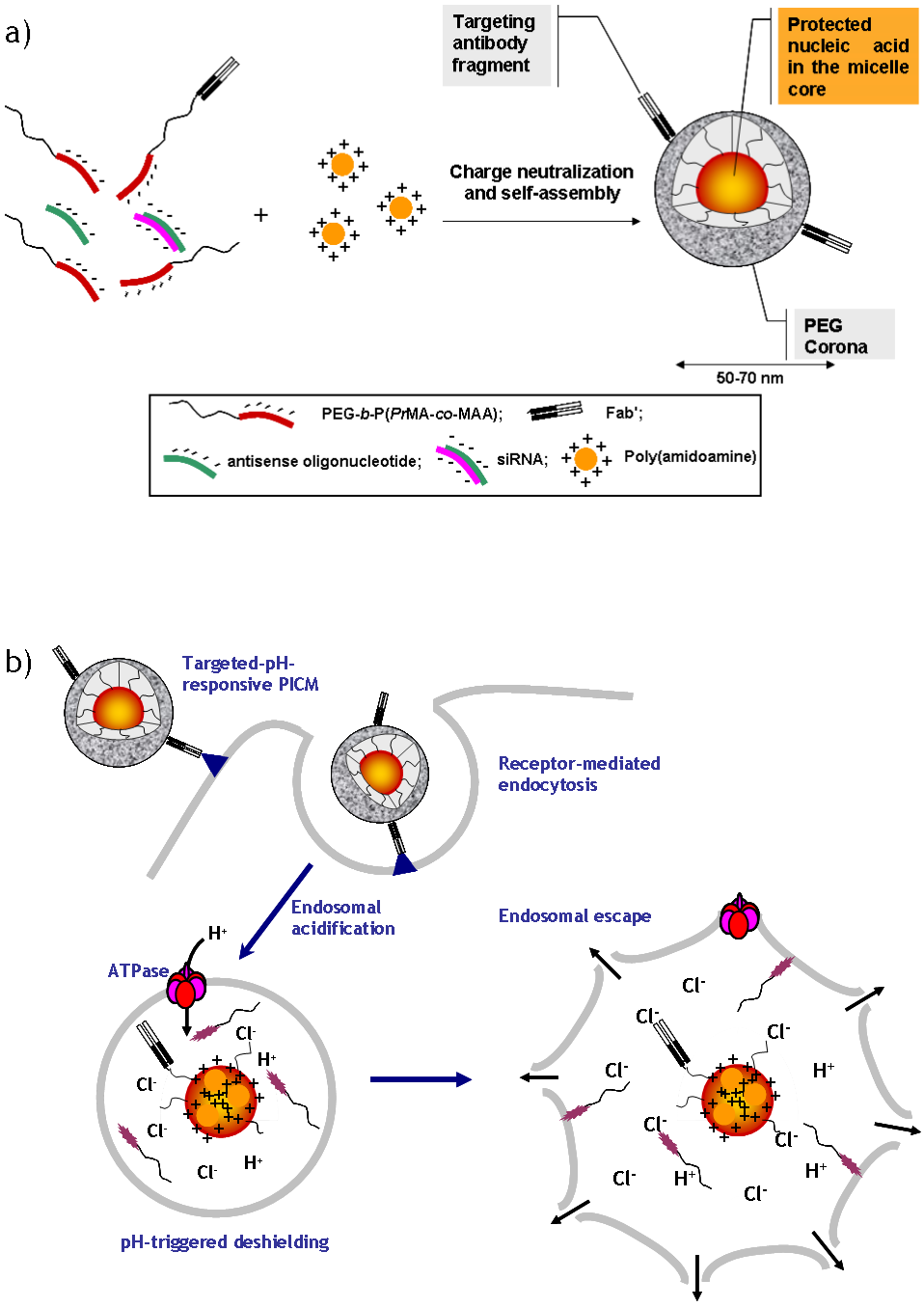

Scheme 1. a) Approach investigated to deliver AON or siRNA: self-assembly of PEG_{115}-*b*-P(*Pr*MA-*co*-MAA)/Fab'-PEG_{145}-*b*-P(*Pr*MA-*co*-MAA) and AON or siRNA with PAMAM to form PICM. b) Proposed mechanism by which the PICM can trigger the endosomal destabilization and facilitate endosomal escape of nucleic acids.

In this work, a PICM system combining several of the essential attributes required for the efficient delivery of polynucleotides into cancer cells is described. The PICMs were designed to exhibit long shelf-life, protection against premature degradation by nucleases, low non-specific cytotoxicity, minimal interactions with blood proteins, efficient uptake by the tumoral cell and high intracellular bioavailability for nucleic acid cargo. They consisted of a poly(amidoamine) (PAMAM) dendrimer-nucleic acid core and a poly(ethylene glycol)-*block*-poly(*propyl* methacrylate-*co*-methacrylic acid) (PEG-*b*-P(*Pr*MA-*co*-MAA)) shell[19, 20] (Scheme 1a). Generally, dendrimers of low molecular weights (generation (G) 5 or less) have low toxicity and are subjected to rapid renal clearance.[21] However, those with cationic surface charge are particularly cleared from the circulation by the liver.[21-23] At physiological pH (7.4), the shell and the core are linked through electrostatic interactions between positive charges of PAMAM and deprotonated MAA moieties of PEG-*b*-P(*Pr*MA-*co*-MAA). Entry in the cell *via* receptor-mediated endocytosis is mediated by a model targeting ligand (fragment antigen binding (Fab')) positioned at the extremity of the PEG segment. Upon cellular uptake and protonation of the MAA units in the acidic endosomal environment, the micelles lose their corona, thereby exposing their positively-charged PAMAM/nucleic acid core (Scheme 1b). PAMAM dendrimers have been shown to destabilize the endosomal membrane through their interaction with the latter and/or *via* the proton sponge effect.[24, 25] We show here that when these pH-responsive Fab'-PICMs are loaded with AON or siRNAs that target the oncoprotein Bcl-2,[26] they exhibit a greater transfection activity than non-targeted PICMs or PAMAM dendrimers.

2. Results and discussion

PEG-*b*-P(*Pr*MA-*co*-MAA) were initially developed to prepare pH-sensitive polymeric micelles for oral drug delivery.[19, 20] The *Pr*MA units were copolymerized with MAA to prevent extensive H-bonding between the later and PEG block in aqueous media. It was discovered that PEG-*b*-P(*Pr*MA-*co*-MAA) could also interact with conventional PAMAM dendrimers to form core-shell type PICMs. More importantly, these PICMs accommodated nucleic acids in their cores. Two different MAA copolymers, *i.e.* PEG_{115}-*b*-P(*Pr*MA_{28}-*co*-MAA_{53}) and PEG_{115}-*b*-P(*Pr*MA_{51}-*co*-MAA_{33}), were synthesized (supplementary Scheme S1 and Table S1) and investigated for the preparation of pH-responsive PICMs. In the presence of G3 or G5 PAMAM, and at an optimal nitrogen-to-(phosphate + carboxylate) ($N/(P + COO^-)$) molar ratio of 1.5, PICMs with mean hydrodynamic diameters ranging from 50 to 70 nm, narrow size distribution (polydispersity indices (PI) < 0.2) and nearly neutral surface charge (1–10 mV) were obtained (supplementary Table S2). Size and PI increased slightly with the PAMAM generation (G3 *vs.* G5) and when the siRNA duplex was used instead of the single stranded AON. The efficient complexation of both MAA copolymer and nucleic acids with the PAMAM dendrimer was assessed by gel electrophoresis. Figure 1 shows the migration of PEG_{115}-*b*-P(*Pr*MA_{28}-*co*-MAA_{53}) and siRNA alone (lanes 1 and 2), and after PICM formation (lanes 3 and 4) using G5 PAMAM. By comparing the PICMs lanes to that of the free components, one can see that the nucleic acid and PEG_{115}-*b*-P(*Pr*MA_{28}-*co*-MAA_{53}) were quantitatively incorporated into the micelles. Entrapment was less efficient when PEG_{115}-*b*-P(*Pr*MA_{51}-*co*-MAA_{33}) or G3 PAMAM were used (data not shown),

possibly due to reduced cooperative electrostatic interactions.[17] Interestingly, these PICMs could be freeze-dried and easily redispersed without any change in complexation efficiency (Fig. 1, lane 4 *vs*. 3), size, PI and zeta-potential (supplementary Table S2). This remarkable resistance to aggregation during the freeze-drying steps in the absence of a lyoprotectant[27] or chemical modification (*i.e.* core crosslinking),[28] might be attributed to a high PEG density in the corona.[29]

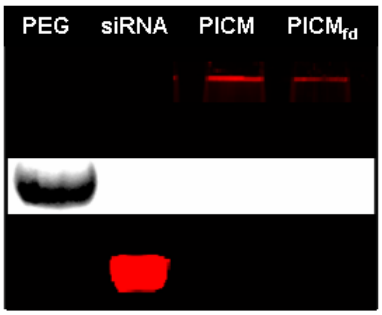

Figure 1. Gel electrophoresis of PICM prepared at N/(P + COO^-) molar ratio of 1.5 using PEG_{115}-*b*-P(*Pr*MA_{28}-*co*-MAA_{53}), siRNA and G5 PAMAM before and after freeze-drying. First 2 lanes represent PEG_{115}-*b*-P(*Pr*MA_{28}-*co*-MAA_{53}) and siRNA controls. The white inset corresponds to the same gel but following iodine staining to reveal PEG.

In order to study the pH-dependent complexation of PEG-*b*-P(*Pr*MA-*co*-MAA) to the PAMAM-nucleic acid core, the zeta potential and light scattering intensity of the PICMs were monitored as a function of pH (Fig. 2). At pH 7.0 and above, micelle formation occurred and was characterized by a strong intensity of scattered light and a zeta potential close to neutrality. The acidification of the external medium resulted in a drastic decrease of scattered light and an increase in zeta potential value (Fig. 2a). These data indirectly suggest that upon protonation, PEG-*b*-

P(*Pr*MA-*co*-MAA) dissociated from the PAMAM/nucleic acid core, leaving excess positive charges available to interact with the endosomal membrane (Fig. 2b).

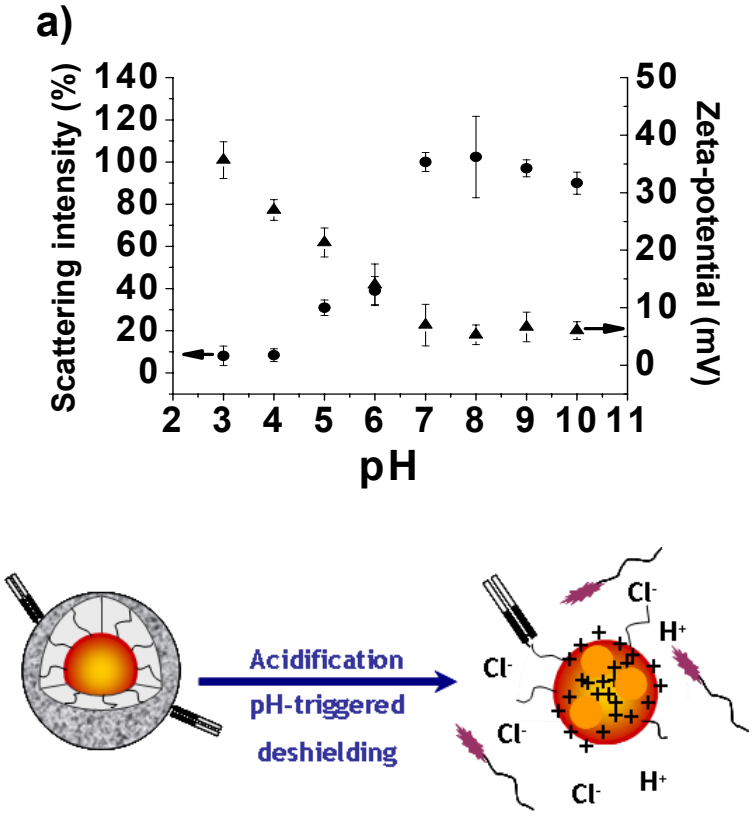

Figure 2. a) Effect of pH on scattering intensity (●) and zeta-potential (▲) of PEG_{115}-*b*-(*Pr*MA_{28}-*co*-MAA_{53})/AON/G5 PAMAM based PICM. Mean ± SD (n=3). b) Proposed mechanism of shell dissociation.

The protection against nucleic acid degradation by nucleases afforded by the PICMs was studied by a fluorescence dequenching assay using dually labeled siRNA, and by gel electrophoresis. The complete degradation of siRNA in fetal bovine serum (FBS) was accompanied by a strong increase in fluorescence intensity of the fluorescein probe and the disappearance of the band corresponding to intact

siRNA (supplementary Fig. S1). The stability of the siRNA, either free, complexed solely to PAMAM or entrapped within the PICMs, was monitored in 50% FBS as a function of time. Free siRNA was rapidly degraded in serum (>90% after 1-h incubation). The siRNA/G3 and G5 PAMAM complexes were more resistant (70 and 45% degradation after 1 h-incubation, respectively). The PICMs were extremely more resistant with less than 30% of the siRNA degraded after 1 h (Fig. 3). The enzymatic attack most probably occurred on the unimers and/or non-micellized PAMAM/siRNA as access to the micelle core was previously shown to be highly restricted.[17] The greatest protection against enzymatic attack was afforded by the PICMs prepared with G5 PAMAM and PEG_{115}-*b*-P(*Pr*MA_{28}-*co*-MAA_{53}), probably due to enhanced cooperative interactions between the nucleic acids and the charged polymers. These findings are in accordance with the gel electrophoresis experiments which revealed the presence of larger fraction of free nucleic acids for micelles formed with G3 PAMAM and/or PEG_{115}-*b*-P(*Pr*MA_{51}-*co*-MAA_{33}) (data not shown). The stability of the nucleic acid could be further improved by increasing the N/(P + COO^-) molar ratio from 1.5 to 3. In this case only 12% of the siRNA was degraded after 1-h incubation with 100% serum (supplementary Fig. S2).[30]

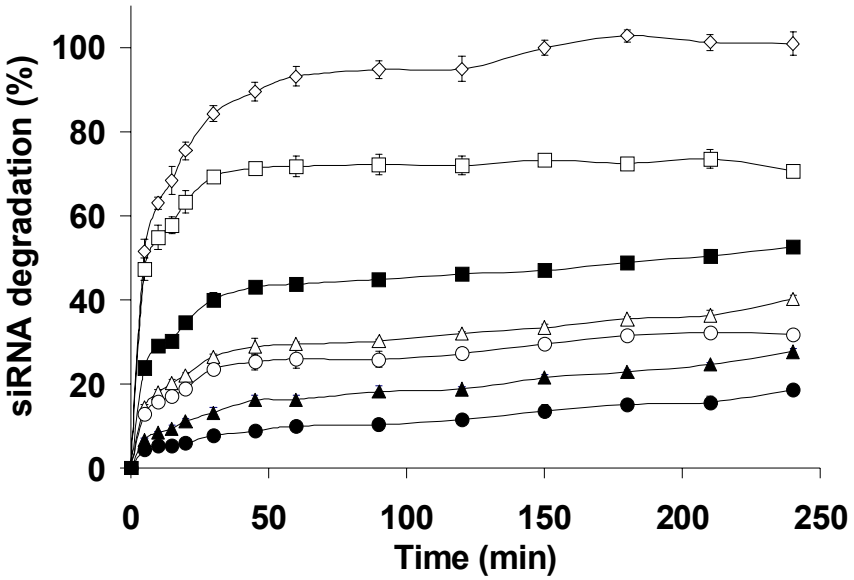

Figure 3. siRNA degradation following incubation with 50% FBS (10 μg/mL siRNA, 37°C, pH 7.4) of free siRNA (◊), siRNA complexed with G3 (□) or G5 (■) PAMAM, PEG_{115}-*b*-P(*Pr*MA_{51}-*co*-MAA_{33}) (triangles) and PEG_{115}-*b*-P(*Pr*MA_{28}-*co*-MAA_{53}) (circles) PICM prepared with G3 (open symbols) or G5 (closed symbols) PAMAM. Mean ± SD (n=3).

The toxicity of the polymers and PICMs was then investigated on prostate cancer (PC-3) cells using MTT assay. Figure 4 presents the cytotoxicity data generated with free PEG_{115}-*b*-P(*Pr*MA_{28}-*co*-MAA_{53}), G5 PAMAM and PICMs resulting from the complexation of these two polymers. PEG_{115}-*b*-P(*Pr*MA_{28}-*co*-MAA_{53}) exhibited no measurable cytotoxicity up to 0.5 mg/mL. In contrast, G5 PAMAM was appreciably more toxic above 0.01 mg/mL. A marked decrease in the cytotoxicity of PAMAM was noted when the dendrimer was complexed with PEG_{115}-*b*-P(*Pr*MA_{28}-*co*-MAA_{53}) to form PICMs. This decrease in cytotoxicity could be explained by the neutralization of the positive charges at the dendrimer surface by the PEG chains.[31] Due to its high complexation efficacy, greater stability against

enzymatic degradation and low cytotoxicity, the PEG_{115}-*b*-P(*Pr*MA_{28}-*co*-MAA_{53})/G5 PAMAM combination was selected for the cellular uptake experiments and transfection assays (*vide infra*).

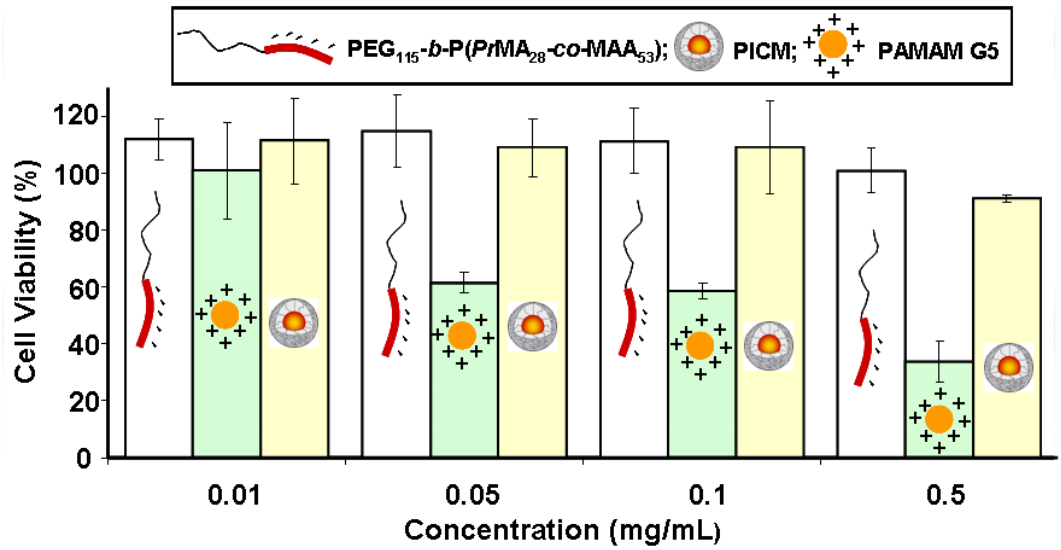

Figure 4. Cell viability of PC-3 cells exposed to PEG_{115}-*b*-P(*Pr*MA_{28}-*co*-MAA_{53}) and G5 PAMAM (0.01-0.5 mg/mL) and PEG_{115}-*b*-P(*Pr*MA_{28}-*co*-MAA_{53})/G5 PAMAM PICM (N/COO^- molar ratio of 1.5). Mean ± SD (n=3).

In order to trigger the internalization of the PICMs, the later were decorated with anti CD71 Fab' which targets the transferrin receptors, that are overexpressed by tumor cells.[32] The antibody fragment was linked to PEG-*b*-P(*Pr*MA-*co*-MAA) through disulfide coupling at the PEG extremity (supplementary scheme S1). PEG of longer chain length (145 *vs.* 115 repeat units, supplementary Table S1) was used to attach the Fab' to ensure its availability on the micelle surface for efficient binding to the receptors. The micelle size and zeta-potential were not changed significantly after decoration with the targeting moiety incorporated at 2 mol% (data not shown). The cellular uptake and intracellular trafficking of the delivered nucleic acid were

examined by flow cytometry and laser scanning confocal microscopy (LSCM), respectively (Fig. 5). The free nucleic acid showed limited uptake (Fig. 5a and supplementary Fig. S3). As expected, the PAMAM/nucleic acid complexes interacted avidly with the cell membrane, as revealed by the strong cell-associated fluorescence. However, a large fraction of AON was localized in acidic compartments (Fig. 5b) as indicated by the yellow color in the merged fluorescence image (Panel A-iii) of the LysoTracker (green, Panel A-i) and the Cy3-labeled oligonucleotide (red, Panel A-ii). Decoration of the PICMs with the anti CD71 Fab' increased the uptake compared to non-targeted micelles (Fig. 5a). The uptake was reduced when the cells were preincubated with free CD71 antibody (supplementary Fig. S4), confirming the specificity of the binding. Interestingly, although targeted PICMs were taken up to a lesser extent than PAMAM/nucleic acid complexes, the oligonucleotide was able to escape more from the lysosomal pathway as indicated by the bright red fluorescence of the cells (Fig. 5b, Panel B-ii). These cells also exhibited a decreased green fluorescence suggesting some leakage from acidic organelles (Panel B-iii).[33, 34]

The formulation of AON or siRNA in Fab'-PICMs prepared with G5 PAMAM and PEG_{115}-*b*-P(*Pr*MA_{28}-*co*-MAA_{53}) was associated to an increased antisense/silencing activity against the oncoprotein Bcl-2 in PC-3 cells *vs.* the nucleic acids in their free form, complexed to PAMAM or incorporated into non targeted micelles (Fig. 5c). In addition, the targeted micelles showed higher activity than lipofectamine (supplementary Fig. S5). Preincubation with excess free antibody (saturation of CD71 receptors) or bafilomycin (inhibition of endosomal acidification) greatly reduced the transfection efficiency. The reduced downregulation after

preincubation with bafilomycin suggests that the endosomal acidification played a pivotal role, possibly by releasing the positively charged PAMAM/nucleic acid complex which became available for endosomal destabilization. As shown in Figure 5c, the PICM activity was only slightly reduced in the presence of serum in the incubation medium. This effect of serum could be ascribed to some degradation of the nucleic acid as the PEGylated shell should prevent non-specific interactions with blood proteins.[14] Targeted micelles prepared at N/(P + COO^-) of 3 were able to efficiently downregulate the Bcl-2 oncoprotein in the presence of 50% FBS. On the contrary, in the presence of the same serum concentration, there was no Bcl-2 inhibition by AON or siRNA that complexed to lipofectamine (supplementary Fig. S5). As opposed to G5 PAMAM, Fab'-PICMs prepared with G3 PAMAM were inefficient at downregulating Bcl-2 (Fig. 5c). The lower transfection efficiency of G3 PAMAM-based PICM can be partially attributed to the reduced entrapment efficiency and enzymatic stability of these micelles. The enhanced activity of AON/siRNA when formulated in G5 PAMAM-based Fab'-PICMs can be rationalized in terms of efficient cellular uptake and greater escape from the endosomal compartment. At the endosomal pH (~5), the dissociation of the micelle corona produced > 10-fold increase in the N/P ratio, leaving positively charged PAMAM/nucleic acids complexes available for interacting with the membrane. Moreover, the protonated PEG-*b*-P(*Pr*MA-*co*-MAA) may also have contributed to the release of the nucleic acid in the cytoplasm, as it has been previously shown that MAA copolymers possess endosomolytic properties.[35]

a)

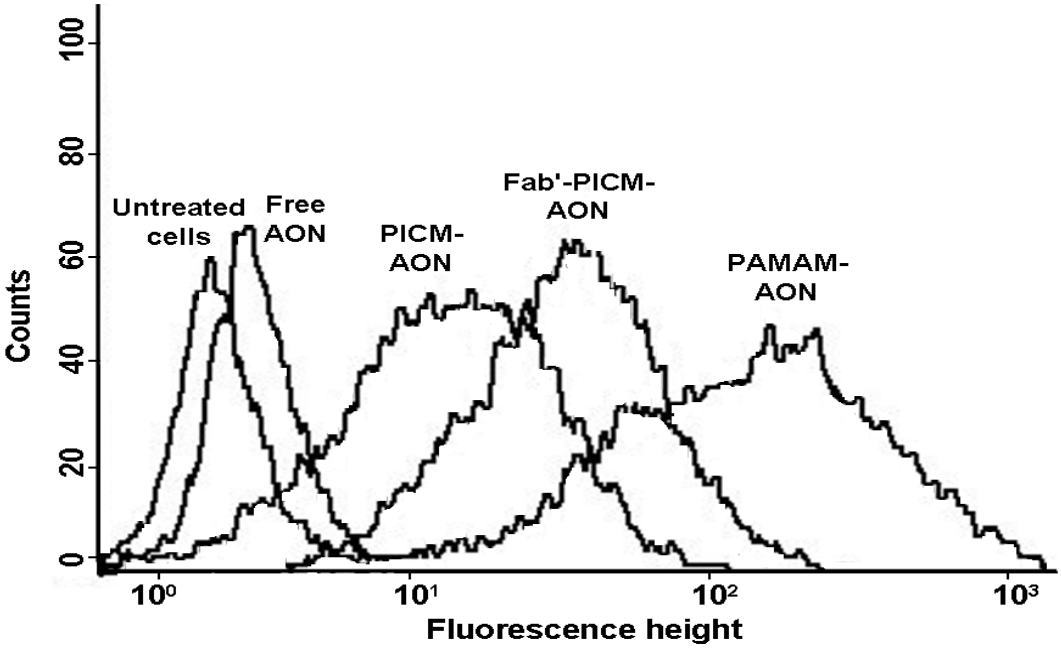
Counts
0
20
40
60
80
100
Untreated cells
Free AON
PICM-AON
Fab'-PICM-AON
PAMAM-AON
10⁰
10¹
10²
10³
Fluorescence height

b)

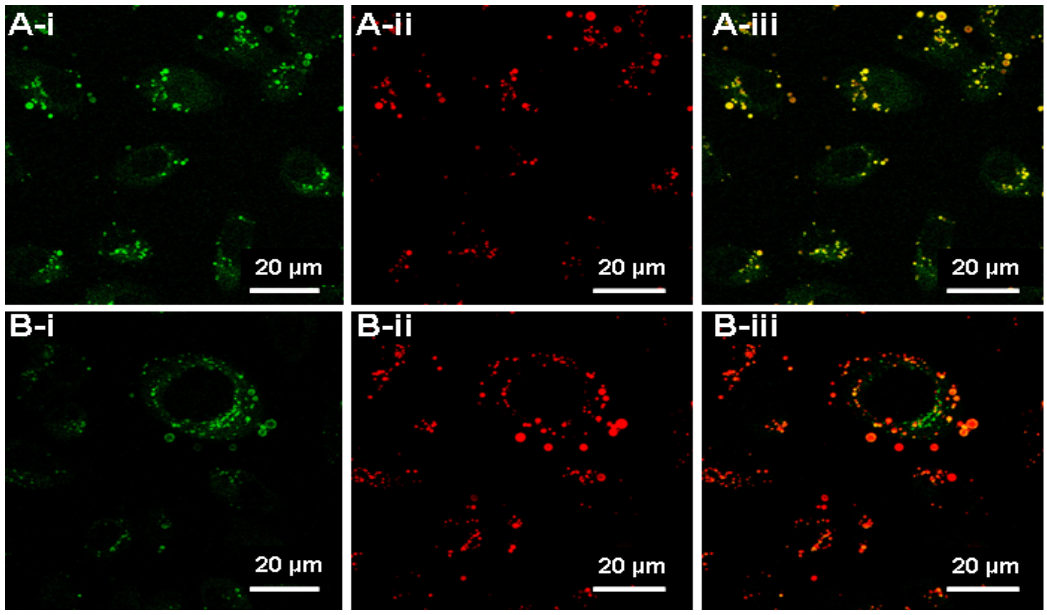
A-i
A-ii
A-iii
B-i
B-ii
B-iii
20 µm

c)

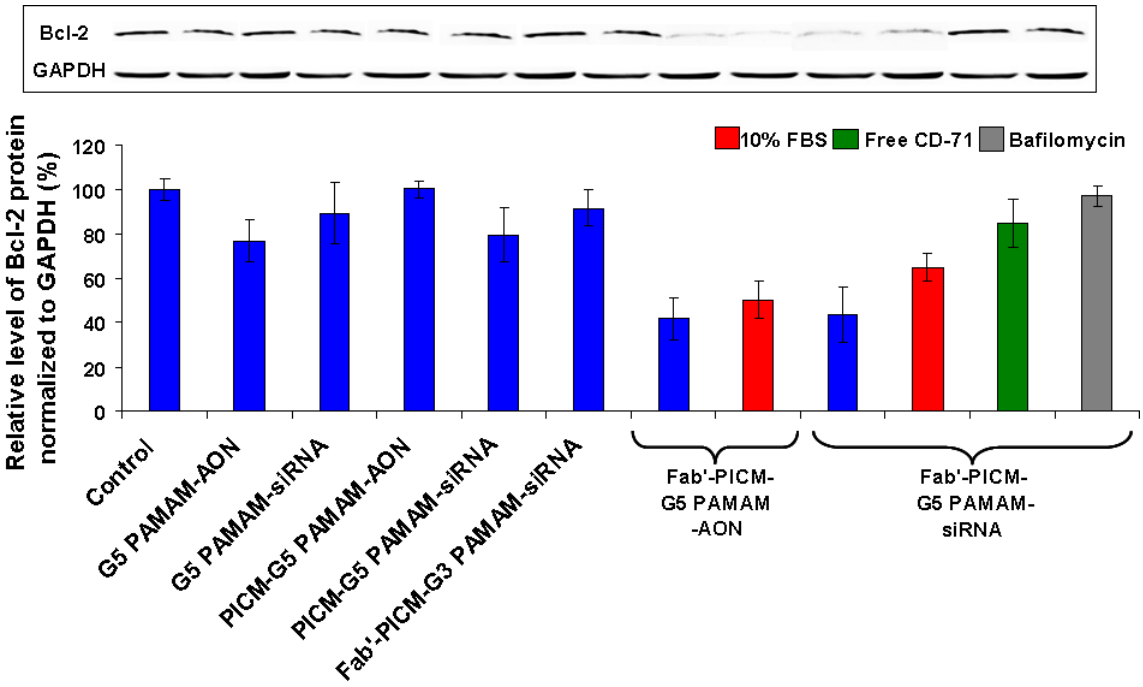

Figure 5. a) Flow cytometry experiment showing the fluorescence intensity of PC-3 cells incubated with Cy3-labeled AON (400 nM) free, complexed to G5 PAMAM or entrapped in plain or Fab'-PEG_{115}-*b*-P(*Pr*MA_{28}-*co*-MAA_{53})/G5 PAMAM PICM (N/(P + COO^-) molar ratio of 1.5). b) Confocal microscopy images of PC-3 cells after treatment with Cy3-AON (red, panel ii) complexed to (A) G5 PAMAM or (B) Fab'-PEG_{115}-*b*-P(*Pr*MA_{28}-*co*-MAA_{53})/G5 PAMAM PICM. Endosomes/lysosomes were stained by LysoTracker (green, panel i), and the images were merged in panel iii. c) Bcl-2 gene silencing in PC-3 cells transfected for 5 h with AON (400 nM) or siRNA (25 nM) complexed to G5 PAMAM or entrapped in plain or Fab'-PEG_{115}-*b*-P(*Pr*MA_{28}-*co*-MAA_{53})/G5 or G3 PAMAM PICM. Control cells were treated with medium alone. The effect of preincubation with 10% FBS, free CD71 or bafilomycin is indicated on the graph. The inset is representative of immunoreactive Bcl-2 and glyceraldehyde-3-phosphate dehydrogenase (GAPDH) as determined by immunoblotting. The molar ratio of the Fab'-PEG_{145}-*b*-P(*Pr*MA_{27}-*co*-MAA_{58}) *vs.* PEG_{115}-*b*-P(*Pr*MA_{28}-*co*-MAA_{53}) is 2% for all the experiments. The results are representative of several independent experiments.

In conclusion, stable PICMs were prepared and found to efficiently protect nucleic acids against enzymatic degradation. The long-term stability of the formulations is also guaranteed by the fact that these micelles could be lyophilized without any additive and thus stored in dried form. pH-triggered deshielding in the acidic organelles was found to unmask the positive charge of the PAMAM/nucleic complexes and facilitate the diffusion of the nucleic acids into the cytoplasm. Herein, the exposure of the membrane destabilizing components does not rely on the chemical hydrolysis of a pH-sensitive bond.[11] This approach would be preferred to ensure fast dissociation kinetics at acidic pH and higher chemical integrity of the construct. The pH-responsive targeted PICMs were endowed with improved transfection efficacy compared to either non-targeted micelles or PAMAM complexes. This *in vitro* proof of concept constitutes our first step toward the development of clinically viable systemic delivery systems for nucleic acid drugs.

3. Experimental Section

Synthesis of PEG_{115}-*b*-(*Pr*MA-*co*-MAA) and Fab'-S-S-PEG_{145}-*b*-(*Pr*MA_{27}-*co*-MAA_{53}) (supplementary sections S1 and S2, Table S1 and Scheme S1): PEG macroinitiator, *i.e.* α-(2-bromoisobutyrylate bromide)-ω-methyl PEG, was synthesized using methoxy-PEG (M_n = 5000) and 2-bromoisobutyryl bromide [32]. The polymerization reactions were carried out by atom transfer radical polymerization (ATRP) of *Pr*MA and *tert*-butyl methacrylate (*t*BMA) as reported previously [33]. For the targeted copolymer, *t*Bu-S-PEG_{145}-OH was synthesized and converted to ATRP macroinitiator by reaction with 2-bromoisobutyryl bromide as

reported previously [34]. The unprotected copolymer was dissolved in a reductive solution (10 mg/mL, DTT in phosphate-buffered saline (PBS) pH 7.4) and recovered by passage through a Sephadex G25 column (GE healthcare, Piscataway, NJ). Fractions containing the copolymer were added directly to an aldrithiol solution in methanol and the reaction was stirred overnight. The solvent was evaporated and the copolymer was purified by passage through a Sephadex G25 column and recovered by freeze-drying (the yield of functionalization ~90%). Antitransferrin antibody was digested to produce $(Fab')_2$ antibody fragments according to $(Fab')_2$ preparation kit (Pierce, Rockford, IL). The *Pyr*-S-S-PEG copolymer was then added to the freshly reduced Fab' (1.4-fold excess) and the coupling reaction was carried out overnight. The excess antibody was removed by passage through an anion exchange column (Hitrap, GE healthcare).

Preparation and characterization of pH-sensitive PICM (supplementary S3 and S4): PEG_{115}-*b*-P(*Pr*MA-*co*-MAA) and either AON or siRNA were mixed with G3 or G5 PAMAM at increasing $N/(P + COO^-)$ molar ratio in Tris buffer (10 mM, pH 7.4) to form PICM. The mean hydrodynamic diameter, PI, and scattering intensity of PICM were measured by dynamic light scattering (DLS) using a Malvern Zetasizer Nanoseries ZS. PICM prepared with fluorescein-labeled siRNA (50 mol%) were used for the gel electrophoresis assays [35]. The stability of siRNA in serum was monitored by spectrofluorimetry as described elsewhere for similar systems [36].

Evaluation of cellular toxicity by MTT assay (supplementary S5): PEG_{115}-*b*-P($PrMA_{28}$-*co*-MAA_{53}), G5 PAMAM or PICM were added at increasing concentrations to PC-3 cells for 4 h. After a total incubation period of 72-h, the cells

were exposed to 10 µL/well of tetrazolium salt 3-(4,5-dimethylthiazol-2-yl)-2,5-diphenyl tetrazolium bromide (MTT) solution for 3.5 h. Then, 100 µL of sodium dodecyl sulfate solution was added to each well and the absorbance was read 24 h later at 570 nm using a Tecan Safire plate reader.

Flow cytometry and intracellular trafficking (supplementary S5): The final concentration of the AON (labeled with Cy3) in the different formulations was adjusted to 400 nM. The plate was then incubated for 2 h under mild agitation at 37°C. Cells were then washed three times with cold PBS, fixed with 1% formaldehyde and resuspended in 0.5 mL PBS. Red fluorescence distributions for 10,000 cells was recorded at the appropriate wavelength with a FacsCalibur flow cytometer (Becton Dickinson, San Jose, CA) at a laser excitation wavelength of 530 nm. For intracellular trafficking, the formulations were incubated with the PC-3 cells for 4 h. Two hours before the end of the incubation period, LysoTracker green was added to each well at a final concentration of 200 nM. Cells were examined by LSCM under a Leica DMIRBE inverted microscope coupled with a Leica TCS SP confocal system (Leica Microsystems, Heidelberg, Germany).

Assessment of the antisense activity: The transfection of the PC-3 cells was carried out as reported elsewhere (See section S5 in the supporting information for detailed method) [22].

4. Acknowledgement

This work was financially supported by the Natural Sciences and Engineering Research Council of Canada (NSERC), the Canada Research Chair program (J. C. Leroux) and the Canadian Institutes of Health Research (M. J. Damha).

5. References

[1] A. Fire, S. Xu, M. K. Montgomery, S. A. Kostas, S. E. Driver, C. C. Mello, *Nature* **1998,** *391*, 806.

[2] S. M. Elbashir, W. Lendeckel, T. Tuschl, *Genes Dev.* **2001**, *15*, 188.

[3] N. M. Dean, C. F. Bennett, *Oncogene* **2003,** *22*, 9087.

[4] R. M. Schiffelers, A. Ansari, J. Xu, Q. Zhou, Q. Tang, G. Storm, G. Molema, P. Y. Lu, P. V. Scaria, M. C. Woodle, *Nucleic Acids Res.* **2004,** *32*, e149.

[5] Y. Chen, G. Cheng, R. I. Mahato, *Pharm. Res.* **2008,** *25*, 72.

[6] J. Kurreck, *Eur. J. Biochem.* **2003,** *270*, 1628.

[7] S. D. Li, L. Huang, *Gene Ther.* **2006,** *13*, 1313.

[8] M. C. De Oliveira, V. Boutet, E. Fattal, D. Boquet, J. M. Grognet, P. Couvreur, J. R. Deverre, *Life Sci.* **2000,** *67*, 1625.

[9] C. Wolfrum, S. Shi, K. N. Jayaprakash, M. Jayaraman, G. Wang, R. K. Pandey, K. G. Rajeev, T. Nakayama, K. Charrise, E. M. Ndungo, T. Zimmermann, V. Koteliansky, M. Manoharan, M. Stoffel, *Nat. Biotechnol* **2007,** *25*, 1149.

[10] C. C. Lee, J. A. MacKay, J. M. Frechet, F. C. Szoka, *Nat. Biotechnol* **2005,** *23*, 1517.

[11] D. B. Rozema, D. L. Lewis, D. H. Wakefield, S. C. Wong, J. J. Klein, P. L. Roesch, S. L. Bertin, T. W. Reppen, Q. Chu, A. V. Blokhin, J. E. Hagstrom, J. A. Wolff, *Proc. Natl. Acad. Sci. U. S. A.* **2007,** *104*, 12982.

[12] N. Nishiyama, K. Kataoka, *Pharmacol. Ther.* **2006,** *112*, 630.

[13] A. Harada, K. Kataoka, *Science* **1999,** *283***,** 65.

[14] M. Oishi, Y. Nagasaki, K. Itaka, N. Nishiyama, K. Kataoka, *J. Am. Chem. Soc.* **2005,** *127*, 1624.

[15] K. Itaka, N. Kanayama, N. Nishiyama, W. D. Jang, Y. Yamasaki, K. Nakamura, H. Kawaguchi, K. Kataoka, *J. Am. Chem. Soc.* **2004,** *126*, 13612.

[16] M. Harada-Shiba, K. Yamauchi, A. Harada, I. Takamisawa, K. Shimokado, K. Kataoka, *Gene Ther.* **2002,** *9*, 407.

[17] M. Elsabahy, M. Zhang, S. Gan, K. C. Waldron, J. C. Leroux, *Soft Matter* **2008,** *4*, 294.

[18] M. H. Dufresne, M. Elsabahy, J. C. Leroux, *Pharm. Res.* **2008,** *25*, 2083.

[19] P. Satturwar, M. N. Eddine, F. Ravenelle, J. C. Leroux, *Eur. J. Pharm. Biopharm.* **2007,** *65*, 379.

[20] V. P. Sant, D. Smith, J. C. Leroux, *J. Control. Release* **2005,** *104*, 289.

[21] R. Duncan, L. Izzo, *Adv. Drug Deliv. Rev.* **2005,** *57*, 2215.

[22] N. Malik, R. Wiwattanapatapee, R. Klopsch, K. Lorenz, H. Frey, J. W. Weener, E. W. Meijer, W. Paulus, R. Duncan, *J. Control. Release* **2000,** *65*, 133.

[23] J. C. Roberts, M. K. Bhalgat, R. T. Zera, *J. Biomed. Mater. Res.* **1996,** *30*, 53.

[24] C. Dufes, I. F. Uchegbu, A. G. Schatzlein, *Adv. Drug Deliv. Rev.* **2005,** *57*, 2177.

[25] S. Hong, P. R. Leroueil, E. K. Janus, J. L. Peters, M. M. Kober, M. T. Islam, B. G. Orr, J. R. Baker, Jr., M. M. Banaszak, *Bioconjugate Chem.* **2006,** *17*, 728.

[26] E. M. Anderson, P. Miller, D. Ilsley, W. Marshall, A. Khvorova, C. A. Stein, L. Benimetskaya, *Cancer Gene Ther.* **2006,** *13*, 406.

[27] M. O. Andersen, K. A. Howard, S. R. Paludan, F. Besenbacher, J. Kjems, *Biomaterials* **2008,** *29*, 506.

[28] K. Miyata, Y. Kakizawa, N. Nishiyama, Y. Yamasaki, T. Watanabe, M. Kohara, K. Kataoka, *J. Control. Release* **2005,** *109*, 15.

[29] N. Kang, M. E. Perron, R. E. Prud'homme, Y. Zhang, G. Gaucher, J. C. Leroux, *Nano Lett.* **2005,** *5*, 315.

[30] M. Elsabahy, M. H. Dufresne, J. C. Leroux, in Materials for Nanomedicine (Eds.: V. Torchilin, M. Amiji), Pan Stanford, Hackensack, **2009,** in press.

[31] R. Jevprasesphant, J. Penny, R. Jalal, D. Attwood, N. B. McKeown, A. D'Emanuele, *Int. J. Pharm.* **2003,** *252*, 263.

[32] D. Hogemann-Savellano, E. Bos, C. Blondet, F. Sato, T. Abe, L. Josephson, R. Weissleder, J. Gaudet, D. Sgroi, P. J. Peters, J. P. Basilion, *Neoplasia* **2003,** 5, 495.

[33] M. A. Yessine, M. H. Dufresne, C. Meier, H. U. Petereit, J. C. Leroux, *Bioconjugate Chem.* **2007,** *18*, 1010.

[34] X. B. Xiong, H. Uludag, A. Lavasanifar, *Biomaterials* **2009,** *30*, 242.

[35] M. A. Yessine, J. C. Leroux, *Adv. Drug Deliv. Rev.* **2004,** *56*, 999.

[36] M. Ranger, M. C. Jones, M. A. Yessine, J. C. Leroux, *J. Polym. Sci. Polym. Chem.* **2001,** *39*, 3861.

[37] V. P. Sant, D. Smith, J. C. Leroux, *J. Control. Release* **2004,** *97*, 301.

[38] M. H. Dufresne, M. A. Gauthier, J. C. Leroux, *Bioconjugate Chem.* **2005,** *16*, 1027.

[39] B. Zimmerman, L. D. Murphy, *Anal. Biochem.* **1996,** *234*, 190.

[40] S. A. Marras, F. R. Kramer, S. Tyagi, *Nucleic Acids Res.* **2003,** *30*, e122.

Supporting information

S1. NMR analysis and molecular weight determination

^{1}H NMR spectra were recorded on a Bruker AMX 300 spectrometer (Bruker Spectrospin, Milton, ON, Canada) in $CDCl_3$ or D_2O at 25°C. M_n and polydispersity indices (PI) were determined by size exclusion chromatography with an Alliance GPCV 2000 system (Waters, Midford, MA), using high sensitivity refractive index detector as reported earlier [1]. Monodisperse PEG standards served to establish the calibration curve.

S2. Synthesis of PEG_{115}-*b*-(*Pr*MA-*co*-MAA) and Fab'-S-S-PEG_{145}-*b*-(*Pr*MA_{27}-*co*-MAA_{58}) (supplementary Scheme S1)

PEG macroinitiator, *i.e.* α-(2-bromoisobutyrylate bromide)-ω-methyl PEG, was synthesized using methoxy-PEG (M_n = 5000) and 2-bromoisobutyryl bromide [1]. The polymerization reactions were carried out by atom transfer radical polymerization (ATRP) of *Pr*MA and *tert*-butyl methacrylate (*t*BMA) as reported previously [2]. The transformation of *t*BMA into MAA was achieved by cleaving the PEG-*b*-P(*Pr*MA-*co*-*t*BMA) in concentrated HCl and dioxane, as described elsewhere [3]. Two copolymers with different compositions were synthesized and characterized (supplementary Table S1).

*t*Bu-S-PEG_{145}-OH was synthesized and converted to ATRP macroinitiator by reaction with 2-bromoisobutyryl bromide for 48 h at room temperature as reported previously [3]. Then, 500 mg of the macroinitiator was dissolved in 2 mL of THF and transferred to flask containing *Pr*MA (280 µL, 25 equiv), *t*BuMA (630 µL, 50 equiv),

bipyridine (24 mg, 2 equiv) and CuBr (I) (7.8 mg, 0.7 equiv). The reaction mixture was degassed, stirred for 15 min and then the flask was placed overnight in an oil bath thermostated at 65°C. The block copolymer was purified by silica column. The terminal thiol and carboxylic acid groups (from MAA units) were generated by adding TFA-DMSO (95:5 *v*/*v*) and let the reaction proceed for 3 h. After removing TFA, the product was basified to pH 10 and washed with ethyl acetate. Aqueous phase was dialyzed against water and lyophilized (23% yield). The unprotected copolymer (9 mg) was dissolved in a reductive solution (10 mg/mL, DTT in phosphate-buffered saline (PBS) pH 7.4, 0.1 M, 0.15 M NaCl) for 6 h. Then the copolymer was recovered by passage through a Sephadex G25 column (GE healthcare, Piscataway, NJ). Fractions containing the copolymer were added directly to an aldrithiol solution in methanol (8 mg in 40 mL), and the reaction was stirred overnight. The solvent was evaporated and the copolymer was purified by passage through a Sephadex G25 column and recovered by freeze-drying. The yield of functionalization (~90%) was determined by reacting an aliquot with DTT and measuring the absorbance at 343 nm (thiopyridone was used as a standard). Antitransferrin antibody (Medicorp, Montreal, QC, Canada) directed against the transferrin receptors was digested to produce $(Fab')_2$ antibody fragments according to $(Fab')_2$ preparation kit (Pierce, Rockford, IL). The *Pyr*-S-S-PEG copolymer was dissolved in degassed Tris (10 mM, pH 7.4), and freshly reduced Fab' (1.4-fold excess) was then added. The coupling reaction was carried out overnight. The excess antibody was removed by passage through an anion exchange column (Hitrap, GE healthcare). The amount of Fab' per copolymer was determined by UV-absorbance at

280 nm and BCA protein assay kit using BSA standards (Pierce) (~15% functionalization).

S3. Preparation and characterization of pH-sensitive PICM

Unlabeled and Cy3-phosphorothioate-AON (5′-TGAAACTCACCAGCGAGAAC) that target the initiation codon of Bcl-2 mRNA [4] was obtained from Alpha DNA (Montreal, QC, Canada). Unlabeled and 5′-DY547 (sense strand)-3′-fluorescein (antisense strand) Bcl-2 targeting siRNA (5′-GCAUGCGGCCUCUGUUUGA) [4], was purchased from Dharmacon (Chicago, IL). PEG_{115}-*b*-P(*Pr*MA-*co*-MAA) and either AON or siRNA were mixed with G3 or G5 PAMAM corresponding to M_w of 6,909 and 28,826 g/mol (Sigma-Aldrich, Oakville, ON, Canada) at increasing N/(P + COO^-) molar ratio in Tris buffer (10 mM, pH 7.4) to form PICM. The N correspond to the amino groups of the PAMAM while P and COO^- account for the phosphate and carboxylate groups of the nucleic acid and MAA copolymer, respectively. To compare the different formulations, the N/(P + COO^-) ratio was selected at 1.5 (unless otherwise indicated) because the micelles formed at this ratio exhibited the lowest PI. The final concentrations of the micelles were adjusted to have 0.1 mg/mL of PEG-*b*-(*Pr*MA-*co*-MAA). The mean hydrodynamic diameter, PI, and scattering intensity of PICM were measured by dynamic light scattering (DLS) using a Malvern Zetasizer Nanoseries ZS (Malvern, Worcestershire, UK) equipped with a backscattered light detector operating at 173°. The CONTIN program was used to extract size distributions from the autocorrelation functions. The scattering intensity and zeta potential of the PICM were determined in

Tris buffer of pH values ranging from 3 to 10 by DLS and laser Doppler anemometry, respectively, with Malvern Zetasizer Nanoseries ZS. Stoichiometric PICM were frozen in liquid ethanol at -50°C, kept at -80°C for 2 h and freeze-dried for 48 h. Changes in micelle size, PI and zeta-potential were evaluated after redispersion of the dried cakes in Tris buffer. For gel electrophoresis experiments, PICM were prepared using siRNA solutions mixed with fluorescein-labeled siRNA (50 mol%). Samples were mixed with glycerol and loaded onto a 20% (*w/v*) acrylamide gel. Following migration, the siRNA was visualized by UV irradiation using a Typhoon^{TM} 9410 Workstation with variable mode imager (Amersham Biosciences, Pittsburgh, PA). The λ_{ex}/ λ_{em} were set at 532/670 nm. Then, the gel was fixed and stained with iodine, as reported elsewhere [5] to assess the presence of free PEG chains. The gel was photographed without destaining using ChemiImager 5500 imaging system (Alpha Innotech Corp., San Leandro, CA).

S4. Stability of siRNA in serum

The degradation of siRNA was monitored by spectrofluorimetry as described elsewhere for similar systems [6]. FRET from fluorescein-labeled antisense strand to the DY547-labeled-sense strand was exploited to follow the degradation of the siRNA as follows (Equation 1):

$$\%\ \text{of}\ siRNA\ \text{degradation} = \left[\frac{\left(I_{(Fl/Dy)\,t=t} - I_{(Fl/Dy)\,t=0}\right)}{\left(I_{(Fl/Dy)\,t=\infty} - I_{(Fl/Dy)\,t=0}\right)}\right] x\,100 \qquad (1)$$

where $I_{(Fl/Dy)}$ is the fluorescence intensity of fluorescein (λ_{em} = 525 nm)/DY547 (λ_{em} = 565 nm) when they are both excited at 488 nm, measured using a Tecan Safire plate reader (Tecan, Durham, NC). $I_{(Fl/Dy)t=0}$, $I_{(Fl/Dy)t=t}$ and $I_{(Fl/Dy)t=\infty}$ correspond to the FRET before siRNA degradation, at different time intervals and at the end of the experiment, respectively. PICM of different compositions were incubated with FBS. At the end of the experiment, heparin was added to destabilize the complexes. The FRET corresponds to 100% degradation was then determined after 24 h-incubation. To assess the siRNA degradation, samples were loaded into 20% acrylamide gel and visualized by UV irradiation.

S5. Cell culture

Evaluation of cellular toxicity by MTT assay: PEG_{115}-*b*-P(*Pr*MA_{28}-*co*-MAA_{53}), G5 PAMAM or PICM (sterilized by filtration) were prepared in Tris buffer at increasing concentrations. PC-3 cells (American Type Culture Collection, Manassas, VA) were maintained in RPMI medium. Cells were seeded in 96-well plates at a density of $5x10^3$ cells/well and cultured for 24 h at 37°C in a humidified atmosphere containing 5% CO_2. The medium was then replaced with Opti-Mem I medium (100 µL) prior to the addition of 20-µL aliquots of the polymers. After a 4-h incubation period, cells were rinsed with PBS, fed with 100 µL of fresh medium. After a total incubation period of 72-h, the cells were exposed to 10 µL/well of tetrazolium salt 3-(4,5-dimethylthiazol-2-yl)-2,5-diphenyl tetrazolium bromide (MTT) solution (5 mg/mL in PBS). After 3.5 h of incubation, 100 µL of sodium dodecyl sulfate solution (10% in HCl 0.01 N) was added to each well to dissolve the blue formazan product

generated by the oxidation of MTT by living cells. The absorbance was read 24 h later at 570 nm using a Tecan Safire plate reader.

Flow cytometry: PC-3 cells were plated in a 24-well tissue culture plate (1 mL medium containing $3x10^5$ viable cells). After 24 h, the cells were washed 3 times with 1 mL Opti-MEM and finally 0.3 mL of the medium was added to the cells prior to the addition of 100-µL aliquots of the formulations. The final concentration of the AON (labeled with Cy3) in the different formulations was adjusted to 400 nM. The plate was then incubated for 2 h under mild agitation at 37°C. Cells were then washed three times with cold PBS, fixed with 1% formaldehyde, washed once more with cold PBS and resuspended in 0.5 mL PBS. Red fluorescence distributions for 10,000 cells was recorded at the appropriate wavelength with a FacsCalibur flow cytometer (Becton Dickinson, San Jose, CA) at a laser excitation wavelength of 530 nm. Profiles are representative of at least 3 replicates.

Intracellular trafficking using LSCM: PC-3 cells were plated in 6-well plates ($5x10^5$ cells/well) containing coverslips. After 24 h, uncomplexed AON, PAMAM-AON or Fab'-PICM-AON (20 µg Cy3-AON) were incubated with cells for 4 h at 37°C in a humid atmosphere containing 5% CO_2. Two hours before the end of the incubation period, LysoTracker green (Invitrogen, Burlington, ON, Canada) was added to each well at a final concentration of 200 nM. After 4 h, the cells were washed five times with cold PBS, fixed in paraformaldehyde for 20 min. The cells were then washed with PBS and stored at 4°C. Cells were then examined by LSCM

under a Leica DMIRBE inverted microscope coupled with a Leica TCS SP confocal system (Leica Microsystems, Heidelberg, Germany). The cells were excited at 488 or 568 nm, and fluorescence was collected by emission windows set at 505-555 and 585-635 nm, respectively. Images collected by *LCS Lite* software (Leica Microsystems) were exported as TIFF files and prepared for publication by *Adobe Photoshop* v 7.0 software (Adobe Systems, San Jose, CA).

Assessment of the antisense activity: PC-3 cells were plated in a 6-well plate ($1.5x10^5$ cells/well). After 24 h, the medium was replaced by Opti-Mem I reduced serum medium. The cells were incubated for 5 h at 37°C with the different formulations in the absence or presence of 10% or 50% FBS. Then, the cells were washed with complete RPMI medium. After total incubation time of 72 h, they were washed with PBS, and extracted in 200-µL lysis buffer consisting of Tris–HCl, pH 8.0 (0.01 M), NaCl (0.14 M), Triton X-100 (1% *v*/*v*), aprotinin (0.1 U/mL) and phenylmethylsulfonyl fluoride (0.5 mM). The cell lysates were incubated for 1 h at 4°C, and centrifuged at 8000 *g* for 10 min at 4°C. Samples protein contents were determined with the BCA protein assay kit. The remaining samples were electrophoresed through a 15% (*w*/*v*) poly(acrylamide) gel, and the resolved proteins were transferred to a poly(vinylidene fluoride) membrane by electrotransfer. Bcl-2 expression was quantified by the use of an anti-Bcl-2 monoclonal antibody (Medicorp). To confirm equal loading, the expression of GAPDH was measured using an anti-GAPDH monoclonal antibody (Advanced Immunochemical Inc., Long Beach, CA). Both the mismatched AON sequence (5'-TCTCCCAGCATGTGCCAT)

(Alpha DNA) and the control siRNA (5'-UAGCGACUAAACACAUCAAUU) (Dharmacon) failed to downregulate the Bcl-2 protein.[4]

Table S1. Molecular characteristics of PEG-*b*-P(*Pr*MA-*co*-MAA)

Diblock copolymer[a]	M_n[a]	M_n[b]	PI[b]
PEG_{115}-*b*-P(*Pr*MA_{28}-*co*-MAA_{53})	13,300	13,500	1.19
PEG_{115}-*b*-P(*Pr*MA_{51}-*co*-MAA_{33})	14,500	11,900	1.20
*t*Bu-S-PEG_{145}-*b*-(*Pr*MA_{27}-*co*-MAA_{58})	14,800	14,400	1.30

[a] The subscripts denote the number of repeat units as measured by ^{1}H NMR.
[b] Measured by GPC.

Table S2. Characteristics of the ternary PICM prepared at N/(P + COO^-) molar ratio of 1.5 before and after lyophilization; mean ± SD (n=3).

Copolymer	PAMAM[a]	Nucleic acid[b]	Diameter [PI]		Zeta potential ± SD (mV)	
			Before lyophilization	Rehydrated PICM	Before lyophilization	Rehydrated PICM
PEG_{115}-*b*-P(*Pr*MA_{28}-*co*-MAA_{53})	G5	AON	60 [0.13]	60 [0.11]	6.3 ± 1.1	3.3 ± 1.5
PEG_{115}-*b*-P(*Pr*MA_{28}-*co*-MAA_{53})	G3	AON	58 [0.16]	56 [0.14]	1.2 ± 3.1	2.5 ± 0.5
PEG_{115}-*b*-P(*Pr*MA_{28}-*co*-MAA_{53})	G5	siRNA	70 [0.14]	68 [0.15]	9.3 (1.3)	5.6 (0.3)
PEG_{115}-*b*-P(*Pr*MA_{28}-*co*-MAA_{53})	G3	siRNA	67 [0.17]	66 [0.15]	0.9 (0.2)	2.0 (0.7)
PEG_{115}-*b*-P(*Pr*MA_{51}-*co*-MAA_{33})	G5	AON	58 [0.16]	56 [0.15]	4.3 ± 3.6	5.4 ± 4.6
PEG_{115}-*b*-P(*Pr*MA_{51}-*co*-MAA_{33})	G3	AON	56 [0.15]	54 [0.13]	2.3 ± 4.1	6.5 ± 2.8
PEG_{115}-*b*-P(*Pr*MA_{51}-*co*-MAA_{33})	G5	siRNA	62 [0.17]	62 [0.16]	4.0 (0.9)	2.6 (1.8)
PEG_{115}-*b*-P(*Pr*MA_{51}-*co*-MAA_{33})	G3	siRNA	61 [0.17]	58 [0.15]	3.6 (1.1)	6.7 (0..8)

[a]G3 = 6,909 g/mol, G5 = 28,826 g/mol.
[b]The AON or siRNA represents 5% of the negative charges in the formulations.

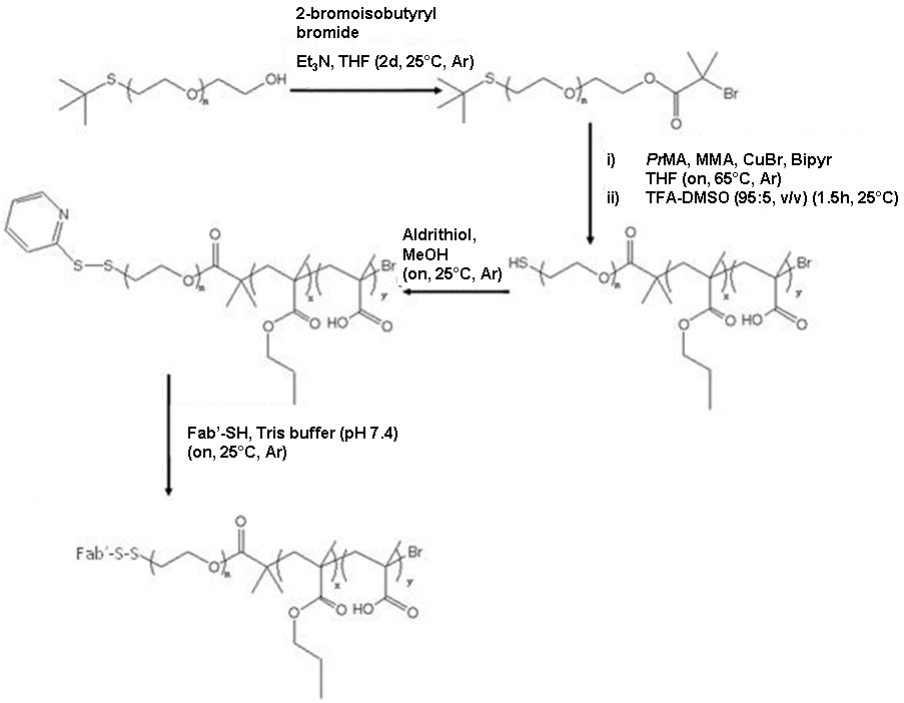

Scheme S1. Synthesis of the targeted block copolymer; Fab'-S-S-PEG-*b*-(*Pr*MA-*co*-MAA). n, x, and y represent the number PEG, *Pr*MA and MAA repeat units, respectively.

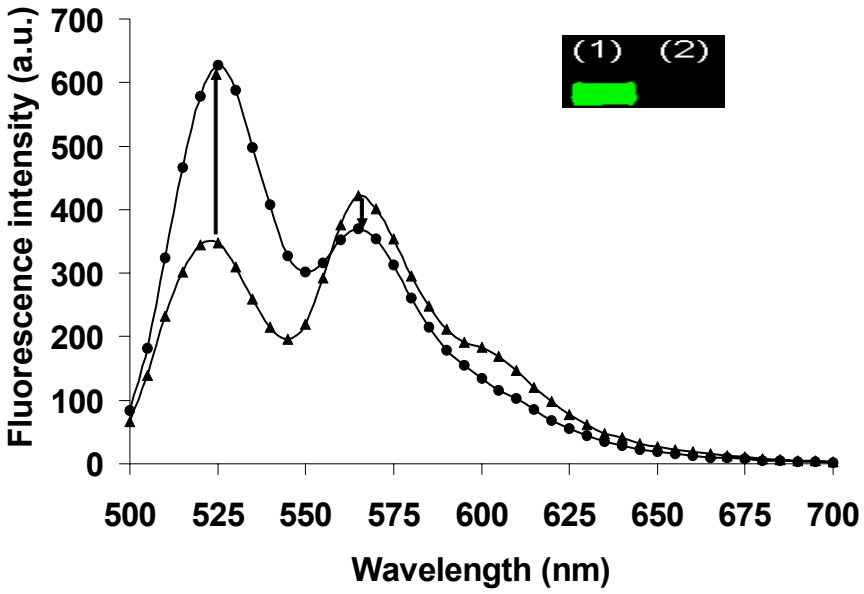

Figure S1. Emission spectrum of fluorescein- and DY547-labeled siRNA prior to (▲) and after (●) degradation in serum (λ_{ex} = 488 nm). The inset is the gel electrophoresis of the siRNA before (1) and after (2) degradation in serum when scanned at $\lambda_{ex}/\lambda_{em}$ of 488/526 nm.

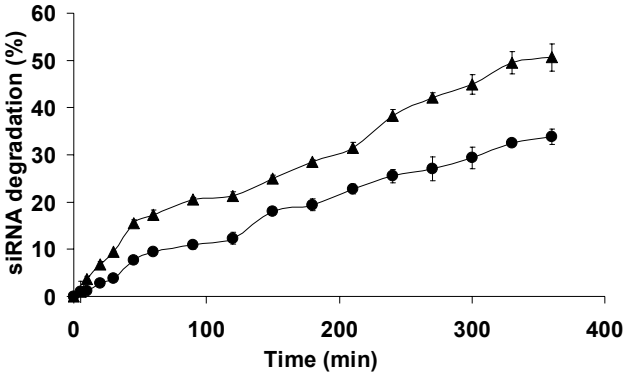

Figure S2. The stability of siRNA in PEG_{115}-*b*-P(*Pr*MA_{28}-*co*-MAA_{53})/ G5 PAMAM PICM following incubation with 100% FBS could be enhanced by increasing the N/(P + COO^-) molar ratio from 1.5 (▲) to 3 (●) (10 μg/mL siRNA, 37°C, pH 7.4). Mean ± SD (n=3).

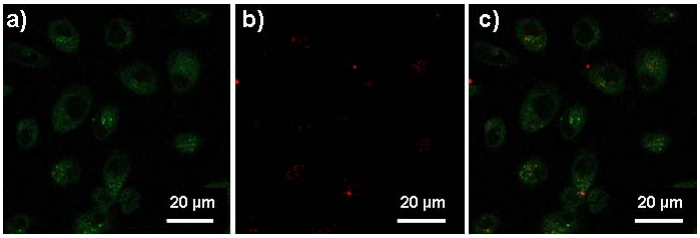

Figure S3. Confocal microscopy images of PC-3 cells after treatment with uncomplexed Cy3-AON (red, panel b). Endosomes/lysosomes were stained by LysoTracker (green, panel a), and the images were merged in panel c.

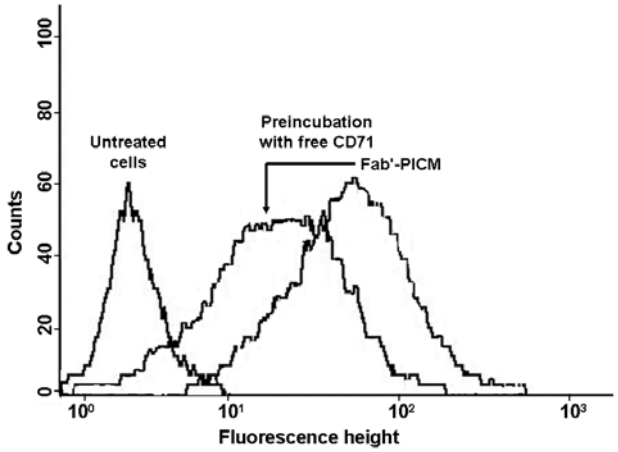

Figure S4. Red fluorescence intensity of PC-3 cells incubated with Cy3-labeled AON entrapped in Fab'-modified PEG_{115}-*b*-P(*Pr*MA_{28}-*co*-MAA_{53})/G5 PAMAM PICM either preincubated with free CD71 antibody or not. Fluorescence of unstained control cells is indicated.

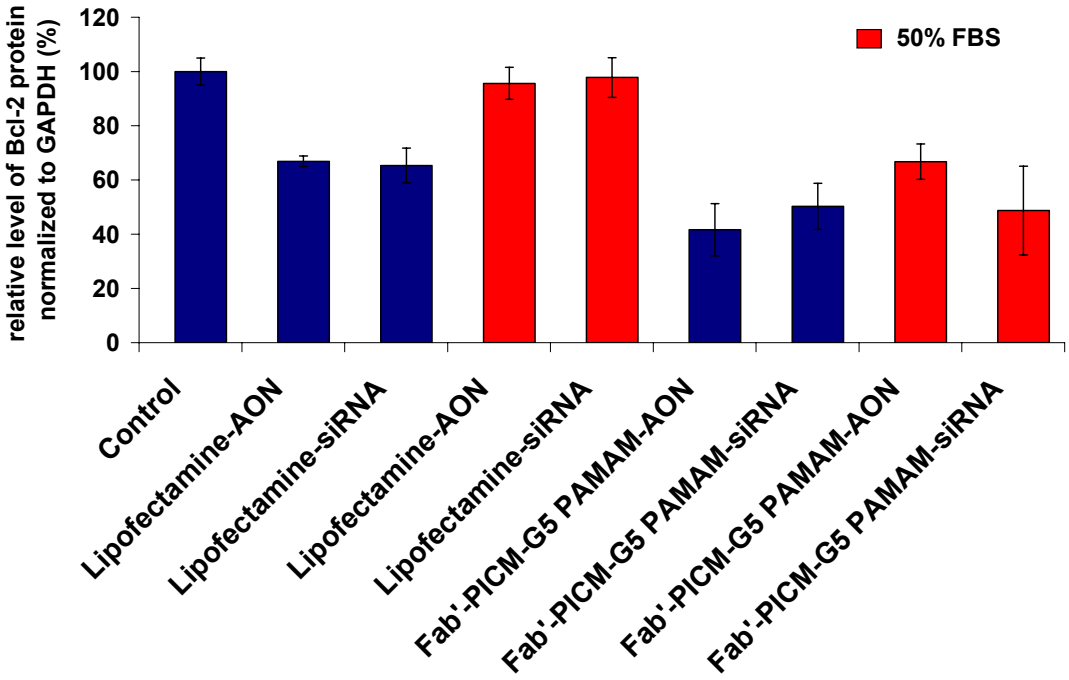

Figure S5. Bcl-2 gene silencing in PC-3 cells transfected for 5 h with AON (400 nM) or siRNA (25 nM) complexed lipofectamine (1 μg/mL) or entrapped in Fab'-PEG_{115}-*b*-P(*Pr*MA_{28}-*co*-MAA_{53})/G5 PAMAM PICMs at N/(P + COO^-) of 3 (final volume of the transfection medium is 2 mL). Control cells were treated with medium alone. The effect of preincubation with 50% FBS is indicated on the graph. The molar ratio of the Fab'-PEG_{145}-*b*-P(*Pr*MA_{27}-*co*-MAA_{58}) *vs.* PEG_{115}-*b*-P(*Pr*MA_{28}-*co*-MAA_{53}) is 2% for all the experiments. The results are representative of several independent experiments.

[1] M. Ranger, M. C. Jones, M. A. Yessine, J. C. Leroux, *J. Polym. Sci. Polym. Chem.* **2001,** *39*, 3861-3874.

[2] V. P. Sant, D. Smith, J. C. Leroux, *J. Control. Release* **2004,** *97*, 301-312.

[3] M. H. Dufresne, M. A. Gauthier, J. C. Leroux, *Bioconjugate Chem.* **2005,** *16*, 1027-1033.

[4] E. M. Anderson, P. Miller, D. Ilsley, W. Marshall, A. Khvorova, C. A. Stein, L. Benimetskaya, *Cancer Gene Ther.* **2006,** *13*, 406-414.

[5] B. Zimmerman, L. D. Murphy, *Anal. Biochem.* **1996,** *234*, 190-193.

[6] S. A. Marras, F. R. Kramer, S. Tyagi, *Nucleic Acids Res.* **2003,** *30*, e122.

CHAPTER 6 – Discussion

1. Hurdles facing current delivery systems

The general objective of this thesis was to develop polymeric nanocarriers for the delivery of hydrophobic anticancer drugs and nucleic acids. We selected docetaxel as a poorly water-soluble drug (2 μg/mL) because it is a clinically well-established treatment of breast, ovarian and non-small cell lung cancer. However, there are some problems associated with the current formulation used to dissolve docetaxel (*i.e.* Taxotere®), such as hypersensitivity reactions and premedication requirement[1]. Hence, a new delivery system is needed to overcome these disadvantages. For nucleic acids, we selected an antisense oligonucleotide (AON) and a short interfering RNA (siRNA) targeting the antiapoptotic oncogene Bcl-2[2]. This gene has been implicated in a number of human cancers, including breast, prostate and lung carcinoma[3]. It is also involved in the resistance to conventional cancer treatment. Downregulation of this gene by either AON or siRNA can sensitize cancer cells to chemotherapy[3,4]. Despite encouraging clinical results after treatment of cancer with G3139 (the Bcl-2-targeting AON), there are many hurdles to overcome. After intravenous injection, the α and β half-lives of the oligonucleotide were 5 and 37 min, respectively[5]. Thus, it was difficult to maintain a sustainable level of intact oligonucleotide after administration. Even with this low concentration, the polyanionic nature of AON and siRNA impairs their ability to penetrate the cellular membranes. Hence, we have focused our efforts on developing targeted polymeric delivery systems to overcome the problems associated with the current therapies. In

this thesis, two types of polymeric micelles (PM) have been developed for the delivery of docetaxel and nucleic acids.

2. PM for drug delivery

2.1 Micellar characterization

Diblock copolymers of poly(ethylene oxide) (PEO) and poly(butylene oxide) (PBO) or poly(styrene oxide) (PSO) can self-assemble at low concentrations into PM of various shapes, depending on relative block lengths, concentration and temperature[6,7]. Although these polymers have been characterized in several studies, their role as solubilizers has been reported only for the antifungal drug griseofulvin (at the time of publication)[8]. PM for docetaxel delivery were prepared using these copolymers. Low critical micelle concentration (CMC) values and high core viscosities were characteristic features of these micelles (Chapter 3, Table 2). Increasing the hydrophobicity by using PSO instead of PBO, or increasing the chain length of PBO or PSO resulted in lower CMC and higher core viscosity. Low CMC values and high core viscosities are indicative of a greater stability upon dilution after intravenous administration. This study also showed, for the first time, the different morphologies (*i.e.* spherical *vs.* cylindrical) of free or docetaxel-loaded PEO-*b*-PBO/PSO micelles by transmission electron microscopy. The importance of investigating micelle morphology lies in the fact that aggregates of different morphologies might display different characteristics. For example, cylindrical assemblies are usually associated with greater solubilization capacity than spherical

assemblies, given their larger core volume[8-11]. The pharmacokinetics are also expected to vary. Discher and coworkers[12-14] found that cylindrical poly(ethylene glycol) (PEG)-*b*-poly(ethylethylene) PM persist in the circulation (in rodents) about 10 times longer than their spherical counterparts. It was observed that the long cylindrical micelles were not taken up by the macrophages. In contrast, shorter micelles are taken up by cells, thus resulting in faster clearance.

2.2 Factors affecting drug-loading

The method of drug-loading, the common solvent utilized for the dissolution of polymer and drug, compatibility between the drug and micellar core, micelle morphology and nature of the drug are the main factors that affect loading capacity. Several procedures have been exploited for the incorporation of docetaxel into PEO-*b*-PBO/PSO micelles. The direct dissolution of docetaxel into a solution of pre-formed micelles resulted in low levels of loading. Hence, both the drug and polymer were dissolved in an organic solvent followed by evaporating the solvent under vacuum. Then, the resulting film was rehydrated with water. The success of this procedure was shown to depend on the nature of the organic solvent employed to form the polymer/drug matrix. Among the different solvent used, only ethanol gave a clear solution after rehydration with water. In another study, Zhang *et al.*[15] found that to incorporate paclitaxel in PEG-*b*-poly(D,L-lactide) (PEG-*b*-PDLLA) PM, only acetonitrile gave a clear solution after reconstitution in water.

PSO-based micelles incorporated more docetaxel (~3-4%) than PBO-micelles (<1%) likely because of the expanded micelle morphology (*i.e.* cylindrical *vs.* spherical). The higher loading capacity of PSO-micelles can be also due to the better

compatibility between docetaxel and PSO (Chapter 3, Tables 4 and 5). The solubilization capacities obtained here were comparable with published data on similar copolymers with different drugs (*e.g.* griseofulvin, furosemide and nabumetone). These are the only other results available for the solubilization of drugs in closely-related copolymers[16].

2.3 *In vitro* evaluation of the micelle formulations

PEO_{45}-*b*-PBO_{24} PM were able to preserve most of docetaxel's chemical integrity against hydrolytic degradation compared to the free drug. The micelles were also able to slow drug release (Chapter 3, Figure 5). The antimitotic activity of docetaxel-loaded micelles was evaluated on human prostate cancer cells (PC-3) (Chapter 3, Figure 6). The PEO_{45}-*b*-PBO_{24} and PEO_{45}-*b*-PSO_{26} micelles were as efficient as the control commercial formulation in inhibiting the growth of these cells. However, at high polymer concentration, PEO_{45}-*b*-PSO_{26} was fairly less toxic than polysorbate 80. D. Le Garrec *et al.*[17] obtained comparable *in vitro* cytotoxicity of docetaxel-loaded poly(*N*-vinylpyrrolidone) (PVP)-*b*-PDLLA PM against C26 murine colon tumoral cells. The PVP-*b*-PDLLA-unloaded micelles also showed less cytotoxicity than polysorbate 80[17]. Thus, at high drug concentrations, PEO-*b*-PSO may potentially improve the therapeutic index of docetaxel by decreasing the formulation's non-specific toxicity. Such polymers could provide useful alternatives to low molecular weight surfactants for the solubilization of taxanes.

2.4 Limitation of the systems

The limitation of the presented systems is their limited loading capacities (~0.4-4% *w*/*w*) (Chapter 3, Table 4). High loading efficiency is crucial in order to reduce the amount of vehicle to be administered. It is required to limit the toxicity or adverse effects that can be associated with the carrier and to minimize the overall cost of the formulation. Hence, we looked for another drug that had a greater affinity for the micellar cores. Indeed, we could obtain up to 10% (*w*/*w*) loading with a new drug for the treatment of hepatitis C that was provided by a pharmaceutical company (data not shown in this thesis for confidentiality reasons). No changes in size and polydispersity indices (PDI) of these loaded micelles were observed for 14 days when they were examined by dynamic light scattering. In addition, no crystals were apparent under the microscope (*i.e.* no precipitation). What remains to be achieved is to test whether drug-loaded micelles can alter the pharmacokinetics of free drug *in vivo* and improve the therapeutic outcomes. PM, when properly designed, can alter the pharmacokinetics of free drugs and reduce the toxicity associated with commercial surfactants. For example, Genexol-PM is a paclitaxel-encapsulated PEG-*b*-poly(D,L-lactide) (PEG-*b*-PDLLA) micelle formulation[18], administered to overcome the side-effects (*e.g.* hypersensitivity reactions) associated with Cremophor® EL-based system[1]. Cremophor® EL and Genexol-PM formulations have similar drug pharmacokinetics at the 230 mg m^{-2} dose level (Table 1). Both Cremophor® EL and Genexol-PM have similar half-lives and clearance rates. However, Genexol-PM is associated with less toxicity and side-effects (*e.g.* hypersensitivity reactions), allowing for a considerable increase in the maximum

tolerated dose (MTD) (Table 1). This dose increment has led to better tumor responses to therapy among patients[18,19].

Table 1. Comparison of the clinical pharmacokinetics of Taxol® (commercial formulation) and Genexol (micellar nanocarrier). Adopted from reference[20].

Formulation	Taxol®	Genexol
Drug	Paclitaxel	Paclitaxel
Carrier	Cremophor® EL	PEG-PDLLA
Dose (mg m^{-2})	230	230
Number of patients	34	21
$T_{1/2, \beta}$ (h)	8.9±1.8	11.0±1.9
Clearance (mL min^{-1} kg^{-1})	3.9±1.1	4.8±1.0
MTD (mg m^{-2})	230	390
Reference	19	18

3. Polyion complex micelles for nucleic acid delivery

3.1 Preparation of polymeric nanocarriers for nucleic acid delivery

The objective of the second part of this thesis was to prepare polymeric delivery systems that would protect nucleic acids against enzymatic degradation and improve their transfection efficiencies. Two different polyion complex micelle (PICM) systems were developed for the sustained release and intracellular delivery of nucleic acids. Firstly, oligonucleotide (ON) conjugates were prepared by covalently attaching a phosphodiester sense ON (SON) to a PEG chain of various molecular weights. The purified PEG-SON was then hybridized to phosphorothioate (PS)-AON and the PEG-duplex was further purified (Chapter 4, Scheme 1). These conjugates

were proposed to gradually release the AON upon the enzymatic degradation of a complementary SON. The PEG conjugates were able to provide a partial protection for the ON against enzymatic degradation. To improve the stability, the PEG-SON/AON duplex was electrostatically complexed to generation (G) 3 or G5 poly(amidoamine)s (PAMAMs) to trigger the self-assembly of the duplexes into monodisperse PICM. Secondly, the incorporation of PEG-*block*-poly(*propyl* methacrylate-*co*-methacrylic acid) (PEG-*b*-P(*Pr*MA-*co*-MAA)) was exploited to impart pH sensitivity to PAMAM-based PICMs. This system was composed of the anionic copolymer mixed with cationic PAMAM dendrimer. Such PICM could accommodate AON or siRNA in their cores (Chapter 5, Scheme 1). Generally, both types of PICM showed mean hydrodynamic diameters ranging from 50 to 100 nm, narrow size distribution (PDI <0.2) and nearly neutral surface charge (-4–10 mV) (Table 1). The smaller size of PEG_{5K}-*b*-P(*Pr*MA-*co*-MAA)-PICM compared to $PEG_{10\ or\ 20K}$-ON duplex-PICM could be explained by the lower molecular weight of PEG used in the preparation of the micelles (5 K *vs.* 10-20 K). The systems were freeze-dried and easily resuspended without any change in size, PDI, zeta-potential and complexation efficacy (Chapter 5, Figure 1 and Supplementary section, Table S2). Thus, lyophilization was achieved without any additive and the micelles could be stored in dried form. Their size and PDI are comparable to the values obtained earlier for similar systems. For example, PICM formed of PEG-ON conjugate/ polyethylenimine had a size of 70 nm and low PDI[21,22]. However, this is the first time that these PICM were shown to be lyophilized without lyoprotectant[23] or chemical modification (*i.e.* core crosslinking)[24] and to retain their characteristics after

reconstitution with water. This remarkable resistance to aggregation might be attributed to high PEG density in the corona[25].

Table 2. Characteristics of ternary PICM-AON; mean ± SD (n=3).

Corona-forming polymer[a]	PAMAM[b]	Diameter (nm)	PDI	Zeta potential ± SD (mV)
PEG_{10K}-ON	G3	68	0.06	-1.8±0.3
PEG_{20K}-ON	G3	88	0.09	-3.2±1.5
$PEG_{20K\text{-}br}$-ON	G3	89	0.14	3.0±1.6
PEG_{10K}-ON	G5	88	0.08	-1.7±0.3
PEG_{20K}-ON	G5	93	0.07	0.5±0.6
$PEG_{20K\text{-}br}$-ON	G5	97	0.11	0.6±2.9
PEG_{5K}-*b*-P(*Pr*MA_{28}-*co*-MAA_{53})	G5	60	0.13	6.3±1.1
PEG_{5K}-*b*-P(*Pr*MA_{28}-*co*-MAA_{53})	G3	58	0.16	1.2±3.1
PEG_{5K}-*b*-P(*Pr*MA_{51}-*co*-MAA_{33})	G5	58	0.16	4.3±3.6
PEG_{5K}-*b*-P(*Pr*MA_{51}-*co*-MAA_{33})	G3	56	0.15	2.3±4.1

[a]In PEG-ON conjugates, the ON is attached to one extremity ($PEG_{10 \text{ or } 20K}$) or to the central part ($PEG_{20K\text{-}br}$) of the PEG chain.
[b]G3 = 6,909 g/mol, G5 = 28,826 g/mol.

3.2 Enzymatic stability of entrapped nucleic acids

A fluorimetric assay was developed to assess AON and siRNA degradation[26]. This was achieved by labeling the two complementary ON strands by two different fluorescent probes (fluorophore (*i.e.* fluorescein (FAM)) and quencher (*i.e.* Cy3)). Depending on the relative position of the fluorophore and quencher, two types of quenching can occur; fluorescence resonance energy transfer (FRET) and contact (static) quenching.

If the fluorophore and quencher are close to each other within a range of 20-100 Å (*e.g.* siRNA (Figure 1A)), FRET is the predominant mode of quenching. Here,

upon excitation of FAM, energy is transferred through non-radiative dipole-dipole coupling, resulting in increase in the emission fluorescence intensity of Cy3 (*i.e.* FRET)[27]. The FRET is detected by the increase in the Cy3 fluorescence intensity and the decrease in FAM fluorescence intensity [28]. In our case, the siRNA degradation could be monitored by measuring the decrease in FRET which occurs upon the degradation of the duplex (Figure 1A).

On the other hand, if the fluorophore and quencher are brought any closer (*i.e.* <20 Å), contact quenching occurs (*e.g.* ON duplex (Figure 1B)). In this case, the fluorescence intensity of both FAM and Cy3 is reduced because at these intimate distances, most of the absorbed energy is dissipated as heat and only a small amount of energy is emitted as light. The degradation of ON duplex brings the FAM and Cy3 apart from each other, resulting in an increase in the fluorescence intensity of FAM and Cy3 (Figure 1B).

The interesting feature of this fluorimetric assay is that degradation of the nucleic acids can be monitored in real time. In addition, this method is much simpler than gel electrophoresis and less time-consuming.

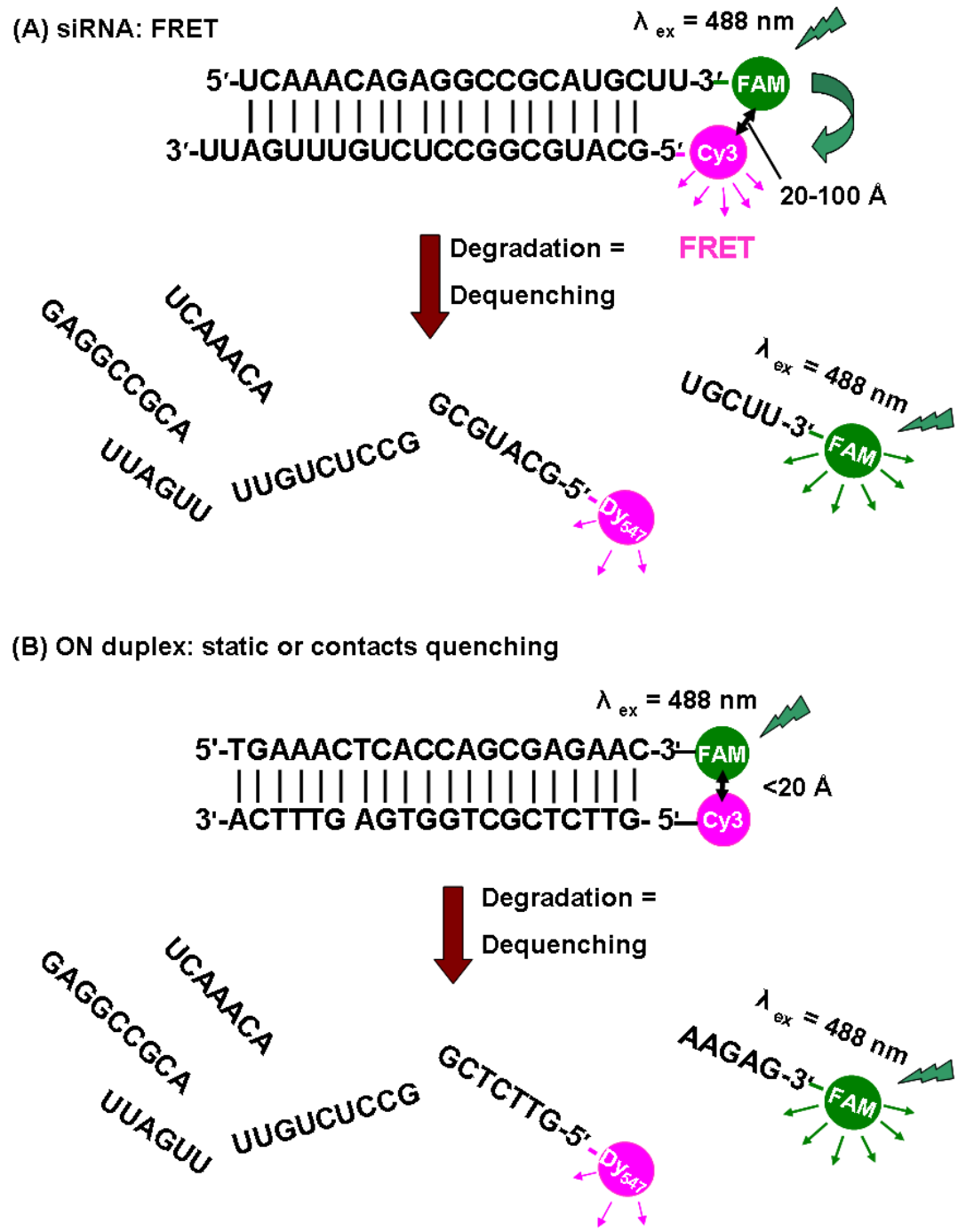

Figure 1. (A) siRNA: the fluorophore (FAM) and the quencher (Cy3) are placed at a distance from each other so that FRET is the predominant mode of quenching. **(B)** ON duplex: the fluorophore and the quencher are placed close to each other so that contact quenching occurs. In both cases, upon the degradation of DNA or RNA duplexes, the fluorophore and quencher become apart from each other and fluorescence dequenching occurs.

Conjugation of ON to PEG partially protected it against enzymatic degradation by DNAse 1. However, the entrapment of nucleic acids (*i.e.* AON or siRNA) in the core of PICM provided greater protection for them against enzymatic degradation by nucleases. Higher generations of PAMAM (*i.e.* G5 *vs.* 3) imparted greater stability to the nucleic acids. Thus, multimeric binding through cooperative effects played a great role in determining the stability of the formed micelles (Chapter 4, Table 2 and Figure 8).

To further study the effect of serum and different plasma proteins on the stability of entrapped siRNA, PEG-*b*-P(*Pr*MA-*co*-MAA)/PAMAM PICM were incubated with serum. Increasing the serum concentration resulted in a faster rate of siRNA degradation (Figure 2). siRNA degradation went from 10 to 40% upon increasing the serum concentration from 20 to 100%. The effects of albumin (40 mg/mL), α- and β-predominant globulins (15 mg/mL), *γ*-globulins (10 mg/mL) and heparin (6×10^{-4} mg/mL) on the degradation profile of the siRNA entrapped in the micelles were examined (Figure 3). These concentrations are representative of the corresponding plasma levels. All plasma proteins and heparin were found to contribute equally to micelle destabilization. A slightly more significant effect was observed for α- and β-globulins. Park, K. and coworkers[29] have recently shown that that α- and β-globulins are major factors for the destabilization of PEG-*b*-PDLLA micelles while other plasma proteins play minor roles. The different results here might be attributed to the difference in micelle composition. PICM are formed *via* electrostatic complexation and are more vulnerable to destabilization by charged plasma proteins.

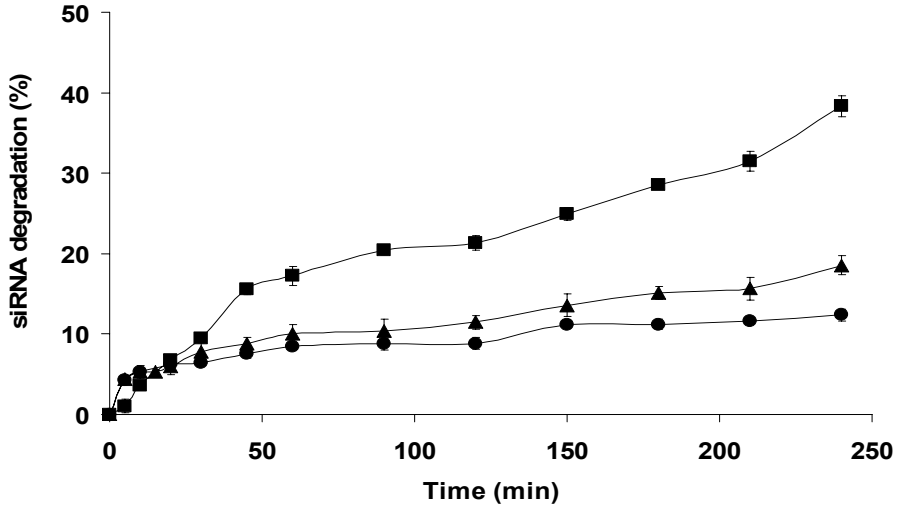

Figure 2. Effect of serum concentration on the stability of siRNA complexed in PEG_{115}-*b*-P(*Pr*MA_{28}-*co*-MAA_{53})/G5 PAMAM PICM (10 µg/mL siRNA, 37°C, pH 7.4). The formulations were incubated in 20% (●), 50% (▲) or 100% (■) FBS. Mean ± SD (n=3).

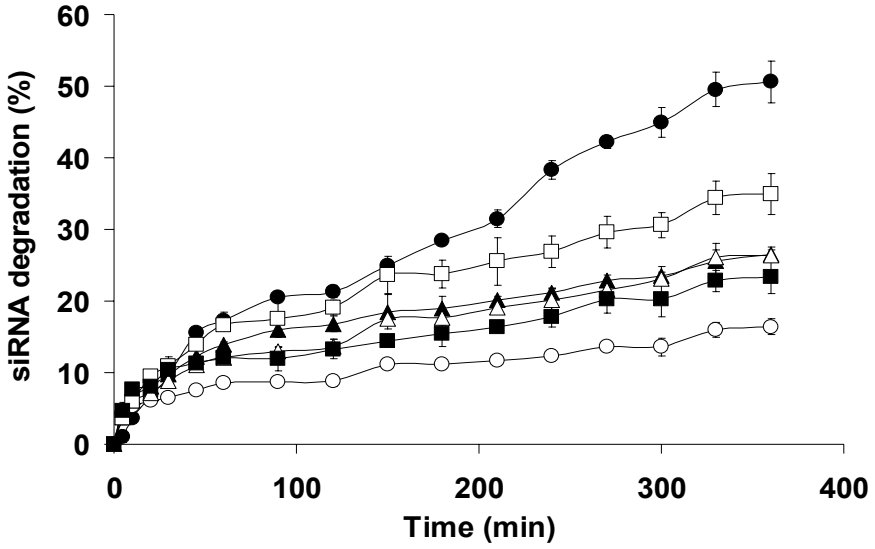

Figure 3. Effect of albumin, 40 mg/mL (▲), γ-globulins, 10 mg/mL (Δ) and α- and β-predominant globulins, 15 mg/mL (□) and heparin, 6 x 10^{-4} mg/mL (■) on the stability of siRNA formulated in PEG_{115}-*b*-P(*Pr*MA_{28}-*co*-MAA_{53})/G5 PAMAM PICM (10 µg/mL siRNA, 37°C, pH 7.4) when incubated with 20% FBS. The stability of PICM in 20% (○) and 100% (●) FBS is also shown. Mean ± SD (n=3).

3.3 Active targeting

An easy way to enhance the intracellular delivery of nucleic acids and to compensate for excessive drug degradation either extra- or intracellularly, is by increasing micelle net positive charge. However, the increase in positive charge usually comes at the expense of toxicity and specificity. These positively-charged complexes are rapidly inactivated in the presence of serum. Moreover, after intravenous injection, the large size and positive character of the complexes result in their rapid opsonization, clearance from the circulation, and the risk of lung capillary occlusion[30-32]. In one study, siRNA-targeting vascular endothelial growth factor (VEGF)-based PICM were tested for anti-angiogenic therapy[33]. The siRNA was conjugated to PEG *via* cleavable disulfide linkage and complexed with cationic polyethylenimine (PEI) for PICM generation. The formulations showed transfection efficiencies superior to PEI/siRNA, even in the presence of serum and despite the absence of any targeting ligand on the micelle surface. This can be explained by the high charge ratio of the formulations (*i.e.* nitrogen-to-phosphate (N/P) = 16). The formulations effectively suppressed VEGF expression after intra-tumoral or intravenous injection, compared to PEI/siRNA. Though interesting, the future applications of such formulations might be limited because of their high charge ratios which can cause toxicity without specific accumulation at target sites. Instead, a targeting ligand should be included to promote the uptake of these micelles at N/P ratio near stoichiometry.

Choosing the antibody as a targeting moiety is advantageous in terms of selectivity, high affinity, and minimal competition for receptors. This is contrary to what is observed with endogenous molecules, such as folic acid or transferrin[34-36]. Whole or fragmented antibodies (*i.e.* fragment antigen binding (Fab')) have been employed to functionalize micelles. In general, targeted micelles show higher cellular uptake than the non-targeted micelles[37,38]. The whole antibody, however, is large and potentially hinders the self-assembly of PICM. Moreover, it can favor the systemic clearance of the carrier *via* Fc region recognition by the mononuclear phagocytic system. In this work, PICM were decorated with anti CD71 Fab' which targets the transferrin receptor. The latter is over-expressed by tumor cells[39]. Decoration of the micelles with the Fab' increased the uptake due to receptor mediated internalization. Then, lowering of pH encountered in the endosomes triggered the deshielding of the micelle corona and released positively-charged AON or siRNA-dendrimer complexes with membrane-destabilizing properties (Chapter 5, Scheme 1). It is worth mentioning that micelles uptake was reduced when the cells were preincubated with free CD71 antibody and became comparable to non-targeted micelles, indicating the specificity of uptake (Chapter 5, Figure S4). Moreover, the micelles were able to escape from the lysosomal pathway as revealed by the confocal microscopy experiments (Chapter 5, Figure 5). In accordance, the Fab'-targeted micelles were able to increase the activity of AON and siRNA directed against Bcl-2 in PC-3 cells more than AON or siRNA that were either free or complexed to plain micelles or PAMAM (Chapter 5, Figure 5). Protection of nucleic acids in the core of the micelles, enhanced cellular uptake and probably the contribution of the MAA

copolymer to endosomal destabilization at acidic pH of the endosomes might be responsible for the enhanced activity of the targeted micelles[40-42]. In addition, at endosomal pH (~5), the deshielding of the micelle corona produced >10-fold increase in (N/P) molar ratio, leaving a positively-charged partially-PEGylated PAMAM/nucleic acids complexes available for interaction with endosomal membranes.

Indeed, targeted and pH-sensitive PICM are promising nanocarriers for siRNA delivery. For example, Kataoka and coworkers[43] prepared lactosylated PEG-siRNA/poly(L-lysine) PICM where the PEG was conjugated to the siRNA *via* β-thiopropionate pH-sensitive linkage. The formulation exhibited gene silencing of firefly luciferase expression in HuH-7 cells that was comparable to cationic liposomes (oligofectamine). However, the application of this formulation may be limited in the treatment of hepatocarcinoma because the targeting ligand (*i.e.* lactose) is used to target hepatocytes. Hepatocytes express carbohydrate receptors (*i.e.* asialoglycoprotein receptors) that recognize different sugar moieties such as lactose, galactose or mannose, allowing liver-specific delivery[44,45]. In addition, our system is preferred because exposure of the membrane-destabilizing components does not rely on the chemical hydrolysis of a pH-sensitive bond[46]. Our approach would also ensure fast dissociation kinetics at acidic pH and higher chemical integrity of the construct.

4. Designing polymeric nanocarriers for drug and nucleic acid delivery

Polymers of different structures and compositions can be used for drug and nucleic acid delivery. Recent data highlight 4 important features of nanocarriers for drug delivery. Firstly, it is essential to incorporate biodegradable polymers. Polymer structure and composition can be changed or even modified according to therapeutic requirements. In many situations, polymer biodegradability and biocompatibility are perquisites for patient safety. Biodegradability can be attained, for example, by endowing polymers with ester[47,48] or disulfide linkages[49,50]. However, the introduction of disulfide bridges in polymer structure might create other problems, such as instability in blood. Disulfide bridges (when not properly designed) can be cleaved in the systemic circulation[51]. Secondly, nanoparticles should be coated with PEG or other neutral polymers to prevent opsonization, decrease clearance and consequently prolong circulation time. The latter allows nanoparticles leakage in leaky vasculature areas (*e.g.* tumors)[52,53]. Thirdly, targeting ligands on the surface of nanoparticles is beneficial in terms of enhancing accumulation at target sites and decreasing the drug exposure of normal cells. Nanoparticles can be decorated with different targeting ligands depending on the purpose of the treatment. For example, targeting transferrin receptors is generally helpful in tumor therapy as they are overexpressed in tumor cells[34,39,54,55]. Alternatively, targeting asialoglycoprotein receptors is particularly beneficial against hepatocellular carcinoma[45,56-58]. Other targeting ligands can be specific in the treatment of prostate cancer[59,60]. Finally, these

nanocarriers can be exploited for combinational therapy, meaning that more than one drug can be incorporated in the same carrier. This can improve drug efficacy (*e.g.* by synergism), reduce the number of injections and ameliorate patient quality of life. For instance, Bae *et al.*[61] combined doxorubicin and wortmannin in PM and could reduce the doxorubicin dose required for cytotoxicity through a synergistic drug action. In addition, Lee *et al*.[62] tested a combination of siRNA and fluorescent dye in magnetic nanoparticles for molecular imaging and siRNA delivery.

Conclusion and perspectives

PM are a promising nanomedicine platform for drug and nucleic acid delivery. These core-shell assemblies can be tailored to increase the solubility of poorly water-soluble drugs just as to protect labile hydrophilic drugs from rapid inactivation. Because of their nanometer size and hydrated outer layer, micelles can prolong the circulation time of encapsulated drugs and passively accumulate at tumor sites, thereby reducing drug systemic toxicity and enhancing its efficacy. Micelles that actively target tissues can also be prepared by utilizing stimuli-responsive components or by attaching recognition groups at their surface.

In this thesis, poly(ethylene oxide)-*block*-poly(butylene oxide/styrene oxide) PM were prepared and found to enhance the aqueous solubility of docetaxel. Poly(ethylene oxide)-*block*-poly(butylene oxide) PM were able to protect docetaxel against hydrolytic degradation. Docetaxel-loaded micelles demonstrated *in vitro* efficacy comparable to the commercial formulation, indicating drug release from the hydrophobic core. In addition, the polymers showed lower toxicity than the commercial surfactants which may increase the therapeutic index of the drug by reducing the adverse reactions associated with the commercial formulations. Pharmacokinetic studies still need to be performed to determine if the half-life of docetaxel can be changed by using these PM.

On the other hand, stable PICM were prepared and found to slow AON and siRNA degradation and increase their intracellular bioavailability. Long-term stability of the formulations is guaranteed by the fact that these micelles can be lyophilized without any additive and thus stored in solid form. Such polymeric

nanocarriers could prove potentially useful to confer prolonged circulating properties to nucleic acids and enhance their intracellular bioavailability.

What remains to be accomplished is further diminution of formulation toxicity compared to current PAMAM systems while providing greater protection for siRNA against degradation in serum. These objectives might be achieved by imparting biodegradability to PAMAM dendrimers and by exploiting chemically-modified siRNA. PAMAM dendrimers of different molecular weights (*i.e.* number of surface amine groups) will be synthesized by convergent method[63]. The dendrimers will be grown *via* ester linkages (Figure 4), which will confer them with biodegradability. Biodegradable PAMAM of G3 to G6 will be synthesized. These PAMAM generations will be selected because they have been shown to form PICM when reacted with PEG-*b*-P(*Pr*MA-*co*-MAA)/siRNA. Lower generations of PAMAM dendrimers do not form PICM[26].

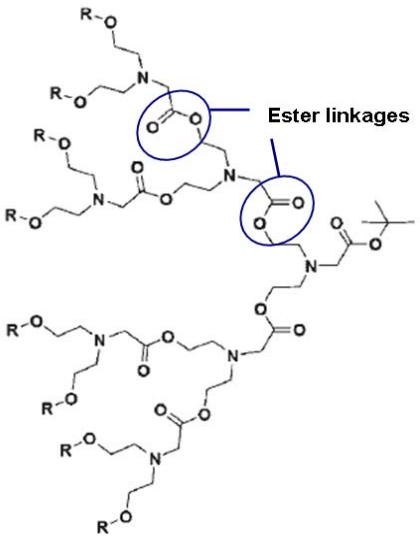

Figure 4. Biodegradable PAMAM dendrimers endowed with ester linkages.

Chemically-modified siRNA will be employed to provide greater protection against enzymatic degradation and possibly greater affinity for the sequences targeted. Indeed, some chemically-modified siRNA have been originally synthesized for our laboratory (Table 3). These siRNA combine more than one kind of chemical modification (2′-deoxy-2′-fluoro-β-D-arabinonucleic acid, 2'fluoro-RNA and locked nucleic acid) but they are still under investigation.

Table 3. Chemically modified siRNA.

Name	Sequence	
BCL2-FF611	5' - **GCA***UGC***GGC***CUC***U***G***U***U***G***AUU**	-3'
	3'- *UUCGUACGCCGGAGACAAACU*	-5'
BCL2-LFL3	5' - **GC*A*UGCGGCC*U*CU*G*U*U*UGAUU**	-3'
	3' - *UUCGUACGCCGGAGACAAACU*	-5'
BCL2-1	5' - **GCA***UGC***GGC***CUC***U***G***U***U***G***AUU**	-3'
	3' - UUCGUACGCCGGAGACAAACU	-5'
BCL2-2	5' - **GC*A*UGCGGCC*U*CU*G*U*U*UGAUU**	-3'
	3' - UUCGUACGCCGGAGACAAACU	-5'

Legend: RNA, **2'F-ANA**, *2'F-RNA*, ***LNA***

Despite the significant progress that has been made in formulating nucleic acids with PICM, no systems have demonstrated sufficient efficacy in animal and/or human models for clinical use. Hence, a pharmacokinetic study will be conducted to determine the half-life of the siRNA *in vivo*. In addition, the feasibility of these systems to efficiently knock down the Bcl-2 oncogene in targeted cells *in vivo* still needs to be established. The long term objective of this research is to construct a clinically-viable pH-responsive PICM system for siRNA systemic administration that would combine most of the essential attributes required for efficient delivery to appropriate cellular compartments.

References

1. ten Tije, A. J., Verweij, J., Loos, W. J., Sparreboom, A. *Clin Pharmacokinet* **42**, 665-685 (2003).
2. Anderson, E. M., Miller, P., Ilsley, D., Marshall, W., Khvorova, A., Stein, C. A., Benimetskaya, L. *Cancer Gene Ther* **13**, 406-414 (2006).
3. Marshall, J., Chen, H., Yang, D., Figueira, M., Bouker, K. B., Ling, Y., Lippman, M., Frankel, S. R., Hayes, D. F. *Ann Oncol* **15**, 1274-1283 (2004).
4. Chanan-Khan, A. *Blood Rev* **19**, 213-221 (2005).
5. Raynaud, F. I., Orr, R. M., Goddard, P. M., Lacey, H. A., Lancashire, H., Judson, I. R., Beck, T., Bryan, B., Cotter, F. E. *J Pharmacol Exp Ther* **281**, 420-427 (1997).
6. Hamley, I. W., Pedersen, J. S., Booth, C. & Nace, V. M. *Langmuir* **17,** 6386-6388 (2001).
7. Yang, Z., Crothers, M., Attwood, D., Collett, J. H., Ricardo, N. M. P. S., Martini, L. G. A. & Booth, C. *J. Colloid Interface Sci.* **263,** 312-317 (2003).
8. Crothers, M., Zhou, Z., Ricardo, N. M., Yang, Z., Taboada, P., Chaibundit, C., Attwood, D., Booth, C. *Int J Pharm* **293**, 91-100 (2005).
9. Chaibundit, C. R., Ricardo, N. M. P. S., Crothers, M. Booth, C. *Langmuir* **18**, 4277 (2002).
10. Elsabahy, M., Perron, M. E., Bertrand, N., Yu, G. E., Leroux, J. C. *Biomacromolecules* **8**, 2250-2257 (2007).
11. Cai, S., Vijayan, K., Cheng, D., Lima, E. M., Discher, D. E. *Pharm Res* **24**, 2099-2109 (2007).

12. Geng, Y., Dalhaimer, P., Cai, S., Tsai, R., Tewari, M., Minko, T., Discher, D. E. *Nat. Nanotechnol.* **2**, 249-255 (2007).

13. Kim, Y., Dalhaimer, P., Christian, D. A., Discher, D. E. *Nanotechnology* **16**, S484–S491 (2005).

14. Dalhaimer, P., Engler, A. J., Parthasarathy, R., Discher, D. E. *Biomacromolecules* **5**, 1714-1719 (2004).

15. Zhange, X., Jackson, J. K., Burt, H. M. *Int. J. Pharm.* **132**, 195-206 (1996).

16. Crothers, M., Ricardo, N. M., Heatley, F., Nixon, S. K., Attwood, D., Booth, C. *Int J Pharm* **358**, 303-306 (2008).

17. Le Garrec, D., Gori, S., Karkan, D., Luo, L., Lessard, D. G., Smith, D., Ranger, M., Yessine, M. A., Leroux, J. C. *J Drug Del Sci Tech* **15,** 115-120 (2005).

18. Kim, T. Y., Kim, D. W., Chung, J. Y., Shin, S. G., Kim, S. C., Heo, D. S., Kim, N. K., Bang, Y. J. *Clin Cancer Res* **10**, 3708-3716 (2004).

19. Wiernik, P. H., Schwartz, E. L., Strauman, J. J., Dutcher, J. P., Lipton, R. B., Paietta, E. *Cancer Res* **47**, 2486-2493 (1987).

20. Sutton, D., Nasongkla, N., Blanco, E., Gao, J. *Pharm Res* **24**, 1029-1046 (2007).

21. Jeong, J. H., Kim, S. W., Park, T. G. *J Control Release* **93**, 183-191 (2003).

22. Jeong, J. H., Kim, S. H., Kim, S. W., Park, T. G. *Bioconjug Chem* **16**, 1034-1037 (2005).

23. Andersen, M. O., Howard, K. A., Paludan, S. R., Besenbacher, F., Kjems, J. *Biomaterials* **29**, 506-512 (2008).

24. Miyata, K., Kakizawa, Y., Nishiyama, N., Yamasaki, Y., Watanabe, T., Kohara, M., Kataoka, K. *J Control Release* **109**, 15-23 (2005).

25. Kang, N., Perron, M. E., Prud'homme, R. E., Zhang, Y., Gaucher, G., Leroux, J. C. *Nano Lett* **5**, 315-319 (2005).

26. Elsabahy, M., Zhang, M., Gan, S., Waldron, K. C., Leroux, J. C. *Soft Matter* **4,** 294-302 (2008).

27. Algar, W. R., Krull, U. J. *Anal Bioanal Chem* **391**, 1609-1618 (2008).

28. Marras, S. A., Kramer, F. R., Tyagi, S. *Nucleic Acids Res* **30**, e122 (2002).

29. Chen, H., Kim, S., He, W., Wang, H., Low, P. S., Park, K., Cheng, J. X. *Langmuir* **24**, 5213-5217 (2008).

30. Ogris, M., Brunner, S., Schuller, S., Kircheis, R., Wagner, E. *Gene Ther* **6**, 595-605 (1999).

31. Mahato, R. I., Kawabata, K., Takakura, Y., Hashida, M. *J Drug Target* **3**, 149-157 (1995).

32. Ward, C. M., Read, M. L., Seymour, L. W. *Blood* **97**, 2221-2229 (2001).

33. Kim, S. H., Jeong, J. H., Lee, S. H., Kim, S. W., Park, T. G. *J Control Release* **129**, 107-116 (2008).

34. Singh, M. *Curr Pharm Des* **5**, 443-451 (1999).

35. King, G. L., Feener, E. P. *Adv Drug Deliv Rev* **29**, 197-213 (1998).

36. Qian, Z. M., Li, H., Sun, H., Ho, K. *Pharmacol Rev* **54**, 561-587 (2002).

37. Torchilin, V. P., Lukyanov, A. N., Gao, Z., Papahadjopoulos-Sternberg, B. *Proc Natl Acad Sci U S A* **100**, 6039-6044 (2003).

38. Merdan, T., Callahan, J., Petersen, H., Kunath, K., Bakowsky, U., Kopeckova, P., Kissel, T., Kopecek, J. *Bioconjug Chem* **14**, 989-996 (2003).

39. Hogemann-Savellano, D., Bos, E., Blondet, C., Sato, F., Abe, T., Josephson, L., Weissleder, R., Gaudet, J., Sgroi, D., Peters, P. J., Basilion, J. P. *Neoplasia* **5**, 495-506 (2003).

40. Yessine, M. A., Dufresne, M. H., Meier, C., Petereit, H. U., Leroux, J. C. *Bioconjug Chem* **18**, 1010-1014 (2007).

41. Yessine, M. A., Leroux, J. C. *Adv Drug Deliv Rev* **56**, 999-1021 (2004).

42. Yessine, M. A., Meier, C., Petereit, H. U., Leroux, J. C. *Eur J Pharm Biopharm* **63**, 1-10 (2006).

43. Oishi, M., Nagasaki, Y., Itaka, K., Nishiyama, N., Kataoka, K. *J Am Chem Soc* **127**, 1624-1625 (2005).

44. Jule, E., Nagasaki, Y., Kataoka, K. *Bioconjug Chem* **14**, 177-186 (2003).

45. Sugahara, K., Togashi, H., Takahashi, K., Onodera, Y., Sanjo, M., Misawa, K., Suzuki, A., Adachi, T., Ito, J., Okumoto, K., Hattori, E., Takeda, T., Watanabe, H., Saito, K., Saito, T., Sugai, Y., Kawata, S. *Hepatology* **38**, 1401-1409 (2003).

46. Rozema, D. B., Lewis, D. L., Wakefield, D. H., Wong, S. C., Klein, J. J., Roesch, P. L., Bertin, S. L., Reppen, T. W., Chu, Q., Blokhin, A. V., Hagstrom, J. E., Wolff, J. A. *Proc Natl Acad Sci U S A* **104**, 12982-12987 (2007).

47. Lee, J. S., Huh, J., Ahn, C. H., Lee, M., Park. T. G. *Macromol Rapid Commun* **27**, 1608-1614 (2006).

48. Xiong, X. B., Uludag, H., Lavasanifar, A. *Biomaterials* **30**, 242-253 (2009).

49. You, Y. Z., Manickam, D. S., Zhou, Q. H., Oupicky, D. *J Control Release* **122**, 217-225 (2007).

50. Kim, S. H., Jeong, J. H., Kim, T. I., Kim, S. W., Bull, D. A. *Mol Pharm* **6**, 718-726 (2009).

51. Zhou, Q. H., Wu, C., Manickam, D. S.,Oupicky, D. *Pharm Res* **26**, 1581-1589 (2009).

52. Jones, M., Leroux, J. C. *Eur J Pharm Biopharm* **48**, 101-111 (1999).

53. Torchilin, V. P. & Trubetskoy, V. S. *Adv Drug Deliv Rev* **16,** 141-155 (1995).

54. Anabousi, S., Bakowsky, U., Schneider, M., Huwer, H., Lehr, C. M., Ehrhardt, C. *Eur J Pharm Sci* **29**, 367-374 (2006).

55. Huang, R. Q., Qu, Y. H., Ke, W. L., Zhu, J. H., Pei, Y. Y., Jiang, C. *FASEB J* **21**, 1117-1125 (2007).

56. Oishi, M., Kataoka, K., Nagasaki, Y. *Bioconjug Chem* **17**, 677-688 (2006).

57. Wakebayashi, D., Nishiyama, N., Yamasaki, Y., Itaka, K., Kanayama, N., Harada, A., Nagasaki, Y., Kataoka, K. *J Control Release* **95**, 653-664 (2004).

58. Jeong, Y. I., Seo, S. J., Park, I. K., Lee, H. C., Kang, I. C., Akaike, T., Cho, C. S. *Int J Pharm* **296**, 151-161 (2005).

59. Farokhzad, O. C., Cheng, J., Teply, B. A., Sherifi, I., Jon, S., Kantoff, P. W., Richie, J. P., Langer, R. *Proc Natl Acad Sci U S A* **103**, 6315-6320 (2006).

60. Farokhzad, O. C., Jon, S., Khademhosseini, A., Tran, T. N., Lavan, D. A., Langer, R. *Cancer Res* **64**, 7668-7672 (2004).

61. Bae, Y., Diezi, T. A., Zhao, A., Kwon, G. S. *J Control Release* **122**, 324-330 (2007).

62. Lee, J. H., Lee, K., Moon, S. H., Lee, Y., Park, T. G., Cheon, J. *Angew Chem Int Ed Engl* **48**, 4174-4179 (2009).

63. Lee, J.-S., Huh, J., Ahn, C.-H., Lee, M., Park, T. G. *Macromol. Rapid Commun.* **27**, 1608–1614 (2006).

Appendix

Protection of the siRNA against degradation in different biological media

Control siRNA or siRNA entrapped in PICMs of PEG_{115}-*b*-P(*Pr*MA_{28}-*co*-MAA_{53})/PAMAM G5 (prepared at N/(P + COO^-) molar ratio of 1.5) were incubated with 20, 50 and 100% FBS. Then, the effect of albumin (40 mg/mL), α- and β-predominant globulins (15 mg/mL), γ-globulins (10 mg/mL) and heparin (6 x 10^{-4} mg/mL) on the degradation profile of the siRNA entrapped in the same micelles was examined. The calculation of the % of siRNA degradation was performed according to Equation 1 (Chapter 5, supplementary S4).

Contributions of Mahmoud El Sabahy as the first author in the following manuscripts

1. **Mahmoud El Sabahy,** Marie-Hélène Dufresne and Jean-Christophe Leroux. Polymeric micelles as versatile carriers for drugs and nucleic acids delivery, In; Torchilin V and Amiji M (Eds), Materials for Nanomedicine, Pan Stanford Publishing, Hackensack, in press (2009).

   This literature review on polymeric micelles (PM) was written by Mahmoud El Sabahy (corresponding to ~90% of the work). The literature survey and book chapter structure were originally proposed and designed by him. In addition, Figure 5 represents some experimental results that were obtained by Mahmoud El Sabahy. Dr. Jean-Christophe Leroux (Research Director) and Dr. Marie-Hélène Dufresne reviewed and monitored the scientific content and structure of the chapter.

2. **Mahmoud El Sabahy**, Marie-Ève Perron, Nicolas Bertrand, Ga-er Yu and Jean-Christophe Leroux, Solubilization of docetaxel in poly(ethylene oxide)-*block*-poly(butylene/styrene oxide) micelles. *Biomacromolecules*, 8, 2250-2257 (2007).

   This peer-reviewed article represents the experimental results obtained by Mahmoud El Sabahy (corresponding to 85% of the work). He designed and optimized a protocol for the preparation of both unloaded and docetaxel-loaded micelles. He found that these micelles could assemble at different morphologies (spherical *vs.* cylindrical). All size measurements, HPLC analysis and

fluorimetric experiments were performed by him. In addition, *in vitro* release kinetics were investigated by Mahmoud El Sabahy. Marie-Ève Perron tested the toxicity of the formulations (MTT assay). Nicolas Bertrand helped in analyzing the kinetics of drug release from the formulations. Ga-er Yu synthesized the polymers and supplied them for our laboratory. Dr. Jean-Christophe Leroux (Research Director) proposed the original idea of this project, revised the scientific content of the article, and provided help as well as advice whenever they were necessary.

3. **Mahmoud El Sabahy**, Mingzhen Zhang, Shao-Ming Gan, Karen C. Waldron and Jean-Christophe Leroux, Synthesis and enzymatic stability of PEGylated oligonucleotide duplexes and their self-assemblies with polyamidoamine dendrimers. *Soft Matter*, 4, 294-302 (2008).

   This peer-reviewed article reports the experimental data obtained by Mahmoud El Sabahy (corresponding to ~90% of the work). Dr. Mingzhen Zhang started the project and designed a protocol for preparing PEGylated oligonucleotide duplexes. However, all the experimental data presented in the article were generated by Mahmoud El Sabahy. Shao-Ming Gan and Dr. Karen C. Waldron allowed the use of their capillary electrophoresis facility and assisted in analyzing the results. Dr. Jean-Christophe Leroux (Research Director) had suggested the original idea of designing PEGylated oligonucleotide duplexes for the delivery of antisense oligonucleotides and revised the scientific content of the article. Then, under his supervision, Mahmoud El Sabahy suggested the use of

poly(amidoamine) dendrimers for the formation of micelles with PEGylated oligonucleotide duplexes to provide greater protection for oligonucleotides against degradation. Dr. Jean-Christophe Leroux was there at every experiment to provide help, advice and direction.

4. **Mahmoud El Sabahy**, Nada Wazen, Núria Bayó-Puxan, Glen Deleavey, Marc Servant, Masad J. Damha and Jean-Christophe Leroux. Delivery of nucleic acids through the controlled disassembly of multifunctional nanocomplexes. *Adv. Funct. Mater*. in press (2009).

   This peer-reviewed article represents the experimental results obtained by Mahmoud El Sabahy (corresponding to 85% of the work). Nada Wazen and Núria Bayó-Puxan synthesized the polymers and developed a protocol for attaching antibody fragments to the anionic copolymers. Then, Mahmoud El Sabahy successfully attached them. He generated all other experimental data and spent about a year trying to find a suitable oncogene that could serve as a model target for inhibition by antisense oligonucleotide and short interfering RNA (siRNA). He also designed the fluorescence resonance energy transfer assay. All *in vitro* cell assays (flow cytometry, cytotoxicity, confocal imaging and Bcl-2 assays) were performed by him. Dr. Marc Servant provided advice regarding the Bcl-2 assay. Scientific meetings were held with Dr. Masad Damha and his graduate student Glen Deleavey to discuss the project. Dr. Masad Damha and Glen Deleavey provided our laboratory with some chemically modified siRNA that are still under investigation and not included in this article. Dr.

Jean-Christophe Leroux (Research Director) had suggested the original idea of using targeted-pH-sensitive PICM for nucleic acid delivery and revised the scientific content of the article. He was also there at every experiment to provide help, advice and direction.